

**AWARD NUMBER: W81XWH-16-1-0104**

**TITLE:** The NUP98 Gene as a Potential Modifier of NF2-Associated Tumors

**PRINCIPAL INVESTIGATOR:** Long-Sheng Chang, Ph.D.

**CONTRACTING ORGANIZATION:** The Research Institute at Nationwide Children's  
Hospital, Columbus, Ohio 43205-2696

**REPORT DATE:** September 30, 2019

**TYPE OF REPORT:** Final

**PREPARED FOR:** U.S. Army Medical Research and Materiel Command  
Fort Detrick, Maryland 21702-5012

**DISTRIBUTION STATEMENT:** Approved for Public Release;  
Distribution Unlimited

The views, opinions and/or findings contained in this report are those of the author(s) and should not be construed as an official Department of the Army position, policy or decision unless so designated by other documentation.

REPORT DOCUMENTATION PAGE				Form Approved OMB No. 0704-0188	
Public reporting burden for this collection of information is estimated to average 1 hour per response, including the time for reviewing instructions, searching existing data sources, gathering and maintaining the data needed, and completing and reviewing this collection of information. Send comments regarding this burden estimate or any other aspect of this collection of information, including suggestions for reducing this burden to Department of Defense, Washington Headquarters Services, Directorate for Information Operations and Reports (0704-0188), 1215 Jefferson Davis Highway, Suite 1204, Arlington, VA 22202-4302. Respondents should be aware that notwithstanding any other provision of law, no person shall be subject to any penalty for failing to comply with a collection of information if it does not display a currently valid OMB control number. <b>PLEASE DO NOT RETURN YOUR FORM TO THE ABOVE ADDRESS.</b>					
1. REPORT DATE SEPTEMBER 2019		2. REPORT TYPE Final		3. DATES COVERED 1 June 2016 – 31 MAY 2019	
4. TITLE AND SUBTITLE  The <i>NUP98</i> Gene as a Potential Modifier of NF2-Associated Tumors				5a. CONTRACT NUMBER W81XWH-16-1-0104	
				5b. GRANT NUMBER GRANT11968353	
				5c. PROGRAM ELEMENT NUMBER	
6. AUTHOR(S)  Long-Sheng Chang, Ph.D.  E-Mail: <a href="mailto:Long-Sheng.Chang@nationwidechildrens.org">Long-Sheng.Chang@nationwidechildrens.org</a>				5d. PROJECT NUMBER	
				5e. TASK NUMBER	
				5f. WORK UNIT NUMBER	
7. PERFORMING ORGANIZATION NAME(S) AND ADDRESS(ES) Research Institute at Nationwide Children's Hospital 700 Children's Drive Columbus, OH 43205-2696				8. PERFORMING ORGANIZATION REPORT NUMBER	
9. SPONSORING / MONITORING AGENCY NAME(S) AND ADDRESS(ES)  U.S. Army Medical Research and Materiel Command Fort Detrick, Maryland 21702-5012				10. SPONSOR/MONITOR'S ACRONYM(S)	
				11. SPONSOR/MONITOR'S REPORT NUMBER(S)	
12. DISTRIBUTION / AVAILABILITY STATEMENT  Approved for Public Release; Distribution Unlimited					
13. SUPPLEMENTARY NOTES					
14. ABSTRACT The objective of this exploratory hypothesis-driven award was to investigate whether the <i>NUP98</i> gene, which plays important roles in nucleocytoplasmic transport, gene expression, mitotic checkpoint, and pathogenesis, is frequently mutated in NF2-related vestibular schwannomas (VS) and whether <i>NUP98</i> mutations are associated with disease severity. By next-generation sequencing and PCR sequencing, we confirmed that the <i>NUP98</i> gene was altered more frequently in patient with NF2 than sporadic VS patients or individuals without VS. The alterations in <i>NUP98</i> identified resulted in changes in three evolutionarily-conserved, charged amino acids, including a D1156N mutation and a Q1142E variant in exon 23 and a K1178R mutation in exon 24. These changes are heterozygous and are present in patients' germline. In addition, we found that NF2-associated VS and meningiomas had low mutational burden and did not have mutations in the genes frequently found in sporadic tumors except <i>NF2</i> . Interestingly, multiple VS and meningiomas from the same patient harbored mutations in the same set of genes, and the genomes of these NF2 tumors were quite stable as a recurrent tumor did not have any new mutation over a long period of time despite after several experimental therapies. However, with the number of samples analyzed particularly those from patients with NF2, we were not able to statistically correlate the <i>NUP98</i> mutations that we identified with disease severity. Additional analysis is ongoing and should allow us to establish whether <i>NUP98</i> is a potential genetic modifier for NF2.					
15. SUBJECT TERMS Neurofibromatosis type 2 (NF2), <i>neurofibromatosis 2 (NF2)</i> gene, genetic modifier, <i>NUP98</i> gene, vestibular schwannoma, meningioma, NF2-associated, sporadic, mutation, variant, polymorphism					
16. SECURITY CLASSIFICATION OF:			17. LIMITATION OF ABSTRACT  Unclassified	18. NUMBER OF PAGES  94	19a. NAME OF RESPONSIBLE PERSON USAMRMC
a. REPORT  Unclassified	b. ABSTRACT  Unclassified	c. THIS PAGE  Unclassified			19b. TELEPHONE NUMBER (include area code)

## Table of Contents

	<u>Page</u>
Cover.....	1
SF298.....	2
Table of Content.....	3
1. Introduction.....	4
2. Keywords.....	4
3. Overall Project Summary.....	4
4. Key Research Accomplishments.....	4 - 13
5. Impact.....	13 - 14
6. Conclusions.....	14
7. Publications, Abstracts, and Presentations.....	14 - 17
8. Inventions, Patents, and Licenses.....	17 - 18
9. Reportable Outcomes.....	18
10. Other Achievements.....	18
11. References.....	18 - 19
12. Appendices.....	19 -

## 1. Introduction

Neurofibromatosis type 2 (NF2) is a neurogenetic disorder characterized by a diverse array of clinical phenotypes, including vestibular schwannomas (VS), meningiomas, ependymomas, spinal and peripheral schwannomas, astrocytomas, and cataracts. Intriguingly, patients with NF2 frequently exhibit a significant amount of phenotypic heterogeneity, including differences in clinical presentation, tumor number, and tumor growth rates. Presently, the causes of this clinical variability are not understood. Studies have shown that genetic modifiers can influence the variability of clinical features, disease severity, and the onset and progression of disease; however, such factors have not been identified for NF2. While loss of the *neurofibromatosis 2* (NF2) tumor suppressor gene plays an important role in the development of NF2-associated tumors, the variability in clinical phenotypes observed in NF2 patients may be explained by genetic modifiers that impact penetrance, expressivity, and disease progression. Identification of a genetic modifier in NF2 should substantially advance our understanding of the disease characteristics and pathobiology of NF2 and may promote the discovery of novel biomarkers and therapeutic targets for drug development.

## 2. Keywords

Neurofibromatosis type 2 (NF2), *neurofibromatosis 2* (NF2) gene, genetic modifier, *NUP98* gene, vestibular schwannoma, meningioma, NF2-associated, sporadic, mutation, variant, polymorphism.

## 3. Overall Project Summary

To better understand genomic alterations in NF2-associated tumors, we previously analyzed 405 cancer-related genes and variants in vestibular schwannomas (VS) from two NF2 patients with large, fast-growing tumors by next-generation sequencing using the FoundationOne Heme genomic test. In addition to the *NF2* gene, mutations were also found in the *nucleoporin 98* (*NUP98*) gene in both patients' VS. Intriguingly, the amino acid residues affected by the *NUP98* mutations identified are evolutionarily conserved among various species, implying that these residues may be important for protein function. The *NUP98* gene encodes a 186-kDa precursor protein that undergoes autoproteolytic cleavage to generate a 98-kDa nucleoporin and 96-kDa nucleoporin (<https://ghr.nlm.nih.gov/gene/NUP98>). These nucleoporins function as components of the nuclear pore complex involved in nucleocytoplasmic transport. The *NUP98* gene products have also been shown to play important roles in gene expression, mitotic checkpoint, and pathogenesis. Alterations in the *NUP98* gene have been found in Beckwith-Wiedemann syndrome and several types of human cancer including Wilms tumor, rhabdomyosarcoma, adrenocortical carcinoma, and lung, ovarian, and breast cancers. In addition, fusions of the *NUP98* gene to several genes have been observed in acute myelogenous leukemia and T-cell acute lymphocytic leukemia. However, whether there is any role of *NUP98* in NF pathogenesis is not known. The objective of this Exploratory Hypothesis-Driven Award was to further examine how frequent the *NUP98* gene is mutated in NF2 patients and whether *NUP98* mutations are associated with disease severity.

## 4. Key Research Accomplishments:

### (i) What were the major goals of the project?

The major goals of this project are to determine the frequency of *NUP98* mutations in a large cohort of patients with NF2-associated and sporadic VS and in individuals without a history of VS and to correlate the presence of *NUP98* mutation with clinical parameters, such as tumor size, growth rate, and tumor recurrence.

### (ii) What was accomplished under these goals?

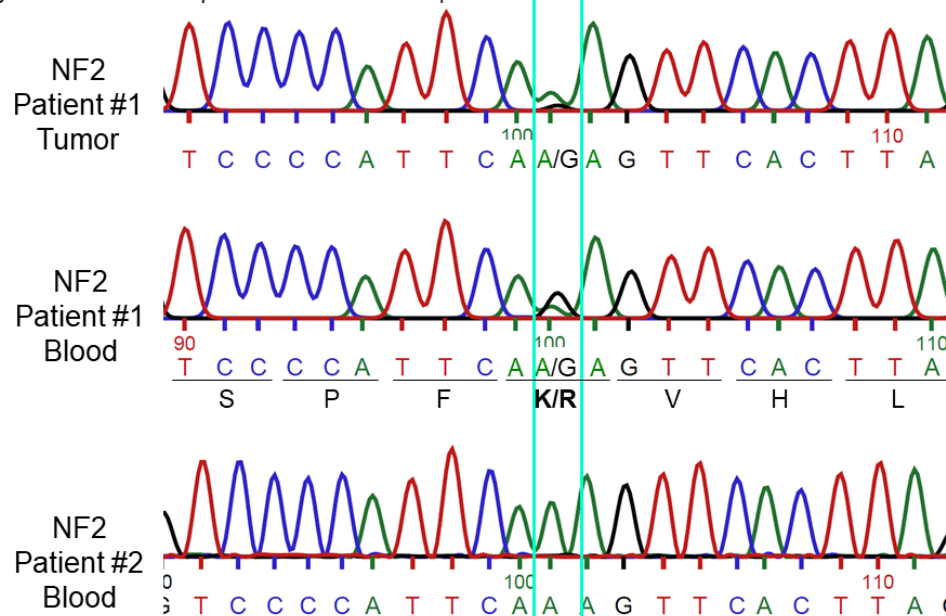
By next-generation sequencing, we initially analyzed two VS from two NF2 patients

(one right VS from each patient) and identified *NUP98* mutations in both patients' tumors in addition to the expected *NF2* gene mutations. Sequence analysis revealed that the first NF2 patient's VS carried a K1178R mutation in exon 24 of the *NUP98* gene, and the second NF2 patient's VS harbored a D1156N mutation in *NUP98* exon 23 (Figure 1).

**Figure 1. Genomic landscape of NF2-associated vestibular schwannomas (VS) and meningiomas.** A total of five tumors including a right VS from NF2 patient #1 and a right VS, a left VS, a left meningioma in the cerebellopontine angle region, and a left orbital meningioma from NF2 patient #2 enrolled in the AR-42 clinical trial were subjected to FoundationOne Heme genomic tests to detect any mutations in 405 cancer-related genes and variants. Mutations in the *NF2* and *NUP98* genes were identified in both NF2 patients' tumors. In addition, the 2 VS and 2 meningiomas from NF2 patient #2 harbor mutations in the same set of genes including *NF2* and *NUP98*.

FoundationOne™ Heme	Genomic Alterations Identified	Variants of Unknown Significance
<b>Right VS</b> (excised 1-month after AR-42 trial) <b>NF2 patient #1</b>	<i>NF2</i> E555*, N485fs*30 <i>NUP98</i> K1178R	<i>DTX1</i> H34P <i>HIST1H2AL</i> N39T <i>STAT4</i> I704V
<b>Right VS</b> (excised 6-month after AR-42 trial) <b>NF2 patient #2</b>	<i>NF2</i> E317*, splice site 240+2T>C, splice site 447+1G>C, V219M <i>MYC</i> duplication exon 2-3	<i>ATML</i> L2307F <i>NF1</i> I2681V <i>NUP98</i> D1156N <i>TET2</i> I1025L
<b>Left VS</b> (excised 2-year after AR-42 trial) <b>NF2 patient #2</b>	<i>NF2</i> splice site 447+1G>C, V146fs*15 <i>MYC</i> duplication exon 2-3	<i>ATML</i> L2307F <i>NF1</i> I2681V <i>NUP98</i> D1156N <i>TET2</i> I1025L
<b>Left meningioma</b> (excised 2-year after AR-42 trial) <b>NF2 patient #2</b>	<i>NF2</i> splice site 447+1G>C <i>MYC</i> duplication exon 2-3	<i>ATML</i> L2307F <i>NF1</i> I2681V <i>NUP98</i> D1156N <i>TET2</i> I1025L
<b>Left orbital meningioma, recurrent</b> (excised 5-year after AR-42 trial) <b>NF2 patient #2</b>	<i>NF2</i> splice site 447+1G>C <i>MYC</i> duplication exon 2-3	<i>ATML</i> L2307F <i>NF1</i> I2681V <i>NUP98</i> D1156N <i>TET2</i> I1025L

**Figure 2. Detection of a heterozygous K1178R mutation in exon 24 of the *NUP98* gene in the germline of NF2 patient #1.** Sequencing analysis identified a heterozygous A/G residue (p. K1178R) in exon 24 of the *NUP98* gene in both the blood and tumor of NF2 patient #1, compared to only the A nucleotide at the corresponding position of the published wild-type *NUP98* gene or the *NUP98* sequence in the blood of NF2 patient #2.



To confirm the presence of these *NUP98* mutations, we analyzed blood and tumor DNA samples from these two patients by polymerase chain reaction (PCR) and DNA sequencing analyses. We found that both the blood and tumor specimens from patient #1 carried a heterozygous K1178R mutation in exon 24 (Figure 2). Also, we detected

another nucleotide change in exon 23, resulting in an amino acid change at Q1142E in this patient #1's blood and tumor DNA (Figure 3).

**Figure 3. Detection of a heterozygous mutation (Q1142E) in exon 23 of the NUP98 gene in the germline of NF2 patient #1.** Sequencing analysis identified a heterozygous G/C residue (p. Q1142E) in exon 23 of the NUP98 gene in both the blood and tumor of NF2 patient #1, compared to only the G nucleotide at the corresponding position of the published wild-type NUP98 gene or the NUP98 sequence in the blood of NF2 patient #2.

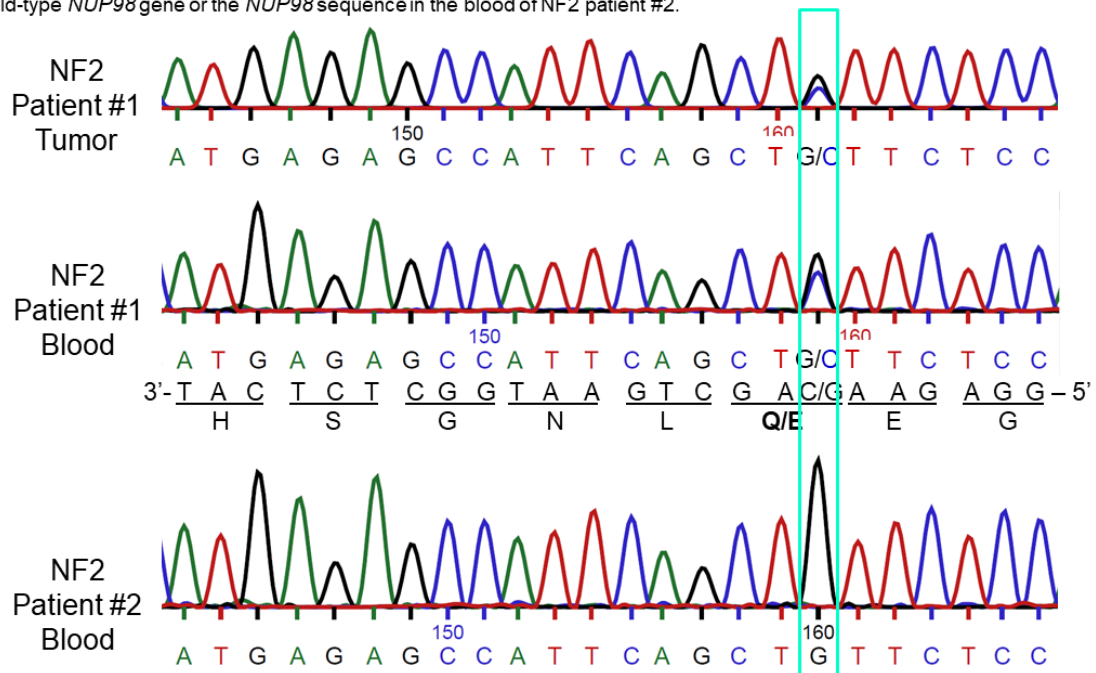
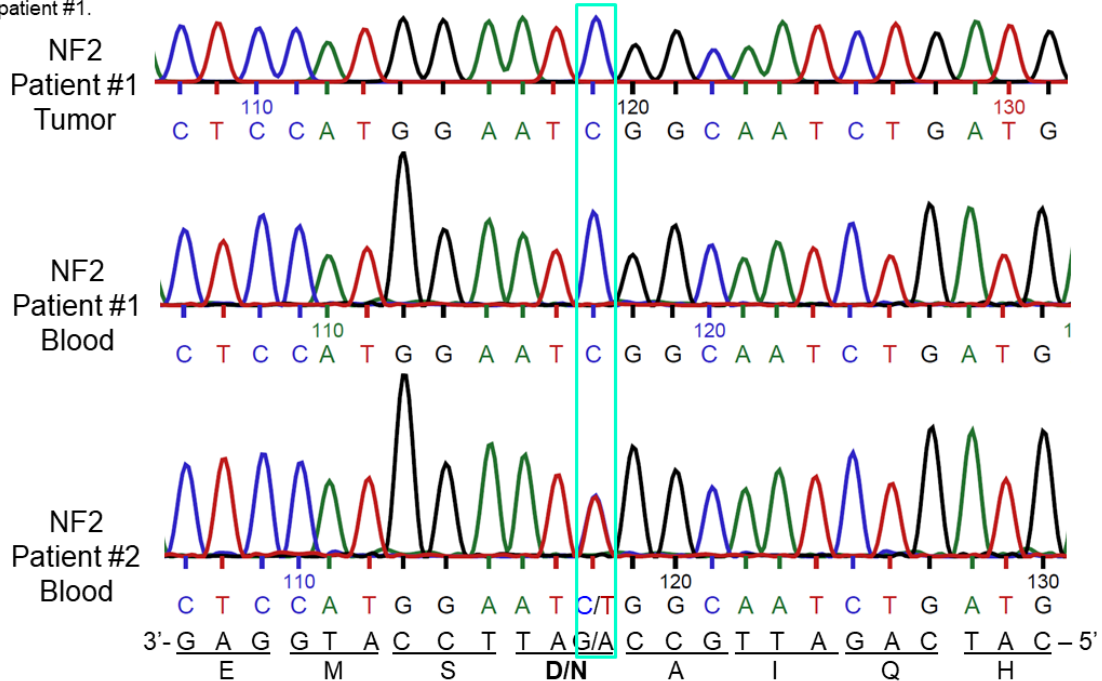


**Figure 4. Detection of a heterozygous mutation in exon 23 of the NUP98 gene in the germline of NF2 patient #2.** Similar to that found in the FoundationOne Heme test of NF2 patient #2's vestibular schwannoma (Figure 1), sequencing analysis identified a heterozygous A/G residue (p. D1156N) in exon 23 of the NUP98 gene in the blood of this patient (NF2 patient #2), compared to only the G nucleotide (complementary to the C residue shown in the sequence) at the corresponding position of the published wild-type NUP98 gene or the NUP98 sequence in both the blood and tumor of NF2 patient #1.



Similarly, we confirmed that both the blood and tumor DNA from patient's #2

harbored a heterozygous D1156N mutation in exon 23 (Figure 4) but did not have any changes for Q1142E in exon 23 or K1178R in exon 24 (data not shown). These results indicate that the K1178R and D1156N mutations were present in the germline of these two NF2 patients. Further analysis of blood samples from the parents of these two NF2 patients revealed that the K1178R mutation found in patient #1 and the D1156N mutation found in patient #2 were inherited from one of their parents (data not shown).

To further confirm the germline origin of the *NUP98* mutations identified in these two NF2 patients, we procured three more tumor specimens from NF2 patient #2 for a total of four tumors; i.e., in addition to the right VS, we also obtained the left VS, a meningioma at the cerebellopontine angle [CPA] region, and a recurrent left orbital meningioma over the past few years. As before, we analyzed these tumor specimens for any genomic alterations in 405 cancer-related genes and variants by FoundationOne Heme tests and found that all four tumors from this NF2 patient #2 harbored few genetic changes but the mutations identified exactly in the same set of genes, including those in *NF2* and *NUP98*, irrespective of whether they are VS or meningiomas (Figure 1). Intriguingly, these NF2-associated VS and meningiomas from both patients 1 and 2 did not have mutations in the genes frequently found in sporadic cases except the *NF2* gene (Brastianos et al., 2013; Clark et al., 2013, 2016; Agnihotri et al., 2016; Suppiah et al., 2019). The only difference in the mutations found in these four tumors from the same patient #2 is the second hit of the *NF2* allele. It is interesting to note that these tumors were procured over five years after patient enrollment in the AR-42 clinical trial (ClinicalTrials.gov identifier: NCT01129193). In addition, the recurrent left orbital meningioma was excised 21 years after the removal of the primary tumor. As this recurrent orbital meningioma only carried mutations in the same set of genes as those found in the other three tumors from this patient, our results indicate that the genomic status of NF2 tumors is amazingly stable despite that this patient has been treated with several experimental drugs.

To verify whether the mutations in the *NUP98* gene that result in K1178R and D1156N changes are true mutations, we searched the COSMIC (Catalogue of Somatic Mutations in Cancer) database and noted that *NUP98* mutations were detected in approximately 1% (452 out of 44832 samples analyzed) of all human cancers analyzed (<http://cancer.sanger.ac.uk/cosmic/gene/analysis?in=NUP98>). Interestingly, missense mutations in *NUP98* (~72%) were the most common types of alterations detected in human cancers, similar to what we found in NF2-associated VS and meningiomas described above. From searching the database of single nucleotide polymorphisms (SNPs) in National Center for Biotechnology Information (NCBI), we noted that the single nucleotide variant (SNV) or mutation responsible for the K1178R A→G change in exon 24 (referred to as rs779147191) and the SNV for the D1156N C→T change in exon 23 (referred to as rs149421589) were rarely found in the general population (0.002% for rs779147191 among 121410 samples analyzed [[http://www.ncbi.nlm.nih.gov/projects/SNP/snp\\_ref.cgi?rs=779147191](http://www.ncbi.nlm.nih.gov/projects/SNP/snp_ref.cgi?rs=779147191)] and 0.02% for rs149421589 among 121412 samples analyzed [[http://www.ncbi.nlm.nih.gov/projects/SNP/snp\\_ref.cgi?rs=149421589](http://www.ncbi.nlm.nih.gov/projects/SNP/snp_ref.cgi?rs=149421589)]). However, the SNV for the Q1142E G→C change (referred to as rs35404087) was detected in ~8% of population among 121412 samples analyzed ([http://www.ncbi.nlm.nih.gov/projects/SNP/snp\\_ref.cgi?rs=35404087](http://www.ncbi.nlm.nih.gov/projects/SNP/snp_ref.cgi?rs=35404087)). These results suggest that the alterations responsible for D1156N and K1178R changes likely represent true mutations, while the Q1142E change may be considered as a genetic variant. Thus, it will be interesting to compare the frequencies of these three *NUP98* changes in NF2-associated tumors and examine the effect of these changes on *NUP98* function and NF2 pathogenesis. Also, are *NUP98* mutations only confined to exons 23

and 24 in NF2-associated tumors?

To examine whether there are mutations in other *NUP98* exons (other than exons 23 and 24), we performed PCR analysis on all 33 *NUP98* exons using the genomic DNA isolated from NF2 patient #1's VS. The PCR products were subjected to DNA sequencing and their sequences were compared with the wild-type *NUP98* sequence. As the FoundationOne Heme test identified mutations only in exons 23 and 24 of the *NUP98* gene in the NF2-associated tumor specimens that we procured, we also did not find nucleotide changes in the remaining 31 *NUP98* exons in the patient #1's VS (Figure 5).

**Figure 5. Mutations were not found in exons other than 23 and 24 of the *NUP98* gene in an NF2-associated VS.** PCR analysis was performed on all 33 *NUP98* exons using the genomic DNA isolated from NF2 patient #1's VS specimen. DNA sequencing of PCR products and their sequence alignment did not reveal any mutations other than those found in exons 23 and 24. Examples of complete alignment of the sequences of *NUP98* exons 21, 22, 25, 28, 30, and 31 from the NF2-associated VS with the corresponding wild-type *NUP98* exon sequences are shown below, indicating no mutations in these exons.

Query 1	AGCCAGAGCCAGAGGTGGAGCAGTTAGGGAGGGTTGTGGAACTGGACAGTGACATGGTA	60	Query 1	CAGAATACCTCTGACAGTGACAGATATGCTCTCCCACTCTCTCGTATCTGGAGGGT	60
Sbjct 275	AGCCAGAGCCAGAGGTGGAGCAGTTAGGGAGGGTTGTGGAACTGGACAGTGACATGGTA	216	Sbjct 191	CAGAATACCTCTGACAGTGACAGATATGCTCTCCCACTCTCTCGTATCTGGAGGGT	132
Query 61	GATATCACCAGGAGCCAGTTTTGGATACCATGTGTAGAAGAGAGCATGCCCTGAGGATCAG	120	Query 61	TCTGGCTGTGTGATAGCGGAGGAGCAAACTCACAGACACCACTTCGAGATGTCTGCTTT	120
Sbjct 215	GATATCACCAGGAGCCAGTTTTGGATACCATGTGTAGAAGAGAGCATGCCCTGAGGATCAG	156	Sbjct 131	TCTGGCTGTGTGATAGCGGAGGAGCAAACTCACAGACACCACTTCGAGATGTCTGCTTT	72
Query 121	GAACCTGTGTCTGCTCAACACATATTCATCTTCACTGGGAATTAATCCACATGTCTTA	180	Query 121	CACCTCTTAAACTCTACAGTGAAG	146
Sbjct 155	GAACCTGTGTCTGCTCAACACATATTCATCTTCACTGGGAATTAATCCACATGTCTTA	96	Sbjct 71	CACCTCTTAAACTCTACAGTGAAG	46
Query 181	CAG	183			
Sbjct 95	CAG	93			
Query 1	ATCATGAAGCATCATTGCTTACTGATGAAGAAGATGTAGATATGGCACTGGATCAACGC	60	Query 1	CATACGTGAGAAAGCTGTTTCGAGAGCTGCTTACCCGGCACTGCGAGCTGTTGGAGACCCC	60
Sbjct 30	ATCATGAAGCATCATTGCTTACTGATGAAGAAGATGTAGATATGGCACTGGATCAACGC	89	Sbjct 54	CATACGTGAGAAAGCTGTTTCGAGAGCTGCTTACCCGGCACTGCGAGCTGTTGGAGACCCC	113
Query 61	TTCAAGTGGCTGCTTCCAAAGCAGATCTCTCAAGAAATCTGTTCTCCAGACTCCCC	120	Query 61	TGAATCTTGGGCTAAAGAGACTTCTTCTACCCGAAGCTCCGTGTACCTGCCAAATGGAT	120
Sbjct 90	TTCAAGTGGCTGCTTCCAAAGCAGATCTCTCAAGAAATCTGTTCTCCAGACTCCCC	149	Sbjct 114	TGAATCTTGGGCTAAAGAGACTTCTTCTACCCGAAGCTCCGTGTACCTGCCAAATGGAT	173
Query 121	ATTTGAGCATCCCACTGCTGAAATCTGTTCACTA	156	Query 121	CCACGAGGCCAAAGCTGTGCGAGCACACATGGAATCTGACAAAGCACTTAGAGGCCCTTTG	180
Sbjct 150	ATTTGAGCATCCCACTGCTGAAATCTGTTCACTA	185	Sbjct 174	CCACGAGGCCAAAGCTGTGCGAGCACACATGGAATCTGACAAAGCACTTAGAGGCCCTTTG	233
			Query 181	CTTATTTAAGGCTGAGCACTGGAACCGCTGCCACAAGCTCATCATCCGACACTTAGCTTC	240
			Sbjct 234	CTTATTTAAGGCTGAGCACTGGAACCGCTGCCACAAGCTCATCATCCGACACTTAGCTTC	293
Query 1	TTGTGAAGCACTGGAGCCTGACATGGACACTATGTGAAGCCCTATGGGGCCACCTGAAGG	60	Query 241	T	241
Sbjct 37	TTGTGAAGCACTGGAGCCTGACATGGACACTATGTGAAGCCCTATGGGGCCACCTGAAGG	96	Sbjct 294	T	294
Query 61	AGCTTGACAGCAGCTAAATGAACCCCTGAATACATTCAAATCTGGAGCGAAGAAGAG	120			
Sbjct 97	AGCTTGACAGCAGCTAAATGAACCCCTGAATACATTCAAATCTGGAGCGAAGAAGAG	156			
Query 121	CTTTCTCCCGTGGCTATCTGTACTGCCACACCTCAGATTGAAGAGGAAATCTCTCTTAA	180	Query 1	GATGCCATCATTAAATGAGAACTATGACTACCTGAAAGGGTCTTCTGGAAAGACTGGACCT	60
Sbjct 157	CTTTCTCCCGTGGCTATCTGTACTGCCACACCTCAGATTGAAGAGGAAATCTCTCTTAA	216	Sbjct 50	GATGCCATCATTAAATGAGAACTATGACTACCTGAAAGGGTCTTCTGGAAAGACTGGACCT	109
Query 181	CCCAAAAAAGCCCTGTGGAGGCTGATTACGCTACCTCAGAGCAAAAGGATCAGTG	240	Query 61	CCAGAGCGCAGCAGCTAATTCAAGATTGGGAAATCTGGGCTGTTTACTGGACAT	120
Sbjct 217	CCCAAAAAAGCCCTGTGGAGGCTGATTACGCTACCTCAGAGCAAAAGGATCAGTG	276	Sbjct 110	CCAGAGCGCAGCAGCTAATTCAAGATTGGGAAATCTGGGCTGTTTACTGGACAT	169
Query 241	AGGCTGCTCTCTGGCCAGCAGTCA	267	Query 121	ATTAGAGTCATTGAAATGCTCCGCCATATACAGCAG	156
Sbjct 277	AGGCTGCTCTCTGGCCAGCAGTCA	303	Sbjct 170	ATTAGAGTCATTGAAATGCTCCGCCATATACAGCAG	205

Exon 21

Exon 22

Exon 25

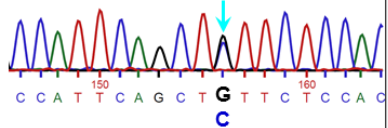
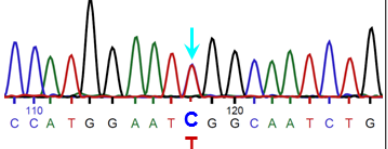
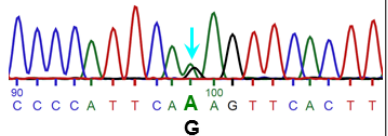
Exon 28

Exon 30

Exon 31

To determine the frequencies of the three SNVs, rs35404087 (Q1142E) and rs149421589 (D1156N) in exon 23 and rs779147191 (K1178R) in exon 24 of the *NUP98* gene that we detected in NF2-associated tumors, we have collaborated with Dr. Miriam Smith, member of the NF Clinic at the University of Manchester, UK. So far, we have analyzed a total of 31 NF2-associated VS, 11 sporadic VS, and 10 blood samples from individuals without VS. We detected 12/31 (39%) NF2 tumors carried one or two of these three SNVs. If we only consider the SNVs for D1156N and K1178R changes as mutations, 3/31 (10%) NF2 patients carried these alterations (Table 1). On the contrary, we did not find D1156N and K1178R changes in sporadic VS or individual without VS. However, we did find the SNV for Q1142E change in 3/25 (9%) patients but not in the 10 individual without VS that we analyzed. As detected in the first two NF2 patients (Figure 1), all of these three variants were heterozygous. Collectively, we conclude that NF2 patients more frequently carry the rs35404087 (Q1142E) variant and/or the rs149421589 (D1156N) and rs779147191 (K1178R) mutations.

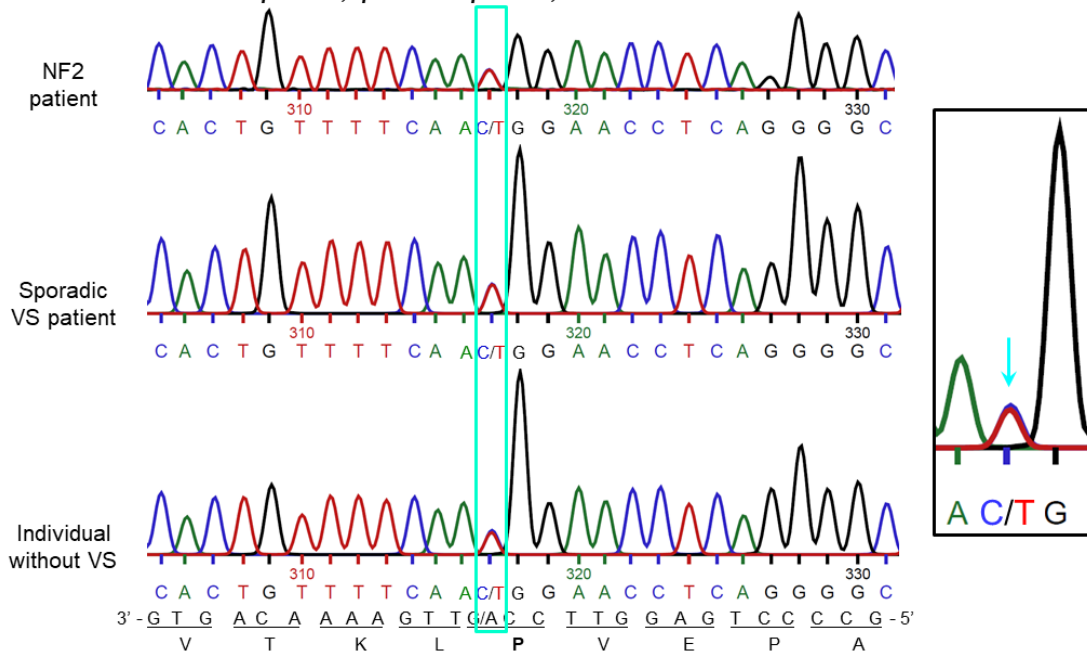
**Table 1. Frequency of single nucleotide variants or mutations in exons 23 and 24 of the NUP98 gene in NF2 patients, sporadic VS patients, and individuals without VS.**

Mutation	Amino acid change	Frequency		
		NF2 patients*	Sporadic VS*	Non-VS
	Q1142E (G→C change in exon 23)	10/31 (32%)	3/25 (12%)	0/10 (0%)
	D1156N (C→T change in exon 23)	1/31 (3.2%)	0/25 (0%)	0/10 (0%)
	K1178R (A→G change in exon 24)	2/31 (6.4%)	0/25 (0%)	0/10 (0%)
Total number of patients with any of the three changes		12/31† (39%)	3/25 (12%)	0/10 (0%)
Total number of patients with D1156N or K1178R changes		3/31 (9.7%)‡	0/25 (0%)‡	0/10 (0%)‡

\*Analysis was performed on VS and/or blood DNA; †One patient exhibited two changes (K1178R and Q1142E); ‡the frequency shown if only considering D1156N and K1178R mutations.

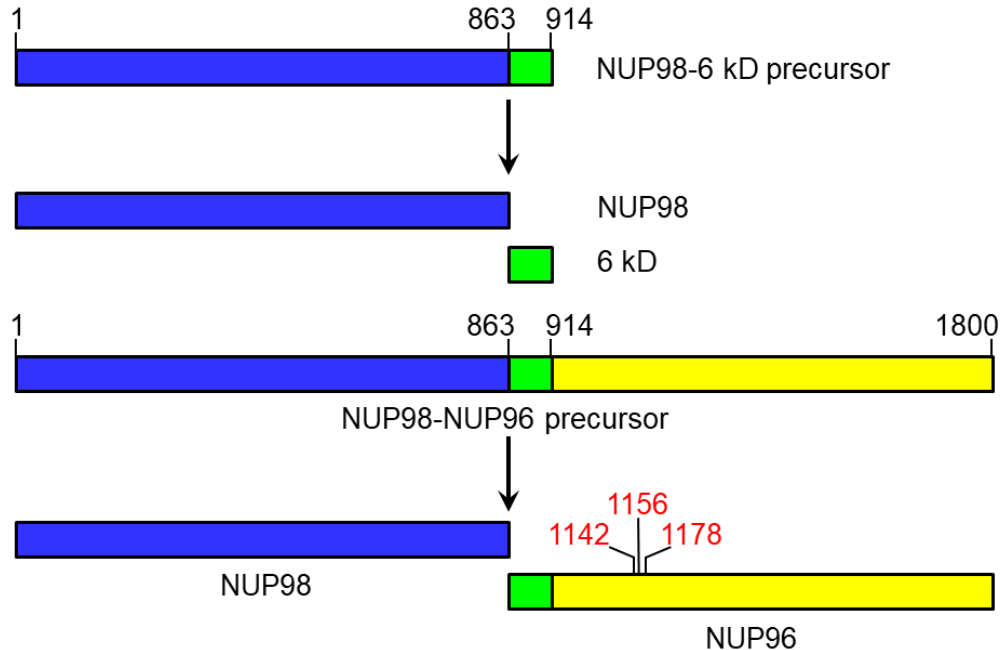
Furthermore, In addition to the SNVs for Q1142E, D1156N, and K1178R changes, we detected another nucleotide polymorphism in *NUP98* exon 23 (referred to as rs3548894; [https://www.ncbi.nlm.nih.gov/projects/SNP/snp\\_ref.cgi?rs=35488940](https://www.ncbi.nlm.nih.gov/projects/SNP/snp_ref.cgi?rs=35488940); Figure 3). This SNV does not change the encoded amino acid (i.e., a silent change) and was detected at a similar frequency in NF2 patients, sporadic VS patients, and individuals without NF2. This is in contrast to the higher frequencies of the SNVs for the Q1142E, D1156N, and K1178R changes detected in NF2 patients (Table1).

**Figure 6. Detection of a nucleotide polymorphism in exon 23 of the NUP98 gene that results in a silent change in the encoded amino acid in NF2 patients, sporadic VS patients, and individuals without VS.**



As mentioned above, the *NUP98* gene encodes a 186-kDa NUP98-NUP96 precursor protein that undergoes autoproteolytic cleavage to generate a 98-kDa nucleoporin (NUP98) and 96-kDa nucleoporin (NUP96) (<https://www.ncbi.nlm.nih.gov/gene/4928>). Sequence alignment analysis revealed that the three SNVs or mutations detected in NF2 patients are located in the N-terminal region of the NUP96 protein (Figure 7).

**Figure 7. The *NUP98* gene encodes the NUP98 and NUP96 proteins.** the *NUP98* gene encodes a 186-kDa NUP98-NUP96 precursor protein that undergoes autoproteolytic cleavage to generate a 98-kDa nucleoporin (NUP98) and 96-kDa nucleoporin (NUP96). The three SNVs identified in NF2 patients are clustered in the N-terminal region of the NUP96 protein.



To better understand potential consequences of the Q1142E, D1156N, and K1178R changes on protein function, we first used the I-TASSER (Iterative Threading ASSEMBly Refinement) protein prediction program to predict the protein structure and function from amino acid sequence (<http://zhanglab.ccmb.med.umich.edu/I-TASSER/>). The NUP96 protein is predicted to be an  $\alpha$ -helical solenoid (Figure 8). Interestingly, the three amino acid changes (Q1142, D1156, and K1178 residues) resulted from the mutations in exon 23 and 24 of the *NUP98* gene were found to be clustered in a coiled region of the NUP96 protein. In addition, these three amino acid residues appear to locate in a natively disordered domain, which is often involved in protein-protein interactions. These results suggest that the exons 23 and 24 of the *NUP98* gene, which contain the three residues more frequently altered in NF2-associated VS and meningiomas, may encode an important functional domain.

Next, from the NCBI database we identified the amino-acid sequences encoded by the *NUP98* genes from various species. Amino-acid sequence alignment on these protein sequences from various species showed that the Q1142, D1156, and K1178 residues are evolutionarily conserved among different species (Figure 9). These results suggest that these three amino acid residues (Q1142, D1156, and K1178) may be important for the function of the NUP96 protein.

**Figure 8. Structural prediction of the NUP96 protein, a NUP98 gene product.** I-TASSER predicts the NUP96 protein to be an  $\alpha$ -helical solenoid (A), and the Q1142, D1156, and K1178 residues are clustered in a coiled region (B). These three amino acid residues are located in a natively disordered domain, which is often involved in protein-protein interactions (C).

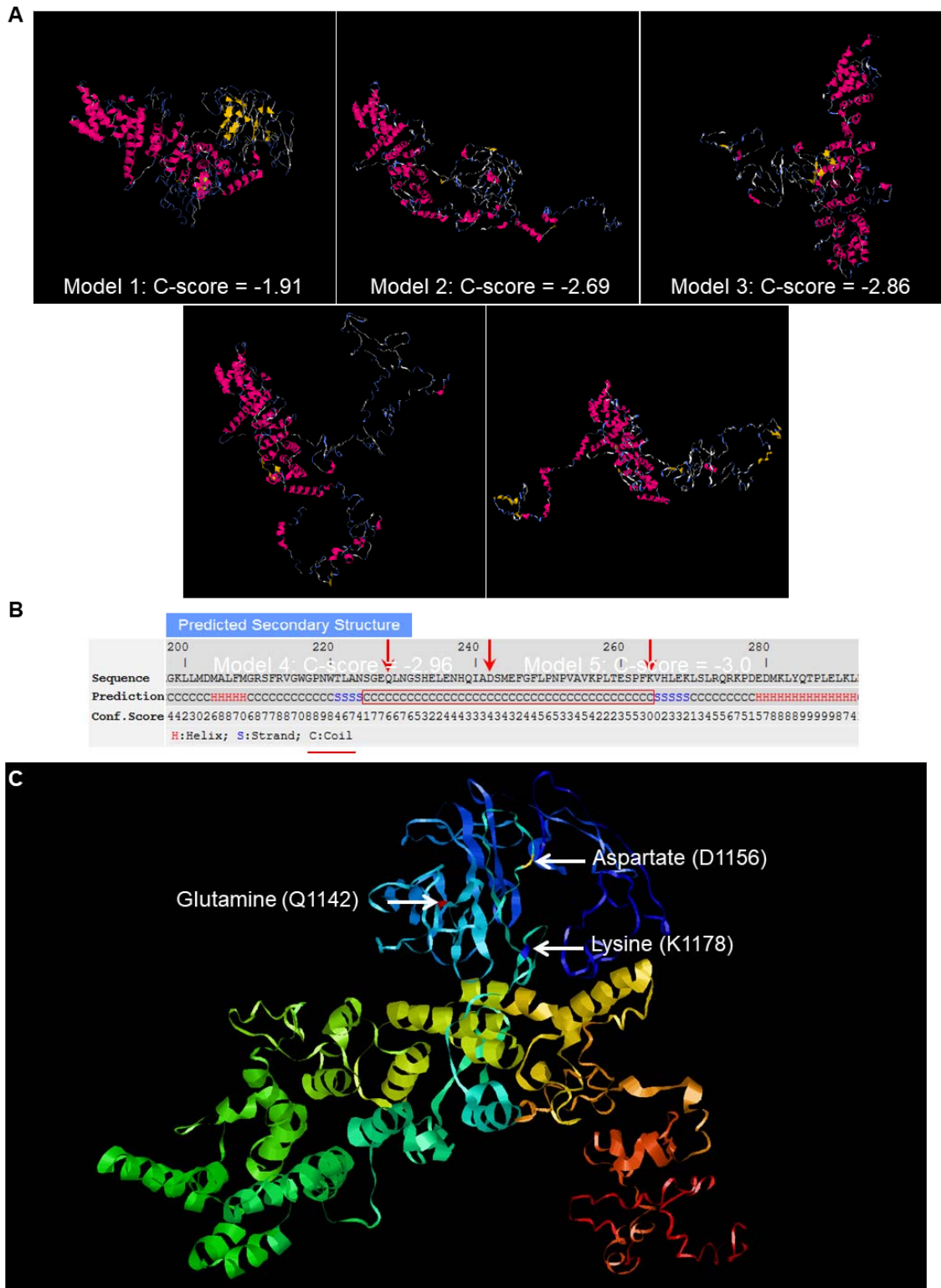
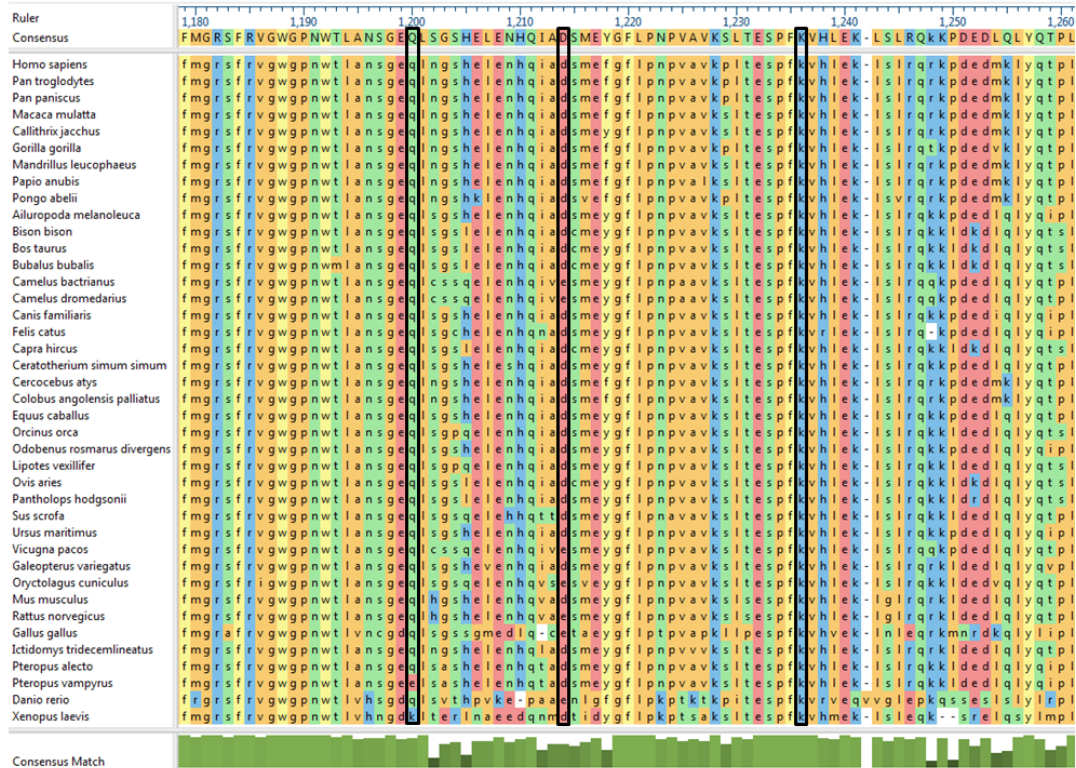


**Figure 9. The three amino acid residues affected by mutations in exons 23 and 24 of the NUP98 gene identified in NF2-associated tumors are evolutionarily conserved.** The NUP98-NUP96 amino acid sequences of various species were identified from the NCBI database and were aligned with each other. Note that the Q1142, D1156, and K1178 residues (boxed) are present in the NUP98-Nup96 protein sequences of most, if not all, species.

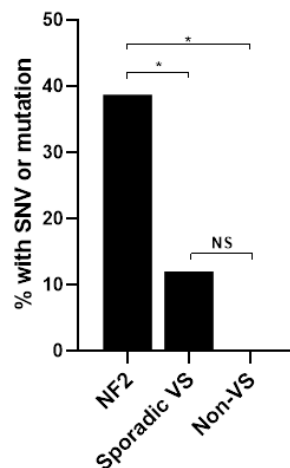


The NUP96 nucleoporin has been shown to play important roles in innate and adaptive immunity (Faria et al., 2006). Dr. Beatriz Fontoura and colleagues at the University of Texas Southwestern Medical Center, Dallas, TX previously showed that mice with homozygous loss of *Nup96* (i.e., *Nup96*<sup>-/-</sup>) are embryonic lethal. While heterozygous *Nup96*<sup>+/-</sup> mice are alive, they exhibit impaired antigen presentation and T cell proliferation and are highly susceptible to viral infection. To examine whether heterozygous loss of *Nup96* can enhance schwannoma tumorigenesis in mice with conditional *Nf2* inactivation in Schwann cells, we attempted to generate a mouse carrying a *Nup96*<sup>+/-</sup> allele. In collaboration with Dr. Fontoura, we obtained from them frozen sperms produced from heterozygous *Nup96*<sup>+/-</sup> mice and attempted to use the sperms to re-derive a heterozygous *Nup96*<sup>+/-</sup> mouse. However, when genotyping the re-derived mice, we did not identify any mice that carried a heterozygous *Nup96*<sup>+/-</sup> allele, suggesting that the *Nup96* mutant allele was not recoverable. Thus, to generate a mouse carrying a *Nup96* mutant allele to study the role of the Nup96 protein in NF2 tumorigenesis, we plan to use the CRISPR/Cas9 genome editing technology to generate mice carrying a heterozygous *Nup96* mutant allele. Then we will cross these *Nup96*<sup>+/-</sup> mice with mice lacking *Nf2* function in Schwann cells (e.g., *P0-Cre; Nf2*<sup>flx/flx</sup> [Giovannini et al., 2000] or *Postn-Cre; Nf2*<sup>flx/flx</sup> [Gehlhausen et al., 2015]) to study whether haplo-insufficiency of *Nup96* enhances schwannoma formation in the future.

As shown in Table 1, we detected the Q1142E SNV in the *NUP98* gene in 10 of 31 (32%) NF2 patients, 3 of 25 (12%) of sporadic VS patients, and 0 of 10 (0%) individuals without VS, the D1156N SNV in 1 of 31 (3.2%) NF2 patient and none of the 25 VS patients and 10 individuals without VS, and the K1178R SNV in 2 of 31 (6.4%) NF2 patient and none of the 25 VS patients and 10 individuals without VS. These results

showed that if considering all three SNVs, patients with NF2 were significantly more likely to have these SNVs or mutations (39% or 12/31) than sporadic VS ( $p = 0.0332$ ) and non-VS samples ( $p = 0.0206$ ) and thus confirmed our hypothesis that the *NUP98* gene is more frequently altered in NF2 patients (Figure 10). However, with the number of samples that we have analyzed so far, we were not able to correlate whether these *NUP98* mutations are associated with disease severity. Therefore, we are continuing to procure additional tumor samples from patients with NF2 or with sporadic VS as well as blood specimens from individuals without VS for *NUP98* mutational analysis in order to achieve a better statistical significance of our correlative study. Nonetheless, the results of the *NUP98* mutations that we have identified in NF2 patients are being written together with the findings from our recent Phase 1 and ongoing Phase 0 clinical trials of the novel histone deacetylase AR-42 as a potential treatment for VS and meningiomas (ClinicalTrials.gov Identifier: NCT01129193 and NCT02282917) into a manuscript. In addition, we have used the VS specimens procured from this study to prepare primary VS cell cultures and establish tumor models for therapeutic evaluation, which resulted in five peer-reviewed publications (see Appendices).

**Figure 10. The *NUP98* gene is more frequently mutated in NF2 patients.** The statistical comparison of the frequencies of the three SNVs or mutations in the *NUP98* gene detected in patients with NF2 or VS and individuals without VS was performed using Fisher Exact tests and confirmed that NF2 samples were significantly more likely to have SNV or mutation than sporadic VS ( $p=0.0332$ ) and non-VS samples ( $p=0.0206$ ).



**(iii) Opportunities for training and professional development:**

This project was not intended to provide training and professional development opportunities; therefore, we have "Nothing to Report."

**(iv) How were the results disseminated to communities of interest?**

As indicated above, part of the research findings has been published and the remaining will be written into manuscripts for publication in the near future. Also, we have presented the findings from this study to the annual Neurofibromatosis Conferences (see Appendices). Based on our findings, a clinical trial to evaluate AR-42 in NF2 patients with vestibular schwannomas and meningiomas (ClinicalTrials.gov Identifier: NCT02282917) is ongoing.

**5. IMPACT**

**(i) Impact on the development of the principal discipline(s) of the project:**

We have found that the *NUP98* gene is more frequently mutated in patients with NF2. Identification of *NUP98* as a genetic modifier for NF2 will substantially enhance our

understanding of the disease characteristics and pathobiology as well as future drug discovery. Further analysis of the potential clinical implications of *NUP98* mutations may allow us to better understand the phenotypic heterogeneity among NF2 patients.

**(ii) Impact on other disciplines:**

Nothing to report

**(iii) Impact on technology transfer:**

Nothing to report

**(iv) Impact on society beyond science and technology:**

Nothing to report

## **6. Conclusion**

By next-generation sequencing, we analyzed five tumors obtained from two NF2 patients, including four of them (two VS and two meningiomas) from one patient. Interestingly, we found that these NF2-associated tumors had low mutational burden and did not have mutations in the genes frequently found in sporadic VS and meningiomas except the *NF2* gene. Intriguingly, we found that the two VS and two meningiomas harvested over several years from the same NF2 patient harbored mutations in the same set of genes. Based on the length of time that these NF2-associated tumors were collected, our results indicate that the genomes of VS and meningiomas from NF2 patients are very stable despite after several experimental treatments. It should be pointed out that we are the first to conduct such a longitudinal analysis of NF2 patient's tumors.

Importantly, we found that in addition to *NF2*, the *NUP98* gene, which encode the nucleoporin proteins involved in nucleocytoplasmic transport, gene expression, mitotic checkpoint, and pathogenesis, is more frequently mutated in patients with NF2 than sporadic VS patients or individuals without VS. The three SNVs or mutations on the *NUP98* gene that we identified are located in exons 23 and 24, and these alterations result in the changes of three evolutionary-conserved, charged amino acids (Q1142E, D1156N, and K1178R). Due to limited numbers of samples analyzed, we were not able to correlate these *NUP98* mutations with disease severity; however, we are continuing to procure and analyze additional specimens from patients with NF2 or sporadic VS as well as individuals without VS for such an analysis.

During the award period, we have presented our findings to the annual Neurofibromatosis Conferences. A manuscript describing the genomic status of NF2-associated VS and meningiomas and the findings on *NUP98* mutation is being prepared. In addition, using the VS specimens procured from this study, we prepared primary VS cell cultures for therapeutic evaluation, which resulted in five peer-reviewed publications.

## **7. Publications, Abstracts, and Presentations**

### **(a) Journal publications**

The works described in the following five publications were supported, in part, by this grant. We have acknowledged this grant support in all of these publications (please see Appendices).

- (i) Burns SS, Chang L-S. Generation of noninvasive, quantifiable, orthotopic animal models for NF2-associated schwannoma and meningioma. *Methods Mol Biol.* 2016;1427:59-72. PMID: 27259921 (<https://www.ncbi.nlm.nih.gov/pubmed/27259921>)

The development of preclinical animal models that accurately capture the clinical characteristics of NF2-associated schwannomas and meningiomas will facilitate the

evaluation of novel therapeutic agents for the treatment of these tumors, ultimately leading to more productive clinical trials. In this methodology paper, we describe the generation of luciferase-expressing *NF2*-deficient schwannoma and meningioma cells and the use of these cells to establish orthotopic, quantifiable tumor models in immunodeficient mice. The growth of these tumors and their response to treatment can be measured effectively by bioluminescence imaging (BLI) and confirmed by small-animal magnetic resonance imaging (MRI). These and other animal models, such as genetically-engineered models, should substantially advance the investigation of promising therapies for schwannomas and meningiomas.

(ii) Petrilli AM, Garcia J, Bott M, Klingeman Plati S, Dinh CT, Bracho OP, Yan D, Zou B, Mittal R, Telischi FF, Liu X-Z, Chang L-S, Welling DB, Copik AJ, Fernández-Valle C. Ponatinib Promotes a G<sub>1</sub> Cell Cycle Arrest of Merlin/NF2-Deficient Human Schwann Cells. *Oncotarget* 2017;8:31666-31681. PMID: 28427224. PMCID: PMC5458238 (<https://www.ncbi.nlm.nih.gov/pubmed/28427224>)

This collaborative publication reported the effect of ponatinib, an FDA-approved ABL/SRC inhibitor, on proliferation and survival of merlin-deficient human Schwann and schwannoma cells. We have established collaboration with Dr. Cristina Fernandez-Valle at the University of Central Florida to use paired human vestibular schwannoma and normal vestibular nerve specimens that we procured to confirm elevated levels of phosphorylated PDGFR $\alpha/\beta$  and SRC in merlin-deficient tumor cells. The study further showed that ponatinib reduced the viability of merlin-deficient Schwann cells by decreasing phospho-PDGFR $\alpha/\beta$  and ERK1/2 and their downstream signals. These changes were associated with decreased cyclin D1 and increased p27<sup>KIP1</sup> levels, leading to a G<sub>1</sub> cell-cycle arrest. These results suggest that ponatinib is a potential therapeutic agent for NF2-associated schwannomas.

(iii) Fuse MA, Plati SK, Burns SS, Dinh CT, Bracho O, Yan D, Mittal R, Shen R, Soulakova JN, Copik AJ, Liu XZ, Telischi FF, Chang L-S, Franco MC, Fernandez-Valle C. Combination therapy with c-Met and Src Inhibition Induces caspase-dependent apoptosis of merlin-deficient Schwann Cells and suppresses growth of schwannoma cells. *Mol Cancer Ther.* 2017;16:2387-2398. PMID: 28775147 (<https://www.ncbi.nlm.nih.gov/pubmed/28775147>)

This study investigated drugs that target c-Met and Src kinases frequently activated in NF2-associated schwannomas. The study demonstrated that merlin/*Nf2*-deficient mouse Schwann cells (MD-MSC) treated with the c-Met inhibitor, cabozantinib, or the Src kinase inhibitors, dasatinib and saracatinib, underwent a G<sub>1</sub> cell-cycle arrest. Interestingly, MD-MSCs treated with a combination of cabozantinib and saracatinib, exhibited caspase-dependent apoptosis. In collaboration with Dr. Cristina Fernandez-Valle at the University of Central Florida, we showed that this combination therapy significantly reduced MD-MSC allograft growth through inhibition of phospho-FAK, phospho-ERK, and cyclin D1. The results indicate that simultaneous inhibition of c-Met and Src signaling in MD-MSCs triggers apoptosis and reveals vulnerable pathways that could be exploited to develop NF2 therapies.

(iv) Oblinger JL, Burns SS, Huang J, Pan L, Ren Y, Shen R, Kinghorn AD, Welling DB, Chang L-S. Overexpression of eIF4F components in meningiomas and suppression of meningioma cell growth by inhibiting translation initiation. *Exp. Neurol.* 2018;299(Pt B):299-307. PMID: 28610844. PMCID: PMC5723558 (<https://www.ncbi.nlm.nih.gov/pubmed/28610844>)

In this paper, we showed that similar to Schwann cell tumors (Oblinger JL et al.,

Neuro Oncol. 2016;18:1265-1277), meningiomas expressed high levels of the three components of the eukaryotic initiation factor 4F (eIF4F) translation initiation complex, eIF4A, eIF4E, and eIF4G. Depletion of eIF4A and eIF4E by shRNAs strongly reduced the growth of *NF2*-deficient meningioma Ben-Men-1 cells. Interestingly, from screening a library of 23 natural compounds, the eIF4A inhibitor silvestrol was identified as having the most potent growth-inhibitory activity in primary meningioma and Ben-Men-1 cells. Silvestrol treatment of meningioma cells prominently induced G2/M arrest. Consistently, silvestrol significantly decreased the amounts of cyclins D1, E1, A, and B, PCNA and Aurora A. In addition, the total and phosphorylated protein levels of mitogenic kinases AKT, ERK and FAK, which are key drivers for meningioma cell proliferation, were markedly reduced in silvestrol-treated Ben-Men-1 cells. Our findings suggest that inhibiting protein translation could be a potential treatment for both meningiomas and schwannomas particularly those associated with *NF2*.

(v) Fuse MA, Dinh CT, Vitte J, Kirkpatrick J, Mindos T, Plati SK, Young JI, Huang J, Carlstedt A, Franco MC, Brnjos K, Nagamoto J, Petrilli A, Copik AJ, Soulakova JN, Bracho O, Yan D, Mittal R, Shen R, Telischi FF, Morrison H, Giovannini M, Liu XZ, Chang LS, Fernandez-Valle C. 2019. Preclinical Assessment of MEK1/2 Inhibitors for Neurofibromatosis Type 2-Associated Schwannomas Reveals Differences in Efficacy and Drug Resistance Development. *Neuro-Oncol.* 21:486-497. PMID: 30615146 (<https://www.ncbi.nlm.nih.gov/pubmed/30615146>)

To identify an effective treatment for *NF2*-associated schwannomas, we collaborated with Dr. Cristina Fernandez-Valle at the University of Central Florida to investigate repurposing drugs targeting MEK1/2 kinases as merlin, the *NF2* gene product, has been shown to modulate activity of the Ras/Raf/MEK/ERK pathway. Among six MEK inhibitors examined, trametinib, PD0325901, and cobimetinib were most effective in reducing the viability of merlin-deficient mouse and human Schwann cells. Also, the three inhibitors slowed the growth of schwannoma allografts. However, when we analyzed drug-treated tumors, we found decreased pERK1/2 levels only in the tumors treated with PD0325901 and cobimetinib but not trametinib. Similarly, tumor burden and average tumor size were reduced in trametinib-treated *NF2* transgenic mice, and we also did not find reduced pERK1/2 in treated mouse tumors. Furthermore, trametinib and PD0325901 modestly reduced viability of several primary human VS cell cultures with *NF2* mutations. DNA methylation analysis of PD0325901-resistant versus -susceptible VS identified genes that could contribute to drug resistance. The results show that MEK inhibitors exhibited differences in anti-tumor efficacy resistance in schwannoma models with possible emergence of trametinib resistance.

#### **(b) Abstracts presented at national/international conferences**

The following 11 abstracts were presented at the annual Neurofibromatosis (NF) Conferences during the award period. We have acknowledged this grant support in these abstracts (please see Appendices).

(i) Burns SS, EM Akhmametyeva, J Blakeley, DB Welling, L-S Chang. 2016. Similarities and Differences in Tumor Characteristics and Treatment Response in *NF2*-Associated Vestibular Schwannomas and Meningiomas. The 2016 NF Conference, Austin, TX. (Platform Presentation)

(ii) Oblinger J, S Burns, M Curley, L-S Chang. 2016. ErbB3 and IGF-1R blockade as a potential treatment for vestibular schwannomas and meningiomas. The 2016 NF Conference, Austin, TX. (Poster Presentation)

(iii) Oblinger J, S Burns, AD Kinghorn, L-S Chang. 2017. Natural Silvestrol-Related Rocaglates as Potential Treatments for Vestibular Schwannomas and Meningiomas. The 2017 NF Conference, Washington, DC. (Poster Presentation)

(iv) Burns S, J Oblinger, E Akhmametyeva, DB Welling, L-S Chang. 2017. A strategy to identify an effective therapy for NF2-associated vestibular schwannomas. The 2017 NF Conference, Washington, DC. (Platform Presentation of Selected Poster)

(v) Chang L-S, J Huang, E Akhmametyeva, S Burns. 2017. Merlin plays an important role in centrosome disjunction. The 2017 NF Conference, Washington, DC. (Platform Presentation of Selected Poster)

(vi) Fernandez-Valle C, M Fuse, C Dinh, J Vitte, J Kirkpatrick, T Mindos, S Campion, K Brnjos, MC Franco, J Huang, J Young, A Petrilli, D Yan, R Mittal, R Shen, F Telischi, L-S Chang, H Morrison, M Giovannini, X-Z Liu. 2018. Preclinical Assessment of MEK1/2 Inhibitors for Neurofibromatosis Type 2-Associated Schwannomas Reveals Differences in Efficacy and Drug Resistance Development. The 2018 Joint Global NF Conference, Paris, France. (Platform Presentation)

(vii) Chang L-S, SS Burns, JL Oblinger, M Ferrer, J Huang, M Poi, V Ramesh, On behalf of the Synodos for NF2 Consortium. 2018. Novel drug discovery for NF2-deficient meningiomas: Brigatinib causes tumor shrinkage in NF2-deficient meningiomas. The 2018 Joint Global NF Conference, Paris, France. (Platform Presentation)

(viii) Chang L-S, JL Oblinger, SS Burns, J Huang, L Anderson, R Shen, L Pan, Y Ren, BR O'Keefe, AD Kinghorn, JM Collins. 2018. Identification of silvestrol-related rocaglates with better bioavailability and high potency against malignant peripheral nerve sheath tumors. The 2018 Joint Global NF Conference, Paris, France. (Poster Presentation)

(ix) Welling DB, SS Burns, JL Oblinger, B Miles-Markley, A Quinkert, J Blakeley, BA Neff, RK Jackler, L-S Chang. 2018. Phase 1 and Phase 0 studies of AR-42, a pan histone deacetylase inhibitor, in subjects with neurofibromatosis type 2 (NF2)-associated vestibular schwannomas and meningiomas. The 2018 Joint Global NF Conference, Paris, France. (Poster Presentation)

(x) Oblinger J, L-S Chang. 2019. Brigatinib as a potential therapy for malignant peripheral nerve sheath tumors. The 2019 NF Conference, San Francisco, CA. (Poster presentation)

(xi) Chang L-S, JL Oblinger, SS Burns, J Huang, L Anderson, R Shen, L Pan, Y Ren, R Roberts, BR O'Keefe, AD Kinghorn, JM Collins. Targeting protein translation with rocaglamide and didesmethylrocaglamide to treat NF1 and NF2 tumors. The 2019 NF Conference, San Francisco, CA. (Platform presentation)

## **8. Inventions, Patents, and Licenses**

### **(i) Individuals who have worked on the project**

Long-Sheng Chang, Ph.D., Professor, Principal Investigator - 0.6 Calendar Months

Janet Oblinger, Ph.D., Research Associate - 7.3 Calendar Months

**(ii) Has there been a change in the active other support of the PD/PI(s) or senior/key personnel since the last reporting period?**

Nothing to report.

**(iii) What other organizations were involved as partners**

Collaborator: Dr. Miriam J. Smith, Ph.D., Lecturer in Cancer Genomics, Centre for Genomic Medicine, Institute of Human Development, University of Manchester.

We have collaborated with Dr. Miriam Smith at The University of Manchester, where the UK NF2 registry is based, to analyze additional VS specimens for *NUP98* mutations. Similar to our findings, Dr. Smith also identified several SNVs in exons 23 and 24 of the *NUP98* gene in VS, particularly those associated with NF2.

**9. Reportable Outcome**

With this support, we have published five peer-reviewed publication and 11 abstracts at the annual Neurofibromatosis Conferences.

**10. Other Achievements**

Nothing to report

**11. References**

- Agnihotri S, Jalali S, Wilson MR, Danesh A, Li M, Klironomos G, Krieger JR, Mansouri A, Khan O, Mamatjan Y, Landon-Brace N, Tung T, Dowar M, Li T, Bruce JP, Burrell KE, Tonge PD, Alamsahebpoor A, Krischek B, Agarwalla PK, Bi WL, Dunn IF, Beroukhir R, Fehlings MG, Bril V, Pagnotta SM, Iavarone A, Pugh TJ, Aldape KD, Zadeh G. 2016. The genomic landscape of schwannoma. *Nat Genet.* 2016;48:1339-1348. <https://www.ncbi.nlm.nih.gov/pubmed/27723760>
- Brastianos PK, Horowitz PM, Santagata S, Jones RT, McKenna A, Getz G, Ligon KL, Palescandolo E, Van Hummelen P, Ducar MD, Raza A, Sunkavalli A, Macconail LE, Stemmer-Rachamimov AO, Louis DN, Hahn WC, Dunn IF, Beroukhir R. Genomic sequencing of meningiomas identifies oncogenic SMO and AKT1 mutations. *Nat Genet.* 2013;45:285-289. <https://www.ncbi.nlm.nih.gov/pubmed/23334667>
- Clark VE, Erson-Omay EZ, Serin A, Yin J, Cotney J, Ozduman K, Avşar T, Li J, Murray PB, Henegariu O, Yilmaz S, Günel JM, Carrión-Grant G, Yilmaz B, Grady C, Tanrikulu B, Bakircioğlu M, Kaymakçalan H, Caglayan AO, Sencar L, Ceyhun E, Atik AF, Bayri Y, Bai H, Kolb LE, Hebert RM, Omay SB, Mishra-Gorur K, Choi M, Overton JD, Holland EC, Mane S, State MW, Bilgüvar K, Baehring JM, Gutin PH, Piepmeier JM, Vortmeyer A, Brennan CW, Pamir MN, Kiliç T, Lifton RP, Noonan JP, Yasuno K, Günel M. Genomic analysis of non-NF2 meningiomas reveals mutations in TRAF7, KLF4, AKT1, and SMO. *Science.* 2013;339:1077-1080. <https://www.ncbi.nlm.nih.gov/pubmed/23348505>
- Clark VE, Harmancı AS, Bai H, Youngblood MW, Lee TI, Baranoski JF, Ercan-Sencicek AG, Abraham BJ, Weintraub AS, Hnisz D, Simon M, Krischek B, Erson-Omay EZ, Henegariu O, Carrión-Grant G, Mishra-Gorur K, Durán D, Goldmann JE, Schramm J, Goldbrunner R, Piepmeier JM, Vortmeyer AO, Günel JM, Bilgüvar K, Yasuno K, Young RA, Günel M. Recurrent somatic mutations in POLR2A define a distinct subset of meningiomas. *Nat*

Genet. 2016;48:1253-1259. <https://www.ncbi.nlm.nih.gov/pubmed/27548314>

Faria AM, Levay A, Wang Y, Kamphorst AO, Rosa ML, Nussenzveig DR, Balkan W, Chook YM, Levy DE, Fontoura BM. The nucleoporin Nup96 is required for proper expression of interferon-regulated proteins and functions. *Immunity*. 2006;24:295-304. <https://www.ncbi.nlm.nih.gov/pubmed/16546098>

Gehlhausen JR, Park SJ, Hickox AE, Shew M, Staser K, Rhodes SD, Menon K, Lajiness JD, Mwanthi M, Yang X, Yuan J, Territo P, Hutchins G, Nalepa G, Yang FC, Conway SJ, Heinz MG, Stemmer-Rachamimov A, Yates CW, Wade Clapp D. A murine model of neurofibromatosis type 2 that accurately phenocopies human schwannoma formation. *Hum Mol Genet*. 2015;24:1-8. <https://www.ncbi.nlm.nih.gov/pubmed/25113746>

Giovannini M, Robanus-Maandag E, van der Valk M, Niwa-Kawakita M, Abramowski V, Goutebroze L, Woodruff JM, Berns A, Thomas G. Conditional biallelic Nf2 mutation in the mouse promotes manifestations of human neurofibromatosis type 2. *Genes Dev*. 2000;14:1617-1630. <https://www.ncbi.nlm.nih.gov/pubmed/10887156>

Suppiah S, Nassiri F, Bi WL, Dunn IF, Hanemann CO, Horbinski CM, Hashizume R, James CD, Mawrin C, Noushmehr H, Perry A, Sahm F, Sloan A, Von Deimling A, Wen PY, Aldape K, Zadeh G; International Consortium on Meningiomas. Molecular and translational advances in meningiomas. *Neuro Oncol*. 2019;21(Supplement\_1):i4-i17. <https://www.ncbi.nlm.nih.gov/pubmed/30649490>

## 12. Appendices

The attachment includes five peer-reviewed publications and 11 abstracts. We have acknowledged the DOD support in all of these publications and abstracts.

# Chapter 4

## Generation of Noninvasive, Quantifiable, Orthotopic Animal Models for NF2-Associated Schwannoma and Meningioma

Sarah S. Burns and Long-Sheng Chang

### Abstract

Schwannomas and meningiomas are nervous system tumors that can occur sporadically or in patients with neurofibromatosis type 2 (NF2). Mutations of the *Neurofibromatosis 2* (NF2) gene are frequently observed in these tumors. Schwannomas and meningiomas cause significant morbidities, and an FDA-approved medical therapy is currently not available. The development of preclinical animal models that accurately capture the clinical characteristics of these tumors will facilitate the evaluation of novel therapeutic agents for the treatment of these tumors, ultimately leading to more productive clinical trials. Here, we describe the generation of luciferase-expressing NF2-deficient schwannoma and meningioma cells and the use of these cells to establish orthotopic tumor models in immunodeficient mice. The growth of these tumors and their response to treatment can be measured effectively by bioluminescence imaging (BLI) and confirmed by small-animal magnetic resonance imaging (MRI). These and other animal models, such as genetically-engineered models, should substantially advance the investigation of promising therapies for schwannomas and meningiomas.

**Key words** Vestibular schwannoma, Meningioma, Neurofibromatosis type 2 (NF2), *Neurofibromatosis 2* (NF2) gene, Xenograft, Allograft, Severe combined immunodeficiency (SCID) mice, Intraneural, Stereotactic, Bioluminescence imaging (BLI), Magnetic resonance imaging (MRI)

---

### 1 Introduction

Vestibular schwannomas (VS) are tumors originating from Schwann cells covering the vestibular branch of the 8th cranial nerve. These tumors are often slow-growing and can occur sporadically or in association with neurofibromatosis type II (NF2; OMIM #101000), a highly penetrant, autosomal-dominant genetic disorder [1]. Nearly all NF2 patients develop bilateral VS, and up to 60 % of these patients develop meningiomas. Other disease features include ependymomas, spinal schwannomas, astrocytomas, and presenile lens opacities. Patients with VS usually present with tinnitus, hearing loss, and imbalance. These tumors can lead to deafness, facial nerve paralysis, brainstem compression, hydrocephalus, and death, if left untreated.

Meningiomas are derived from cells of the meninges lining the brain. About 80 % of meningiomas are benign (WHO grade I), whereas the remaining are atypical (grade II) and anaplastic (grade III) [2]. These tumors cause significant morbidity, including cranial nerve palsy, seizures, and brainstem compression, which may lead to paralysis, aspiration pneumonia, and death. Approximately 20 % of benign meningiomas recur over ten years, while grade II and grade III tumors possess greater rates of recurrence. Meningiomas in NF2 patients are associated with disease severity and increased risk of mortality [3, 4].

Currently, an FDA (U.S. Food and Drug Administration)-approved drug is not available for the treatment of VS and meningiomas. Treatment options for these tumors are presently limited to observation, surgical removal, and stereotactic radiation [1]. However, surgery may not be possible if the tumor is inaccessible or when there are too many tumors. Radiation treatment may cause malignant transformation and/or growth acceleration of benign tumor cells. In addition, preservation of hearing and balance along with the facial nerve and lower cranial nerves for swallowing and airway protection are often not achieved with current methods. Together, these factors underscore the importance of developing effective medical therapies that stop tumor growth.

Evaluation of potential novel therapeutic agents requires animal models that accurately reflect disease characteristics. Most, if not all, of NF2-associated VS and the more common sporadic unilateral schwannomas harbor mutations in the *Neurofibromatosis 2* (*NF2*) tumor suppressor gene [5, 6]. Additionally, *NF2* mutations are found in most NF2-associated meningiomas and about 50–60 % of sporadic meningiomas [4, 7, 8]. To address the tumor suppressor role of merlin, mice that lack *Nf2* function in Schwann or meningeal cells have been generated and develop schwannomas and meningiomas, respectively [9–11]. These genetically engineered mouse (GEM) models have been used in therapeutic evaluation; however, tumor latency, penetrance, and detection in these GEM models are important considerations. Also, xenograft models in severe combined immunodeficiency (SCID) mice implanted with VS specimens have been established, but the tumors do not exhibit consistent growth [12, 13]. Thus, additional models that closely mimic the clinical presentation of *NF2*-deficient benign schwannomas and meningiomas and that facilitate efficient quantitation of tumor growth will further enhance therapeutic testing.

Accurate measurement of tumor size and longitudinal monitoring of tumor growth are critical in evaluating drug responses. Magnetic resonance imaging (MRI) has been the gold standard for evaluating NF2-associated tumors in situ [14]. Likewise, small-animal MRI has been used to noninvasively monitor tumor growth in mouse models. To facilitate longitudinal monitoring of

drug response, bioluminescence imaging (BLI) has significantly advanced the ability to quantitate tumor growth in animal models and is particularly valuable for intracranial tumors whose growth cannot be monitored externally [15]. Here, we describe the use of luciferase-expressing schwannoma and meningioma cells to generate orthotopic animal models. Tumor growth in these models can be quantified over time by BLI and confirmed by MRI.

## 2 Materials

### 2.1 Cell Culture

1. Dulbecco's modified Eagle (DME) and DME/F-12 (v/v) media (Life Technologies, Grand Island, NY) are supplemented with 10 % fetal bovine serum (FBS).
2. 100× Penicillin/Streptomycin stock solution: Mix 5000 units/ml penicillin G sodium and 5000 µg/ml streptomycin sulfate in 0.85 % saline (*see Note 1*).
3. Phosphate-buffered saline (PBS) without  $\text{Ca}^{2+}$ / $\text{Mg}^{2+}$ : 137 mM NaCl, 2.7 mM KCl, 10 mM  $\text{Na}_2\text{HPO}_4$ , and 1.8 mM  $\text{KH}_2\text{PO}_4$ , pH 7.4.
4. Tris-buffered saline (TBS): 50 mM Tris-HCl, pH 7.4 and 150 mM NaCl.
5. Trypsin solution: 0.25 % trypsin-0.53 mM EDTA in Hanks' Balanced Salt Solution (HBSS).
6. Reconstitute recombinant human neuregulin-β1/hereregulin-β1 epidermal growth factor domain (rhuHRG-β1) in PBS, aliquot in small volumes, and store at  $-80^\circ\text{C}$ .
7. Forskolin stock solution: Prepare 5 mM forskolin in dimethyl sulfoxide (DMSO), sterilize using a 0.2-µm filter, aliquot, and store at  $-20^\circ\text{C}$ . HRG-β1 and forskolin are freshly added to culture medium (*see Subheading 3.1, step 1*).
8. 100× Poly-L-lysine or Poly-D-lysine (molecular weight 75–150 kDa) stock solution: Prepare 5 mg/ml in TBS and store at  $4^\circ\text{C}$ .
9. 250× Laminin stock: Purchased as 1 mg/ml solution from, e.g., Sigma and stored at  $-80^\circ\text{C}$ .
10.  $Nf2^{P0}$  ( $P0Cre;Nf2^{flox/flox}$ ) schwannoma cells.
11.  $Nf2^{P0}$  schwannoma cell culture medium: DME/F-12 medium supplemented with 10 % FBS, 10 ng/ml HRG-β1, and 2 µM forskolin.
12.  $NF2$ -deficient benign human meningioma cell line Ben-Men-1.
13. Ben-Men-1 culture medium: Supplement DME medium with 10 % FBS.

## **2.2 Lentiviral Transduction and Isolation of Luciferase-Expressing Clones**

1. Lenti-CMV-Luc lentiviruses containing a cytomegalovirus (CMV) promoter-driven luciferase-expression unit and a puromycin-resistance gene (Qiagen, Germantown, MD).
2. 10,000× Polybrene (hexadimethrine bromide; Sigma-Aldrich) solution: Prepare polybrene by dissolving 80 mg in 1 ml of H<sub>2</sub>O, sterilize by filtration, and store at 4 °C (*see Note 5*).
3. Puromycin dihydrochloride stock solution: Prepare a 5 mg/ml solution in DME medium, sterilize by filtration, aliquot, and store at –20 °C (*see Subheading 3.2, step 5*).
4. Cloning cylinders (Bellco Glass, Vineland, NJ) are used to isolate individual puromycin-resistant colonies.
5. The Protein Assay Dye Reagent Concentrate (Bio-Rad, Hercules, CA) is diluted five-fold prior to protein concentration measurements (*see Subheading 3.2, step 7*).
6. The Luciferase Reporter Assay System (Promega, Madison, WI) is used according to the manufacturer's instruction.
7. A SpectraMax microplate reader (Molecular Devices, Sunnyvale, CA) is used to detect luciferase activity in cultured cells (*see Subheading 3.2, step 8*).

## **2.3 Mice and Tumor Cell Injection**

1. SCID C.B17 mice are purchased from a certified vendor, such as The Jackson Laboratory, Charles River Laboratories, and Taconic Biosciences (*see Subheadings 3.3 and 3.4, step 3*).
2. PROTEXIS sterile powder-free surgical gloves, Curity™ gauze sponges, Webcol™ alcohol prep, and Duo-Swab® Povidone-Iodine Cleansing Scrub and Prep Swabsticks.
3. Isoflurane (Forane) and an Inhalation Anesthesia System and Vapor Guard activated charcoal adsorption filters (VET Equip® Instrument, Livermore, CA).
4. Fine surgical instruments, including iris scissors, forceps, scalpels, blades, and a high-speed micro drill with carbon steel burrs (0.5 mm diameter) (Fine Science Tools, Foster City, CA).
5. A Mini ARCO hair clipper (Wahl Clipper Corp, Sterling, IL).
6. A model 940 small-animal stereotaxic instrument with a BENCHMark™ 3-axes digital counter display (Leica Biosystems, Inc., Buffalo Grove, IL) equipped with an inhalation anesthesia system (VET Equip® Instrument) and a KDS310 Nano single syringe infusion/withdraw pump (KD Scientific, Holliston, MA).
7. Hamilton Neuros™ 10 µl syringes with removable 33-gauge or 26-gauge needles are used for intranerve or intracranial injection, respectively.
8. An OPMI Pro Magis surgical microscope (Carl Zeiss Microscopy, LLC, Thornwood, NY).

9. Vetbond™ tissue adhesive (3M, St. Paul, MN).
10. Small-animal thermo-controlled recovery pads, to enhance post-surgical recovery.

## 2.4 Bioluminescence Imaging

1. D-luciferin potassium stock: D-luciferin potassium salt (Gold Biotechnology, St. Louis, MO) is dissolved as a 15 mg/ml stock in PBS. The stock solution should be sterilized by filtration. Alternatively, a ready-to-inject solution of D-luciferin (Xenolight RediJect; Perkin Elmer, Waltham, MA) is also available (*see* Subheading 3.5, step 1).
2. Insulin syringes with 28-gauge needles are used for luciferin injection into mice.
3. An IVIS Spectrum Preclinical In Vivo Imaging System and Living Image® software (Perkin Elmer) (*see* Subheading 3.5, step 4).
4. Isoflurane (Forane) is used to anesthetize mice throughout the imaging process.

---

## 3 Methods

Orthotopic animal models of tumors are essential tools in evaluating the safety and efficacy of potential therapeutics. These models can complement cell culture models by providing the native environment for tumor growth on the organismal level. In addition, they facilitate assessment of drug distribution and the ability of a drug to reach the tumor tissue and to inhibit target molecules. Effective animal models accurately recapitulate the specific features of the human tumors. As benign schwannomas and meningiomas tend to be slow-growing, an ideal animal model for these tumors would incorporate this growth characteristic. We discuss approaches for generating orthotopic, quantifiable schwannoma allograft and meningioma xenograft models, which can be used to evaluate potential therapeutic agents.

### 3.1 Schwannoma and Meningioma Cell Cultures

1. Dissect and use schwannomas developed in *P0Cre;Nf2<sup>flax/flax</sup>* (*Nf2<sup>P0</sup>*) mice with conditional *Nf2* inactivation in Schwann cells [9] to prepare schwannoma cell cultures as described previously [16].
2. Grow *Nf2<sup>P0</sup>* schwannoma cells in DME/F-12 (*see* Subheading 2.1, step 5) and plate on dishes coated with polylysine and laminin.
3. Confirm *Nf2*/Merlin status of these schwannomas by PCR genotyping and Western blotting [16, 17] (*see* Note 2).
4. Grow *NF2*-deficient benign human meningioma cell line Ben-Men-1 in DME medium supplemented with 10 % FBS on non-coated dishes [18, 19] (*see* Note 3).

**3.2 Generation  
of Luciferase-  
Expressing Sch10545-  
Luc Schwannoma  
and Ben-Men-1-LucB  
Meningioma Cells**

1. Trypsinize and plate Sch10545 schwannoma (derived from an *Nf2<sup>po</sup>* mouse) and Ben-Men-1 meningioma cells in fresh growth medium so that they will be about 25–50 % confluent by the next day. An extra dish of cells is plated at the same dilution to determine the number of cells in the dish.
2. The next day, trypsinize and count cells in the extra dish to determine the amount of lentivirus needed for infection (*see Note 4*). We usually infect Sch10545 or Ben-Men-1 cells with Lenti-CMV-Luc lentiviruses at a multiplicity of infection (MOI) of 1 to 10 (*see Note 5*). The MOI is defined as the number of infectious viral particles per cell (*see Note 6*).
3. For lentiviral transduction, remove medium from the dish. Based on the number of cells determined, mix an appropriate amount of lentiviruses with growth media supplemented with 8 µg/ml of polybrene and add to the cells. Incubate dish at 37 °C from 4 h to overnight (*see Note 7*).
4. Change media the next day following transduction and incubate the transduced dish at 37 °C for another day.
5. Two days after transduction, add puromycin to the cells to a final concentration of 2 µg/ml and replenish the growth medium containing puromycin every 3 days until puromycin-resistant colonies are visible (*see Note 8*).
6. Isolate individual puromycin-resistant colonies using cloning cylinders and expand in separate dishes containing growth medium and puromycin (*see Note 9*).
7. Trypsinize cells when dishes containing individual puromycin-resistant clones approach confluence. Expand half of the cells from each clone into a new dish to continue propagating as a stock. Wash the other half of the cells with PBS 2× and lyse in the Luciferase Reporter Lysis Buffer (Subheading 2.2, **step 6**). To determine the protein concentration, mix 2 µl of each clear lysate with 1 ml of diluted Bio-Rad Protein Assay Dye Reagent (*see Subheading 2.2, step 5*) and measure the absorbance at a wavelength of 595 nm. Generate a standard curve for protein concentration by measuring the absorbance of a series of standards with known amounts of protein at 595 nm and use these data to extrapolate each sample's protein concentration.
8. Measure luciferase activity by using equal amounts of proteins from each lysate (10 µg) using a Promega Luciferase Assay Kit and a microplate reader, according to the manufacturer's instructions. Inject clones expressing robust luciferase activity (e.g., Sch10545-Luc and Ben-Men-1-LucB) into mice to generate luciferase-expressing schwannoma allograft and meningioma xenograft tumors as described in the following sections.

**3.3 Intranerve  
Injection  
of Luciferase-  
Expressing Mouse  
*Nf2<sup>-/-</sup>* Schwannoma  
Cells into the Nerves  
of SCID Mice**

1. Acquire approval from the institutional animal care and use committee (IACUC) prior to initiating any studies involving animals.
2. Trypsinize and count actively-growing, luciferase-expressing Sch10545-Luc schwannoma cells. Wash in PBS 2× and spin down at 2000×*g* for 30 s in an Eppendorf microfuge. Resuspend cell pellet in an appropriate volume of PBS and place on ice until injection. To establish schwannoma allografts, inject ~10<sup>5</sup> Sch10545-Luc cells in 3 µl of PBS per mouse.
3. To perform intranerve injections, anesthetize an 8-to-10-month-old SCID mouse (*see Note 10*) using 5 % isoflurane in oxygen in an induction chamber until it is under deep anesthesia and does not respond to toe pinches. The induction chamber is connected to an Inhalation Anesthesia System to regulate isoflurane flow rate and to a Vapor Guard activated charcoal adsorption filter to capture the waste gas.
4. Once anesthetized, place the mouse on its stomach with its hind legs outstretched on a clean surgical platform. To maintain anesthesia during surgery, place a nose cone connected to an Inhalation Anesthesia System on the nose to continue administering isoflurane gas. Use a mini-hair clipper to remove hair from the right (or left) thigh and hind leg area, since only one sciatic nerve is injected with cells (*see Note 11*).
5. Disinfect the surgical site with a Povidone-Iodine Cleansing Scrub Swabstick and then with a Povidone-Iodine Antiseptic Prep Swabstick. Make a small incision (~1 cm) in the skin of the flank just below and parallel to the femur. Use scissors to separate the skin from the muscle of the leg. To expose the sciatic nerve, blunt dissect through the biceps femoris muscle using a pair of sharp scissors. The sciatic nerve should appear as a white fascicle of nerve fibers extending parallel to the femur.
6. To access the sciatic nerve for intranerve injection, insert a pair of fine forceps underneath the nerve to gently elevate and stabilize the nerve above the muscle. Load 3 µl of the Sch10545-Luc cell suspension in a Hamilton Neuros™ 10 µl syringe with a 33-gauge needle. To inject the cells, the needle of the Neuros™ syringe should be carefully inserted into the nerve by positioning the needle along the nerve. Gradually inject the contents of the syringe into the nerve, while holding the needle steady.
7. Once the syringe is empty, remove the needle slowly and place the nerve back into its original position beneath the muscle. Close and seal the incision using Vetbond™ tissue adhesive. Give the mouse a dose of buprenorphine (0.05 mg/kg) subcutaneously as an analgesic, remove the isoflurane nose cone, and place the animal on a thermo-controlled recovery pad until fully recovered and ambulatory.

**3.4 Stereotactic  
Injection  
of Luciferase-  
Expressing NF2-  
Deficient Benign  
Meningioma Cells  
to the Skull Base  
of SCID Mice**

1. As in Subheading 3.3, all animal experiments should be approved by the IACUC before initiating any studies.
2. Harvest actively-growing, luciferase-expressing Ben-Men-1-LucB for injection as described in Subheading 3.3, step 2. We find that injection of approximately  $10^6$  cells suspended in 5  $\mu$ l of PBS per mouse results in reproducible establishment of intracranial tumors.
3. As in Subheading 3.3, step 3, anesthetize 8–12-month-old SCID mice using 5 % isoflurane in oxygen until they are under deep anesthesia and do not respond to toe pinches.
4. Stabilize the anesthetized mouse on a secure platform and position in a small-animal stereotaxic device using a nose cone connected to an Inhalation Anesthesia System. Insert the ear pins carefully into the ear canals. When positioned properly, the head of the mouse is immobilized to minimize movement of the head during stereotactic injection.
5. Remove the hair on the top of the head using a pair of iris scissors and cleanse the surface area of the head from the nose to the back of the skull with Duo-Swab® Povidone-Iodine Cleansing Scrub and Antiseptic Prep Swabsticks. Using a scalpel with a No. 10 surgical blade, make a longitudinal midline incision from the forehead to the back of the skull. Use a sterile cotton-tipped applicator to stabilize the skin to facilitate the incision. Gently push scalp skin to the sides so that an area of the skull is exposed from the bregma, which is located near the middle of the skull, to the eyes. The bregma is a juncture in the cranial plates, where the coronal suture intersects perpendicularly to the sagittal suture.
6. Stabilize a 26-gauge needle attached to a Neuros™ 10  $\mu$ l syringe filled with 5  $\mu$ l of cell suspension, containing  $\sim 1 \times 10^6$  Ben-Men-1-LucB cells, in the stereotactic device and position it above the bregma. An OPMI Pro Magis surgical microscope is helpful in visualizing the bregma.
7. After the needle of the syringe is positioned directly above the bregma, set each of the stereotactic coordinates to zero. Then, using the stereotactic axes, move the syringe 1.5 mm anterior to the bregma and 1.5 mm lateral to the right of the bregma. Make a small burr hole at this location using a high-speed micro drill.
8. Once the drill has completely penetrated the skull so that the brain is exposed, lower the syringe until the tip of the needle is at the surface of the brain. Prior to inserting the needle into the brain, set the coordinate of the Z-axis to zero, and confirm coordinates for the X- and Y-axes (1.5 mm anterior and 1.5 mm lateral to the right of the bregma).

9. Once positioned, lower the needle slowly 4.5 mm into the brain to the skull base (*see Note 12*).
10. Using an automatic injector, inject tumor cells into the skull base at a rate of 1.5 ml/min. After the cells have been completely dispensed, maintain the needle in place for one minute to permit the injected cells to settle, followed by slowly withdrawing the needle from the brain.
11. Using a pair of forceps, close the surgical incision with Vetbond tissue adhesive.
12. As in Subheading 3.3, **step 7**, inject a dose of buprenorphine (0.05 mg/kg) subcutaneously near the surgical site as an analgesic. Remove the mouse from the stereotactic device and place on a thermo-controlled recovery pad until full recovery.

**3.5 Monitoring  
Growth of  
Schwannoma  
Allografts and  
Meningioma  
Xenografts by BLI**

1. BLI is used to assess successful tumor engraftment and growth. Prior to imaging, inject mice, implanted with Sch10545-Luc or Ben-Men-1-LucB cells, intraperitoneally with 150 mg/kg of D-luciferin (*see Note 11*).
2. As in Subheadings 3.3 and 3.4, **steps 3**, anesthetize mice using 5 % isoflurane in oxygen. Place the anesthetized mouse in the IVIS Spectrum Preclinical In Vivo Imaging System and position the nose in the nose cone for isoflurane gas administration during imaging.
3. Capture bioluminescent images of tumor-bearing mice at the peak time of luciferase activity following injection of D-luciferin (*see Note 13*).
4. Using BLI, tumor growth is measured noninvasively over time. The intensity of the BL signal correlates with changes in tumor size and is measured in each mouse using region-of-interest analysis in the LivingImage software (*see Note 14*). To determine tumor establishment and growth prior to treatment, at least two bioluminescent images should exhibit robust and increasing signals. We have found that tumor growth in the Sch10545-Luc schwannoma allograft model is effectively detected over one-week time intervals, whereas growth in the Ben-Men-1-LucB meningioma xenograft model is best observed over 1-month intervals.
5. To assess the efficacy of a particular therapeutic agent, compare the intensity of the BL signal (*see Note 15*) and its changes over time among animals treated with a therapeutic agent and untreated controls (*see Note 16*). Treatment responses can be confirmed by small-animal MRI [12, 19].

---

## 4 Notes

1. Antibiotics, such as penicillin and streptomycin, are used to reduce contamination, particularly during preparation of primary cultures of VS and meningioma cells. The details regarding preparation of these primary tumor cell cultures have been described previously [16]. However, we try to avoid using antibiotics, whenever it is possible, e.g., culturing established cell lines.
2. To generate an *Nf2*-deficient schwannoma cell line, schwannoma cells from *Nf2*<sup>p0</sup> mice were cultured for more than 25 passages and subcloned. We isolated a clone, designated Sch10545, which exhibits continuous growth. Loss of the *Nf2* gene in these cells was confirmed by PCR genotyping and Western blotting [16, 17]. Interestingly, these cells are no longer dependent on HRG and can grow in medium supplemented with 10 % FBS.
3. The benign human meningioma cell line Ben-Men-1 was established from a grade I meningioma by telomerase immortalization [18]. By Western blotting and DNA sequencing, we previously showed that Ben-Men-1 cells are Merlin-deficient [19].
4. Lentiviral vectors, such as Lenti-CMV-Luc, are considered Biosafety Level 2 (BSL-2) agents. Although they are replication-deficient, all handling and storage of lentiviral vectors and disposal of contaminated waste must be conducted according to institutional rules and regulations and NIH guidelines. Lentiviral vectors should be aliquoted in small amounts and stored at -80 °C. Repeated freeze-thawing will decrease the viral titer.
5. Other optimized firefly luciferase expression vectors [20–22] can be used, as well as luciferase-expressing vectors from other species [23, 24].
6. The optimal MOI is dependent on the target cell type and should be titrated to enhance viral gene delivery. Infection time may be decreased, or purified viral particles are used if viral toxicity is observed in the cell line of interest, particularly when using viral supernatant.
7. Polybrene is a cation polymer that can enhance retroviral or lentiviral transduction efficiency, by neutralizing the charge repulsion between viral particles and sialic acid moieties on the cell surface [25]. However, polybrene may be toxic to some cell lines, calling for a shorter incubation time. Alternatively, protamine sulfate [26] or other reagent systems, such as ViraDuctin™ or Sigma's ExpressMag bead system, are used to increase the efficiency of viral infection.

8. The optimal concentration of puromycin for the selection of puromycin-resistant clones should be determined in advance. For this purpose, we usually use the minimal concentration of puromycin that is sufficient to kill all non-transduced cells. Puromycin should be added 24 h after infection to allow for sufficient expression of the puromycin-resistant gene.
9. Different sizes of cloning cylinders can be purchased and used to isolate individual puromycin-resistant colonies. Alternatively, dilution cloning can be performed using 96-well plates. Also, it is possible to plate cells at a low density and directly select individual puromycin-resistant colonies in 96-well plates 24 h or more after lentiviral transduction.
10. For engraftment of schwannoma and meningioma cells, we routinely use the *scid* strain of immunodeficient mice, which carry the defective DNA-activated protein kinase *Prkdc*, important for the rearrangement of the immunoglobulin and T-cell receptor genes [27]. Other immunodeficient mouse strains, such as nonobese diabetic (NOD)-*scid*  $\beta 2m$ null and NOD-*scid* *IL2R $\gamma$* null (also called NSG or NOD *scid* gamma), may be considered as they give rise to more rapid tumor engraftment in some tumor models [28, 29]. Due to the  $\beta 2m$ null mutation, NOD-*scid*  $\beta 2m$ null mice are deficient in MHC class I expression, and their natural killer (NK) cells are unable to kill susceptible targets upon activation [30]. The NOD-*scid* *IL2R $\gamma$* null strain harbors a mutation in *IL2R $\gamma$* , which encodes the cytokine-receptor  $\gamma$ -chain shared by IL-2, IL-4, IL-7, IL-9, IL-15, and IL-21 receptors, and exhibits impaired NK cell development [31].
11. It can be helpful to stabilize mouse legs by taping their toes to the platform during surgery. The sciatic nerve can be accessed from either the dorsal or ventral sides of the mouse. It is preferable to graft only one sciatic nerve in each mouse as grafting both nerves will lead to impaired function of both hind legs due to tumor growth, resulting in early removal of mice from the study.
12. The depth to which the needle needs to be lowered to reach the skull base may vary slightly, depending on the age of the mice. Using 8-to-12-week-old mice, a depth of 4.5 mm is a useful guideline for skull base injection.
13. The sensitivity with which tumors are measured depends on the level of luciferase expression in the clones. Stronger luciferase activity yields a strong BL signal for a smaller number of cells, enabling the detection of fewer cells in a tumor. D-luciferin is commonly used for BLI in mice. Recently, a synthetic luciferin, the cyclic alkylaminoluciferin (CycLuc1), was shown to exhibit improved light output and to enhance BL detection in deep tissues, such as the brain [32].

14. The kinetics of luciferin circulation and uptake by tumor cells may vary in different models. To facilitate accurate quantitation of tumor growth, measurements are performed when luciferase activity is highest. This peak time is determined by measuring in vivo luciferase activity at various time intervals after D-luciferin injection. All subsequent bioluminescence measurements should be performed at this time interval.
15. As a sensitive and efficient way to noninvasively monitor tumor growth, BLI facilitates longitudinal studies, particularly for benign tumors [19]. Studies suggest that BL signals detected in luciferase-expressing tumors correlate with tumor size detected by MRI. BLI and MRI complement each other well by quantifying viable tumor cells and measuring the volume of the tumor mass by clinical standards, respectively.
16. Recently, interest is gaining in orthotopic patient-derived xenografts (PDX) as preclinical models for drug screening and development [33]. Loss of the *NF2* gene product Merlin leads to deregulation of multiple signaling pathways, such as the mitogen-activated protein kinase (MAPK) and PI3K/AKT/mTOR pathways, which may serve as viable therapeutic targets [1]. Study of these pathways has led to the initiation of several clinical trials. These schwannoma and meningioma animal models should enhance evaluation of additional novel therapeutic compounds.

---

## Acknowledgments

The authors would like to thank Dr. D. Bradley Welling for discussion. This work was supported by grants from the Department of Defense, Children's Tumor Foundation, Advocure NF2, Meningioma Mommas, and the Galloway Family.

## References

1. Yates C, Welling DB, Chang L-S (2011) Research advances in therapeutics for neurofibromatosis type 2-associated vestibular schwannomas. In: Cunha KS, Geller M (eds) *Advances in neurofibromatosis research*. Nova Science Publishers, Inc., Hauppauge, NY
2. Wiemels J, Wrensch M, Claus EB (2010) Epidemiology and etiology of meningioma. *J Neurooncol* 99:307–314
3. Baser ME, Friedman JM, Aeschliman D, Joe H, Wallace AJ, Ramsden RT, Evans DG (2002) Predictors of the risk of mortality in neurofibromatosis 2. *Am J Hum Genet* 71:715–723
4. Goutagny S, Kalamirides M (2010) Meningiomas and neurofibromatosis. *J Neurooncol* 99:341–347
5. Rouleau GA, Merel P, Lutchman M et al (1993) Alteration in a new gene encoding a putative membrane-organising protein causes neurofibromatosis type 2. *Nature* 363:515–521
6. Trofatter JA, MacCollin MM, Rutter JL et al (1993) A novel Moesin-, Exrin-, Radixin-like gene is a candidate for the neurofibromatosis 2 tumor-suppressor. *Cell* 72:791–800
7. Bianchi AB, Hara T, Ramesh V et al (1994) Mutations in transcript isoforms of the neurofibromatosis 2 gene in multiple human tumour types. *Nat Genet* 6:185–192
8. Bianchi AB, Mitsunaga SI, Cheng JQ, Klein WM, Jhanwar SC, Seizinger B, Kley N, Klein-Szanto AJ, Testa JR (1995) High frequency of inactivating mutations in the neurofibromatosis

- type 2 gene (*NF2*) in primary malignant mesotheliomas. *Proc Natl Acad Sci U S A* 92:10854–10858
9. Giovannini M, Robanus-Maandag E, van der Valk M, Niwa-Kawakita M et al (2000) Conditional biallelic *Nf2* mutation in the mouse promotes manifestations of human neurofibromatosis type 2. *Genes Dev* 14:1617–1630
  10. Kalamarides M, Stemmer-Rachamimov AO, Niwa-Kawakita M, Chareyre F, Taranchon E, Han ZY, Martinelli C, Lusi EA, Hegedus B, Gutmann DH, Giovannini M (2011) Identification of a progenitor cell of origin capable of generating diverse meningioma histological subtypes. *Oncogene* 30:2333–2344
  11. Gehlhausen JR, Park SJ, Hickox AE et al (2015) A murine model of neurofibromatosis type 2 that accurately phenocopies human schwannoma formation. *Hum Mol Genet* 24:1–8
  12. Chang L-S, Jacob A, Lorenz M, Rock J et al (2006) Growth of benign and malignant schwannoma xenografts in severe combined immunodeficiency mice. *Laryngoscope* 116:2018–2026
  13. Neff BA, Voss SG, Allen C, Schroeder MA, Driscoll CL, Link MJ, Galanis E, Sarkaria JN (2009) Bioluminescent imaging of intracranial vestibular schwannoma xenografts in NOD/SCID mice. *Otol Neurotol* 30:105–111
  14. Lin AL, Gutmann DH (2013) Advances in the treatment of neurofibromatosis-associated tumours. *Nat Rev Clin Oncol* 10:616–624
  15. Wang Y, Tseng JC, Sun Y, Beck AH, Kung AL (2015) Noninvasive imaging of tumor burden and molecular pathways in mouse models of cancer. *Cold Spring Harb Protoc* 2015:135–144
  16. Chang L-S, Welling DB (2009) Molecular biology of vestibular schwannomas. In: Sokolowski B (ed) *Auditory/vestibular research*, The Humana Press, Totowa, NJ, *Methods Mol Biol* 493:163–177
  17. Spear SA, Burns SS, Oblinger JL, Ren Y, Pan L, Kinghorn AD, Welling DB, Chang L-S (2013) Natural compounds as potential treatments of *NF2*-deficient schwannoma and meningioma: cucurbitacin D and goyazensolide. *Otol Neurotol* 34:1519–1527
  18. Püttmann S, Senner V, Braune V, Hillmann B, Exeler R, Rickert C et al (2005) Establishment of a benign meningioma cell line by hTERT-mediated immortalization. *Lab Invest* 85:1163–1171
  19. Burns SS, Akhmeteva EA, Oblinger JL, Bush ML, Huang J, Senner V, Chen C-S, Jacob A, Welling DB, Chang L-S (2013) AR-42, a histone deacetylase inhibitor, differentially affects cell-cycle progression of meningeal and meningioma cells and potently inhibits *NF2* meningioma growth. *Cancer Res* 73:792–803
  20. Rabinovich BA, Ye Y, Etto T, Chen JQ, Levitsky HI, Overwijk WW, Cooper LJ, Gelovani J, Hwu P (2008) Visualizing fewer than 10 mouse T cells with an enhanced firefly luciferase in immunocompetent mouse models of cancer. *Proc Natl Acad Sci U S A* 105:14342–14346
  21. Kim JB, Urban K, Cochran E, Lee S, Ang A, Rice B, Bata A, Campbell K, Coffee R, Gorodinsky A, Lu Z, Zhou H, Kishimoto TK, Lassota P (2010) Non-invasive detection of a small number of bioluminescent cancer cells *in vivo*. *PLoS One* 5:e9364
  22. Harwood KR, Mofford DM, Reddy GR, Miller SC (2011) Identification of mutant firefly luciferases that efficiently utilize aminoluciferins. *Chem Biol* 18:1649–1657
  23. Prescher JA, Contag CH (2010) Guided by the light: visualizing biomolecular processes in living animals with bioluminescence. *Curr Opin Chem Biol* 14:80–89
  24. Mezzanotte L, Fazzina R, Michelini E, Tonelli R, Pession A, Branchini B, Roda A (2010) In vivo bioluminescence imaging of murine xenograft cancer models with a red-shifted thermostable luciferase. *Mol Imaging Biol* 12:406–414
  25. Davis HE, Morgan JR, Yarmush ML (2002) Polybrene increases retrovirus gene transfer efficiency by enhancing receptor-independent virus adsorption on target cell membranes. *Biophys Chem* 97:159–172
  26. Cornetta K, Anderson WF (1989) Protamine sulfate as an effective alternative to polybrene in retroviral-mediated gene-transfer: implications for human gene therapy. *J Virol Methods* 23:187–194
  27. Shultz LD, Ishikawa F, Greiner DL (2007) Humanized mice in translational biomedical research. *Nat Rev Immunol* 7:118–130
  28. Ito M, Hiramatsu H, Kobayashi K et al (2002) NOD/SCID/ $\gamma$ cnul mouse: an excellent recipient mouse model for engraftment of human cells. *Blood* 100:3175–3182
  29. Carreno BM, Garbow JR, Kolar GR, Jackson EN, Engelbach JA, Becker-Hapak M, Carayannopoulos LN, Pivnicka-Worms D, Linette GP (2009) Immunodeficient mouse strains display marked variability in growth of human melanoma lung metastases. *Clin Cancer Res* 15:3277–3286
  30. Kim S, Poursine-Laurent J, Truscott SM et al (2005) Licensing of natural killer cells by host

- major histocompatibility complex class I molecules. *Nature* 436:709–713
31. Shultz LD, Lyons BL, Burzenski LM, Gott B, Chen X, Chaleff S et al (2005) Human lymphoid and myeloid cell development in NOD/LtSz-scid IL2R gamma null mice engrafted with mobilized human hemopoietic stem cells. *J Immunol* 174:6477–6489
  32. Evans MS, Chaurette JP, Adams ST Jr, Reddy GR, Paley MA, Aronin N, Prescher JA, Miller SC (2014) A synthetic luciferin improves bioluminescence imaging in live mice. *Nat Methods* 11:393–395
  33. Wilding JL, Bodmer WF (2014) Cancer cell lines for drug discovery and development. *Cancer Res* 74:2377–2384

## Ponatinib promotes a G<sub>1</sub> cell-cycle arrest of merlin/NF2-deficient human schwann cells

Alejandra M. Petrilli<sup>1</sup>, Jeanine Garcia<sup>1</sup>, Marga Bott<sup>1</sup>, Stephani Klingeman Plati<sup>1</sup>, Christine T. Dinh<sup>2</sup>, Olena R. Bracho<sup>2</sup>, Denise Yan<sup>2</sup>, Bing Zou<sup>2</sup>, Rahul Mittal<sup>2</sup>, Fred F. Telischi<sup>2</sup>, Xue-Zhong Liu<sup>2</sup>, Long-Sheng Chang<sup>3</sup>, D. Bradley Welling<sup>3,4</sup>, Alicja J. Copik<sup>1</sup> and Cristina Fernández-Valle<sup>1</sup>

<sup>1</sup>Burnett School of Biomedical Sciences, College of Medicine, University of Central Florida, Lake Nona-Orlando, FL 32827, USA

<sup>2</sup>University of Miami Miller School of Medicine, Department of Otolaryngology, Miami, FL 33136, USA

<sup>3</sup>Center for Childhood Cancer and Blood Diseases, The Research Institute at Nationwide Children's Hospital and Department of Pediatrics, The Ohio State University College of Medicine, Columbus, OH 43205, USA

<sup>4</sup>Current Affiliation: Department of Otolaryngology, Massachusetts Eye and Ear Infirmary, Massachusetts General Hospital and Harvard University, Boston, MA 02114, USA

**Correspondence to:** Cristina Fernández-Valle, **email:** cfv@ucf.edu

**Keywords:** neurofibromatosis type 2, schwannoma, PDGFR, SRC, STAT3

**Received:** August 17, 2016

**Accepted:** February 20, 2017

**Published:** March 06, 2017

**Copyright:** Petrilli et al. This is an open-access article distributed under the terms of the Creative Commons Attribution License (CC-BY), which permits unrestricted use, distribution, and reproduction in any medium, provided the original author and source are credited.

### ABSTRACT

**Neurofibromatosis type 2 (NF2) is a genetic syndrome that predisposes individuals to multiple benign tumors of the central and peripheral nervous systems, including vestibular schwannomas. Currently, there are no FDA approved drug therapies for NF2. Loss of function of merlin encoded by the NF2 tumor suppressor gene leads to activation of multiple mitogenic signaling cascades, including platelet-derived growth factor receptor (PDGFR) and SRC in Schwann cells. The goal of this study was to determine whether ponatinib, an FDA-approved ABL/SRC inhibitor, reduced proliferation and/or survival of merlin-deficient human Schwann cells (HSC). Merlin-deficient HSC had higher levels of phosphorylated PDGFR $\alpha$ / $\beta$ , and SRC than merlin-expressing HSC. A similar phosphorylation pattern was observed in phospho-protein arrays of human vestibular schwannoma samples compared to normal HSC. Ponatinib reduced merlin-deficient HSC viability in a dose-dependent manner by decreasing phosphorylation of PDGFR $\alpha$ / $\beta$ , AKT, p70S6K, MEK1/2, ERK1/2 and STAT3. These changes were associated with decreased cyclin D1 and increased p27<sup>Kip1</sup> levels, leading to a G<sub>1</sub> cell-cycle arrest as assessed by Western blotting and flow cytometry. Ponatinib did not modulate ABL, SRC, focal adhesion kinase (FAK), or paxillin phosphorylation levels. These results suggest that ponatinib is a potential therapeutic agent for NF2-associated schwannomas and warrants further *in vivo* investigation.**

### INTRODUCTION

Neurofibromatosis type 2 (NF2) is a non-malignant tumor disorder affecting the peripheral and central nervous systems. Although bilateral vestibular schwannomas (VS) are a diagnostic hallmark of the disorder, NF2 patients typically develop multiple meningiomas, ependymomas and other schwannomas as well. VS lead to deafness, tinnitus, imbalance and can cause life-threatening brainstem compression [1]. NF2 is caused by mutations in the NF2 gene that encodes the tumor suppressor protein

known as merlin or schwannomin [2, 3]. Merlin belongs to the Band 4.1 family of proteins that link the actin cytoskeleton to membrane receptors and transporters. Merlin modulates the activity of multiple signaling pathways that control cell size, morphology, cell adhesion, proliferation, and survival. These include receptor tyrosine kinase (RTK; e.g. ErbB2/3, PDGFR, EGFR, HGFR), small GTPases, FAK/SRC, the mammalian target of rapamycin (mTOR)/PI3K/AKT, and Hippo pathways [4]. Currently, surgery and radiation are the mainstream treatment options for NF2-associated tumors. Depending on the tumor

size and location, there are significant adverse effects associated with their removal. While an understanding of the biological functions of merlin is progressing, well-defined druggable molecular targets have yet to emerge. Increasingly, patients are treated off-label with the anti-angiogenic agent bevacizumab that also reduces edema in schwannomas without affecting the tumor cells. Dosing regimens are being optimized to reduce associated kidney toxicity observed with prolonged bevacizumab treatment [1, 5]. However, to date there are no FDA-approved therapies that target schwannoma cells directly and reduce morbidity and mortality of NF2 patients [1, 6].

Because of the slow-growing and benign nature of NF2 schwannomas, conventional chemotherapeutic agents are unsuccessful. Several RTK inhibitors have been investigated in preclinical studies and clinical trials with limited patient response. These include lapatinib (an EGFR/Erbb2 inhibitor; NCT00973739, NCT00863122), nilotinib (a PDGFR and c-kit inhibitor; NCT01201538), sorafenib (a VEGFR-2, PDGFR $\beta$ , and c-kit inhibitor), and axitinib (a VEGFR, c-kit, and PDGFR $\beta$  inhibitor; NCT02129647) [1, 7]. We selected ponatinib for evaluation because it is an FDA-approved drug that inhibits a relevant RTK, the PDGFR, and a downstream effector common to several *NF2* activated pathways, the non-receptor tyrosine kinase SRC. PDGFR and SRC signaling regulate cell survival, proliferation, migration and angiogenesis in many cell types [8, 9]. PDGFR is over-expressed and activated in VS and primary human schwannoma cells, consistent with merlin's role in downregulating surface levels of growth factor receptors [10-13]. In HEI-193 schwannoma cells, merlin overexpression inhibits cell proliferation by promoting PDGFR internalization and degradation [14]. There is evidence that SRC activity is deregulated in cells with loss of merlin function and thus is a candidate for therapeutic targeting. In human schwannoma cells, SRC activity is increased compared to normal Schwann cells, and in mouse glia cells, merlin inhibits proliferation by modulating SRC activity [15, 16]. Lastly, primary human schwannoma cells treated with the SRC inhibitor SU6656 exhibit decreased transcription of proliferation-associated genes [17]. Thus, an inhibitor that targets both PDGFR and SRC might have therapeutic value for NF2-associated tumors.

Ponatinib (AP24534, brand name: Iclusig<sup>®</sup>) is a third generation type IIA inhibitor of ABL/SRC tyrosine kinase (TK). It is orally active and initially received accelerated approval in 2012 for adult patients with chronic myeloid leukemia (CML) and Philadelphia chromosome-positive acute lymphoblastic leukemia (Ph+ ALL) that are T315I-positive and are not candidates for other TK inhibitors. Ponatinib binds the inactive, DFG-out (aspartic acid, phenylalanine and glycine) ABL/SRC conformation [18, 19]. In a cell-free kinase screen, ponatinib inhibited SRC with IC<sub>50</sub> of 5.4nM and PDGFR $\alpha$  and PDGFR $\beta$  with IC<sub>50</sub> of 1.1nM and 7.7nM, respectively [19].

In this study, we measured the ability of ponatinib to decrease proliferation and survival of merlin-deficient HSC and vestibular schwannoma cells with *NF2* mutations. We found that ponatinib caused a G<sub>1</sub> cell-cycle arrest and mapped the regulatory signaling cascades modulated by the inhibitor. Our findings support further *in vivo* evaluation of ponatinib as a candidate drug for NF2 schwannomas.

## RESULTS

### Ponatinib decreases viability of merlin-deficient HSC and vestibular schwannoma (VS) cells

To create a suitable cell line for drug discovery studies, we first authenticated primary HSC based on their expression of human nuclear antigen and Schwann cell markers, S100, PLP, and O4 (Figure 1A). We then used lentiviral delivery of *NF2*-shRNA to reduce expression of merlin in the primary HSC. Merlin levels were stably reduced to nearly undetectable levels in the transduced cells compared to the parental HSC (Figure 1B, C). The merlin-deficient HSC did not contact inhibit but did not form aggregates and grows in multiple layers; many of these merlin-deficient HSC maintained an elongated morphology when cultured in the presence of serum and mitogens (Supplementary Figure 1AB). We measured basal levels of PDGFR $\alpha/\beta$  and SRC phosphorylation in primary HSC prior to and following knockdown of merlin. We found that depletion of merlin expression was associated with increased levels of p-PDGFR $\alpha/\beta$  and p-SRC compared to the parental HSC (Figure 1B). This finding agrees with previous reports of increased activation of the PDGFR and SRC pathways in human schwannomas compared to normal human nerve [10, 20, 21].

We screened the ability of ponatinib to reduce viability of multiple control and merlin-deficient HSC lines. As controls, we tested the parental wild-type HSC (HSC-WT), HSC expressing a scrambled shRNA construct (HSC-SCR), HSC expressing a Turbo-GFP shRNA (HSC-GFP), and merlin-deficient HSC lines (MD-HSC) expressing shRNA sequences that target the human *NF2* gene, (MD-HSC #45, #74 #75 and #77). All control HSC expressed merlin, whereas the HSCs transduced with shRNA constructs targeting the *NF2* gene had nearly undetectable merlin levels (Figure 1D). We performed 48 hour dose-response viability assays on the seven HSC lines in complete growth medium containing serum and growth factors. The results indicated that ponatinib reduced viability of all of the cell lines in a dose-dependent manner (Figure 1E). Under the conditions tested, ponatinib was not selective for MD-HSC over scrambled, GFP or untransduced HSC (IC<sub>50</sub> HSC-SCR= 3.3 $\mu$ M, HSC-GFP=2.4  $\mu$ M, HSC-WT= 2.3  $\mu$ M, MD-HSC#45= 2.2  $\mu$ M, MD-HSC#74= 3.3  $\mu$ M, MD-HSC#75= 1.9  $\mu$ M and MD-HSC#77=3.7  $\mu$ M). The average maximal response at 10 $\mu$ M was a 71% decrease in cell viability. However, when control merlin-expressing cell

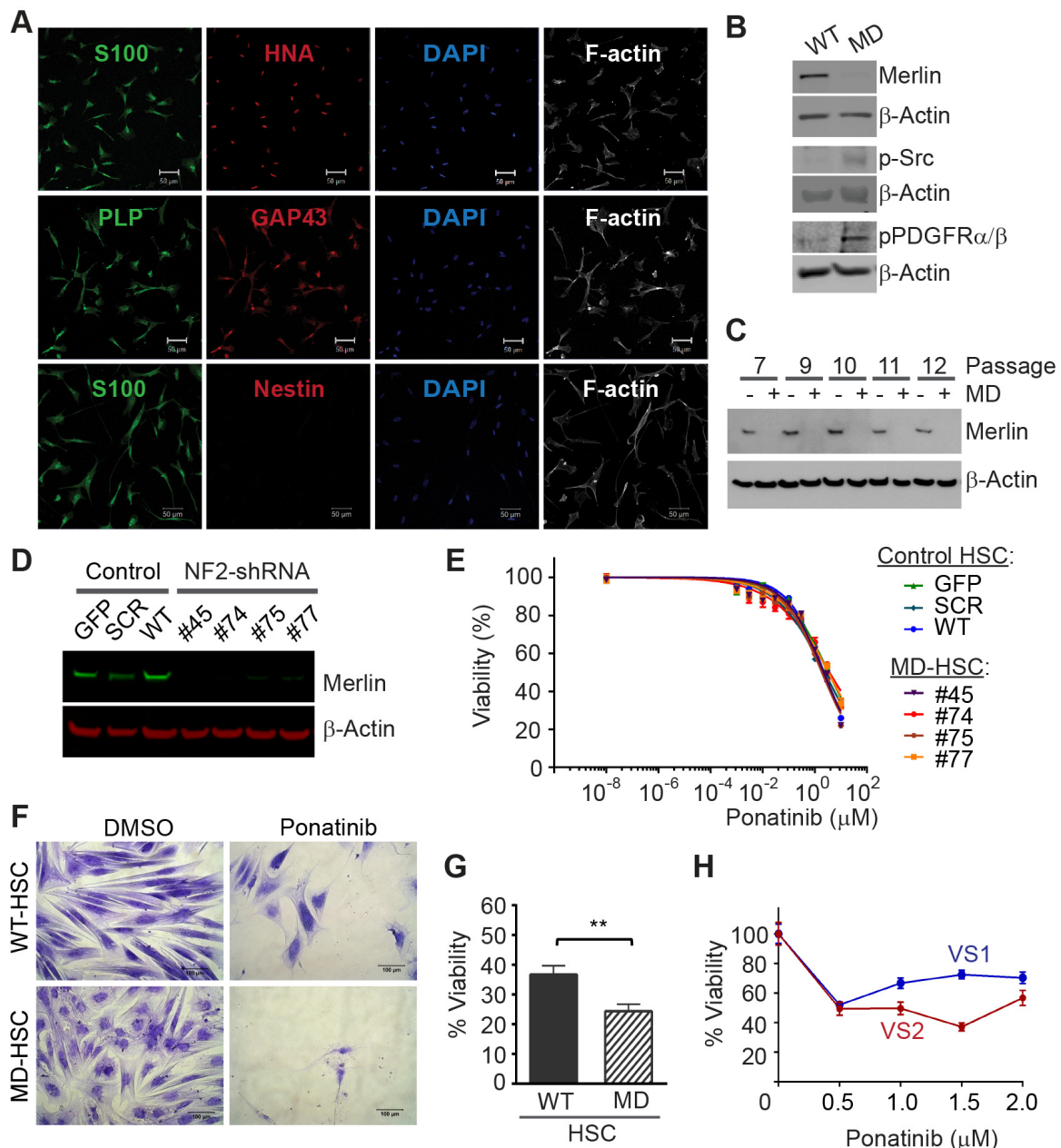


**Figure 1: Ponatinib decreases HSC viability.** (A) Characterization of primary HSC. Confocal Images of HSC expressing human and SC lineage markers: human nuclear antigen (HNA, red), S100 (green), GAP43 (red), proteolipid protein (PLP, green), negative nestin (red), DAPI stained nuclei (blue) and F-actin was visualized with phalloidin-Alexa633 (white). Scale bar: 50 $\mu$ m. (B) Representative Western blots of primary HSC and merlin-deficient HSC (MD-HSC) lysates, merlin silencing increased levels of phosphorylated SRC and PDGFR $\alpha/\beta$ . (C) Western blotting for merlin and  $\beta$ -actin in control HSC and merlin deficient cells at increasing cell passages. (D) Western blot for merlin and  $\beta$ -actin in three control HSC lines and four merlin-deficient (knock-down) HSC lines. (E) Ponatinib dose-response CellTiter-Fluor viability assay. Control HSC lines: SCR-HSC, GFP-HSC and WT-HSC and merlin-deficient HSC: #45, 74, 75, 77 were treated with increasing concentrations of ponatinib in constant 0.1% DMSO or vehicle alone for 48h. Viability is presented as a % of the DMSO control. Graph represents the mean  $\pm$  SEM of three independent experiments. (F-G) WT-HSC and MD-HSC (#45) were maintained in serum free medium for 5-10 days and then treated with 0.25 $\mu$ M ponatinib for one week. Relative cell numbers was assessed using a crystal violet assay: (F) Representative 20X phase contrast images of cells. Scale bar= 100 $\mu$ m. (G) Cell viability calculated as a % of their respective DMSO control. Graph represent mean  $\pm$  SEM of three independent experiments (\*\*  $p < 0.01$ , unpaired  $t$ -test, two tailed). (H) Viability of primary human VS cells treated for 48h with increasing ponatinib concentrations. Relative cell viability was assessed using a crystal violet assay and presented as % viability normalized to DMSO group. Plot of mean  $\pm$  SEM of 6 replicates. VS1 (heterozygous deletion of 23 nucleotides in exon 8 of the *NF2* gene, non-irradiated, passage 2); VS2 (heterozygous missense c.1460T>A and p. I487N in exon 14 of the *NF2* gene, non-irradiated, passage 2).

line (HSC-WT) and merlin-deficient HSC (MD-HSC#45) were cultured in the absence of serum and mitogens, merlin-deficient HSC were significantly more sensitive to 0.25  $\mu$ M ponatinib than the merlin-expressing HSC (Figure 1F,G).

We tested ponatinib's effect on cultured human vestibular schwannoma cells with *NF2* mutations. We assessed relative cell viability using a crystal violet assay following 48 hour incubation with ponatinib. Cell viability was reduced by approximately 40% at 2  $\mu$ M in VS1 and VS2 compared to DMSO-treated cells in agreement with the  $IC_{50}$  obtained with our MD-HSC lines. (Figure 1H).

### Ponatinib decreases viability of merlin-deficient HSC independent of the SRC/FAK/paxillin pathway

Ponatinib did not reduce net levels of ABL phosphorylation in merlin-deficient HSC (Figure 2A). Ponatinib

induced a dose-dependent increase in the total SRC protein level but did not alter the levels of the other SRC family members, FYN and YES, that play important roles in SC biology as well (Figure 2B) [22, 23]. We found a slight increase in SRC-Tyr416 phosphorylation in merlin-deficient HSC treated with 0.3 to 3  $\mu$ M (with a peak at 1  $\mu$ M). The phosphorylation pattern, however, did not coincide with the increase in the SRC protein levels (Figure 2B).

Key effectors transducing extracellular matrix adhesion and growth factor-dependent stimuli in Schwann cells are the SRC substrates, FAK and paxillin, a focal adhesion-associated adaptor [24]. FAK is a key mediator of extracellular matrix-integrin and RTK signaling that is upregulated in schwannomas [10]. Upon FAK autophosphorylation at Tyr397, SRC binds the phosphorylated residue and phosphorylates FAK on Tyr576 and Tyr577, resulting in stabilizing the activation loop of FAK in the active conformation and its binding to substrates,

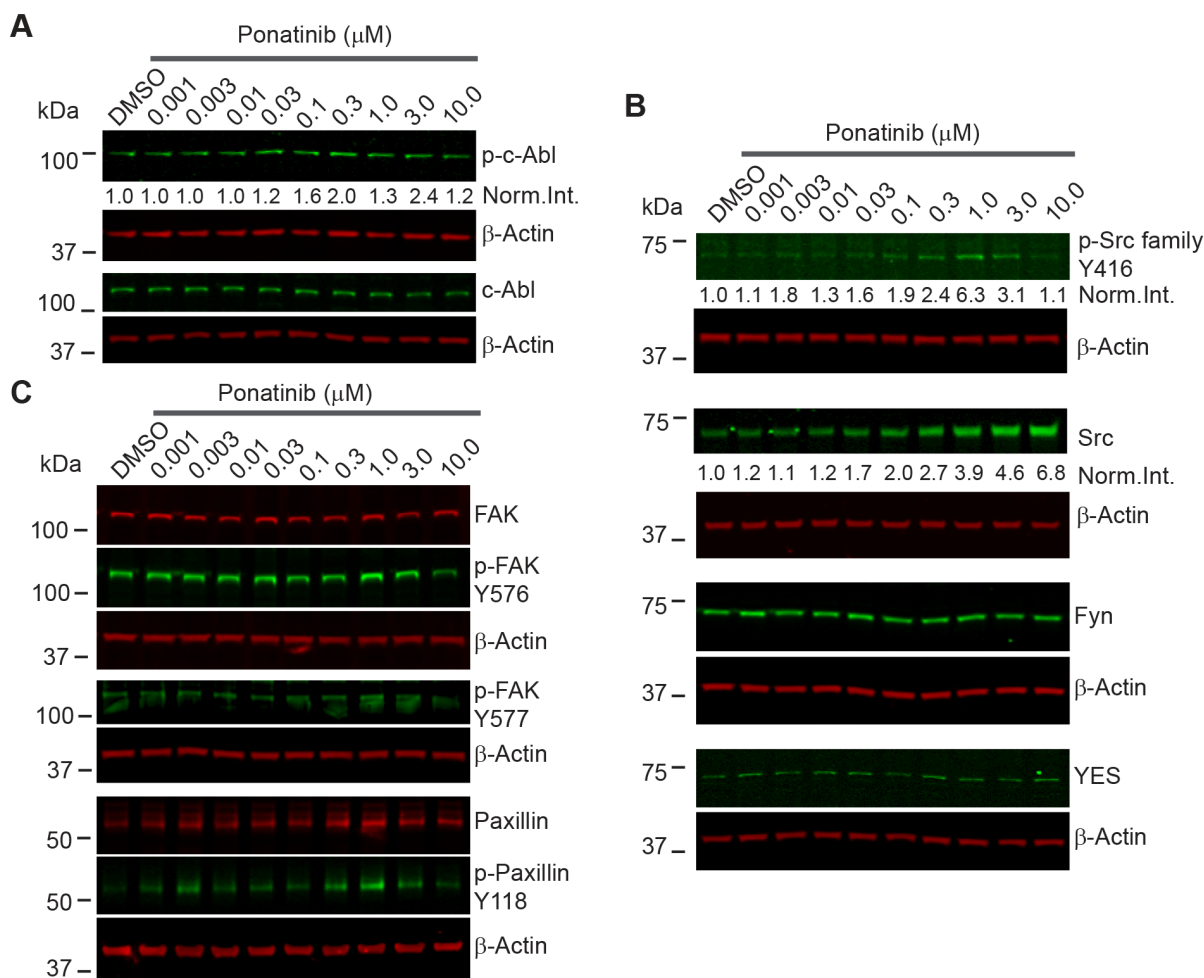


**Figure 2: Ponatinib decreased merlin-deficient HSC viability independent of ABL/SRC/FAK pathway inhibition.** Representative ponatinib dose-response Western blots (n=3). MD- HSC#45 plated in 12-well plates were treated with increasing concentrations of ponatinib for 2h as indicated. Cells were harvested, lysed, resolved by SDS-PAGE and blotted for: (A) p-ABL-Tyr452, c-ABL and β-actin as a loading control; (B) p-SRC-Tyr416 and total SRC, FYN, YES, p-FAK-Tyr576, p-FAK-Tyr577, total FAK, p-Paxillin-Tyr118, and total paxillin. The β-actin levels were used as loading controls.

thereby providing FAK with maximal activity [25]. In turn, FAK either directly or via SRC, phosphorylates paxillin at Tyr118 [26]. We therefore assessed FAK and paxillin phosphorylation in merlin-deficient HSC treated for 2h with increasing ponatinib concentrations. Western blot analysis showed that ponatinib did not reduce FAK-Tyr576 or Tyr577 or paxillin-Tyr118 phosphorylation similar to the SRC-Tyr416 phosphorylation pattern (Figure 2C and Supplementary Figure 2). Together the results demonstrate that the ABL, SRC, FAK and paxillin pathways are not inhibited by ponatinib in merlin-deficient HSC.

### Ponatinib decreases activation of the PDGFR $\alpha/\beta$ , PI3K, MEK1/2, ERK1/2 and STAT3 signaling pathways

To identify the signaling pathways modulated by ponatinib, we conducted a series of Western blots of merlin-deficient HSC treated for 2 hours with increasing

concentrations of ponatinib. We found that ponatinib reduced phosphorylation of PDGFR $\alpha/\beta$  at Tyr849/Tyr857, the autophosphorylation sites in the activation loop of these kinases, in a dose-dependent manner without altering the PDGFR $\alpha/\beta$  protein levels (Figure 3). In addition, ponatinib reduced phosphorylation of three additional tyrosine residues in PDGFR $\beta$  at positions 740, 771 and 1021 (Figure 3). Phosphorylation of these residues increases affinity for binding and activating PI3K, SRC, the GTPase Activator of Ras (GAP), GRB2, and PLC $\gamma$  [27]. When cells are stimulated with growth factors, AKT (also known as protein kinase B) and p70 S6 kinase are activated in a phosphatidylinositol 3-kinase (PI3K)-dependent pathway. Thr308 in the AKT activation loop and Thr229 in the p70S6 kinase catalytic domain are phosphorylated by 3-phosphoinositide-dependent protein kinase-1 (PDK1) *in vivo* and *in vitro* [28, 29]. Therefore to probe activity of the PI3K pathway in ponatinib-treated cells, we assessed AKT-Thr308 phosphorylation and p70S6 kinase-Thr229

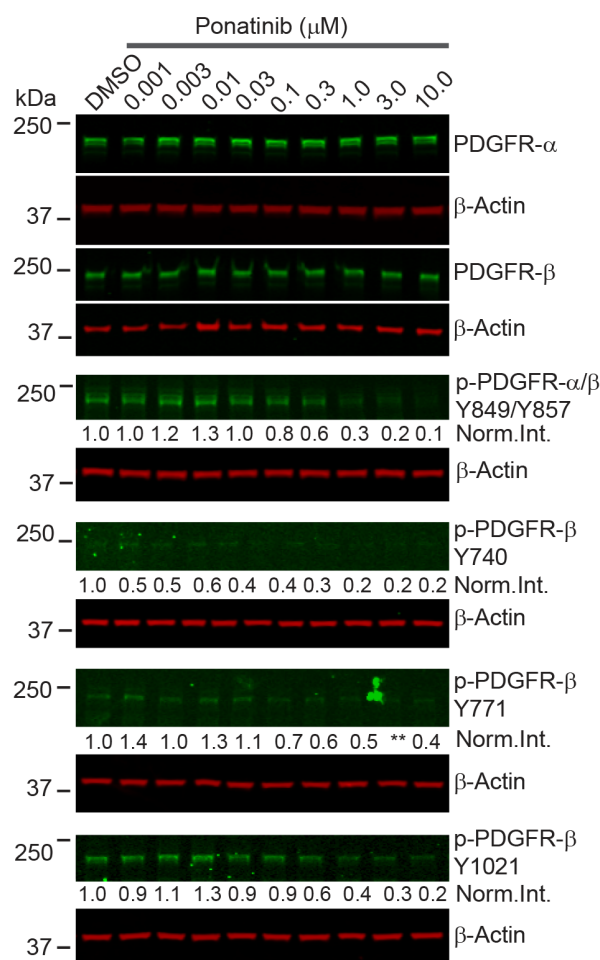


**Figure 3: Ponatinib inhibited PDGFR $\alpha/\beta$  phosphorylation in merlin-deficient HSC.** Representative ponatinib dose-response Western blots (n=3). MD-HSC#45 plated in 12-well plates were treated with increasing concentrations of ponatinib for 2h as indicated. Cells were harvested, lysed, resolved by SDS-PAGE and blotted for p-PDGFR $\alpha/\beta$ -Tyr849/Tyr857, p-PDGFR $\beta$ -Tyr740, p-PDGFR $\beta$ -Tyr771, p-PDGFR $\beta$ -Tyr1021 and total PDGFR $\alpha$  and PDGFR $\beta$ . The  $\beta$ -actin levels were used as loading controls.

phosphorylation by Western blots. We found that both AKT-Thr308 and p70S6 kinase-Thr229 underwent a dose-dependent decrease in phosphorylation (Figure 4A,B).

Previous studies demonstrated that overexpression and activation of PDGFR $\beta$  strongly activates MEK1/2 and ERK1/2 in human schwannoma cells leading to enhanced proliferation [10]. We assessed the phosphorylated MEK1/2 and ERK1/2 levels in merlin-deficient HSC after ponatinib treatment. We found that ponatinib treatment was associated with a dose-dependent decrease in MEK1/2-Ser217/Ser221 and ERK1/2-Thr202/Tyr204 phosphorylation in merlin-deficient HSC (Figure 4C).

Although net inhibition of SRC phosphorylation was not observed, ligand binding to PDGFR promotes receptor binding to SRC and recruitment of STAT3,

followed by Tyr705 auto-phosphorylation of STAT3 and its dimerization and translocation into the nucleus to directly drive gene expression needed for cell proliferation [30-32]. Western blot analysis showed that ponatinib decreased STAT3 phosphorylation in a dose-dependent manner in merlin-deficient HSC (Figure 4D).

Lastly, to further evaluate the contribution of PI3K/AKT, MEK, or STAT3 inhibition downstream to PDGFR responsible for ponatinib's effect, we individually inhibited AKT with perifosine/KRX-0401, MEK with selumetinib/AZD6244, and STAT3 with S3I-201/NSC-74859 and compared the results to ponatinib's effects on cell viability. MEK, AKT or STAT3 inhibition alone only partially decreased merlin-deficient HSC viability. Inhibition of STAT3 with S3I-201 was the least effective,

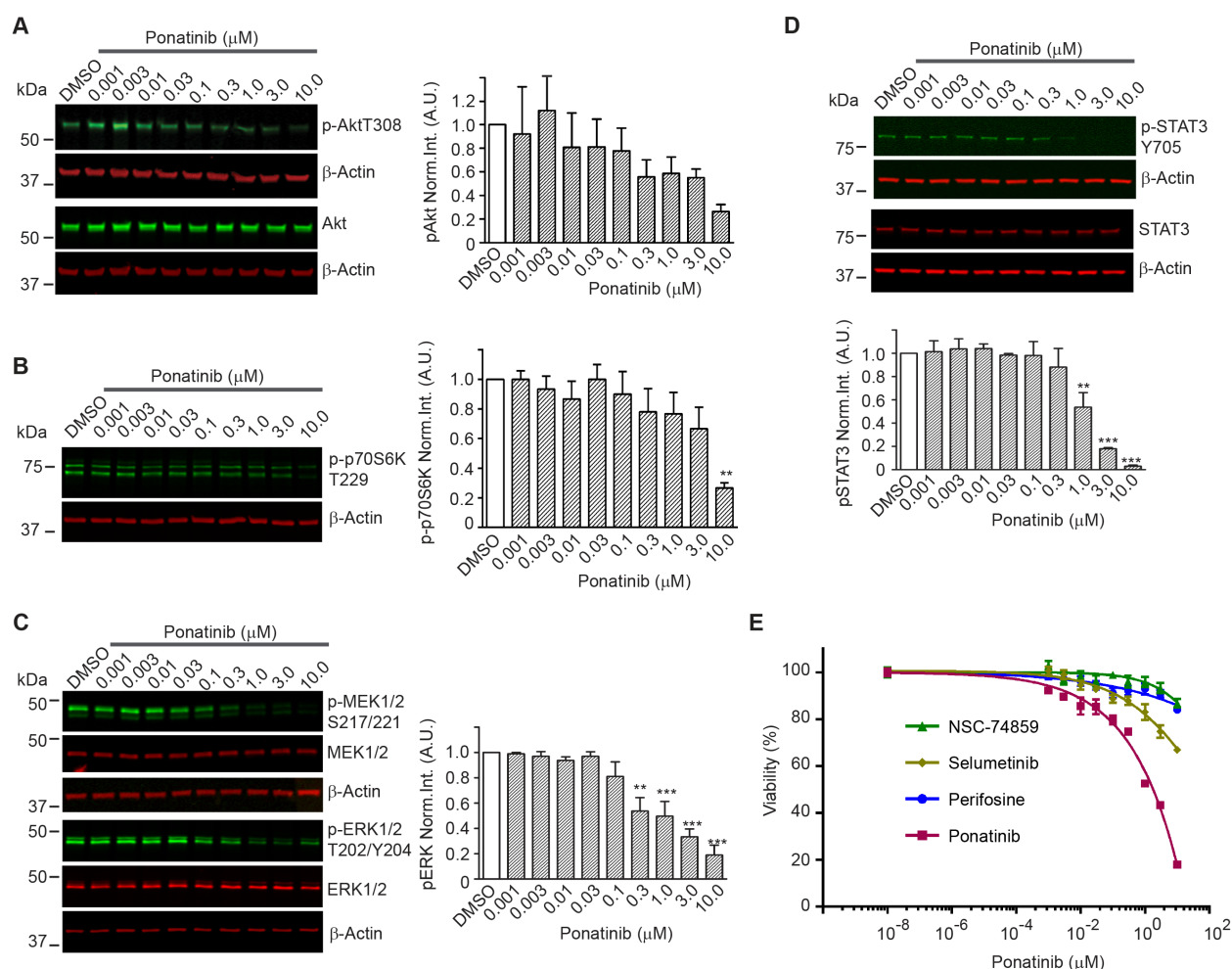


**Figure 4: Downstream signaling pathways inhibited by ponatinib in merlin-deficient HSC.** Western blots of extracts prepared from merlin-deficient HSC#45 treated with increasing ponatinib concentrations. Quantitation was done by fluorescence intensity analysis, normalized to  $\beta$ -actin, and plotted as mean  $\pm$  SEM (n=3). One-way analysis of variance and Dunnett's multiple comparison post-test were used for statistical analysis (\* $p$ <0.1; \*\* $p$ <0.01 and \*\*\* $p$ <0.001). Representative Western blots of dose response experiments at 2h for: (A) p-AKT-Thr308 and AKT; (B) p-p70S6K-Thr229; (C) MEK1/2, p-MEK1/2-Ser217/Ser221, ERK1/2, and p-ERK1/2-Thr202/Tyr204; (D) p-STAT3-Tyr705, and total STAT3. (E) Ponatinib dose-response CellTiter-Fluor viability assay. MD- HSC#45 were treated with semi-log serial dilutions of ponatinib, NSC-74859, selumetinib, perifosine in 0.1% DMSO for 48h, or vehicle alone. Viability is presented as % of the DMSO control. Graph represents the mean  $\pm$  SEM of three independent experiments.

and although selumetinib was more efficacious than perifosine and S3I-201, none of individual inhibitors even at the highest concentration tested (10  $\mu$ M) matched ponatinib's efficacy (Figure 4E). These results suggest that simultaneous inhibition of these three pathways occurs in response to ponatinib and similarly contributes to the loss of viability of merlin-deficient HSC.

### Ponatinib arrests merlin-deficient HSC in $G_1$ by decreasing cyclin D1 and increasing p27<sup>Kip1</sup> levels

A molecular link between ERK1/2 and STAT3 to proliferation is through cyclin D1 to regulate  $G_1$ -to-S cell cycle progression. ERK1/2 activity is required for

expression of cyclin D1 in the  $G_1$  phase of the cell cycle. Moreover, STAT3 transcriptionally regulates cyclin-D1 by binding to its promoter region [33, 34]. We assessed the level of cyclin D1 in merlin-deficient HSC after a 24h incubation with ponatinib. We found that ponatinib strongly decreased cyclin D1 protein levels in a dose-dependent manner (Figure 5A). These results suggest that ponatinib reduces the viability of merlin-deficient HSC by inhibiting PDGFR $\alpha$ / $\beta$ -dependent activation of MEK/ERK and STAT3 pathways, leading to decreased cyclin D1 expression.

To test the possibility that the decrease in the viability of merlin-deficient HSC by ponatinib was a consequence of cell-cycle blockage due to reduced cyclin

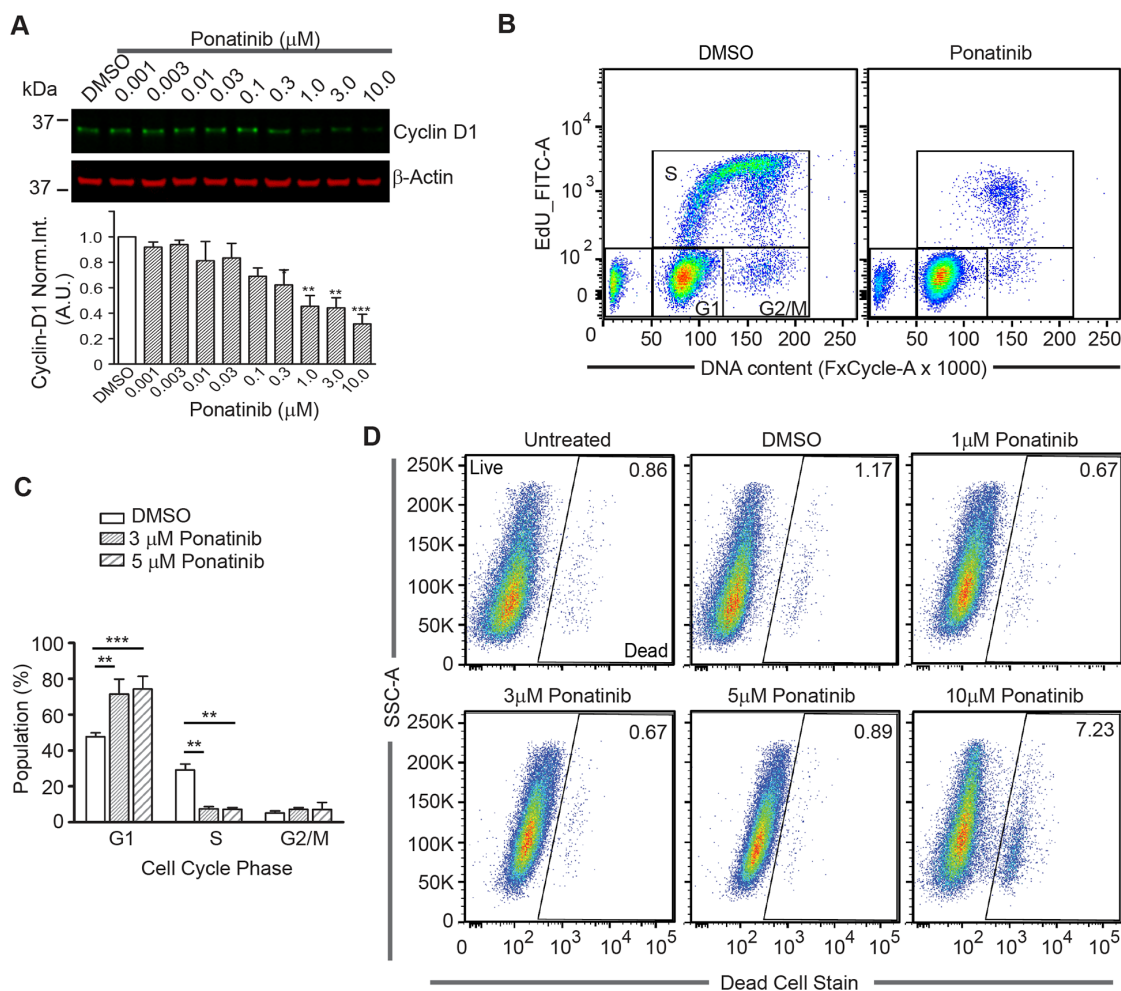


**Figure 5: Ponatinib arrests merlin-deficient HSC at the  $G_1$  phase of the cell cycle.** (A) Representative Western blots for Cyclin D1 of lysates prepared from merlin-deficient HSC#45 treated 24h with increasing concentrations of ponatinib. Plotted below as mean  $\pm$  SEM (n=3). One-way analysis of variance and Dunnett's multiple comparison post-test were used for statistical analysis (\*\*  $p < 0.01$  and \*\*\*  $p < 0.001$ ). (B,C) Merlin-deficient HSC were treated with 3 and 5  $\mu$ M ponatinib for 24h and during the last 3h, 10  $\mu$ M EdU was added. Cells were harvested, labeled with live/dead fixable dye, and analyzed by flow cytometry. (B) Representative plots of the distribution of EdU- and FxCycle-labelled cells of 0.1% DMSO vehicle control and ponatinib treated cells. (C) Graph of the distribution of the cell cycle phases (gated for the live population) of all the experiments as mean  $\pm$  SEM, n=4; \*\*  $p < 0.01$  and \*\*\*  $p < 0.001$  were determined by two-way ANOVA and Bonferroni multiple comparisons post-test. (D) Representative plots of the distribution of live and dead cell population in these experiments with increasing concentrations of ponatinib as indicated.

D1 expression, we analyzed the distribution of cells among the different phases of the cell cycle. There was a significant increase in the number of cells in the G<sub>1</sub> phase when treated with 3 and 5  $\mu$ M ponatinib compared to vehicle controls (72%  $\pm$ 8% and 74%  $\pm$ 7% vs. 47%  $\pm$ 2% of control). This was accompanied by a concomitant decrease

in the number of S-phase cells observed in ponatinib-treated samples as compared with control samples (7.5%  $\pm$ 1% for 3  $\mu$ M and 7%  $\pm$ 1% at 5  $\mu$ M vs. 29%  $\pm$ 3% of control) (Figure 5B–5C). At the lower concentrations (1 through 5  $\mu$ M), ponatinib arrested merlin-deficient HSC at G<sub>1</sub>, indicating a cytostatic mechanism of action. However,

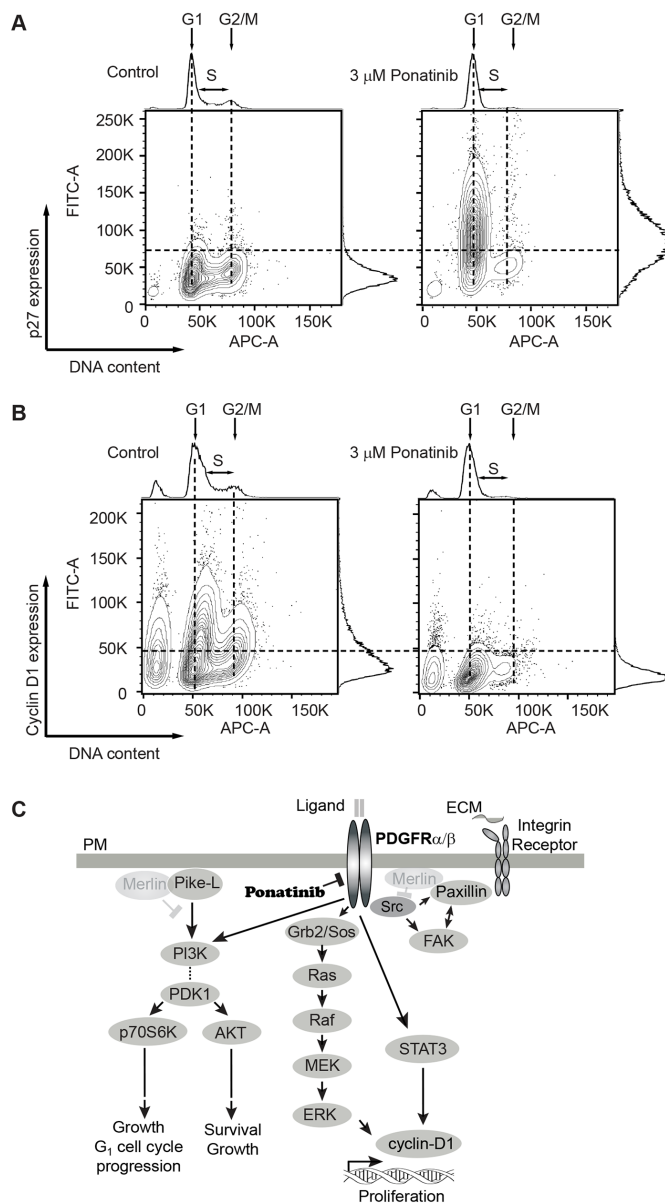


**Figure 6: Analysis of G<sub>1</sub> regulatory proteins during the cell-cycle in merlin-deficient HSC treated with ponatinib.** MD-HSC were treated with 3  $\mu$ M ponatinib or vehicle control for 24h. Cells were harvested, fixed, and permeabilized. DNA was stained with FxCycle, and intracellular G<sub>1</sub> regulatory proteins were immunostained and analyzed by flow cytometry. (A) Distribution plots of cells with positive/negative p27<sup>Kip1</sup> immunostain vs DNA content. Data shown are representative plots of four independent experiments. (B) Distribution of cells analyzed by flow cytometry with positive/negative cyclin D1 immunostain vs DNA content. Shown are representatives of four independent experiments. (C) Diagram of signaling pathways inhibited by ponatinib in merlin-deficient HSC. Merlin deficiency leads to activation of PDGFR, SRC and PI3K. Activation of PI3K potentiates AKT and p70S6K phosphorylation and leads to cell survival, growth and G<sub>1</sub> cell cycle progression. PDGFR activity triggers ERK and STAT3 activation, leading to cyclin D1 expression and cell proliferation. SRC activation of FAK and paxillin is not modulated by ponatinib. Ponatinib decreases cell viability through downstream inhibition of AKT, ERK, and STAT3.

by analyzing the live/dead populations, at a higher concentration (10 $\mu$ M), ponatinib became cytotoxic (Figure 5D). The increase in the number of dead cells present in the cells treated with 10 $\mu$ M ponatinib coincides with the decrease in phosphorylated proteins studied here.

Lastly, we analyzed the correlation of the cell-cycle phases with levels of several cell cycle regulators. Cyclin-dependent kinase (Cdk) inhibitor p27 (p27<sup>Kip1</sup>) is a key negative regulator of Cdk activity in cells progressing from G<sub>1</sub> toward S phase [35]. We analyzed the expression of p27<sup>Kip1</sup> in conjunction with DNA content by flow cytometry. We found fewer p27<sup>Kip1</sup>-positive cells in G<sub>1</sub> in control cells compared with a large increase in p27<sup>Kip1</sup>-positive cells in G<sub>1</sub> in ponatinib-treated samples (Figure 6A). Similarly, we found a greater number of cyclin D1-positive cells in control samples in G<sub>1</sub> in contrast to ponatinib-treated samples (Figure 6B). This result correlates with that observed from the Western blot experiment (Figure 5A). Overlay of the p27<sup>Kip1</sup> and cyclin D1 plots with the cell-cycle plots clearly demonstrate that ponatinib induced G<sub>1</sub> arrest with associated changes in the cyclin D1 and p27<sup>Kip1</sup> levels in merlin-deficient HSC (Supplementary Figure 3AB). Our results are consistent with ponatinib inhibition of PDGFR and downstream PI3K activity leading to a G<sub>1</sub> cell-cycle arrest of merlin-deficient HSC by blocking ERK- and STAT3-dependent expression of cyclin D1 (Figure 6C).

### **PDGFR $\alpha$ / $\beta$ , SRC, STAT 3 and MEK1/2 are highly phosphorylated in human vestibular schwannomas**

To assess activation of PDGFR $\alpha$ / $\beta$  and SRC in human schwannomas, we surveyed a phospho-proteome profile comparing five human vestibular schwannoma specimens with primary normal adult human Schwann cells cultured in the presence of mitogens to stimulate their proliferation. Analysis of phospho-receptor tyrosine kinase and phospho-kinases proteome profiler arrays revealed that schwannomas consistently had higher levels of phosphorylated PDGFR $\alpha$ , PDGFR $\beta$ , SRC, MEK and STAT3 compared with control primary HSC (Figure 7 A-D). Schwannomas exhibited averaged 6.6 times higher PDGFR $\alpha$  phosphorylation, 5.4 times higher PDGFR $\beta$  phosphorylation, 30 times higher SRC phosphorylation, 5.6 times higher MEK phosphorylation and 7.4 times higher STAT3 phosphorylation compared with control primary HSC (Figure 7 A-D).

## **DISCUSSION**

In this study, we evaluated whether ponatinib, a BCR-ABL/SRC inhibitor approved for use in leukemia, could potentially be repurposed for treatment of NF2 schwannomas. Following merlin depletion, HSC increased the levels of phosphorylated SRC and

PDGFR $\alpha$ / $\beta$ , in agreement with studies in primary human NF2 schwannoma cells [36]. Ponatinib stimulated a robust G<sub>1</sub> cell cycle arrest of merlin-deficient HSC in a dose-dependent manner by inhibiting PDGFR $\alpha$ / $\beta$  and its downstream effectors AKT, p70S6 kinase, MEK/ERK and STAT3, leading to reduced levels of cyclin D1 and increased levels of p27<sup>Kip1</sup>. Intriguingly, ponatinib did not reduce ABL/SRC/FAK/paxillin net phosphorylation in merlin-deficient HSC. We did not find clear evidence of ABL and SRC inhibition in merlin-deficient HSC treated with ponatinib. However, we found that ponatinib induced a dose-dependent increase in the SRC levels in the HSC. Similar results been reported for SRC inhibition with AZD0530 of Philadelphia chromosome-positive leukaemia cell lines. We speculate that this is due to a compensatory feedback mechanism, suggesting SRC kinase inhibition by ponatinib [37]. Other SRC family members, such as Fyn and Yes, did not change their protein levels in ponatinib-treated cells. In some CML cases of imatinib resistance, upregulation of SRC kinase has been implicated as a BCR-ABL-independent mechanism responsible for imatinib failure [38-40]. Therefore the increase in SRC protein levels observed ponatinib-treated HSC may be an adaptive response. It would be interesting to investigate if other SRC inhibitors, including SU6656, that have anti-proliferative activity in primary human schwannoma cells, also increase SRC levels [20, 41].

Ponatinib lacked selectivity for the merlin-deficient HSC over NF2 wild-type HSC when cultured in the presence of serum and mitogens. This is comparable to results reported by others with the MEK1 inhibitor AZD6244 in primary human schwannoma cells and normal Schwann cells grown in serum-containing medium [21]. Notably, when cells were incubated in growth arresting medium (SCM base + N2 supplement) in the presence of 0.25  $\mu$ M ponatinib for one week, merlin-deficient HSC showed a greater sensitivity to the drug than merlin-expressing HSC. To maintain fetus derived cell lines amenable to drug discovery studies, we routinely culture these embryonic Schwann cells in the presence of serum and other mitogenic supplements, which induces Schwann cells to proliferate. In contrast, both myelinating and non-myelinating Schwann cells are post-mitotic in normal nerves [42-44]. Only after nerve injury do adult Schwann cells de-differentiate and proliferate as part of the nerve repair process [21, 45-48]. Thus, ponatinib's lack of *in vitro* selectivity is not a cause for concern for *in vivo* studies and its potential as a therapeutic for NF2-associated schwannomas.

Ponatinib strongly inhibited PDGFR phosphorylation in merlin-deficient HSC. Studies with other RTK inhibitors that primarily target PDGFR and c-KIT (e.g., nilotinib, imatinib and sorafenib) showed that these RTK inhibitors exhibited strong anti-proliferative activity on primary human schwannoma and HEI-193 cells [10, 12, 41]. Merlin was shown to promote the

internalization of activated PDGFR $\beta$ , a role consistent with increased expression and activation of mitogenic receptors in NF2 schwannomas [13, 14]. In Schwann cells, PDGFR $\alpha$  and  $\beta$  signaling are central to cell proliferation and survival through the Ras/Raf/MEK/ERK and PI3K/AKT signaling pathways [49-51]. In the four schwannoma samples with chronic merlin loss, the p-AKT Ser473 levels downstream of mTORC2 were reported as consistently reduced across tumor samples relative to normal arachnoid and meningioma tissues, as well as in

one immortalized human SC line with acute loss of merlin achieved by an RNAi compared to the immortalized human merlin-expressing SC line [52]. The consistent decrease in mTORC2 signaling activity in schwannoma and merlin-deficient Schwann cells mimics the PDGFR activity results in schwannomas reported by others and our phospho-receptor tyrosine kinase arrays showing a high PDGFR phosphorylation levels in all tumors tested (Figure 7 and 1) [10-12]. Consistent with PDGFR inhibition, we observed a dose-dependent decrease in AKT-Thr308

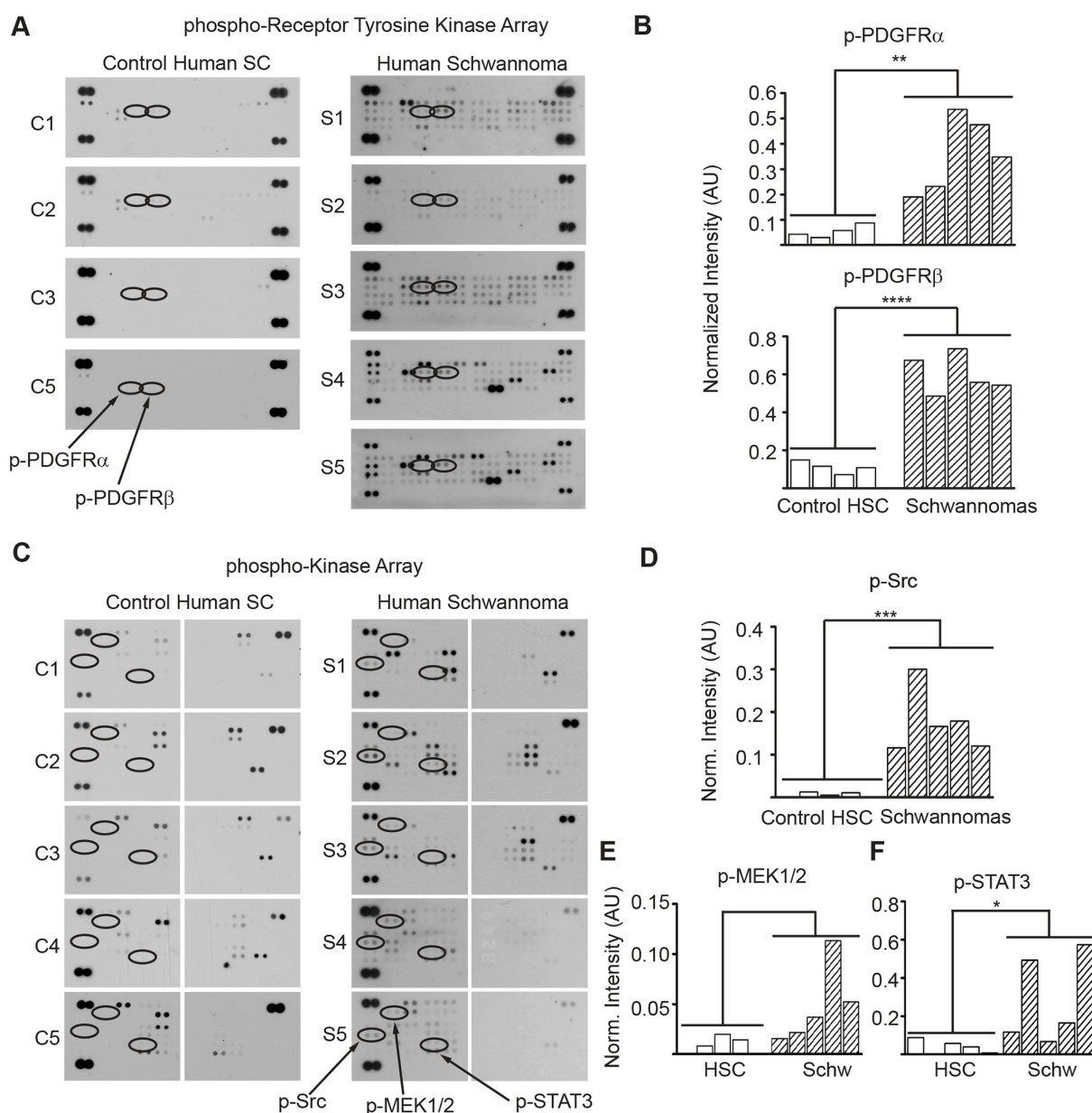


**Figure 7: PDGFR $\alpha/\beta$ , SRC, MEK and STAT3 are overactive in human schwannomas.** (A) Phospho-RTK membrane profile of schwannomas and control cultured primary HSC. (B) Bar graph of the quantitation of p-PDGFR $\alpha$  and p-PDGFR $\beta$  membrane dot intensity normalized to positive controls.  $**p<0.005$ ;  $****p<0.0001$  determined using unpaired *t*-test of control HSC vs. VS populations, two-tailed. (C) Phospho-kinase membrane profile of schwannomas and control cultured primary HSC samples. (D) Bar graph of the quantitation of phospho-SRC, phospho-MEK1/2 and phospho-STAT3 membrane intensity normalized to positive controls.  $*p<0.05$ ;  $***p<0.001$  determined using unpaired *t*-test of control HSC vs. VS populations, two-tailed.

phosphorylation, a PI3K-dependent phosphorylation site, and a decrease in MEK/ERK phosphorylation, similar to those reported in sorafenib-treated schwannoma cells [10, 53, 54]. Moreover, we demonstrated a dose-dependent reduction of cyclin D1 levels that correlates with STAT3 inactivation. STAT3 induces cyclin D1 transcription by binding its promoter region; and ERK1/2 has plays a critical role for induction of cyclin D1 (Figure 6C) [33, 34, 55, 56]. Decreased cyclin-D1 expression together with an increase in the p27<sup>Kip1</sup> level are key to the G<sub>1</sub> to S phase progression block that we observed in ponatinib-treated HSCs.

Unlike traditional dual SRC/ABL inhibitors, ponatinib is a reversible, third-generation inhibitor that binds the unphosphorylated inactive DFG-out conformation of both enzymes [57]. Ponatinib was designed to overcome resistance-inducing BCR-ABL mutations in CML and ALL treated with the first- and second-generation TK inhibitors. It is considered a pan-BCR-ABL inhibitor because it is potently active on ABL-T315I and fourteen other mutants [19]. Ponatinib shows inhibitory activity against ABL/SRC, PDGFR and other kinases, including the FGFR (fibroblast growth factor receptor), Ephrin receptors, FLT3 (FMS-like tyrosine kinase 3), VEGFR1-3 (vascular endothelial growth factor receptor 1-3), Ret (rearranged during transfection) and KIT (mast/stem cell growth factor receptor) [19]. Ponatinib therapy, similar to other TK inhibitors, is associated with severe adverse events, such as arterial thrombosis and liver toxicity, and older patients (>65 years) had higher risk of experiencing adverse effect than younger patients [58, 59]. In a large group of children and adolescents with CML treated with imatinib, assessment of long term growth revealed growth deceleration in both genders [60]. Therefore, adverse effects of long-term treatment in children should be carefully weighed.

Whereas short-term treatment with ponatinib leads to cytostasis, prolonged treatment could lead to cell death or senescence [61, 62]. These sequelae have been reported for B precursor or T cells from ALL patients treated with ponatinib; the treated cells underwent apoptosis after a G<sub>1</sub> cell-cycle arrest by increasing endogenous TNF-related apoptosis-inducing ligand (TRAIL) [63]. Drugs that simply slow schwannoma growth would benefit NF2 patients enormously. If a long-term use of ponatinib is envisioned, we speculate that ponatinib may be used at lower doses in a combinatorial therapeutic approach with other compounds targeting interconnecting pathways, thereby limiting adverse effects. The different mechanisms of kinase inhibition and diverse range and selectivity of small-molecule kinase inhibitors requires that each drug be studied in NF2-relevant cell types, and weighed independently. To this extent, ponatinib treatment effectively reduced viability of merlin-deficient HSC with a robust arrest at the G<sub>1</sub> phase. Ponatinib therapy may be applicable to a larger patient population than

NF2, considering that merlin inactivation also occurs in sporadic schwannomas. Future *in vivo* studies addressing ponatinib alone or in combination as an effective therapy for schwannomas in NF2 mouse models are warranted.

## MATERIALS AND METHODS

### Cell cultures and human vestibular schwannomas

The merlin-deficient HSC line was generated from primary fetal HSC purchased from ScienCell (lot #7228) and authenticated by immunostaining for expression of human nuclear antigen, and SC markers, S100, PLP, O4, and Gap43, and Nestin. Cells were transduced with lentiviral particles expressing human NF2 gene-specific shRNA (GenBank accession no. NM\_000268; TRCN0000237845; TRCN0000039974; TRCN0000039975 and TRCN0000039977, Sigma-Aldrich), shRNA Scrambled, or Turbo-GFP control (Sigma-Aldrich) and then selected with 0.5 mg/ml puromycin. Wild-type and merlin-deficient HSC were cultured in CellBIND dishes (Corning) in complete Schwann cell media (SCM) from ScienCell (basal Schwann cell medium plus 5% fetal bovine serum, Schwann cell growth supplements which contains growth factors, hormones, and proteins necessary for the culture of normal human Schwann cells and 1X-penicillin/streptomycin) unless otherwise specified. Cells were used between passages 9 to 18. Merlin levels were assessed by Western blotting.

Frozen human schwannomas used in phospho-proteome studies were procured with patient informed consent at The Ohio State University College of Medicine according to Institutional Review Board regulations. Human vestibular schwannoma (VS) cells cultured to test ponatinib efficacy were isolated from dissociated fresh human tumors. Fresh VS specimens were procured with patient informed consent at University of Miami Miller School of Medicine according to Institutional Review Board regulations through the Tissue Bank Core Facility.

Normal primary human SCs, a gift from Dr. Patrick Wood (The Miami Project to Cure Paralysis, University of Miami Miller School of Medicine), were used in phospho-proteome studies, and cultured as previously described [64].

### Antibody proteome profiler arrays

Human phospho-RTK (ARY001) and phospho-kinase array (ARY003) kits were purchased from R&D systems. Human schwannoma homogenates and control HSC lysates were prepared and analyzed according to manufacturer's instructions. Arrays were visualized with chemiluminescence and were quantified with ImageJ MicroArray\_Profile.jar plugin or Carestream software; mean intensity of duplicate spots was calculated.

## Antibodies and inhibitors

Rabbit antibodies against merlin (D1D8), c-ABL, phospho-AKT (Thr308; C31E5E), cyclin-D1 (92G2), FYN, p-MEK1/2 (Ser217/221), PDGFR $\alpha$  and  $\beta$ , SRC (36D10), p-SRC family (Tyr416), p-ERK1/2 (D13.14.4E), YES and mouse antibodies recognizing AKT (40D4),  $\beta$ -Actin (8H10D10), MEK1/2 (L38C12), ERK1/2, p27<sup>Kip1</sup> (SX53G8.5) were purchased from Cell Signaling. Rabbit antibodies against p-paxillin (Tyr118) and p-FAK (Tyr577/Tyr576) were purchased from Invitrogen. Rabbit p70 S6 kinase (Thr229) was purchased from ThermoFisher Scientific. Rabbit anti-p-ABL (Tyr245), and human nuclear antigen antibodies were obtained from Millipore and antibodies for myelin-proteolipid protein and GAP43 were from Abcam. The anti-S100 antibody was purchased from Dako. Mouse anti-paxillin antibody was from BD bioscience. Secondary antibodies, goat anti-rabbit IgG conjugated with DyLight 800 4X-PEG, goat anti-Mouse IgG conjugated with DyLight 680, were purchased from Cell Signaling. Ponatinib, perifosine/KRX-0401, and selumetinib/AZD6244 were purchased from SelleckChem. The STAT3 inhibitor S3I-201/NSC-74859 was purchased from MedChem Express.

## Western blot analysis

Cultured HSCs were lysed in modified RIPA buffer as previously described [65] or in 1X-SDS loading buffer plus 2.5 U/ml benzonase. 10  $\mu$ g of protein or 10  $\mu$ l 1X-loading buffer lysate were resolved in 4–20% polyacrylamide gels (Pierce), transferred to PVDF membranes (Immobilon-FL; Millipore), blocked with 5% BSA in TBS, and incubated with primary antibodies overnight at 4°C, and then with their corresponding fluorescence-conjugated secondary antibodies at 1:25,000–1:40,000 dilution. Image acquisition was done using LI-COR® Biosciences Odyssey® Infrared Imaging System and quantification using Odyssey Image Studio Version 3.1 software and ImageJ 1.46r.

## Immunocytochemistry

Cells were grown on German glass coverslips coated with 200  $\mu$ g/ml poly-L-lysine (Sigma-Aldrich). HSCs were fixed in 4% paraformaldehyde and immunostained, and stained images were acquired with a Zeiss LSM710 confocal microscope as previously described [64]. Images were processed with ZEN2011 software.

## Cell viability assay

HSC were seeded at 2,500 cells/well in 20  $\mu$ l of phenol-red free SCM (SCM phenol-red free base, 5% serum, Schwann cell growth supplements containing growth factors, hormones, and proteins and 1X-penicillin/streptomycin) in 384-well plates and incubated with

increasing concentrations of ponatinib in 0.1% DMSO or vehicle alone for 48h. The CellTiter-Fluor cell viability assay (Promega) was used according to manufacturer's specifications [53].

To evaluate cell viability without artificially stimulating proliferation, control and merlin-deficient HSC were cultured and assayed in growth suppressive medium (SCM base, 1X-penicillin/streptomycin –ScienCell, plus N2 supplement-Invitrogen). Cells were seeded in 24 well plates (Corning-CellBIND) at 60,000 cells/well in four replicates, after 4 days incubation at 37°C, 7% CO<sub>2</sub>, cells were treated with 0.25 $\mu$ M ponatinib or a vehicle control for one week. Viability was assessed with a crystal violet assay as previously described [64].

To evaluate cell viability of primary VS cells with *NF2* mutations, two fresh VS were obtained from the Tissue Bank Core Facility at the University of Miami Miller School of Medicine. VS tumors were cut into 1 mm pieces and dissociated in 0.5 mg/ml collagenase (~150U/ml) and dispase (2.5 mg/ml) in Dulbecco's Modified Eagle Medium (Sigma) for 1h followed by 0.25% Trypsin for 30 minutes at 37°C. Digested tissue was triturated and centrifuged at 1500 rpm at 4°C for 10 minutes. Supernatant was discarded and cells were resuspended and cultured using Schwann Cell Media (ScienCell) on culture flasks pre-treated with 0.1% poly-L-lysine (Sigma) and 25 mg/ml laminin (ThermoScientific). Cells from Passage 2 were then seeded in a 96 well plate (Costar, Corning) at 5,000 cells/well in six replicates. After 24 hours of incubation at 37°C, 5% CO<sub>2</sub>, cells were treated with ponatinib at different concentrations or 0.05% DMSO for 48h. Viability was assessed with a crystal violet assay as previously described [64].

## DNA sequencing of VS

Genomic DNA was isolated and purified using Trizol (Invitrogen) as per the manufacturer's protocol. A total of 17 pairs of primers were designed for the amplification and sequencing of the coding exons and their flanking splice sites using the Primer 3 program (<http://bioinfo.ut.ee/primer3-0.4.0/>). The complete coding sequences of *NF2* were amplified by PCR. DNA (~1  $\mu$ g) was amplified with *NF2*-specific primer pairs in 50 $\mu$ L, containing 10XPCR Buffer (pH 8.5), 0.4 mM dNTP mix (Promega Corporation), 0.4 pmol/ $\mu$ L of each primer, and 0.0625 units of *Taq* DNA polymerase (Eppendorf AG). DNA templates were amplified using the following program: 95°C for 3 min; 35 cycles of 94°C for 50 s, 60°C for 50 s, 72°C for 60 s; and final extension of 72°C for 5 min. Direct sequencing of PCR products were performed on both strands using the ABI Prism BigDye Terminator reaction kit and ABI 3100 DNA sequencer or with Beckman Coulter 2000 XL instrument and appropriate kits.

## Cell-cycle and G<sub>1</sub> proteins analysis by flow cytometry

The Click-iT EdU, FxCycle stain and Live/Dead fixable dead cell stain kits were purchased from Molecular Probes (ThermoFisher Scientific). Cells were seeded in 6-well plates and treated overnight with an inhibitor or vehicle. On the next day, 10  $\mu$ M EdU was added to the cultures for 3 h, and then cells were harvested (total 24-h inhibitor incubation), stained with fixable violet live/dead stain, and permeabilized. EdU and DNA labeling was conducted according to manufacturer's instruction. Cell cycle analysis was done on gated live cells. For the cyclin D1/p27<sup>Kip1</sup> expression study [66], cultures were treated with an inhibitor or vehicle for 24 h and then harvested, fixed with 4% paraformaldehyde for 10 min at 37°C, chilled for 1 min, and permeabilized for 30 min in 90% methanol. Fixed cells were transferred to a Falcon 5 ml tube through a cell strainer cap, rinsed twice with 0.5% BSA in PBS, and immunostained by incubating for 1h at room temperature with a cyclin D1 (1:400) or p27<sup>Kip1</sup> (1:3,000) antibody, followed by a 30-min incubation with a goat anti-rabbit or anti-mouse-Alexa488 secondary antibody. After one wash, cells were resuspended in 1 ml of 0.5% BSA and stained for 30 min with 200nM FxCycle Far Red DNA stain supplemented with 0.1mg/ml of ribonucleaseA (Invitrogen). A BD FACS Canto-II flow cytometer (BD Biosciences) with the BD FACSDiva™ 6.1.3 software was used for data acquisition and FlowJo software was used for data analysis.

## Statistical analysis

Statistical analysis was performed using GraphPad Prism v5.0 for Windows. Ponatinib dose-response experiments were analyzed by non-linear regression (four parameters). Other experiments were analyzed by applying two-way ANOVA and Bonferroni multiple comparisons post-test, one-way ANOVA, and Dunnett's multiple comparison post-test or unpaired *t*-test, two-tailed as noted.

## Author contributions

A.M.P. designed experiments, performed research, analyzed and interpreted data, and wrote the manuscript; J.G., M.B., S.K.P., O.R.B., B.Z. and R.M. performed research and analyzed data; C.T.D., D.Y., F.F.T., X.Z.L., L.S.C., D.B.W., and A.J.C. designed experiments, analyzed data, contributed to intellectual development of the manuscript, and revised the manuscript; C.F.V. supervised the project, analyzed data, and wrote the manuscript.

## ACKNOWLEDGMENTS

We thank Dr. Michael Ivan and Dr. Jacques Morcos for their generosity and time harvesting tumors. We thank Drs. Annette Khaled and Deborah Altomare for helpful discussions, and Jeremiah Oyer for assistance with flow cytometry.

## CONFLICTS OF INTEREST

The authors reported no potential conflicts of interest.

## GRANT SUPPORT

This work was supported by a Department of Defense (NF140044 to CFV and NF150080 to LSC) and a Children's Tumor Foundation Drug Discovery Award 2014 to CFV. JG received support from UCF's Office of Undergraduate Research.

## REFERENCES

1. Blakeley JO, Plotkin SR. Therapeutic advances for the tumors associated with neurofibromatosis type 1, type 2, and schwannomatosis. *Neuro-oncology*. 2016; 18:624-38.
2. Rouleau GA, Merel P, Lutchman M, Sanson M, Zucman J, Marineau C, Hoang-Xuan K, Demczuk S, Desmaze C, Plougastel B, et al. Alteration in a new gene encoding a putative membrane-organizing protein causes neurofibromatosis type 2. *Nature*. 1993; 363:515-521.
3. Trofatter JA, MacCollin MM, Rutter JL, Murrell JR, Duyao MP, Parry DM, Eldridge R, Kley N, Menon AG, Pulaski K, et al. A novel moesin-, ezrin-, radixin-like gene is a candidate for the neurofibromatosis 2 tumor suppressor. *Cell*. 1993; 72:791-800.
4. Petrilli AM, Fernandez-Valle C. Role of Merlin/NF2 inactivation in tumor biology. *Oncogene*. 2015; 35:537-48.
5. Farschtschi S, Kollmann P, Dalchow C, Stein A and Mautner VF. Reduced dosage of bevacizumab in treatment of vestibular schwannomas in patients with neurofibromatosis type 2. *Eur Arch Otorhinolaryngol*. 2015; 272:3857-3860.
6. Karajannis MA and Ferner RE. Neurofibromatosis-related tumors: emerging biology and therapies. *Current opinion in pediatrics*. 2015; 27:26-33.
7. Ammoun S and Hanemann CO. Emerging therapeutic targets in schwannomas and other merlin-deficient tumors. *Nature reviews Neurology*. 2011; 7:392-399.
8. Andrae J, Gallini R and Betsholtz C. Role of platelet-derived growth factors in physiology and medicine. *Genes Dev*. 2008; 22:1276-1312.
9. Roskoski R, Jr. Src protein-tyrosine kinase structure, mechanism, and small molecule inhibitors. *Pharmacol Res*. 2015; 94:9-25.

10. Ammoun S, Flaiz C, Ristic N, Schuldt J and Hanemann CO. Dissecting and targeting the growth factor-dependent and growth factor-independent extracellular signal-regulated kinase pathway in human schwannoma. *Cancer Res.* 2008; 68:5236-5245.
11. Lallemand D, Manent J, Couvelard A, Watilliaux A, Siena M, Chareyre F, Lampin A, Niwa-Kawakita M, Kalamarides M and Giovannini M. Merlin regulates transmembrane receptor accumulation and signaling at the plasma membrane in primary mouse Schwann cells and in human schwannomas. *Oncogene.* 2009; 28:854-865.
12. Mukherjee J, Kamnasaran D, Balasubramaniam A, Radovanovic I, Zadeh G, Kiehl TR and Guha A. Human schwannomas express activated platelet-derived growth factor receptors and c-kit and are growth inhibited by Gleevec (Imatinib Mesylate). *Cancer Res.* 2009; 69:5099-5107.
13. Ammoun S, Cunliffe CH, Allen JC, Chiriboga L, Giancotti FG, Zagzag D, Hanemann CO and Karajannis MA. ErbB/HER receptor activation and preclinical efficacy of lapatinib in vestibular schwannoma. *Neuro-oncology.* 2010; 12:834-843.
14. Fraenzer JT, Pan H, Minimo L, Jr., Smith GM, Knauer D and Hung G. Overexpression of the NF2 gene inhibits schwannoma cell proliferation through promoting PDGFR degradation. *Int J Oncol.* 2003; 23:1493-1500.
15. Houshmandi SS, Emnett RJ, Giovannini M and Gutmann DH. The neurofibromatosis 2 protein, merlin, regulates glial cell growth in an ErbB2- and Src-dependent manner. *Molecular and cellular biology.* 2009; 29:1472-1486.
16. Zhou L and Hanemann CO. Merlin, a multi-suppressor from cell membrane to the nucleus. *FEBS Lett.* 2012; 586:1403-1408.
17. Zhou T, Commodore L, Huang WS, Wang Y, Thomas M, Keats J, Xu Q, Rivera VM, Shakespeare WC, Clackson T, Dalgarno DC and Zhu X. Structural mechanism of the Pan-BCR-ABL inhibitor ponatinib (AP24534): lessons for overcoming kinase inhibitor resistance. *Chem Biol Drug Des.* 2011; 77:1-11.
18. Blanc J, Geney R and Menet C. Type II kinase inhibitors: an opportunity in cancer for rational design. *Anticancer Agents Med Chem.* 2013; 13:731-747.
19. O'Hare T, Shakespeare WC, Zhu X, Eide CA, Rivera VM, Wang F, Adrian LT, Zhou T, Huang WS, Xu Q, Metcalf CA 3rd, Tyner JW, Loriaux MM, et al. AP24534, a pan-BCR-ABL inhibitor for chronic myeloid leukemia, potently inhibits the T315I mutant and overcomes mutation-based resistance. *Cancer Cell.* 2009; 16:401-412.
20. Zhou L, Ercolano E, Ammoun S, Schmid MC, Barczyk MA and Hanemann CO. Merlin-deficient human tumors show loss of contact inhibition and activation of Wnt/beta-catenin signaling linked to the PDGFR/Src and Rac/PAK pathways. *Neoplasia.* 2011; 13:1101-1112.
21. Ammoun S, Ristic N, Matthies C, Hilton DA and Hanemann CO. Targeting ERK1/2 activation and proliferation in human primary schwannoma cells with MEK1/2 inhibitor AZD6244. *Neurobiology of disease.* 2010; 37:141-146.
22. Hossain S, Fragoso G, Mushynski WE and Almazan G. Regulation of peripheral myelination by Src-like kinases. *Exp Neurol.* 2010; 226:47-57.
23. Kumar A, Jaggi AS and Singh N. Pharmacology of Src family kinases and therapeutic implications of their modulators. *Fundam Clin Pharmacol.* 2015; 29:115-130.
24. McLean GW, Carragher NO, Avizienyte E, Evans J, Brunton VG and Frame MC. The role of focal-adhesion kinase in cancer - a new therapeutic opportunity. *Nat Rev Cancer.* 2005; 5:505-515.
25. Calalb MB, Polte TR and Hanks SK. Tyrosine phosphorylation of focal adhesion kinase at sites in the catalytic domain regulates kinase activity: a role for Src family kinases. *Molecular and cellular biology.* 1995; 15:954-963.
26. Turner CE. Paxillin interactions. *J Cell Sci.* 2000; 113 Pt 23:4139-4140.
27. Heldin CH and Lennartsson J. Structural and functional properties of platelet-derived growth factor and stem cell factor receptors. *Cold Spring Harb Perspect Biol.* 2013; 5:a009100.
28. Alessi DR, Andjelkovic M, Caudwell B, Cron P, Morrice N, Cohen P and Hemmings BA. Mechanism of activation of protein kinase B by insulin and IGF-1. *EMBO J.* 1996; 15:6541-6551.
29. Alessi DR, Kozlowski MT, Weng QP, Morrice N and Avruch J. 3-Phosphoinositide-dependent protein kinase 1 (PDK1) phosphorylates and activates the p70 S6 kinase *in vivo* and *in vitro*. *Curr Biol.* 1998; 8:69-81.
30. Bowman T, Broome MA, Sinibaldi D, Wharton W, Pledger WJ, Sedivy JM, Irby R, Yeatman T, Courtneidge SA and Jove R. Stat3-mediated Myc expression is required for Src transformation and PDGF-induced mitogenesis. *Proc Natl Acad Sci U S A.* 2001; 98:7319-7324.
31. Kortylewski M, Jove R and Yu H. Targeting STAT3 affects melanoma on multiple fronts. *Cancer Metastasis Rev.* 2005; 24:315-327.
32. Wang YZ, Wharton W, Garcia R, Kraker A, Jove R and Pledger WJ. Activation of Stat3 preassembled with platelet-derived growth factor beta receptors requires Src kinase activity. *Oncogene.* 2000; 19:2075-2085.
33. Kim DJ, Chan KS, Sano S and Digiovanni J. Signal transducer and activator of transcription 3 (Stat3) in epithelial carcinogenesis. *Mol Carcinog.* 2007; 46:725-731.
34. Meloche S and Pouyssegur J. The ERK1/2 mitogen-activated protein kinase pathway as a master regulator of the G1- to S-phase transition. *Oncogene.* 2007; 26:3227-3239.
35. Jakel H, Peschel I, Kunze C, Weinl C and Hengst L. Regulation of p27 (Kip1) by mitogen-induced tyrosine phosphorylation. *Cell Cycle.* 2012; 11:1910-1917.

36. Ammoun S, Schmid MC, Zhou L, Ristic N, Ercolano E, Hilton DA, Perks CM and Hanemann CO. Insulin-like growth factor-binding protein-1 (IGFBP-1) regulates human schwannoma proliferation, adhesion and survival. *Oncogene*. 2012; 31:1710-1722.
37. Gwanmesia PM, Romanski A, Schwarz K, Bacic B, Ruthardt M and Ottmann OG. The effect of the dual Src/Abl kinase inhibitor AZD0530 on Philadelphia positive leukaemia cell lines. *BMC Cancer*. 2009; 9:53.
38. Donato NJ, Wu JY, Stapley J, Lin H, Arlinghaus R, Aggarwal BB, Shishodia S, Albitar M, Hayes K, Kantarjian H and Talpaz M. Imatinib mesylate resistance through BCR-ABL independence in chronic myelogenous leukemia. *Cancer Res*. 2004; 64:672-677.
39. Huang WS, Zhu X, Wang Y, Azam M, Wen D, Sundaramoorthi R, Thomas RM, Liu S, Banda G, Lentini SP, Das S, Xu Q, Keats J, et al. 9-(Arenethenyl) purines as dual Src/Abl kinase inhibitors targeting the inactive conformation: design, synthesis, and biological evaluation. *J Med Chem*. 2009; 52:4743-4756.
40. Jabbour E, Kantarjian H and Cortes J. Use of second- and third-generation tyrosine kinase inhibitors in the treatment of chronic myeloid leukemia: an evolving treatment paradigm. *Clin Lymphoma Myeloma Leuk*. 2015; 15:323-334.
41. Ammoun S, Schmid MC, Triner J, Manley P and Hanemann CO. Nilotinib alone or in combination with selumetinib is a drug candidate for neurofibromatosis type 2. *Neuro-oncology*. 2011; 13:759-766.
42. Giovannini M, Robanus-Maandag E, van der Valk M, Niwa-Kawakita M, Abramowski V, Goutebroze L, Woodruff JM, Berns A and Thomas G. Conditional biallelic Nf2 mutation in the mouse promotes manifestations of human neurofibromatosis type 2. *Genes Dev*. 2000; 14:1617-1630.
43. Jessen KR, Mirsky R and Morgan L. Role of cyclic AMP and proliferation controls in Schwann cell differentiation. *Ann N Y Acad Sci*. 1991; 633:78-89.
44. Zorick TS and Lemke G. Schwann cell differentiation. *Curr Opin Cell Biol*. 1996; 8:870-876.
45. Atanasoski S, Boentert M, De Ventura L, Pohl H, Baranek C, Beier K, Young P, Barbacid M and Suter U. Postnatal Schwann cell proliferation but not myelination is strictly and uniquely dependent on cyclin-dependent kinase 4 (cdk4). *Mol Cell Neurosci*. 2008; 37:519-527.
46. Mirsky R, Woodhoo A, Parkinson DB, Arthur-Farraj P, Bhaskaran A and Jessen KR. Novel signals controlling embryonic Schwann cell development, myelination and dedifferentiation. *J Peripher Nerv Syst*. 2008; 13:122-135.
47. Atanasoski S, Shumas S, Dickson C, Scherer SS and Suter U. Differential cyclin D1 requirements of proliferating Schwann cells during development and after injury. *Mol Cell Neurosci*. 2001; 18:581-592.
48. Kim HA, Pomeroy SL, Whoriskey W, Pawlitzky I, Benowitz LI, Sicinski P, Stiles CD and Roberts TM. A developmentally regulated switch directs regenerative growth of Schwann cells through cyclin D1. *Neuron*. 2000; 26:405-416.
49. Heldin CH and Westermark B. Mechanism of action and *in vivo* role of platelet-derived growth factor. *Physiol Rev*. 1999; 79:1283-1316.
50. Meier C, Parmantier E, Brennan A, Mirsky R and Jessen KR. Developing Schwann cells acquire the ability to survive without axons by establishing an autocrine circuit involving insulin-like growth factor, neurotrophin-3, and platelet-derived growth factor-BB. *J Neurosci*. 1999; 19:3847-3859.
51. Peulve P, Laquerriere A, Paresy M, Hemet J and Tadie M. Establishment of adult rat Schwann cell cultures: effect of b-FGF, alpha-MSH, NGF, PDGF, and TGF-beta on cell cycle. *Exp Cell Res*. 1994; 214:543-550.
52. James MF, Stivison E, Beauchamp R, Han S, Li H, Wallace MR, Gusella JF, Stemmer-Rachamimov AO and Ramesh V. Regulation of mTOR complex 2 signaling in neurofibromatosis 2-deficient target cell types. *Mol Cancer Res*. 2012; 10:649-659.
53. Petrilli AM, Fuse MA, Donnan MS, Bott M, Sparrow NA, Tondera D, Huffziger J, Frenzel C, Malany CS, Echeverri CJ, Smith L and Fernandez-Valle C. A chemical biology approach identified PI3K as a potential therapeutic target for neurofibromatosis type 2. *American journal of translational research*. 2014; 6:471-493.
54. Rong R, Tang X, Gutmann DH and Ye K. Neurofibromatosis 2 (NF2) tumor suppressor merlin inhibits phosphatidylinositol 3-kinase through binding to PIKE-L. *Proc Natl Acad Sci U S A*. 2004; 101:18200-18205.
55. Masuda M, Suzui M, Yasumatu R, Nakashima T, Kuratomi Y, Azuma K, Tomita K, Komiyama S and Weinstein IB. Constitutive activation of signal transducers and activators of transcription 3 correlates with cyclin D1 overexpression and may provide a novel prognostic marker in head and neck squamous cell carcinoma. *Cancer Res*. 2002; 62:3351-3355.
56. Sinibaldi D, Wharton W, Turkson J, Bowman T, Pledger WJ and Jove R. Induction of p21WAF1/CIP1 and cyclin D1 expression by the Src oncoprotein in mouse fibroblasts: role of activated STAT3 signaling. *Oncogene*. 2000; 19:5419-5427.
57. Hari SB, Perera BG, Ranjitkar P, Seeliger MA and Maly DJ. Conformation-selective inhibitors reveal differences in the activation and phosphate-binding loops of the tyrosine kinases Abl and Src. *ACS Chem Biol*. 2013; 8:2734-2743.
58. Hoy SM. Ponatinib: a review of its use in adults with chronic myeloid leukaemia or Philadelphia chromosome-positive acute lymphoblastic leukaemia. *Drugs*. 2014; 74:793-806.
59. Moslehi JJ and Deininger M. Tyrosine Kinase Inhibitor-Associated Cardiovascular Toxicity in Chronic Myeloid Leukemia. *J Clin Oncol*. 2015; 33:4210-4218.
60. Millot F, Guilhot J, Baruchel A, Petit A, Leblanc T, Bertrand Y, Mazingue F, Lutz P, Verite C, Berthou C, Galambrun

- C, Nicolas S, Yacouben K, et al. Growth deceleration in children treated with imatinib for chronic myeloid leukaemia. *Eur J Cancer*. 2014; 50:3206-3211.
61. Mombach JC, Bugs CA and Chaouiya C. Modelling the onset of senescence at the G1/S cell cycle checkpoint. *BMC Genomics*. 2014; 15:S7.
  62. Pucci B, Kasten M and Giordano A. Cell cycle and apoptosis. *Neoplasia*. 2000; 2:291-299.
  63. Ehrhardt H, Wachter F, Grunert M and Jeremias I. Cell cycle-arrested tumor cells exhibit increased sensitivity towards TRAIL-induced apoptosis. *Cell Death Dis*. 2013; 4:e661.
  64. Petrilli A, Copik A, Posadas M, Chang LS, Welling DB, Giovannini M and Fernandez-Valle C. LIM domain kinases as potential therapeutic targets for neurofibromatosis type 2. *Oncogene*. 2014; 33:3571-3582.
  65. Petrilli A, Bott M and Fernandez-Valle C. Inhibition of SIRT2 in merlin/NF2-mutant Schwann cells triggers necrosis. *Oncotarget*. 2013; 4:2354-2365. doi: 10.18632/oncotarget.1422.
  66. Darzynkiewicz Z, Gong J, Juan G, Ardel B and Traganos F. Cytometry of cyclin proteins. *Cytometry*. 1996; 25:1-13.



# Combination Therapy with c-Met and Src Inhibitors Induces Caspase-Dependent Apoptosis of Merlin-Deficient Schwann Cells and Suppresses Growth of Schwannoma Cells

Marisa A. Fuse<sup>1</sup>, Stephani Klingeman Plati<sup>1</sup>, Sarah S. Burns<sup>2,3</sup>, Christine T. Dinh<sup>4</sup>, Olena Bracho<sup>4</sup>, Denise Yan<sup>4</sup>, Rahul Mittal<sup>4</sup>, Rulong Shen<sup>5</sup>, Julia N. Soulakova<sup>1</sup>, Alicja J. Copik<sup>1</sup>, Xue Zhong Liu<sup>4</sup>, Fred F. Telischi<sup>4</sup>, Long-Sheng Chang<sup>2,3,5</sup>, Maria Clara Franco<sup>1</sup>, and Cristina Fernandez-Valle<sup>1</sup>

## Abstract

Neurofibromatosis type 2 (NF2) is a nervous system tumor disorder caused by inactivation of the merlin tumor suppressor encoded by the *NF2* gene. Bilateral vestibular schwannomas are a diagnostic hallmark of NF2. Mainstream treatment options for NF2-associated tumors have been limited to surgery and radiotherapy; however, off-label uses of targeted molecular therapies are becoming increasingly common. Here, we investigated drugs targeting two kinases activated in NF2-associated schwannomas, c-Met and Src. We demonstrated that merlin-deficient mouse Schwann cells (MD-MSC) treated with the c-Met inhibitor, cabozantinib, or the Src kinase inhibitors, dasatinib and saracatinib, underwent a G<sub>1</sub> cell-cycle arrest.

However, when MD-MSCs were treated with a combination of cabozantinib and saracatinib, they exhibited caspase-dependent apoptosis. The combination therapy also significantly reduced growth of MD-MSCs in an orthotopic allograft mouse model by greater than 80% of vehicle. Moreover, human vestibular schwannoma cells with *NF2* mutations had a 40% decrease in cell viability when treated with cabozantinib and saracatinib together compared with the vehicle control. This study demonstrates that simultaneous inhibition of c-Met and Src signaling in MD-MSCs triggers apoptosis and reveals vulnerable pathways that could be exploited to develop NF2 therapies. *Mol Cancer Ther*; 16(11); 2387–98. ©2017 AACR.

## Introduction

Neurofibromatosis type 2 (NF2) is a genetic disorder characterized by the development of vestibular schwannomas (VS) and meningiomas. NF2 is caused by mutations in the *NF2* gene encoding the tumor suppressor merlin (1, 2). Loss of merlin function in Schwann cells leads to aberrant signaling in molecular pathways involved in cell survival and proliferation, resulting in schwannoma formation (3).

VS treatment relies on surgical removal of tumors, frequently causing nerve damage. A less invasive option, stereotactic radiosurgery, controls tumor growth with hearing preservation rates

consistently approaching approximately 20% to 44% at 10 years (4, 5). However, the rate of malignant transformation or secondary malignancies following radiation for NF2 is estimated to be approximately 5%, representing a seven-fold increase compared with NF2 patients without irradiation (6). Clinical trials with off-label use of FDA-approved drugs, such as lapatinib and everolimus (RAD001), have shown moderate success in slowing NF2 schwannoma growth (7, 8). More success has been achieved with bevacizumab, a mAb against the VEGF-A (9). Bevacizumab promotes VS tumor shrinkage and hearing response in approximately 40% to 50% of NF2 patients (10), but has adverse side-effects, including hypertension and proteinuria, and amenorrhea in women (11, 12). Thus, it is imperative to identify drugs suitable for prolonged treatment in NF2 patients. Identifying molecular targets that allow re-purposing of FDA-approved drugs would accelerate development of NF2 therapies.

Microarray and qPCR analysis revealed that expression of c-Met, a receptor tyrosine kinase (RTK), is elevated in human VS compared with nerves or Schwann cells (13, 14). Additionally, hepatocyte growth factor (HGF), the c-Met ligand, is a potential NF2 biomarker (15). Merlin directly interacts with HGF-regulated tyrosine kinase substrate (HRS), supporting a role of merlin in c-Met/HRS signaling (16). The loss of merlin function could contribute to aberrant c-Met signaling, leading to schwannoma formation. C-Met activates several cell proliferation and survival signaling pathways and is mitogenic for Schwann cells (17, 18). Cabozantinib (XL184, Cabometyx™, Exelixis) is a small-molecule

<sup>1</sup>Division of Neuroscience, Burnett School of Biomedical Science, College of Medicine, University of Central Florida, Orlando, Florida. <sup>2</sup>Center for Childhood Cancer and Blood Diseases, Nationwide Children's Hospital, The Ohio State University, Columbus, Ohio. <sup>3</sup>Department of Pediatrics, The Ohio State University, Columbus, Ohio. <sup>4</sup>Department of Otolaryngology, University of Miami Miller School of Medicine, Miami, Florida. <sup>5</sup>Department of Pathology, The Ohio State University, Columbus, Ohio.

**Note:** Supplementary data for this article are available at Molecular Cancer Therapeutics Online (<http://mct.aacrjournals.org/>).

**Corresponding Author:** Cristina Fernandez-Valle, University of Central Florida, 6900 Lake Nona Blvd., Orlando, FL 32827. Phone: 407-266-7033; Fax: 407-266-7002; E-mail: cfv@ucf.edu

doi: 10.1158/1535-7163.MCT-17-0417

©2017 American Association for Cancer Research.

inhibitor of c-Met and other RTKs involved in cell motility and metastasis, and inhibits VEGFR2-dependent angiogenesis (19). It is FDA-approved for treatment of tumors with elevated c-Met and HGF expression, such as medullary thyroid cancer (20) and renal cell carcinoma (21). Cabozantinib also reduces proliferation of NF1-associated malignant peripheral nerve sheath tumor (MPNST) cells *in vitro* and suppresses tumor growth in mouse models (22, 23).

Src-family kinases are another promising drug target for NF2-associated schwannomas. Compared with normal Schwann cells, VS have increased levels of phosphorylated Src and focal adhesion kinase (FAK), resulting in deregulation of cell proliferation pathways (24). Dasatinib (SPRYCEL<sup>®</sup>, Bristol-Myers Squibb) is a type I, ATP-competitive Src/Abl kinase inhibitor. It is FDA-approved for chronic myeloid leukemia and acute lymphocytic leukemia with mutant Abl kinase expression (25, 26) and reduces growth of both solid tumors and blood cancers (27). In tumor cell lines, dasatinib is a cytostatic agent that inhibits cell proliferation, invasion, and metastasis (28). Similar to dasatinib, saracatinib (AZD0530, AstraZeneca) is another type I, ATP-competitive Src/Abl inhibitor, but binds the inactive Src conformation (29). Preclinical studies confirm the ability of saracatinib to reduce proliferation and migration/invasion of tumor cells (30). Moreover, Src inhibition by saracatinib enhances the sensitivity of gastric tumors to c-Met inhibitors (31), supporting the use of Src and c-Met inhibitors in combination.

In this study, we identified a potential combination therapy for NF2-associated schwannomas. Although cabozantinib and saracatinib each promoted G<sub>1</sub> cell-cycle arrest, their combination induced apoptosis and suppressed the growth of merlin-deficient Schwann cell allografts as well as primary human VS cells. Our results support targeting c-Met and Src kinases as a potential treatment for NF2-associated schwannomas.

## Materials and Methods

### Cell culture

Wild-type (WT) and merlin-deficient (MD) mouse Schwann cells (MSC) were generated and authenticated as previously described (ref. 32; MD-MSCs created in-house in 2010) and routinely tested for *Mycoplasma* contamination (LookOut *Mycoplasma* PCR Detection Kit; Sigma). VS were obtained according to the Institutional Review Board-approved human subject protocol with patient informed consent at University of Miami Miller School of Medicine through the Tissue Bank Core Facility and were used to prepare primary VS cultures (33). A description of the genetic analysis of human VS samples and the generation of human SC lines is provided in Supplementary Methods.

### MD-MSC transduction

MD-MSCs were grown in six-well CellBind plates (Corning) at 200,000 cells/well for 24 hours and then received transduction growth media with 8 µg/mL of polybrene. Lentiviral luciferase particles [prepared from pLenti PGK V5-LUC Neo (Addgene #21471)] were added at five multiplicity of infection (MOI) for 18 hours, followed by growth media for 24 hours prior to selection media containing 1 µg/mL puromycin. The same protocol was followed for the lentiviral shRNA knockdown of c-Met (Sigma-Aldrich catalog no. SHCLNV-NM\_008591-TRCN0000023529 for c-Met shRNA and catalog no. SHC202V for scrambled shRNA viruses).

### Drugs and high-content screening

Cabozantinib, saracatinib (Selleckchem and MedChemExpress), and dasatinib (Selleckchem) were dissolved in DMSO (10 mmol/L stock) for *in vitro* experiments. MD-MSCs and WT-MSCs were seeded in a 384-well CellBind plate at 1,000 and 3,250 cells/well, respectively, and treated with drug for 48 hours, followed by paraformaldehyde fixation and Hoechst dye staining. Images were acquired with Image Express (micro-automated microscope) and analyzed using the Definiens platform (Definiens, Inc.).

### Cell viability and caspase 3/7 activation assays

MD-MSCs were seeded in 384-well CellBind plates at 2,500 cells/well in phenol red-free (prf) growth media. WT-MSCs were seeded at 15,000 to 20,000 cells/well in 96-well plates coated with poly-L-lysine (200 µg/mL) and laminin (25 µg/mL). After attachment, cells were treated with drugs or DMSO for 48 hours. Cell viability was determined using the CellTiter-Fluor Assay (Promega). Primary VS cells were seeded in a 96-well plate at 5,000 cells/well. After 24 hours, cells were treated with drugs or DMSO for 48 hours. Cell viability was determined with a crystal violet assay as previously described (32). For caspase activation assays, MD-MSCs were seeded in 384-well CellBind plates at 5,000 cells/well in prf growth media and were treated with drugs for 18 hours. The Apo-ONE Homogeneous Caspase 3/7 Assay (Promega) was used per the manufacturer's instructions with fluorescence measurement using an H1 Synergy plate reader.

### Apoptosis inhibitors

MD-MSCs were seeded as described for cell viability assays. Cells were treated for 24 hours with drugs and/or inhibitors of apoptosis: Fas(human):Fc(human) (ALX-522-002, Enzo Life Sciences), Z-DEVD-FMK Caspase-3 Inhibitor, Z-LEHD-FMK Caspase-9 Inhibitor (#550378, #550381, BD Pharmingen), and Z-IETD-FMK Caspase-8 Inhibitor (#FMK007, R&D Systems). The inhibitors were dissolved at 20 mmol/L in DMSO. Fas:Fc was dissolved at 1 mg/mL in water. A cross-linking enhancer (#ALX-203-001, Enzo Life Sciences) was used with the Fas:Fc treatment. Cell viability was measured using the CellTiter-Fluor assay.

### Genetic analysis of NF2 mutations in human VS samples

Genomic DNA was isolated and purified using Trizol (Invitrogen). Samples were subjected to NF2 multiplex ligation-dependent probe amplification (MLPA) using the NF2 MLPA Kit (MRC-Holland) per the manufacturer's instructions.

### Violet ratiometric assay

MD-MSCs were grown in six-well CellBind plates to approximately 80% confluence and treated with drugs or DMSO for 19 hours. Cells were harvested with 0.05% Trypsin and resuspended in 1 mL of HBSS/million cells. The Violet Ratiometric Assay (Invitrogen) was used according to the manufacturer's instructions. Cell populations were measured with a Cytotflex (Beckman Coulter) flow cytometer and analyzed with CytExpert (Beckman Coulter) software.

### Western blots

Western blots were performed as previously described (34). Cells were extracted with 4% SDS, 0.01% bromophenol blue, 10% glycerol, and 100 mmol/L dithiothreitol. The following antibodies were used: anti-cleaved caspase 3 (17 to 19 kDa), total

caspase 3 (35 kDa), p-Src (Y416), Src (60 kDa), p-FAK (Y576), p-c-Met (Y1234/Y1235),  $\beta$ -actin (45 kDa), p-VEGFR2/3 (230 kDa), p-ERK1/2, ERK1/2 (42–44 kDa), p-Akt (T308), Akt (60 kDa), cyclin D<sub>1</sub> (36 kDa), and P27<sup>Kip1</sup> (27 kDa) from Cell Signaling Technology; FAK (125 kDa) and paxillin (68 kDa) from BD Biosciences; Fas (45 kDa) from Santa Cruz Biotechnology; p-paxillin (Y118) and c-Met (145 kDa) from Thermo Fisher Scientific. Primary antibodies were prepared in 1:1 Odyssey Blocking Buffer (TBS-0.1% Tween) and incubated overnight at 4°C or for 1 hour at room temperature. Secondary antibodies were prepared similarly but with 0.02% SDS and incubated for 45 to 60 minutes in the dark at room temperature. Western blots were quantified using the Odyssey System (LI-COR Biosciences).

### Pharmacokinetics

NSG (*NOD.Cg-Prkdcscid Il2rgtm1Wjl/SzJ*) mice were cared for as approved by the University of Central Florida (UCF) Institutional Animal Care and Usage Committee. The animal facility at UCF is accredited by the Association for Assessment and Accreditation of Laboratory Animal Care. Three mice were dosed by oral gavage (20 mg/kg dasatinib, 25 mg/kg saracatinib, or 40 mg/kg cabozantinib in a vehicle containing 1.25% polyethylene glycol, 2.5% Tween-80, and 5% DMSO) and one mouse received vehicle only. At the indicated times, mice were sacrificed. Blood and sciatic nerves were collected and analyzed by mass spectrometry at Sanford Burnham Prebys Medical Discovery Institute (Lake Nona, FL).

### Orthotopic sciatic nerve allograft model

Male and female NSG mice were bred in house and used at 6 to 8 weeks of age. Following anesthesia with isoflurane (1–3% in oxygen), the right sciatic nerve was injected with 5,000 luciferase-expressing MD-MSCs in 3  $\mu$ L of L-15 prf media. Wounds were sealed with Vetbond. Mice were imaged with an In Vivo Imaging System (IVIS, Caliper) 15 minutes after intraperitoneal injection of luciferin (150 mg/kg) to confirm engraftment, were assigned to treatment groups (Day 0) and began daily treatment with the vehicle (as above), saracatinib (25 mg/kg), cabozantinib (12.5 mg/kg), or a combination of saracatinib and cabozantinib (25 and 12.5 mg/kg, respectively). Mice were imaged with IVIS every 7 days and were sacrificed at day 14. Tumor grafts and contralateral sciatic nerves were removed, weighed and photographed, followed by fixation overnight in 4% paraformaldehyde and storage in 30% sucrose/0.02% azide.

### Immunohistochemistry

Fixed grafts and nerves were embedded in paraffin and cut into 4- $\mu$ m sections. Antigen retriever reaction was performed by heating sections in 0.1 mol/L sodium citrate, pH 6.0 in a pressure cooker for 30 minutes. To block endogenous peroxidase activity, sections were treated with 3% hydrogen peroxide for 15 minutes. Following blocking (Super Block solution, ScyTek Lab), sections were incubated with primary antibody at 4°C overnight. After washing, an UltraTek anti-polyvalent biotinylated secondary antibody (ScyTek Lab) was added to the sections for 10 minutes, followed by serial treatment with UltraTek HRP (ScyTek Lab), an AEC substrate, and hematoxylin counterstaining. Stained sections were mounted with Immu-mount (Thermo Fisher Scientific) and photographed under a Nikon Eclipse microscope. Images were taken from multiple areas in each section, and representative images are shown.

### Statistical analysis

Statistical analysis was performed using GraphPad Prism 6. Comparisons were made using ANOVA with Bonferroni posttest or Kruskal–Wallis test with Dunn's comparison. For mouse study, statistical analysis was performed using SAS version 9.4 (SAS Institute Inc. SAS/STAT 9.4 User's Guide, SAS Institute Inc.; 2014) and GraphPad Prism 6. Bonferroni adjustments were used when performing multiple comparisons and significance was fixed at the 5% level.

## Results

### C-Met inhibition promotes G<sub>1</sub> cell-cycle arrest of MD-MSCs

We performed a high-content drug screen to assess the effect of c-Met inhibitors on proliferation of MD-MSCs. All inhibitors tested reduced proliferation of MD-MSCs after 48 hours (Supplementary Fig. S1). We further evaluated cabozantinib, a c-Met/VEGFR2 inhibitor, because it is FDA-approved and would target Schwann cells and the vasculature. Cabozantinib significantly reduced viability of MD-MSCs after 48 hours of treatment, with IG<sub>50</sub> of 2.2  $\mu$ mol/L, an 85% maximum effect, and five-fold selectivity over WT-MSCs (IG<sub>50</sub> = 10  $\mu$ mol/L; Fig. 1A). MD-MSCs treated with increasing cabozantinib concentrations had a dose-dependent decrease in c-Met (Y1234/1235) phosphorylation (Fig. 1B), but no change in the VEGFR2/3 phosphorylation levels (Fig. 1C). Knockdown of c-Met in MD-MSCs decreased their growth rate by approximately 30% over 72 hours (Fig. 1D), confirming that c-Met contributes to enhanced MD-MSC proliferation. Downstream of c-Met, cabozantinib decreased the phosphorylation levels of Erk1/2 and Akt(T308) in MD-MSCs within 6 hours, and the effect was maintained at 24 hours (Fig. 1E and F). These changes were accompanied by decreased cyclin D<sub>1</sub> and increased p27 levels at 24 hours of treatment (Fig. 1G), consistent with a G<sub>1</sub> cell-cycle arrest (35). To assess suitability for *in vivo* testing, we performed a pharmacokinetic analysis of cabozantinib in NSG mice. Plasma and nerve concentrations of cabozantinib peaked at 4 hours (6,500 and 1,650 ng/ml, respectively) and were detectable for at least 17 hours with a t<sub>1/2</sub> of approximately 7 hours following a single 40 mg/kg oral dose (Fig. 1H).

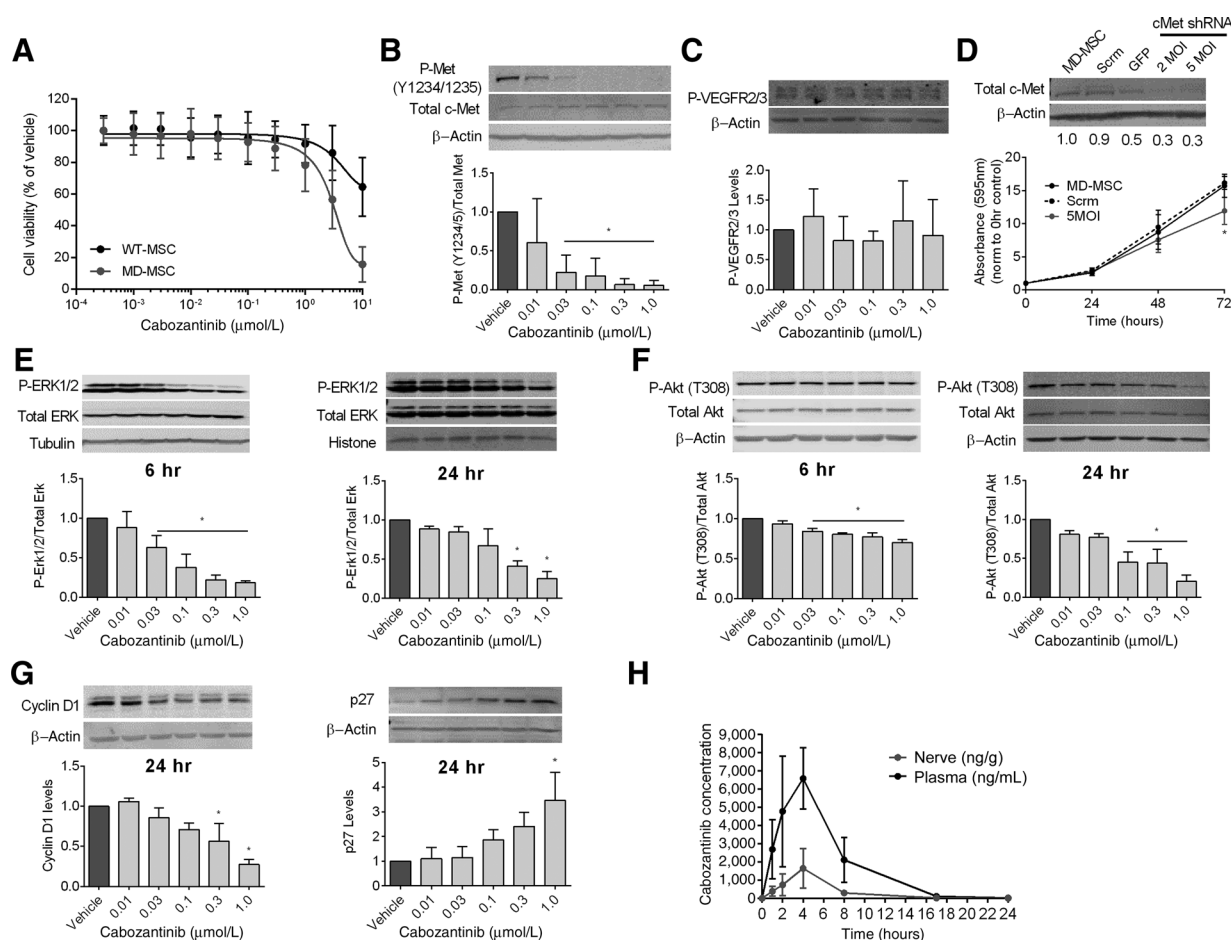
### Cabozantinib synergizes with the Src inhibitor, dasatinib, in MD-MSCs

High-content screening of drug combinations identified that combination treatment of cabozantinib with the Src inhibitor, dasatinib, selectively reduced the number of MD-MSCs compared with WT-MSCs (Fig. 2A). Synergy scores revealed that cabozantinib and dasatinib synergized in MD-MSCs at low concentrations (Fig. 2B). In addition, the combination index (CI) of cabozantinib and dasatinib was 0.6 (Fig. 2C), indicating a synergistic relationship of the two inhibitors and supporting their use in combination for these studies.

### Src inhibition promotes G<sub>1</sub> cell-cycle arrest of MD-MSCs

Antibody array analysis revealed increased Src phosphorylation in human VS compared with normal Schwann cells (33), supporting Src as a potential target for NF2 therapeutics (24). The Src inhibitor, dasatinib, reduced MD-MSC viability with IG<sub>50</sub> = 9 nmol/L, a maximum effect of approximately 80%, and 100-fold selectivity over WT-MSCs (IG<sub>50</sub> = 1.45  $\mu$ mol/L; Fig. 3A). In addition to reducing Src(Y416) phosphorylation, dasatinib decreased Src-dependent phosphorylation of FAK(Y576) and

Fuse et al.

**Figure 1.**

C-Met inhibition promotes G<sub>1</sub> cell-cycle arrest of MD-MSCs *in vitro*. **A**, Dose-response curves of MD-MSCs and WT-MSCs treated with cabozantinib for 48 hours (IG<sub>50</sub> = 2.2 and 10 μmol/L for MD-MSCs and WT-MSCs, respectively). *n* = 3 cultures, eight replicates each). Representative Western blot analysis and densitometry show that cabozantinib reduces phosphorylation of c-Met (Y1234/5) (**B**) and has no effect on phosphorylation of VEGFR2/3 (**C**) after 6 hours of treatment (*n* = 3–4). **D**, Lentiviral-mediated shRNA knockdown of c-Met in MD-MSCs decreases cell growth (*n* = 3, eight replicates each; SCRM, scrambled shRNA; MOI, multiplicity of infection). Representative Western blots and densitometry show that cabozantinib reduces phosphorylation of Erk1/2 (**E**), Akt (T308) (**F**) after 6 and 24 hours, and reduces cyclin D<sub>1</sub> and increases p27 protein levels (**G**) after 24 hours of treatment (*n* = 3–4). One-way ANOVA, \**P* < 0.05. **H**, Drug concentrations were measured in plasma and nerves at the indicated times following a single oral dose of 40 mg/kg cabozantinib (*n* = 3 mice per time point). One-way ANOVA or Kruskal-Wallis. \*, *P* < 0.05.

Src/FAK-dependent phosphorylation of paxillin (Y118) in a dose-dependent manner (Fig. 3B). Dasatinib promoted a G<sub>1</sub> cell-cycle arrest in MD-MSCs, as evidenced by decreased cyclin D<sub>1</sub> and increased p27 levels at 24 hours of treatment (Fig. 3C). A pharmacokinetic analysis revealed that dasatinib (20 mg/kg oral dose) had poor nerve penetration and it peaked in the plasma at 1 hour (200 ng/mL). Consistent with previous reports (36), the half-life (*t*<sub>1/2</sub>) of dasatinib in plasma was approximately 2.5 hours (Fig. 3D). These results do not support *in vivo* evaluation of dasatinib.

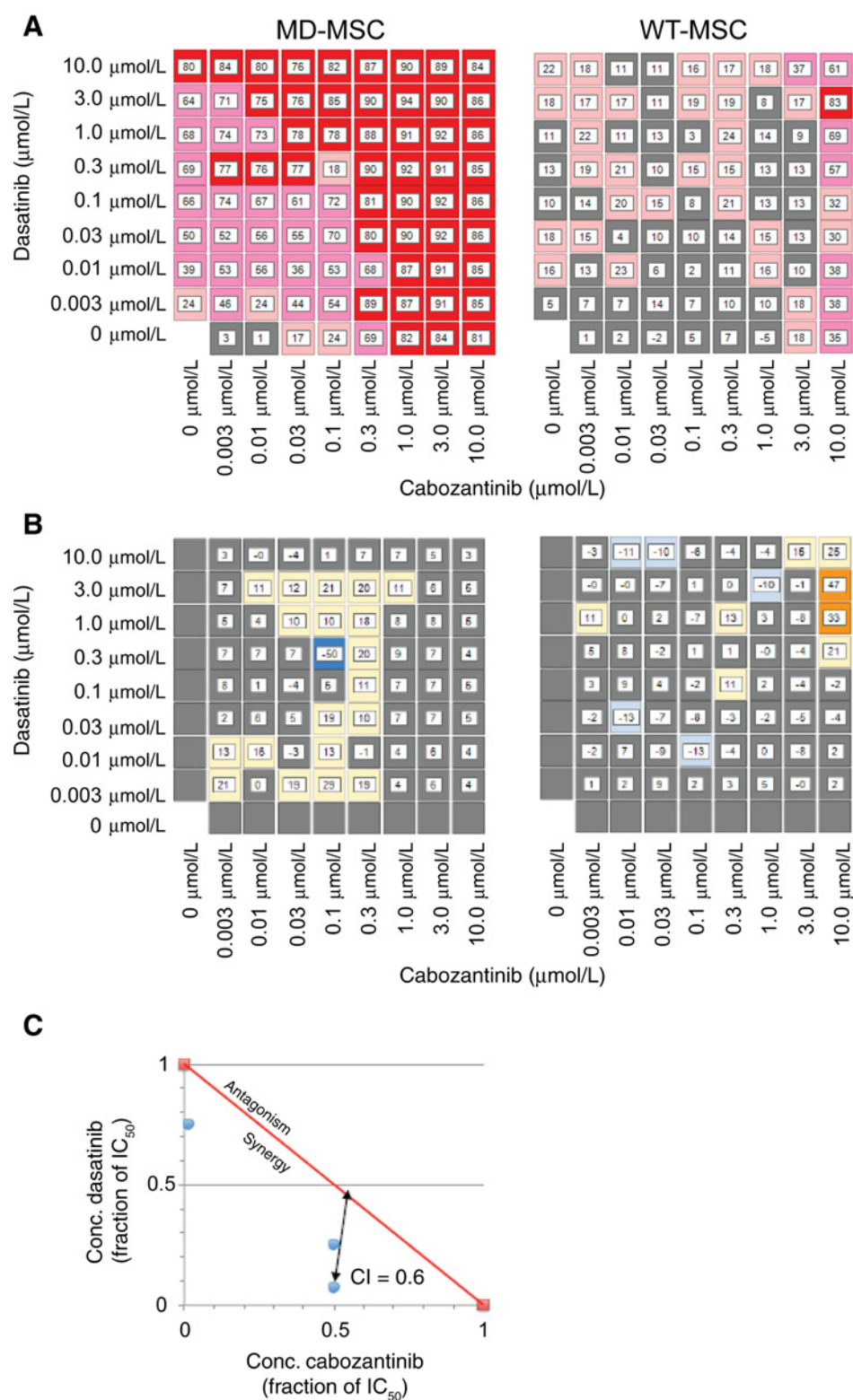
#### Saracatinib reduces MD-MSC viability and has good nerve penetration

A pharmacokinetic study of saracatinib (25 mg/kg oral dose) in NSG mice revealed that plasma and nerve concentrations of saracatinib peaked at 0.5 hours with a *t*<sub>1/2</sub> of 4.4 hours, but remained constant in the nerve at approximately 300–400 ng/g

for at least 8 hours, the longest time point measured (Fig. 3D). Saracatinib selectively reduced MD-MSC viability (IG<sub>50</sub> = 0.3 μmol/L) but had a low maximum effect of approximately 40%–50%, compared with an 80% maximum effect for dasatinib (Fig. 3E). Saracatinib decreased the levels of Src (Y416) phosphorylation compared with total Src levels, and also decreased Src-dependent phosphorylation of FAK (Y576), and Src/FAK-dependent phosphorylation of paxillin (Y118) at 6 hours of treatment (Fig. 3F). After 24 hours of saracatinib treatment, MD-MSCs had increased p27 levels compared with controls (Fig. 3G).

#### Dual c-Met and Src inhibition is more effective than either inhibitor alone

MD-MSCs treated with saracatinib (0.5 μmol/L) together with increasing cabozantinib concentrations had a three-fold decrease in the IG<sub>50</sub> of cabozantinib (0.6 μmol/L, compared with

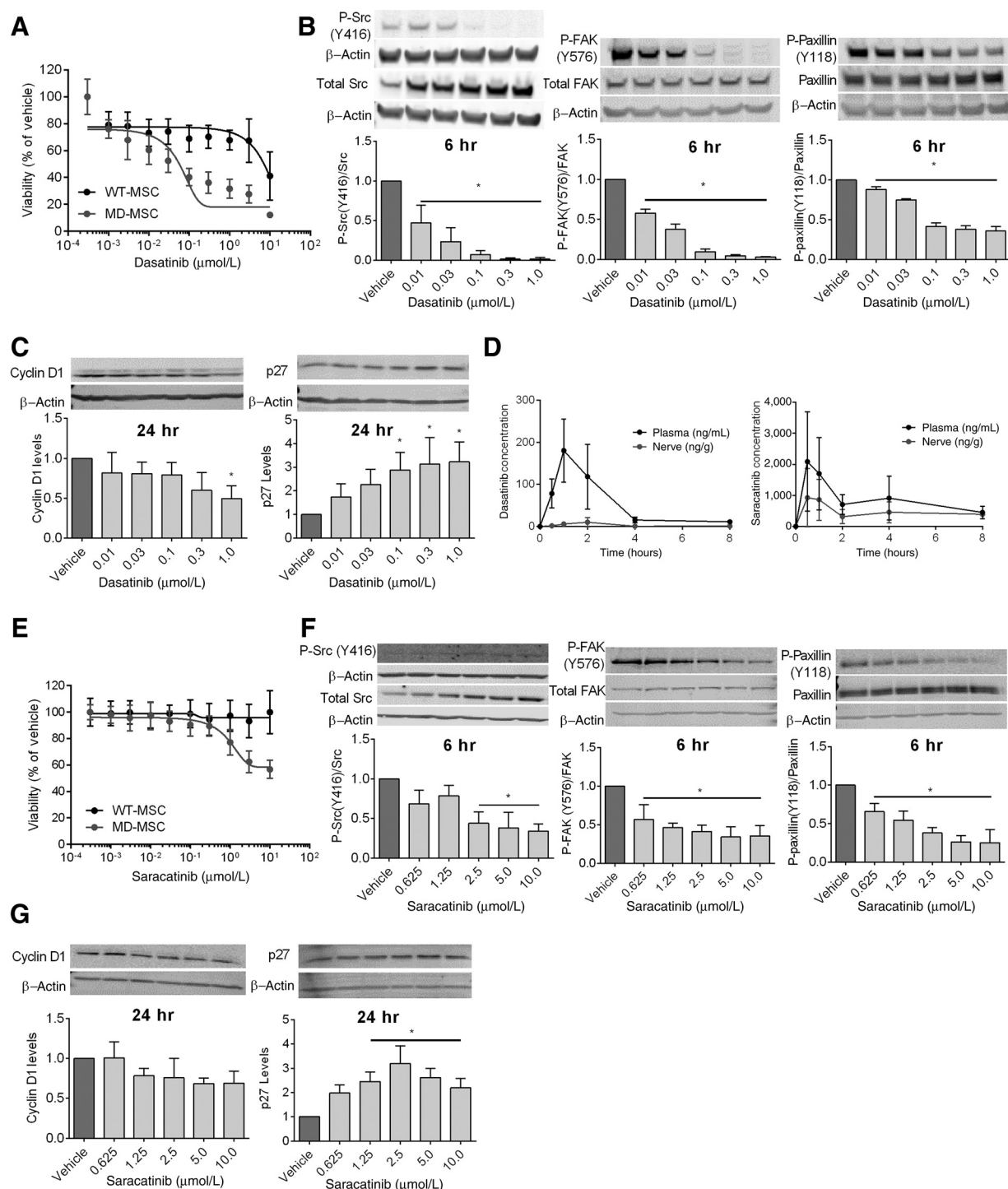
**Figure 2.**

Src and c-Met inhibitors synergize to reduce MD-MSC number. **A**, Dasatinib/cabozantinib combination matrix analyses of % decrease in nuclear number (Hoescht staining; red: >75%; dark pink: 36–75%; light pink: 16–35%; gray: 0–15%). **B**, Synergy over model scores (ref. 49; gray: no synergy; yellow-orange: moderate to strong synergy; blue: antagonistic effects). **C**, Dasatinib and cabozantinib showed a synergistic CI score of 0.6 (CI = 1: no interaction; CI < 1: synergy; CI > 1: antagonism).

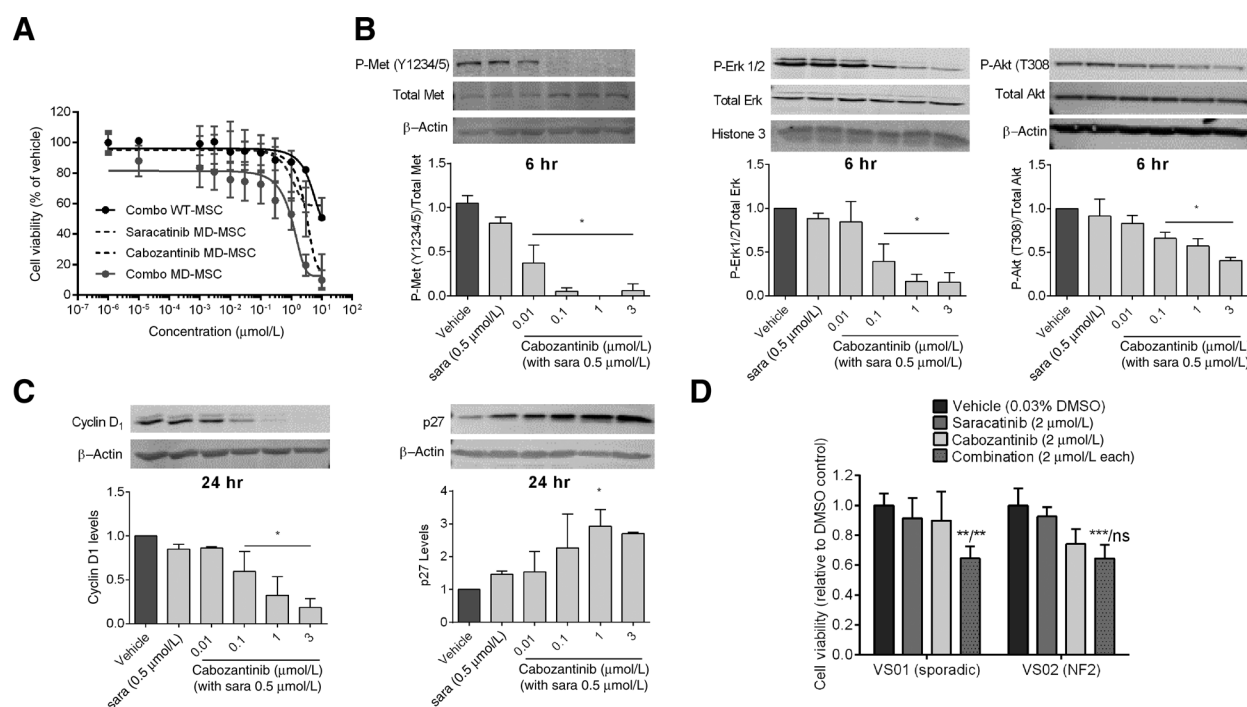
2.2  $\mu\text{mol/L}$  for cabozantinib alone), and more than five-fold selectivity over WT-MSCs ( $\text{IC}_{50}$  = 3.4  $\mu\text{mol/L}$ ; Fig. 4A). Treatment of MD-MSCs with saracatinib (0.5  $\mu\text{mol/L}$ ) and increasing cabo-

zantinib concentration resulted in decreased phosphorylation levels of c-Met(Y1234/1235), Erk1/2, and Akt(T308) after 6 hours (Fig. 4B). After 24 hours of the combination treatment, MD-MSCs

Fuse et al.

**Figure 3.**

Src inhibition promotes G<sub>1</sub> cell-cycle arrest of MD-MSCs *in vitro*. **A**, Dose-response curves of MD-MSCs and WT-MSCs treated with dasatinib for 48 hours ( $\text{IG}_{50}$  = 9 nmol/L and 1.45  $\mu\text{mol/L}$  for MD-MSCs and WT-MSCs, respectively).  $n$  = 3 cultures, eight replicates each). Representative Western blots and densitometry show that dasatinib decreased phosphorylation levels of Src(Y416), FAK(Y576), and paxillin(Y118) after 6 hours (**B**) and decreased cyclin D<sub>1</sub> and increased p27 levels after 24 hours of treatment ( $n$  = 3–4; **C**). **D**, Drug concentrations were measured in plasma and nerves at the indicated times following a single oral dose of 20 mg/kg of dasatinib or 25 mg/kg of saracatinib in NSG mice ( $n$  = 3 mice per time point). **E**, Dose-response curves of MD-MSCs and WT-MSCs treated with saracatinib for 48 hours ( $\text{IG}_{50}$  = 0.3  $\mu\text{mol/L}$  for MD-MSCs and was ineffective on WT-MSCs).  $n$  = 3 cultures, eight replicates each). Representative Western blots and densitometry show that saracatinib decreased phosphorylation levels of Src(Y416), FAK(Y576), and paxillin(Y118) relative to total levels after 6 hours (**F**) and did not change the level of cyclin D<sub>1</sub>, but increased p27 expression after 24 hours of treatment ( $n$  = 3–4; **G**). One-way ANOVA or Kruskal-Wallis. \*,  $P$  < 0.05.

**Figure 4.**

Combination treatment modulates similar signaling pathways as single drugs and reduces the viability of primary human VS cells. **A**, Dose-response curves of MD-MSCs treated with saracatinib (0.5  $\mu\text{mol/L}$ ) and increasing concentration of cabozantinib ( $\text{IG}_{50}$  = 0.6  $\mu\text{mol/L}$  in MD-MSCs and 3.4  $\mu\text{mol/L}$  in WT-MSCs;  $n$  = 3 cultures, eight replicates each). Single drug curves are replotted for comparison. Representative Western blots and densitometry show that simultaneous treatment of 0.5  $\mu\text{mol/L}$  saracatinib with increasing cabozantinib concentrations decreased phosphorylation levels of Met(Y1234/5), Erk1/2, and Akt(T308) after 6 hours (**B**), and decreased cyclin D1 and increased p27 after 24 hours of treatment ( $n$  = 3, one-way ANOVA; \*,  $P$  < 0.05; **C**). **D**, VS cell viability was reduced by treatment of saracatinib and cabozantinib (2  $\mu\text{mol/L}$  each) for 48 hours. Two-way ANOVA, compared with single agents. \*\*,  $P$  < 0.01; \*\*\*,  $P$  < 0.001,  $n$  = 6 replicates.

had decreased cyclin D1 levels and increased p27 levels at lower cabozantinib concentrations than those treated with cabozantinib alone (Fig. 4C).

#### Dual c-Met and Src inhibition reduces viability of primary VS cells

We investigated the efficacy of this drug combination in decreasing viability of primary VS cells obtained from two patients. VS01 was a sporadic VS with a heterozygous duplication of *NF2* exon 5 and a homozygous duplication of exon 7. VS02 was from an NF2 patient with an exon 14 deletion. VS cells were cultured with cabozantinib (2  $\mu\text{mol/L}$ ) and saracatinib (2  $\mu\text{mol/L}$ ), alone or in combination, for 48 hours. For both VS01 and VS02, the combination treatment reduced VS cell viability by approximately 35%–40% compared with vehicle (0.3% DMSO) and was significantly more effective than saracatinib alone. In addition, for VS01 cells, the combination treatment was more effective than cabozantinib alone (Fig. 4D).

#### Dual c-Met and Src inhibition slows MD-MSC growth *in vivo*

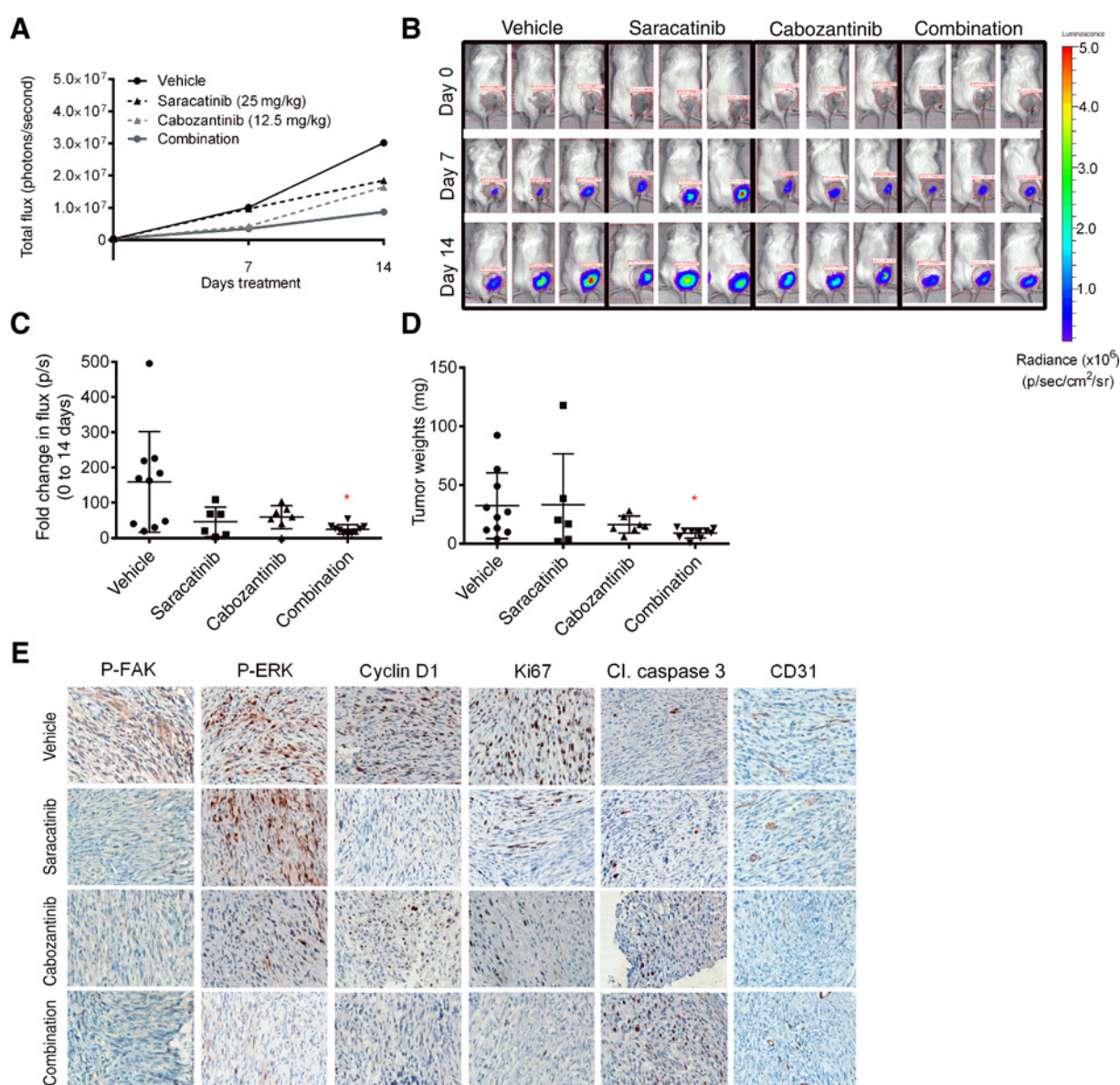
To evaluate the efficacy of cabozantinib and saracatinib *in vivo*, luciferase-expressing MD-MSCs were grafted into the sciatic nerves of NSG mice, and the graft size was monitored by bioluminescence imaging (BLI). Upon confirmation of successful grafting (Supplementary Fig. S2A), mice were assigned into vehicle, cabozantinib (12.5 mg/kg/day), saracatinib (25 mg/kg/day),

and combination (cabozantinib and saracatinib at 12.5 mg/kg/day and 25 mg/kg/day, respectively) treatment cohorts. BLI showed that grafts in the combination-treated group had a significantly slower growth rate compared with those in the single-agent groups (Fig. 5A and B). Although the vehicle-treated allografts had a 160-fold increase in BL signal over 14 days, the grafts treated with saracatinib or cabozantinib had a 50- and 60-fold increase in BL signal, respectively. Significantly, the allografts from the combination group had only a 25-fold increase in BL signal after 14 days of treatment (Fig. 5C). The reduction in BL signals correlated with lower tumor weights in the combination-treated group compared with the vehicle group (Fig. 5D; Supplementary Fig. S2B).

#### Dual c-Met and Src inhibition modulates FAK and ERK signaling pathways in allografts

To assess the signaling pathways modulated by drug treatments, allograft sections were analyzed by immunohistochemistry. Similar to the *in vitro* findings, saracatinib decreased the FAK phosphorylation levels, and cabozantinib decreased the ERK1/2 phosphorylation levels compared with vehicle controls (Fig. 5E). These changes were also observed in the combination-treated allografts. Moreover, CD31 staining of endothelial cells was decreased in grafts treated with cabozantinib compared with vehicle controls, indicating that cabozantinib targets the vasculature *in vivo* as well (Fig. 5E). Grafts from mice treated with

Fuse et al.

**Figure 5.**

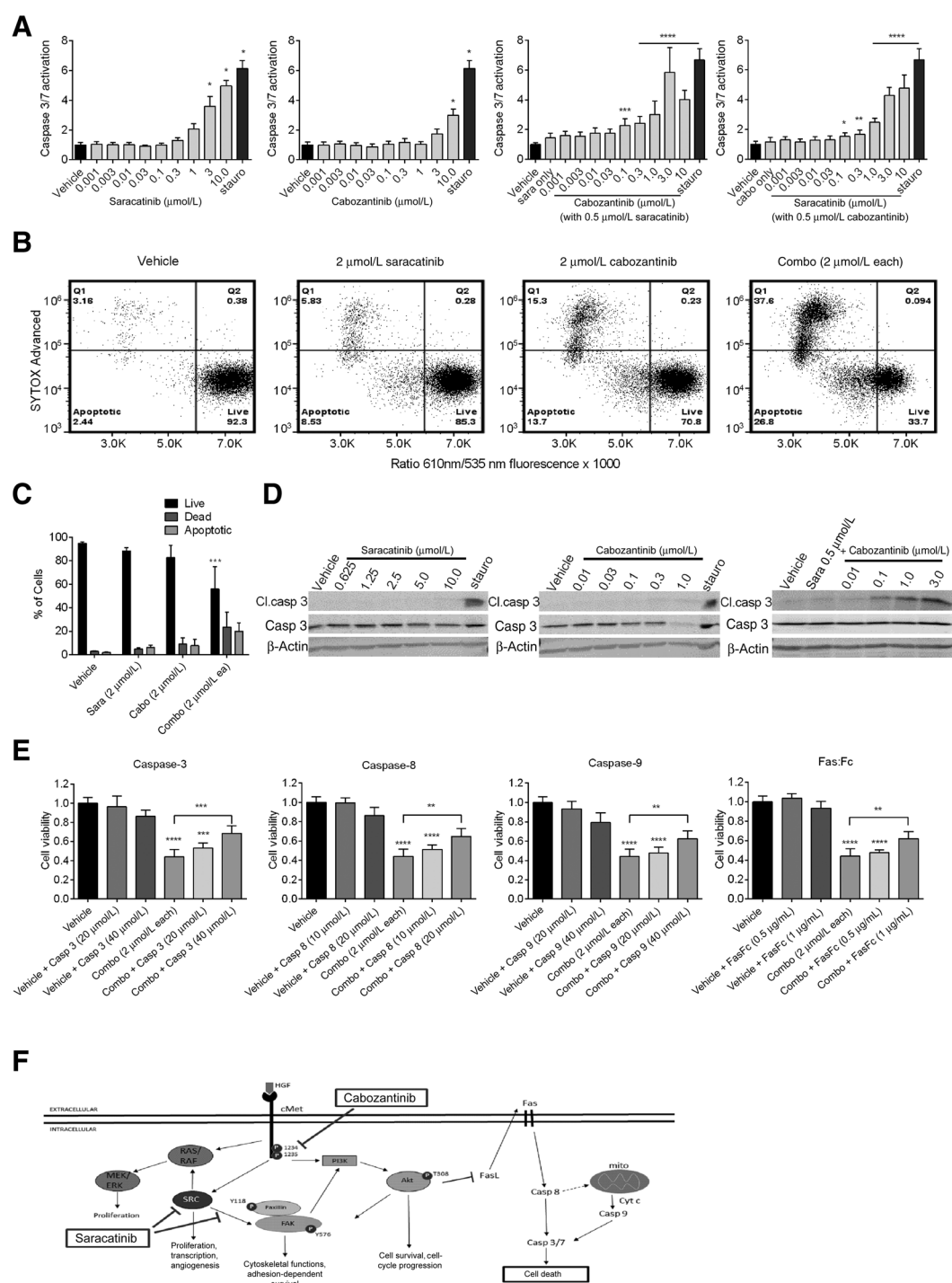
C-Met and Src inhibition reduces growth of orthotopic MD-MSC allografts. **A**, The relative BL signals are shown at 0, 7, and 14 days after treatment (total flux, photons/sec,  $n = 6-10$  mice) and representative BL images are presented in **B**. **C**, The flux values were normalized to day 0, and the fold changes are shown for each treatment group. **D**, Graft weights support the BL quantitation results. **E**, Graft IHC for p-FAK, p-ERK, cyclin D<sub>1</sub>, Ki-67, cleaved caspase-3, and CD31. A representative image for each section is shown.

cabozantinib or saracatinib, alone or in combination, had fewer cyclin D<sub>1</sub> and Ki67-positive cells compared with those from vehicle-treated mice. In addition, grafts in the combination-treated group had elevated cleaved caspase 3 staining, compared with those in the vehicle and single treatment groups (Fig. 5E), supporting the conclusion that the drug combination induces apoptosis of MD-MSCs *in vivo*.

#### Dual c-Met and Src inhibition induces MD-MSC apoptosis

To confirm the *in vivo* findings, we studied caspase-dependent apoptosis in cultured MD-MSCs. Caspase 3/7 activity was trig-

gered by cabozantinib or saracatinib alone only when administered at high doses (3  $\mu\text{mol/L}$  saracatinib or 10  $\mu\text{mol/L}$  cabozantinib) for 19 to 24 hours (Fig. 6A). However, cotreatment of MD-MSCs with saracatinib (0.5  $\mu\text{mol/L}$ ) and increasing cabozantinib concentrations induced caspase 3/7 activity at 100-fold lower concentrations of cabozantinib compared with cabozantinib administered alone (0.1  $\mu\text{mol/L}$  vs. 10  $\mu\text{mol/L}$ ; Fig. 6A). Similarly, MD-MSCs treated with cabozantinib (0.5  $\mu\text{mol/L}$ ) and increasing saracatinib concentrations induced caspase 3/7 activity at approximately 30-fold lower saracatinib concentrations compared with saracatinib administered alone (0.1  $\mu\text{mol/L}$  vs. 3  $\mu\text{mol/L}$ ; Fig. 6A).

**Figure 6.**

Combined c-Met and Src inhibition induces caspase-dependent apoptosis in MD-MSCs. **A**, Caspase-3/7 activation in MD-MSCs treated with saracatinib and cabozantinib, alone, and in combination. Staurosporine (1  $\mu\text{mol/L}$ ) was used as a positive control [fluorescence (RFU) normalized to DMSO vehicle control.  $n = 2$ , eight replicates each]. **B**, Representative membrane asymmetry assay of MD-MSCs treated with 2  $\mu\text{mol/L}$  each of saracatinib and cabozantinib, alone, and in combination. DMSO was used as vehicle control. Quantitation is shown in **C** ( $n = 3$ , two-way ANOVA). **D**, Representative Western blots show cleaved caspase-3 after 24 hours of treatment with a single drug or drug combination. **E**, MD-MSC viability after treatment with the indicated drug or drug combination for 24 hours in the presence and absence of inhibitors of apoptosis: Fas:Fc (FasL decoy), Z-DEVD-FMK (caspase 3), Z-IETD-FMK (caspase 8), and Z-LEHD-FMK (caspase 9) at the indicated concentrations ( $n = 2$ , 6–10 replicate wells each). Wells treated with the drug and inhibitor were compared with wells treated with inhibitor alone (Kruskal-Wallis,  $*P < 0.05$ ,  $**P < 0.01$ ,  $***P < 0.001$ ,  $****P < 0.0001$ ). **F**, Combination treatment of MD-MSCs with cabozantinib and saracatinib decreases pro-survival signaling through ERK and Akt, leading to Fas activation and caspase-dependent apoptosis.

A membrane asymmetry assay confirmed that the drug combination induced a larger apoptotic cell population than either drug alone (Fig. 6B). Treatment with 2  $\mu\text{mol/L}$  saracatinib resulted in 6.2% apoptotic cells, 4.8% dead cells, and 88.4% live cells, whereas treatment with 2  $\mu\text{mol/L}$  cabozantinib had 7.7% apoptotic cells, 9% dead cells, and 82.8% live cells. The combination treatment increased the apoptotic population to 20% after 19 hours (Fig. 6C). When administered alone, saracatinib did not induce cleavage of caspase 3. Cabozantinib induced caspase cleavage at 1  $\mu\text{mol/L}$  whereas in the presence of 0.5  $\mu\text{mol/L}$  saracatinib, caspase cleavage was detected at 0.1  $\mu\text{mol/L}$  cabozantinib (Fig. 6D). Collectively, our results indicate that although the individual drugs promote a  $G_1$  cell-cycle arrest of MD-MSCs, saracatinib and cabozantinib combination is cytotoxic and promotes caspase 3/7-dependent apoptosis.

#### Dual c-Met and Src inhibition activates extrinsic and intrinsic apoptotic pathways

To examine the apoptotic pathway activated by dual inhibition of c-Met and Src, MD-MSCs were cultured in the presence of 2  $\mu\text{mol/L}$  saracatinib and 2  $\mu\text{mol/L}$  cabozantinib, alone and in combination, for 24 hours with or without inhibitors for caspase 3 (Z-DEVD-FMK), caspase 8 (Z-IETD-FMK), and caspase 9 (Z-LEHD-FMK). The three caspase inhibitors significantly prevented the loss of viability of MD-MSCs treated with cabozantinib and saracatinib together (Fig. 6E), suggesting that the combination treatment activates both the extrinsic and intrinsic apoptotic pathways. Incubation of MD-MSCs with the Fas ligand (FasL) decoy Fas:Fc partially prevented the loss of MD-MSC viability (Fig. 6E), supporting the conclusion that the Fas receptor is activated by the combination treatment, leading to activation of caspases and cell death. Furthermore, basal expression of Fas receptor was higher in MD-MSCs compared with WT-MSCs (Supplementary Fig. S3), suggesting a possible explanation for drug selectivity.

## Discussion

Individuals with NF2 develop multiple meningiomas and schwannomas over their lifetime. Although there is a low incidence of malignancy, repetitive surgeries to remove tumors increase morbidity and considerably decrease a patient's lifespan (10). Removal or irradiation of bilateral VS that occur in all NF2 patients can lead to deafness and facial nerve paralysis. This outcome in particular leads to social isolation and decreased quality of life. Currently, there is no approved pharmacologic treatment for NF2 tumors; however, patients are increasingly treated off-label with cancer drugs. The majority of drug therapies in clinical use for NF2 are cytostatic or target the tumor vasculature (7–9).

To date, only an HDAC and PI3K inhibitors have been found to induce apoptosis of MD-MSCs and human VS cells (32, 37, 38). A 3-phosphoinositide-dependent protein kinase-1 (PDK-1) inhibitor, OSU-03012, induced caspase-9-dependent apoptosis in NF2-associated Schwann cells and malignant schwannomas (38). Our screen of the Library of Pharmaceutically Active Compounds (LOPAC) revealed that multiple PI3K inhibitors reduced viability of MD-MSCs by inducing caspase-dependent apoptosis and autophagy (32). Currently, there are over 300 ongoing clinical trials of PI3K inhibitors due to their relevance to oncology (clinicaltrials.gov). However, only one PI3K inhibitor, Idelalisib (Zydelig, Gilead Sciences) has been FDA-approved (39). This

drug, however, carries a black box warning for adverse effects (40). Recently, six clinical trials of drug combinations with Idelalisib have been halted due to toxicity (41).

Here, we demonstrate that simultaneous inhibition of c-Met and Src with cabozantinib and saracatinib, respectively, reduced the viability of MD-MSCs *in vitro* and in nerve allografts by inducing caspase-dependent apoptosis. Moreover, the drug combination inhibited growth of primary VS cells carrying genetic inactivation of NF2. Treatment of MD-MSCs with cabozantinib reduced activation of ERK1/2 and Akt signaling pathways downstream of c-Met. *In vivo*, cabozantinib also reduced microvessel density. Both dasatinib and saracatinib inhibited Src activity in MD-MSCs as evidenced by reductions in phosphorylated FAK and paxillin. FAK signaling is elevated in NF2-associated VS compared with normal nerves (24). A previous study showed that FAK inhibition with crizotinib reduced allograft growth in mice (42). Merlin modulates activity of the  $\beta 1$  integrin pathway activated by extracellular matrix and transduced by Src and FAK (43, 44). This pathway mediates extracellular matrix-dependent cell survival, and converges with proliferative signals from mitogen receptor-dependent activation of ERK1/2 and PI3K/Akt (3). The absence of merlin activates these pathways, leading to enhanced cell survival and proliferation. Simultaneous inhibition of c-Met-ERK1/2-Akt and Src-FAK-paxillin could prevent schwannoma cells from using a compensatory mechanism of adhesion-dependent cell survival.

Inhibition of these two pathways which converge on PI3K/Akt in Schwann cells may contribute to induction of apoptosis. Akt modulates transcription factors that regulate cell cycle and apoptosis (45), and may mediate the cytostatic and cytotoxic effects observed in cabozantinib and saracatinib-treated MD-MSCs. Our results suggest that the efficacy of the combination treatment is due, in part, to activation of the Fas/FasL cell death pathway. Inhibition of Fas with a FasL decoy partially prevented cell death induced by the drug combination. We observed activation of both the extrinsic and intrinsic apoptotic pathways downstream of Fas receptor, as evidenced by the ability of caspase 8, 9, and 3 inhibitors to prevent MD-MSC death caused by the drug combination. This could be attributed to decreased pro-survival and pro-proliferative signaling involving ERK and Akt, leading to upregulation of FasL (46). In addition, stimulation of the Fas receptor by FasL activates both the extrinsic and intrinsic apoptotic pathways, resulting in cytochrome *c* release from mitochondria and apoptosome formation with caspase-9 (47). Merlin loss in SCs leads to accumulation of multiple receptors in the plasma membrane (48), potentially explaining the elevated basal levels of Fas receptor in MD-MSCs compared with WT-MSCs. A proposed pathway summarizing our findings is shown in Fig. 6F.

This study demonstrates that simultaneous c-Met and Src inhibition induced apoptosis of merlin-deficient mouse Schwann cells in culture and in allografts, and reduced growth of primary VS cells with NF2 mutations. The drug combination also decreased the viability of two merlin-deficient human SC lines and a human benign meningioma line *in vitro* (Supplementary Fig. S4), confirming that the effects are not cell-line or species-dependent. Both ERK and Src-FAK kinases converge onto the PI3K/Akt pathway; inhibitors of which induce apoptosis in NF2-associated cells. Considering the severe toxicity associated with direct targeting of PI3K with Idelalisib, and until additional PI3K inhibitors are approved, simultaneous inhibition of c-Met-ERK and Src-FAK pathways with cabozantinib and dasatinib/saracatinib may

promote schwannoma cell apoptosis with fewer adverse effects. This study provides preclinical data supporting further investigation of dual inhibition of c-Met and Src as a potential therapy for NF2-associated schwannomas.

### Disclosure of Potential Conflicts of Interest

C. Fernandez-Valle is an unpaid research advisory board member for the Children's Tumor Foundation. No potential conflicts of interest were disclosed by the other authors.

### Authors' Contributions

**Conception and design:** M.A. Fuse, C.T. Dinh, R. Mittal, J.N. Soulaikova, X.Z. Liu, L.-S. Chang, M.C. Franco, C. Fernandez-Valle

**Development of methodology:** M.A. Fuse, R. Mittal, L.-S. Chang, M.C. Franco, C. Fernandez-Valle

**Acquisition of data (provided animals, acquired and managed patients, provided facilities, etc.):** M.A. Fuse, S.K. Plati, S.S. Burns, C.T. Dinh, O. Bracho, D. Yan, R. Mittal, R. Shen, L.-S. Chang, M.C. Franco, C. Fernandez-Valle

**Analysis and interpretation of data (e.g., statistical analysis, biostatistics, computational analysis):** M.A. Fuse, S.K. Plati, S.S. Burns, C.T. Dinh, D. Yan, R. Mittal, R. Shen, J.N. Soulaikova, A.J. Copik, X.Z. Liu, L.-S. Chang, M.C. Franco, C. Fernandez-Valle

**Writing, review, and/or revision of the manuscript:** M.A. Fuse, S.K. Plati, C.T. Dinh, R. Mittal, J.N. Soulaikova, X.Z. Liu, F.F. Telischi, L.-S. Chang, M.C. Franco, C. Fernandez-Valle

**Administrative, technical, or material support (i.e., reporting or organizing data, constructing databases):** M.A. Fuse, S.K. Plati, R. Mittal, M.C. Franco, C. Fernandez-Valle

**Study supervision:** C.T. Dinh, X.Z. Liu, C. Fernandez-Valle

### Acknowledgments

We thank Dr. Jacques Morcos for harvesting human VS tumors and Cenix Bioscience for conducting the c-Met inhibitor screen and synergy studies through the Industry-Academia collaboration program.

### Grant Support

This study was supported by the Children's Tumor Foundation (to C. Fernandez-Valle and M.A. Fuse, YIA 2015-01-012), DOD NF140044 (to C. Fernandez-Valle), and DOD NF150080 (to L.-S. Chang).

The costs of publication of this article were defrayed in part by the payment of page charges. This article must therefore be hereby marked *advertisement* in accordance with 18 U.S.C. Section 1734 solely to indicate this fact.

Received May 11, 2017; revised July 7, 2017; accepted July 17, 2017; published OnlineFirst August 3, 2017.

### References

- Rouleau GA, Merel P, Lutchman M, Sanson M, Zucman J, Marineau C, et al. Alteration in a new gene encoding a putative membrane-organizing protein causes neuro-fibromatosis type 2. *Nature* 1993;363:515–21.
- Trofatter JA, MacCollin MM, Rutter JL, Murrell JR, Duyao MP, Parry DM, et al. A novel moesin-, ezrin-, radixin-like gene is a candidate for the neurofibromatosis 2 tumor suppressor. *Cell* 1993;72:791–800.
- Petrilli AM, Fernandez-Valle C. Role of Merlin/NF2 inactivation in tumor biology. *Oncogene* 2016;35:537–48.
- Kim BS, Seol HJ, Lee JI, Shin HJ, Park K, Kong DS, et al. Clinical outcome of neurofibromatosis type 2-related vestibular schwannoma: treatment strategies and challenges. *Neurosurg Rev* 2016;39:643–53.
- Meijer OW, Vandertop WP, Lagerwaard FJ, Slotman BJ. Linear accelerator-based stereotactic radiosurgery for bilateral vestibular schwannomas in patients with neurofibromatosis type 2. *Neurosurgery* 2008;62:A37–42.
- Baser ME, Evans DG, Jackler RK, Sujansky E, Rubenstein A. Neurofibromatosis 2, radiosurgery and malignant nervous system tumours. *Br J Cancer* 2000;82:998.
- Goutagny S, Raymond E, Esposito-Farese M, Trunet S, Mawrin C, Bernardeschi D, et al. Phase II study of mTORC1 inhibition by everolimus in neurofibromatosis type 2 patients with growing vestibular schwannomas. *J Neuro-Oncol* 2015;122:313–20.
- Karajannis MA, Legault G, Hagiwara M, Ballas MS, Brown K, Nusbaum AO, et al. Phase II trial of lapatinib in adult and pediatric patients with neurofibromatosis type 2 and progressive vestibular schwannomas. *Neuro-Oncology* 2012;14:1163–70.
- Hochart A, Gaillard V, Baroncini M, André N, Vannier JP, Vinchon M, et al. Bevacizumab decreases vestibular schwannomas growth rate in children and teenagers with neurofibromatosis type 2. *J Neuro-Oncol* 2015;124:229–36.
- Blakeley JO, Plotkin SR. Therapeutic advances for the tumors associated with neurofibromatosis type 1, type 2, and schwannomatosis. *Neuro Oncol* 2016;18:624–38.
- Morris KA, Golding JE, Blessing C, Evans DG, Ferner RE, Foweraker K, et al. Toxicity profile of bevacizumab in the UK Neurofibromatosis type 2 cohort. *J Neuro-Oncol* 2017;131:117–24.
- Slusarz KM, Merker VL, Muzikansky A, Francis SA, Plotkin SR. Long-term toxicity of bevacizumab therapy in neurofibromatosis 2 patients. *Cancer Chemothera Pharmacol* 2014;73:1197–204.
- Dilwali S, Roberts D, Stankovic KM. Interplay between VEGF-A and cMET signaling in human vestibular schwannomas and schwann cells. *Cancer Biol Ther* 2015;16:170–5.
- Torres-Martin M, Lassaletta L, San-Roman-Montero J, De Campos JM, Isla A, Gavilan J, et al. Microarray analysis of gene expression in vestibular schwannomas reveals SPP1/MET signaling pathway and androgen receptor deregulation. *Int J Oncol* 2013;42:848–62.
- Hanemann CO, Blakeley JO, Nunes FP, Robertson K, Stemmer-Rachamimov A, Mautner V, et al. Current status and recommendations for biomarkers and biobanking in neurofibromatosis. *Neurology* 2016;87:S40–S8.
- Scoles DR, Huynh DP, Chen MS, Burke SP, Gutmann DH, Pulst SM. The neurofibromatosis 2 tumor suppressor protein interacts with hepatocyte growth factor-regulated tyrosine kinase substrate. *Human Mol Genet* 2000;9:1567–74.
- Krasnoselsky A, Massay MJ, DeFrances MC, Michalopoulos G, Zarnegar R, Ratner N. Hepatocyte growth factor is a mitogen for Schwann cells and is present in neurofibromas. *J Neurosci* 1994;14:7284–90.
- Organ SL, Tsao MS. An overview of the c-MET signaling pathway. *Thera Adv Med Oncol* 2011;3:S7–S19.
- Yakes FM, Chen J, Tan J, Yamaguchi K, Shi Y, Yu P, et al. Cabozantinib (XL184), a novel MET and VEGFR2 inhibitor, simultaneously suppresses metastasis, angiogenesis, and tumor growth. *Mol Cancer Ther* 2011;10:2298–308.
- Bentzien F, Zuzow M, Heald N, Gibson A, Shi Y, Goon L, et al. In vitro and in vivo activity of cabozantinib (XL184), an inhibitor of RET, MET, and VEGFR2, in a model of medullary thyroid cancer. *Thyroid* 2013;23:1569–77.
- Singh H, Brave M, Beaver JA, Cheng J, Tang S, Zahalka E, et al. U.S. food and drug administration approval: cabozantinib for the treatment of advanced renal cell carcinoma. *Clin Cancer Res* 2017;23:330–5.
- Lock R, Ingraham R, Maertens O, Miller AL, Weledji N, Legius E, et al. Cotargeting MNK and MEK kinases induces the regression of NF1-mutant cancers. *J Clin Invest* 2016;126:2181–90.
- Torres KE, Zhu QS, Bill K, Lopez G, Ghadimi MP, Xie X, et al. Activated MET is a molecular prognosticator and potential therapeutic target for malignant peripheral nerve sheath tumors. *Clin Cancer Res* 2011;17:3943–55.
- Ammoun S, Flaiz C, Ristic N, Schuldt J, Hanemann CO. Dissecting and targeting the growth factor-dependent and growth factor-independent extracellular signal-regulated kinase pathway in human schwannoma. *Cancer Res* 2008;68:5236–45.
- Kujak C, Kolesar JM. Treatment of chronic myelogenous leukemia. *Am J Health System Pharmacy* 2016;73:113–20.
- Talpaz M, Shah NP, Kantarjian H, Donato N, Nicolli J, Paquette R, et al. Dasatinib in imatinib-resistant Philadelphia chromosome-positive leukemias. *N Engl J Med* 2006;354:2531–41.

Fuse et al.

27. Bolos V, Gasent JM, Lopez-Tarruella S, Grande E. The dual kinase complex FAK-Src as a promising therapeutic target in cancer. *OncoTargets Thera* 2010;3:83–97.
28. Araujo J, Logothetis C. Dasatinib: a potent SRC inhibitor in clinical development for the treatment of solid tumors. *Cancer Treat Rev* 2010;36:492–500.
29. Hennequin LF, Allen J, Breed J, Curwen J, Fennell M, Green TP, et al. N-(5-chloro-1,3-benzodioxol-4-yl)-7-[2-(4-methylpiperazin-1-yl)ethoxy]-5-(tetrahydro-2H-pyran-4-yloxy)quinazolin-4-amine, a novel, highly selective, orally available, dual-specific c-Src/Abl kinase inhibitor. *J Med Chem* 2006;49:6465–88.
30. Green TP, Fennell M, Whittaker R, Curwen J, Jacobs V, Allen J, et al. Preclinical anticancer activity of the potent, oral Src inhibitor AZD0530. *Mol Oncol* 2009;3:248–61.
31. Bertotti A, Bracco C, Girolami F, Torti D, Gastaldi S, Galimi F, et al. Inhibition of Src impairs the growth of met-addicted gastric tumors. *Clin Cancer Res* 2010;16:3933–43.
32. Petrilli AM, Fuse MA, Donnan MS, Bott M, Sparrow NA, Tondera D, et al. A chemical biology approach identified PI3K as a potential therapeutic target for neurofibromatosis type 2. *Am J Translat Res* 2014;6:471–93.
33. Petrilli AM, Garcia J, Bott M, Klingeman Plati S, Dinh CT, Bracho OR, et al. Ponatinib promotes a G1 cell-cycle arrest of merlin/NF2-deficient human schwann cells. *Oncotarget* 2017;8:31666–81.
34. Franco MC, Ricart KC, Gonzalez AS, Dennys CN, Nelson PA, Janes MS, et al. Nitration of Hsp90 on tyrosine 33 regulates mitochondrial metabolism. *J Biol Chem* 2015;290:19055–66.
35. Wander SA, Zhao D, Slingerland JM. p27: a barometer of signaling deregulation and potential predictor of response to targeted therapies. *Clin Cancer Res* 2011;17:12–8.
36. Lombardo LJ, Lee FY, Chen P, Norris D, Barrish JC, Behnia K, et al. Discovery of N-(2-chloro-6-methyl-phenyl)-2-(6-(4-(2-hydroxyethyl)-piperazin-1-yl)-2-methylpyrimidin-4-ylamino)thiazole-5-carboxamide (BMS-354825), a dual Src/Abl kinase inhibitor with potent antitumor activity in preclinical assays. *J Med Chem* 2004;47:6658–61.
37. Bush ML, Oblinger J, Brendel V, Santarelli G, Huang J, Akhmeteyeva EM, et al. AR42, a novel histone deacetylase inhibitor, as a potential therapy for vestibular schwannomas and meningiomas. *Neuro Oncol* 2011;13:983–99.
38. Lee TX, Packer MD, Huang J, Akhmeteyeva EM, Kulp SK, Chen CS, et al. Growth inhibitory and anti-tumour activities of OSU-03012, a novel PDK-1 inhibitor, on vestibular schwannoma and malignant schwannoma cells. *Eur J Cancer* 2009;45:1709–20.
39. Forcello N, Saraiya N. Idelalisib: the first-in-class phosphatidylinositol 3-kinase inhibitor for relapsed CLL, SLL, and indolent NHL. *J Adv Pract Oncol* 2014;5:455–9.
40. Coutre SE, Barrientos JC, Brown JR, de Vos S, Furman RR, Keating MJ, et al. Management of adverse events associated with idelalisib treatment: expert panel opinion. *Leukemia Lymphoma* 2015;56:2779–86.
41. Smith SM, Pitcher BN, Jung SH, Bartlett NL, Wagner-Johnston N, Park SI, et al. Safety and tolerability of idelalisib, lenalidomide, and rituximab in relapsed and refractory lymphoma: the alliance for clinical trials in oncology A051201 and A051202 phase 1 trials. *Lancet Haematol* 2017;4:e176–e82.
42. Troutman S, Moleirinho S, Kota S, Nettles K, Fallahi M, Johnson GL, et al. Crizotinib inhibits NF2-associated schwannoma through inhibition of focal adhesion kinase 1. *Oncotarget* 2016;7:54515–25.
43. Fernandez-Valle C, Tang Y, Ricard J, Rodenas-Ruano A, Taylor A, Hackler E, et al. Paxillin binds schwannomin and regulates its density-dependent localization and effect on cell morphology. *Nat Genet* 2002;31:354–62.
44. Obrebski VJ, Hall AM, Fernandez-Valle C. Merlin, the neurofibromatosis type 2 gene product, and beta1 integrin associate in isolated and differentiating Schwann cells. *J Neurobiol* 1998;37:487–501.
45. Chang F, Lee JT, Navolanic PM, Steelman LS, Shelton JG, Blalock WL, et al. Involvement of PI3K/Akt pathway in cell cycle progression, apoptosis, and neoplastic transformation: a target for cancer chemotherapy. *Leukemia* 2003;17:590–603.
46. Zhang X, Tang N, Hadden TJ, Rishi AK. Akt, FoxO and regulation of apoptosis. *Biochim Biophys Acta* 2011;1813:1978–86.
47. Roy S, Nicholson DW. Cross-talk in cell death signaling. *J Exp Med* 2000;192:F21–5.
48. Lallemand D, Manent J, Couvelard A, Watilliaux A, Siena M, Chareyre F, et al. Merlin regulates transmembrane receptor accumulation and signaling at the plasma membrane in primary mouse Schwann cells and in human schwannomas. *Oncogene* 2009;28:854–65.
49. Lehar J, Krueger AS, Zimmermann GR, Borisy AA. Therapeutic selectivity and the multi-node drug target. *Discov Med* 2009;8:185–90.

# Molecular Cancer Therapeutics

## Combination Therapy with c-Met and Src Inhibitors Induces Caspase-Dependent Apoptosis of Merlin-Deficient Schwann Cells and Suppresses Growth of Schwannoma Cells

Marisa A. Fuse, Stephani Klingeman Plati, Sarah S. Burns, et al.

*Mol Cancer Ther* 2017;16:2387-2398. Published OnlineFirst August 3, 2017.

**Updated version** Access the most recent version of this article at:  
doi:[10.1158/1535-7163.MCT-17-0417](https://doi.org/10.1158/1535-7163.MCT-17-0417)

**Supplementary Material** Access the most recent supplemental material at:  
<http://mct.aacrjournals.org/content/suppl/2017/08/02/1535-7163.MCT-17-0417.DC1>

**Cited articles** This article cites 49 articles, 10 of which you can access for free at:  
<http://mct.aacrjournals.org/content/16/11/2387.full#ref-list-1>

**E-mail alerts** [Sign up to receive free email-alerts](#) related to this article or journal.

**Reprints and Subscriptions** To order reprints of this article or to subscribe to the journal, contact the AACR Publications Department at [pubs@aacr.org](mailto:pubs@aacr.org).

**Permissions** To request permission to re-use all or part of this article, use this link  
<http://mct.aacrjournals.org/content/16/11/2387>.  
Click on "Request Permissions" which will take you to the Copyright Clearance Center's (CCC) Rightslink site.



## Research Paper

## Overexpression of eIF4F components in meningiomas and suppression of meningioma cell growth by inhibiting translation initiation



Janet L. Oblinger<sup>a,b,c</sup>, Sarah S. Burns<sup>a,b,c</sup>, Jie Huang<sup>a,b,c</sup>, Li Pan<sup>e</sup>, Yulin Ren<sup>e</sup>, Rulong Shen<sup>d</sup>, A. Douglas Kinghorn<sup>e</sup>, D. Bradley Welling<sup>c,1</sup>, Long-Sheng Chang<sup>a,b,c,d,\*</sup>

<sup>a</sup> Center for Childhood Cancer and Blood Diseases, The Research Institute at Nationwide Children's Hospital, Columbus, OH, USA

<sup>b</sup> Department of Pediatrics, The Ohio State University College of Medicine, Columbus, OH, USA

<sup>c</sup> Department of Otolaryngology-Head and Neck Surgery, The Ohio State University College of Medicine, Columbus, OH, USA

<sup>d</sup> Department of Pathology, The Ohio State University College of Medicine, Columbus, OH, USA

<sup>e</sup> Division of Medicinal Chemistry and Pharmacognosy, The Ohio State University College of Pharmacy, Columbus, OH, USA

## ARTICLE INFO

## Article history:

Received 21 December 2016

Received in revised form 3 June 2017

Accepted 9 June 2017

Available online 10 June 2017

## Keywords:

Protein translation

eIF4F

eIF4A

eIF4E

eIF4G

Meningioma

Neurofibromatosis type 2 (NF2)

Merlin

Silvestrol

## ABSTRACT

Meningiomas frequently display activation of the PI3K/AKT/mTOR pathway, leading to elevated levels of phospho-eukaryotic translation initiation factor 4E binding proteins, which enhances protein synthesis; however, it is not known whether inhibition of protein translation is an effective treatment option for meningiomas. We found that human meningiomas expressed high levels of the three components of the eukaryotic initiation factor 4F (eIF4F) translation initiation complex, eIF4A, eIF4E, and eIF4G. The expression of eIF4A and eIF4E was important in sustaining the growth of NF2-deficient benign meningioma Ben-Men-1 cells, as shRNA-mediated knock-down of these proteins strongly reduced cell proliferation. Among a series of 23 natural compounds evaluated, silvestrol, which inhibits eIF4A, was identified as being the most growth inhibitory in both primary meningioma and Ben-Men-1 cells. Silvestrol treatment of meningioma cells prominently induced G<sub>2</sub>/M arrest. Consistently, silvestrol significantly decreased the amounts of cyclins D1, E1, A, and B, PCNA, and Aurora A. In addition, total and phosphorylated AKT, ERK, and FAK, which have been shown to be important drivers for meningioma cell proliferation, were markedly lower in silvestrol-treated Ben-Men-1 cells. Our findings suggest that inhibiting protein translation could be a potential treatment for meningiomas.

© 2017 Elsevier Inc. All rights reserved.

## 1. Introduction

Meningiomas, accounting for over one third of all primary brain tumors, cause significant morbidity, including cranial nerve palsy, seizures, and brainstem compression, which may lead to paralysis, aspiration pneumonia, and death (Ostrom et al., 2015). Current treatment options for these tumors are limited to surgery and radiation. However, incomplete tumor resection is not uncommon and is one of the main causes of tumor recurrence (Goldbrunner et al., 2016). Even after total gross resection, the 5-year recurrence rate is about 7–23% (Rogers et al., 2015). Meningiomas can occur sporadically or in patients with neurofibromatosis type 2 (NF2), which is caused by the inactivation of NF2/merlin tumor suppressor function (Rouleau et al., 1993; Trofatter et al., 1993). Importantly, patients with NF2 are at increased risk for multiple meningiomas, which often requires them to undergo several arduous treatment cycles. Development of an effective systemic medical therapy for meningiomas is therefore of urgent clinical need.

In addition to NF2-associated meningiomas, about 50% of sporadic tumors also harbor NF2 mutations. Loss of merlin abnormally activates several mitogenic signals, such as the PI3K/AKT/mTOR pathway (Ammoun et al., 2008; Jacob et al., 2008). Indeed, meningiomas often exhibit elevated levels of phospho-AKT (p-AKT), which can promote protein biosynthesis by stimulating p70 S6-kinase, leading to phosphorylation of the S6 ribosomal protein (Sorrells et al., 1999; De Benedetti and Graff, 2004; Holland et al., 2004; Anjum and Blenis, 2008; Menon and Manning, 2008; Kleiner et al., 2009; Ma and Blenis, 2009; Silvera et al., 2010; Li et al., 2012). Other important signaling proteins downstream of the PI3K/AKT/mTOR pathway include the 4E-binding protein (4E-BP) translational repressors; upon phosphorylation, these proteins are inactivated and protein biosynthesis is facilitated. Consistent with this notion, meningiomas display high p-4E-BP levels (Pachow et al., 2013), suggesting that protein translation initiation is likely enhanced in these tumors.

\* Corresponding author at: Center for Childhood Cancer and Blood Diseases, The Research Institute at Nationwide Children's Hospital, 700 Children's Drive, Columbus, OH 43205, USA. E-mail address: [Long-Sheng.Chang@nationwidechildrens.org](mailto:Long-Sheng.Chang@nationwidechildrens.org) (L.-S. Chang).

<sup>1</sup> Present address: Department of Otolaryngology, Harvard Medical School and Massachusetts Eye and Ear Infirmary, Massachusetts General Hospital, 243 Charles Street, Boston, MA 02114.

Initiation of protein translation is strictly-controlled and occurs when the eukaryotic initiation factor 4F (eIF4F) complex is recruited to the 5' cap structure of mRNA, followed by the unwinding of the secondary structure of its 5' untranslated region (Jackson et al., 2010; Silvera et al., 2010; Blagden and Willis, 2011). The eIF4F complex is composed of three components: eIF4E binds the 5' cap; the eIF4A RNA helicase unwinds the secondary structure; and eIF4G is a scaffold for other eIFs and enhances the eIF4A helicase activity. Studies have shown that the 4E-BP proteins repress translation by binding to eIF4G and preventing its association with eIF4E. Phosphorylation of 4E-BPs causes these proteins to dissociate from eIF4G, thus promoting eIF4F assembly. The effective formation of the eIF4F complex may require sufficient levels of each eIF4F component.

As uncontrolled growth of tumor cells often requires a high degree of protein translation, increased expression of the eIF4F components has been reported in several cancer types (Sorrells et al., 1999; De Benedetti and Graff, 2004; Kleiner et al., 2009; Silvera et al., 2010; Li et al., 2012). Overexpression of eIF4E promotes cell transformation (Lazaris-Karatzas et al., 1990) and frequently correlates with high tumor grade and poor patient prognosis (Li et al., 1997; Berkel et al., 2001; Li et al., 2012). While the oncogenicity of eIF4A and eIF4G has not been as well characterized as for eIF4E, elevated eIF4A and eIF4G levels have been reported in hepatocellular and lung carcinomas, respectively (Shuda et al., 2000; Bauer et al., 2001; Comtesse et al., 2007). Also, forced overexpression of eIF4A enhances malignant progression in an acute lymphocytic leukemia mouse model (Wolfe et al., 2014). Furthermore, enhanced protein translation has been described in a spectrum of neurological disorders, including autism spectrum disorders and fragile X syndrome (Silvera et al., 2010; Gkogkas et al., 2013; Gkogkas et al., 2014), suggesting that targeting translation initiation may have therapeutic potential. Recently, we reported elevated expression of all three eIF4F components in *NF2*-deficient vestibular schwannomas, and depletion of these eIF4F components reduced schwannoma cell growth (Oblinger et al., 2016). However, the protein levels of eIF4A, eIF4E, and eIF4G have not been rigorously explored in meningiomas.

In this study, we used meningioma tumors, primary meningioma cell cultures, and the benign *NF2*-deficient meningioma Ben-Men-1 cell line to demonstrate that meningiomas overexpress all three eIF4F components. Overexpression of these components is an important driver of meningioma cell proliferation, as confirmed by short-hairpin RNA-mediated knockdown and pharmacological inhibition. Our results suggest that inhibition of translation initiation factors should be further evaluated as a potential treatment for these tumors.

## 2. Materials and methods

### 2.1. Tissue acquisition and cell cultures

The Ohio State University (OSU) Institutional Review Board (IRB) approved the human subjects protocols for the acquisition of meningioma specimens, the diagnosis of which was confirmed by a pathologist. Fresh meningioma tissues were finely minced and digested with collagenase/dispase at 37 °C overnight as previously described (Chang and Welling, 2009). Primary meningioma cells, normal human meningeal cells (ScienCell), and *NF2*-deficient benign meningioma Ben-Men-1 cells were grown in Dulbecco's modified Eagle medium (DMEM) and 10% fetal bovine serum (FBS) (Thermo Fisher) as described previously (Burns et al., 2013). All primary cell cultures were used at early passages (less than five passages).

### 2.2. Natural compound treatment, cell proliferation assays, and flow cytometry

A series of 23 natural compounds, including silvestrol (Fig. 3A), was isolated and their structures and absolute configurations were previously reported (Kingham et al., 2011; Oblinger et al., 2016). Purified

compounds were dissolved in dimethyl sulfoxide (DMSO) to 1–10 mM and then diluted for cell proliferation assays. Briefly, Ben-Men-1 and primary meningioma cells were seeded in 96-well plates at 4000 cells/well and treated the next day with various concentrations of each natural compound or DMSO as a control. After three days, cell proliferation was assessed using resazurin, and the IC<sub>50</sub> values were determined (Burns et al., 2013).

Cell cycle analysis of drug-treated Ben-Men-1 cells was performed as previously described (Oblinger et al., 2016). A FACSCalibur flow cytometer (Becton Dickinson) was used to analyze samples after gating around the diploid population (FL2-A/FL2-W). Histograms and cell cycle distribution were determined using ModFit LT software (Verity Software House).

### 2.3. Western blots

Subconfluent Ben-Men-1 cells were treated with the indicated concentrations of silvestrol or DMSO vehicle for 24 h, followed by cell lysis and Western blotting according to Oblinger et al. (2016). The antibodies used included anti-eIF4A1 (2490), AKT (9272), phospho-AKT [p-AKT(Ser<sup>473</sup>)] (4060), extracellular signal-regulated kinases 1 and 2 (ERK1/2; 4695), p-ERK (4370), proline-rich Akt substrate of 40 kDa (PRAS40; 2691), p-PRAS40(Thr<sup>246</sup>) (2997), focal adhesion kinase (FAK; 3285), cyclin B1 (4138), cyclin D1 (2978), cyclin E1 (4129), glyceraldehyde 3-phosphate dehydrogenase (GAPDH; 5174), merlin (12888) (all from Cell Signaling Technology), proliferating cell nuclear antigen (PCNA; sc-56), cyclin A (sc-751), eIF4A2 (sc-137148), and eIF4G (sc-133155) (all from Santa Cruz Biotechnology), p-FAK(Tyr<sup>397</sup>) (700255 from Thermo Fisher), and eIF4E (ab33768 from Abcam). Protein bands were detected using an HRP-conjugated secondary antibody and the ECL Plus Western Blotting Substrate (Thermo Fisher) or a fluorescently-labeled secondary antibody and the Odyssey CLx imaging system (LI-COR Biosciences).

### 2.4. Lentiviral-mediated short-hairpin RNA (shRNA) transduction

Ben-Men-1 cells were seeded in 6-well plates at 9000 cells/well. The next day, cells were fed with fresh DMEM/10% FBS containing 8 µg/mL polybrene and then incubated overnight with MISSION shRNA lentiviruses targeting *EIF4A1* (TRCN0000288729; target sequence 5'-GCCGTAAAGGTGTGGCTATTA-3'), *EIF4A2* (TRCN0000051869; target sequence 5'-CGGGAGAGTGTGGATATGTT-3'), *EIF4E* (TRCN0000062573; target sequence 5'-CCAATCTGTAATAGTTCAGTA-3') or shNon-targeting lentivirus (#SHC002V, insert sequence 5'-CAACAAGATGAAGAGCACCAA-3'; all from Sigma) at a multiplicity of infection (MOI) of 10. Two days following transduction, puromycin (Corning) was added to the culture medium to a final concentration of 2.5 µg/mL. Cells were grown for another 8 days before counting on a hemocytometer. Subsequently, the cells were centrifuged, and the resulting pellets were lysed in 2% SDS with protease and phosphatase inhibitors (Sigma). Equal amounts of protein were analyzed by Western blot for eIF4A1, eIF4A2, eIF4E, and GAPDH (Oblinger et al., 2016). Fluorescently-labeled protein bands were captured on an Odyssey CLx Imager (LI-COR BioSciences), quantitated using Image Studio, and calculated as percent of the nontargeting control after normalization to GAPDH.

### 2.5. Immunohistochemistry (IHC)

Archived formalin-fixed, paraffin-embedded sections of human meningioma tissues were acquired, deparaffinized, and immunostained for eIF4A1-II (sc-50354) and eIF4G (sc-133155) (both from Santa Cruz) and eIF4E (ab33768 from Abcam) as previously described (Burns et al., 2013). Quantification of immunostaining signal was performed by a pathologist and an investigator using visual analysis based on the intensity and percentage of immunopositive cells.

### 3. Results

#### 3.1. Meningiomas expressed elevated levels of eIF4A, eIF4E, and eIF4G compared to normal meningeal cells

To determine the expression levels of the eIF4F components, we performed immunohistochemical staining for eIF4A, eIF4E, and eIF4G on 16 meningiomas, including six grade I sporadic tumors, four grade I NF2-associated tumors, five grade II sporadic tumors, and one grade III sporadic tumor. All of these meningiomas showed more intense labeling of eIF4F components compared to adjacent normal meningeal tissues (Fig. 1 and Table 1). Fifty percent of the meningioma specimens (8/16) were scored as having 1+ or greater labeling for eIF4A, 94% of the tumors (15/16) were scored as having 1+ or greater labeling for eIF4E, and 75% percent of the tumors (12/16) were scored as having 1+ or greater labeling for eIF4G. Notably, all four NF2-associated tumors had intense staining for eIF4A and eIF4E (Table 1).

The RNA helicase eIF4A had prominent perinuclear staining, consistent with its role in translation initiation and localization to the rough endoplasmic reticulum. Staining for eIF4E occurred more diffusely throughout the cytoplasm, with faint nuclear labeling (Rosenwald et al., 1995; Culjkovic et al., 2008). The labeling pattern for eIF4G was diffusely cytoplasmic, with some conspicuous rimming around the nucleus that resembled the perinuclear concentrations observed with eIF4A. While the sample size was limited, the six high grade meningiomas (five grade II and one grade III) tended to show higher labeling in eIF4G, when compared to grade I tumors (Table 1).

To confirm these findings, we compared eIF4A, eIF4E, and eIF4G protein expression in four primary grade I meningioma cultures prepared from two sporadic (Primary meningiomas #1 and 2 in Fig. 2A) and two NF2-associated tumors (Primary meningiomas #3 and 4) and the telomerase-immortalized Ben-Men-1 benign meningioma line with those in primary meningeal cells. All four primary cultures of

meningioma cells and Ben-Men-1 cells uniformly exhibited higher levels of all three eIF4F components relative to normal meningeal cells (Fig. 2A). As previously reported (Burns et al., 2013), Ben-Men-1 cells did not express merlin protein. In addition, merlin was not detected in three of the four primary meningioma cultures and was greatly reduced in the fourth meningioma culture. Collectively, these results indicate increased expression of eIF4A, eIF4E, and eIF4G in meningiomas.

#### 3.2. Inhibition of eIF4A and eIF4E impaired meningioma cell proliferation

To verify the importance of eIF4F components in meningioma cell growth, we used shRNA-containing lentiviruses to silence eIF4A and eIF4E expression in Ben-Men-1 cells. Consistent with the knockdown efficiencies (Fig. 2B), depletion of eIF4A2 or eIF4E dramatically reduced cell numbers by about 87% and 80%, respectively, relative to control cells that were transduced with a nontargeting shRNA construct (Fig. 2C). Silencing eIF4A1 gave rise to partial growth suppression, which was commensurate with a moderate knockdown efficiency (Fig. 2B and C). These results indicate that silencing of either eIF4A1 or eIF4A2 impairs meningioma cell proliferation. We also noted that knockdown of any individual eIF resulted in modest decreases in the other eIF4F components. In these conditions, the levels of eIF4E seemed to be particularly sensitive, decreasing by 53% and 36% after depletion of eIF4A1 or eIF4A2, respectively.

As an FDA-approved medical therapy is currently not available for the treatment of meningiomas, identification of new therapeutics for patients with meningiomas is of great clinical interest. The growth inhibition observed from the eIF4A and eIF4E RNA interference experiments (Fig. 2B and C) suggested that meningioma cells may be susceptible to pharmacological inhibition of these eIF4F components. Interestingly, we found that among a series of botanical compounds evaluated, the eIF4A inhibitors silvestrol and episilvestrol, an isomer of silvestrol, were the most potent in inhibiting proliferation of Ben-Men-1 cells and primary meningioma cells based on the IC<sub>50</sub> values and maximal killing effects

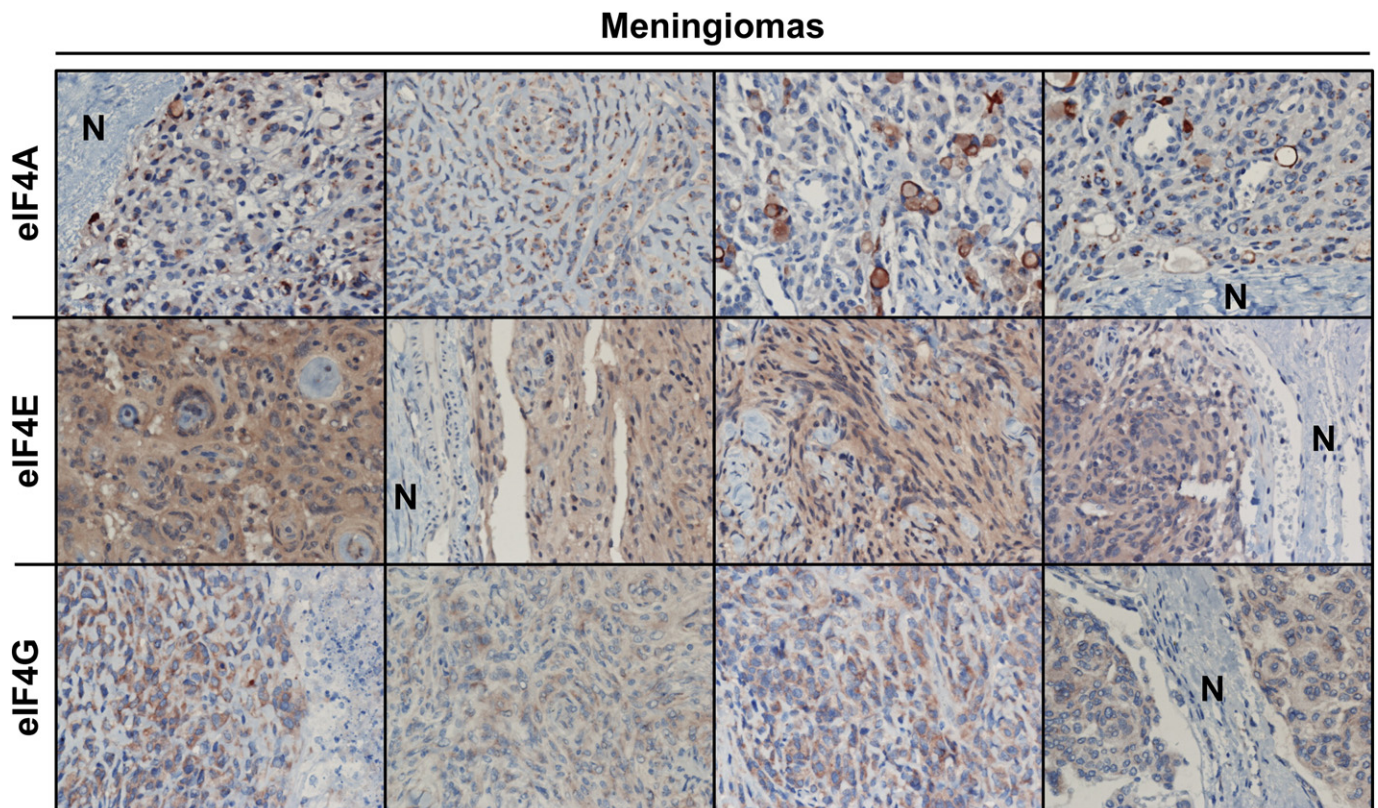


**Fig. 1.** Meningioma tissues overexpressed all three components of the eIF4F complex. Shown are representative images of meningioma sections immunostained for eIF4A, eIF4E, and eIF4G. "N" indicates adjacent normal meninges. The staining scores for all tumors are reported in Table 1.

**Table 1**  
Clinicopathological information of meningiomas and their relative IHC staining signals for eIF4A, eIF4E, and eIF4G. Meningioma tumor sections were processed for immunohistochemistry analysis as described in the [Materials and methods](#). Immunostaining signals were quantified using visual analysis based on the intensity and percentage of immunopositive cells (0 as negative, 0.5 = weak positive, 1 = moderate positive, 2 = strong positive, and 3 = very strong positive). Adjacent normal meningeal cells showed little to no staining and were scored as 0 ([Fig. 1](#)).

Tumor ID	Gender	Tumor grade	Histological type	Clinical diagnosis	Tumor size (cm)	IHC staining signals		
						eIF4A	eIF4E	eIF4G
Men01	F	WHO grade I	Meningothelial	Sporadic	3.3 × 2.7 × 1.6	0.5 +	1 +	0–0.5 +
Men02	F	WHO grade I	Meningothelial	Sporadic	2.0 × 1.0 × 1.0	1–2 +	0.5 +	1–2 +
Men03	F	WHO grade I	Fibrous	Sporadic	3.2 × 2.6 × 1.3	0.5 +	2 +	0.5–1 +
Men04	F	WHO grade I	Meningothelial	Sporadic	2.5 × 2.0 × 1.8	0.5 +	2 +	1–1.5 +
Men05	N/A <sup>a</sup>	WHO grade I	Meningothelial	Sporadic	2.5 × 1.5 × 1.0	1–2 +	1–2 +	1–2 +
Men06	F	WHO grade I	Meningothelial	Sporadic	2.5 × 1.8 × 0.9	0.5 +	2 +	0.5–1 +
Men07	M	WHO grade I	Meningothelial	NF2	2.0 × 1.2 × 0.8	1–3 +	2–3 +	2–3 +
Men08	F	WHO grade I	Meningothelial	NF2	3.4 × 2.8 × 1.7	0.5–1 +	1–2 +	0.5 +
Men09	M	WHO grade I	Meningothelial	NF2	3.2 × 2.9 × 3.4	1–3 +	1–2 +	0.5 +
Men10	M	WHO grade I	Meningothelial	NF2	2.0 × 2.2 × 2.5	2–3 +	1–2 +	0.5 +
Men11	F	WHO grade II	Atypical	Sporadic	3.2 × 1.4 × 2.1	0.5–1 +	1–3 +	1–2 +
Men12	F	WHO grade II	Atypical	Sporadic	9.0 × 4.0 × 3.0	0.5 +	1–1.5 +	1–2 +
Men13	F	WHO grade II	Atypical	Sporadic	3.0 × 2.5 × 1.1	0.5 +	2 +	1 +
Men14	M	WHO grade II	Atypical	Sporadic	1.5 × 1.0 × 0.8	0.5 +	0.5–1 +	0.5–1 +
Men15	F	WHO grade II	Chordoid	Sporadic	6.5 × 6.0 × 3.0	0.5–1 +	1 +	1 +
Men16	M	WHO grade III	Anaplastic	Sporadic	5.8 × 4.0 × 3.1	0.5 +	1 +	1–1.5 +

<sup>a</sup> N/A, not available.

([Fig. 3A](#)). Silvestrol consistently inhibited meningioma cell proliferation at very low IC<sub>50</sub> values (~10 nM in Ben-Men-1 and ~25 nM in primary meningioma cultures) ([Fig. 3A and B](#)). These results highlight the importance of eIF4F components in the growth of meningioma cells.

### 3.3. Silvestrol treatment induced G<sub>2</sub>/M arrest and reduced the levels of several cell-cycle and mitogenic proteins

Consistent with previous reports ([Mi et al., 2006a; Oblinger et al., 2016](#)), silvestrol induced cell cycle arrest at the G<sub>2</sub>/M phase. Ben-Men-1 cells treated with the IC<sub>50</sub> dose of silvestrol for three days had an over two-fold increase in the proportion of cells in G<sub>2</sub>/M (untreated, 5.68% versus silvestrol-treated, 12.86%; [Fig. 4](#)). This effect became even more pronounced at twice the IC<sub>50</sub> dose, in which over half the cell population was in the G<sub>2</sub>/M fraction. To further examine the effects of silvestrol on the cell cycle, we profiled the expression of various cell cycle proteins. Ben-Men-1 cells treated with silvestrol exhibited sharp reductions in all examined cyclins (D1, E1, A, and B1) as well as the mitotic Aurora A kinase ([Fig. 5](#)). PCNA, which acts during S phase to facilitate DNA synthesis, was also markedly reduced. This is consistent with the finding that silvestrol treatment of Ben-Men-1 cells reduced the S phase fraction ([Fig. 4](#)).

NF2-deficient tumors often exhibit increased phosphorylation of the AKT, ERK1/2, and FAK kinases ([Poulikakos et al., 2006; Jacob et al., 2008; Hilton et al., 2009; Endo et al., 2013; Ammoun et al., 2014](#)), and activation of these kinases can lead to enhanced protein biosynthesis ([Silvera et al., 2010](#)). We found that silvestrol treatment decreased both the total and phosphorylated AKT as well as its downstream substrate PRAS40 in Ben-Men-1 cells ([Fig. 5](#)). Likewise, both the total and phosphorylated ERK1/2 and FAK were suppressed in silvestrol-treated meningioma cells. Taken together, these results suggest that silvestrol exerts its anti-proliferative action by simultaneously reducing multiple pro-growth signaling molecules.

## 4. Discussion

Despite being the most frequent brain tumors, the biology of meningiomas is not well understood and an FDA-approved medical therapy is currently not available for these tumors. While alterations in the NF2 gene frequently occur, recent molecular genetic studies have identified mutations in *AKT1*, *SMO*, *KLF4*, *TRAF7*, and *POLR2A* in non-NF2 meningiomas ([Brastianos et al., 2013; Clark et al., 2013; Clark et al., 2016](#)). In

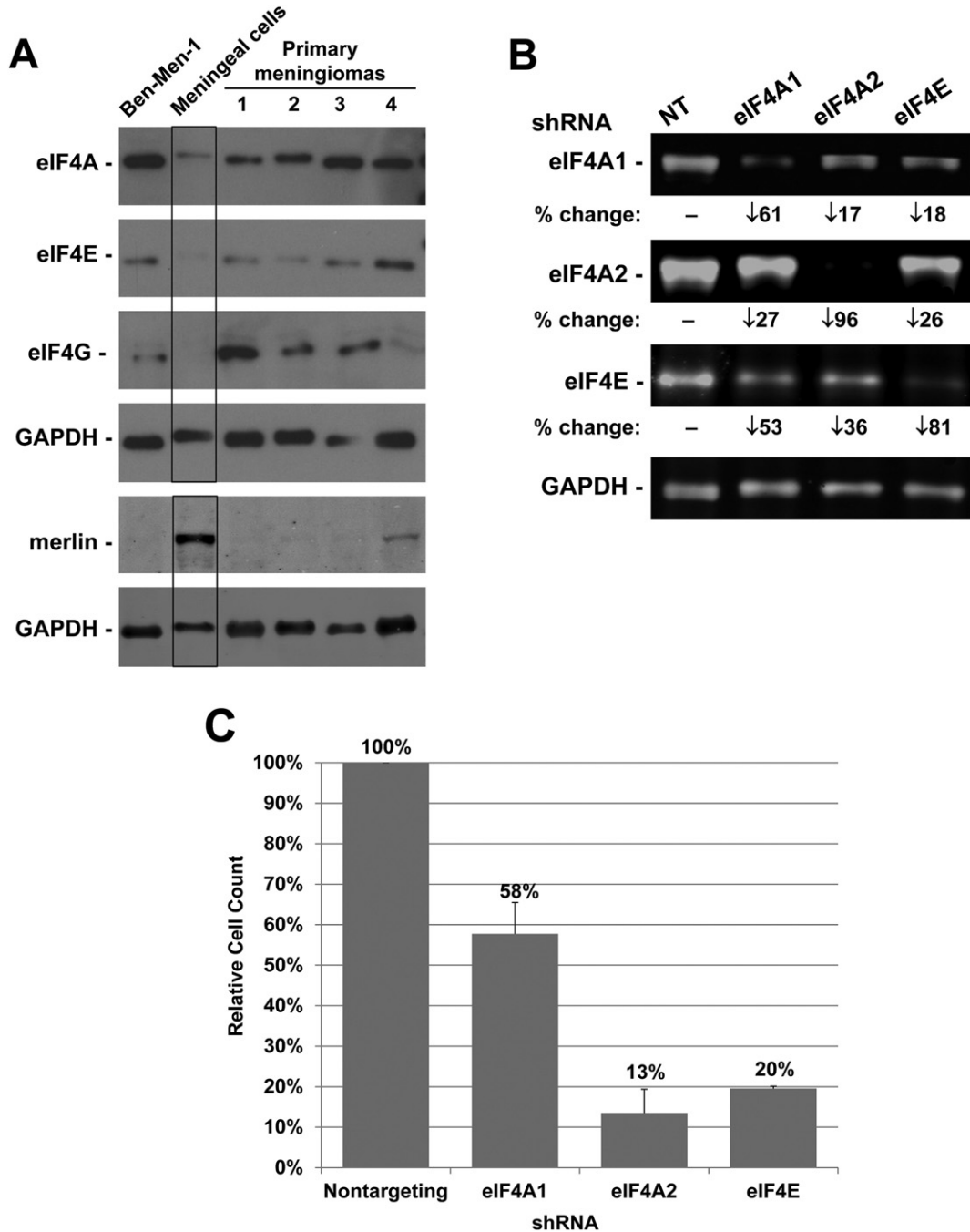
addition, gene expression analyses have identified AKT as one of the key drivers for meningioma growth ([Wang et al., 2012; Hilton et al., 2016](#)). Activation of AKT promotes protein translation initiation, which is dependent upon expression and assembly of several eIF complexes ([Jackson et al., 2010; Silvera et al., 2010](#)). Intriguingly, high levels of eIF4E correlate with meningioma grade ([Tejada et al., 2009](#)). Meningiomas lacking NF2 frequently have more abundant eIF3C than NF2-expressing tumors ([Scoles et al., 2006](#)). We now report that all three components of the eIF4F complex are overexpressed in meningiomas. While the number of meningiomas that we analyzed is small, the NF2-associated grade I meningiomas that we analyzed exhibited high levels of these proteins, particularly eIF4A and eIF4E, when compared to sporadic grade I tumors ([Table 1 and Fig. 2A](#)). Similarly, we recently reported that NF2-associated vestibular schwannomas also appeared to have more eIF4F components ([Oblinger et al., 2016](#)). In addition, we observed that the six high grade (II and III) tumors expressed higher amounts of eIF4E and eIF4G, compared to sporadic grade I tumors ([Table 1](#)). In line with this tumor study, our primary cultures of meningioma cells also showed elevated levels of eIF4F components compared with normal meningeal cells. It would be interesting to extend our study to a larger cohort of tumors to see if these findings can be confirmed and if they correlate with any clinical outcome parameters.

Both RNA silencing and pharmacological inhibition verified that these eIF4F components are critical for meningioma cell growth. Using shRNA-mediated knockdown in Ben-Men-1 cells, we found that silencing eIF4A1, eIF4A2, or eIF4E was sufficient to inhibit cell growth. Curiously, eIF4A2 appeared to be as important for proliferation as eIF4A1 since eIF4A2 knockdown profoundly impaired proliferation of meningioma cells ([Fig. 2C](#)). Previously, we observed similar results in malignant peripheral nerve sheath tumor (MPNST) cells ([Oblinger et al., 2016](#)). However, the role of eIF4A2 on cell proliferation may depend upon the cell type ([Galicia-Vázquez et al., 2012](#)). In a similar context, it would be also interesting to investigate the role of eIF4G in meningioma cell growth. As isoforms exist in eIF4G ([Silvera et al., 2010](#)), the contribution of each isoform should be evaluated as we did with eIF4A1 and eIF4A2. Unexpectedly, we did not observe that depletion of eIF4A1, eIF4A2, or eIF4E resulted in a compensatory increase of the other two eIF4F components, but instead, we saw modest decreases in the levels of these components ([Fig. 2B](#)). Our previous study in MPNST cells also showed reduced eIF4E levels following knockdown of eIF4A1 or eIF4A2 protein ([Oblinger et al., 2016](#)), suggesting coordinate regulation of these eIF4F components.

The importance of eIF4A activity for meningioma cell proliferation was also validated by the identification of the eIF4A inhibitor silvestrol as being profoundly growth inhibitory in both primary meningioma and Ben-Men-1 cells. Consistent with previous reports (Mi et al., 2006a; Oblinger et al., 2016), silvestrol treatment resulted in a prominent G<sub>2</sub>/M arrest in meningioma cells (Fig. 4). Cyclin levels are induced during specific phases of the cell cycle and are well-known for having a fast protein turnover rate (Pines, 1996). While tumor cells frequently exhibit an abnormal G<sub>1</sub> checkpoint, sharp declines in multiple cyclins

following silvestrol treatment render them liable to G<sub>2</sub>/M arrest. Additionally, the pro-growth signaling molecules AKT, ERK1/2, and FAK are frequently phosphorylated and activated in NF2-related tumor cells (Poulidakos et al., 2006; Jacob et al., 2008). Reducing the levels of these mitogenic signals would be expected to reinforce silvestrol's growth inhibitory properties.

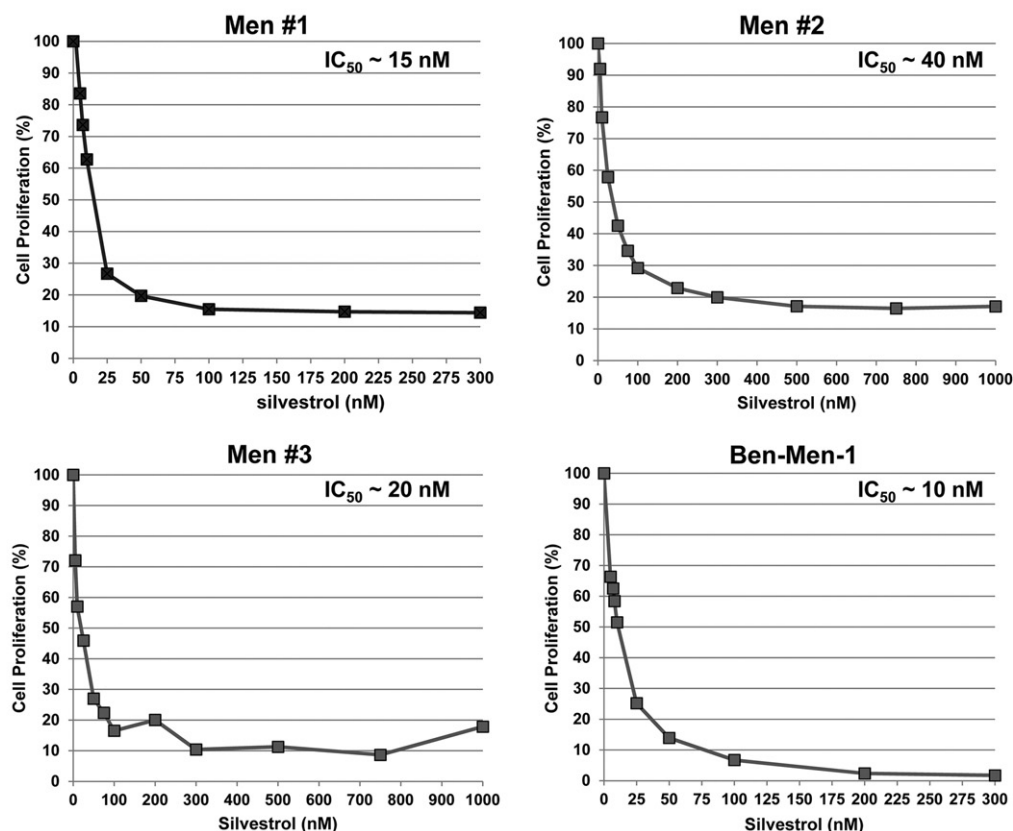
With its high potency in several tumor types, silvestrol has been rigorously investigated as a potential cancer therapeutic (Pan et al., 2014). While it is well tolerated in mice, studies are ongoing to determine



**Fig. 2.** Meningioma cells expressed higher levels of eIF4F components. (A) Overexpression of eIF4F components in primary meningioma cells and the Ben-Men-1 benign meningioma cell line. Total cell lysates from four primary cultures of meningioma cells, normal human meningeal cells, and Ben-Men-1 cells were resolved by SDS-PAGE and probed for eIF4E, eIF4A, eIF4G, merlin, and GAPDH (loading control). The four meningiomas used to prepare primary cell cultures included two sporadic (#1 and #2) and two NF2-associated (#3 and #4) grade I tumors. (B) Silencing each indicated eIF4F component by shRNA. Ben-Men-1 cells were transduced with 10 MOI of lentiviruses expressing the indicated shRNAs (Materials and methods). After 8 days, cells were lysed and analyzed by Western blotting for eIF4A1, eIF4A2, eIF4E, and GAPDH. Fluorescently-labeled protein bands were detected on the Odyssey CLx and quantitated in Image Studio. Shown below the blots is the % decrease in the eIF4A1, eIF4A2, or eIF4E protein level in shRNA-transduced cells relative to the nontargeting (NT) control. (C) Suppression of meningioma cell growth following depletion of eIF4A or eIF4E. Ben-Men-1 cells transduced as described in (B) were counted. Shown are the means and standard deviations (SDs) from two independent experiments run in technical duplicates.

**A**

Compound \ IC <sub>50</sub>	Ben-Men-1 cells	Primary meningioma cells
Silvestrol	10 nM	25 nM
Episilvestrol	32 nM	25 nM
Bruceantin	200 nM	256 nM
Bruceine A	960 nM	1190 nM
13-Acetoxyrolandrolide	800 nM	1 $\mu$ M
2 $\alpha$ ,13-diacetoxy-4 $\alpha$ -hydroxy-8 $\alpha$ -methacryloyloxybourbonen-12,6 $\alpha$ -olide	> 10 $\mu$ M	> 10 $\mu$ M
Cucurbitacin D	200 nM	200 nM
Dichamanetin	27 $\mu$ M	27 $\mu$ M
Antidesmone	4 $\mu$ M	36 $\mu$ M
(-)-Isogaudichaudiic acid	7 $\mu$ M	15 $\mu$ M
Artonin O	13 $\mu$ M	18 $\mu$ M
Artobioxanthone	30 $\mu$ M	32 $\mu$ M
Artorigidin A	7 $\mu$ M	12 $\mu$ M
$\alpha$ -Mangostin	> 18 $\mu$ M	> 18 $\mu$ M
1,3,7-trihydroxy-2,4-diisoprenylxanthone	30 $\mu$ M	30 $\mu$ M
Cochinchinone A	24 $\mu$ M	22 $\mu$ M
3,4'-dimethoxy-5,7,3'-trihydroxyflavone	> 4 $\mu$ M	> 4 $\mu$ M
Goyazensolide	1 $\mu$ M	> 4 $\mu$ M
[3-(3,5-dimethoxy-4-hydroxyphenyl)]propanol-trans-coumarate	> 45 $\mu$ M	45 $\mu$ M
CAPE	> 20 $\mu$ M	ND
Curcumin	7 $\mu$ M	ND
Resveratrol	> 30 $\mu$ M	ND
Sulforaphane	8 $\mu$ M	ND

**B**

**Fig. 3.** Silvestrol potently inhibited proliferation of meningioma cells. (A) The natural compounds used in this study and their IC<sub>50</sub> values in Ben-Men-1 and primary meningioma cells are summarized. Data shown are the mean IC<sub>50</sub> values from three independent experiments. CAPE, caffeic acid phenethyl ester; ND, not determined. (B) Resazurin assays for cell proliferation were performed on primary meningioma cells and Ben-Men-1 cells treated with various concentrations of silvestrol for three days. Primary meningioma cells were derived from three separate tumors (Men #1–3) and assays were performed in six replicate wells; the IC<sub>50</sub> values for each experiment are shown in the graph insets. The mean IC<sub>50</sub> value for primary meningioma cells across the three experiments was ~25 nM. Experiments on Ben-Men-1 cells were performed in six replicates, and the experiments were independently repeated three times. Data shown are the mean of the six replicate wells from one representative experiment. The mean IC<sub>50</sub> value for Ben-Men-1 cells across all three experiments was ~10 nM.

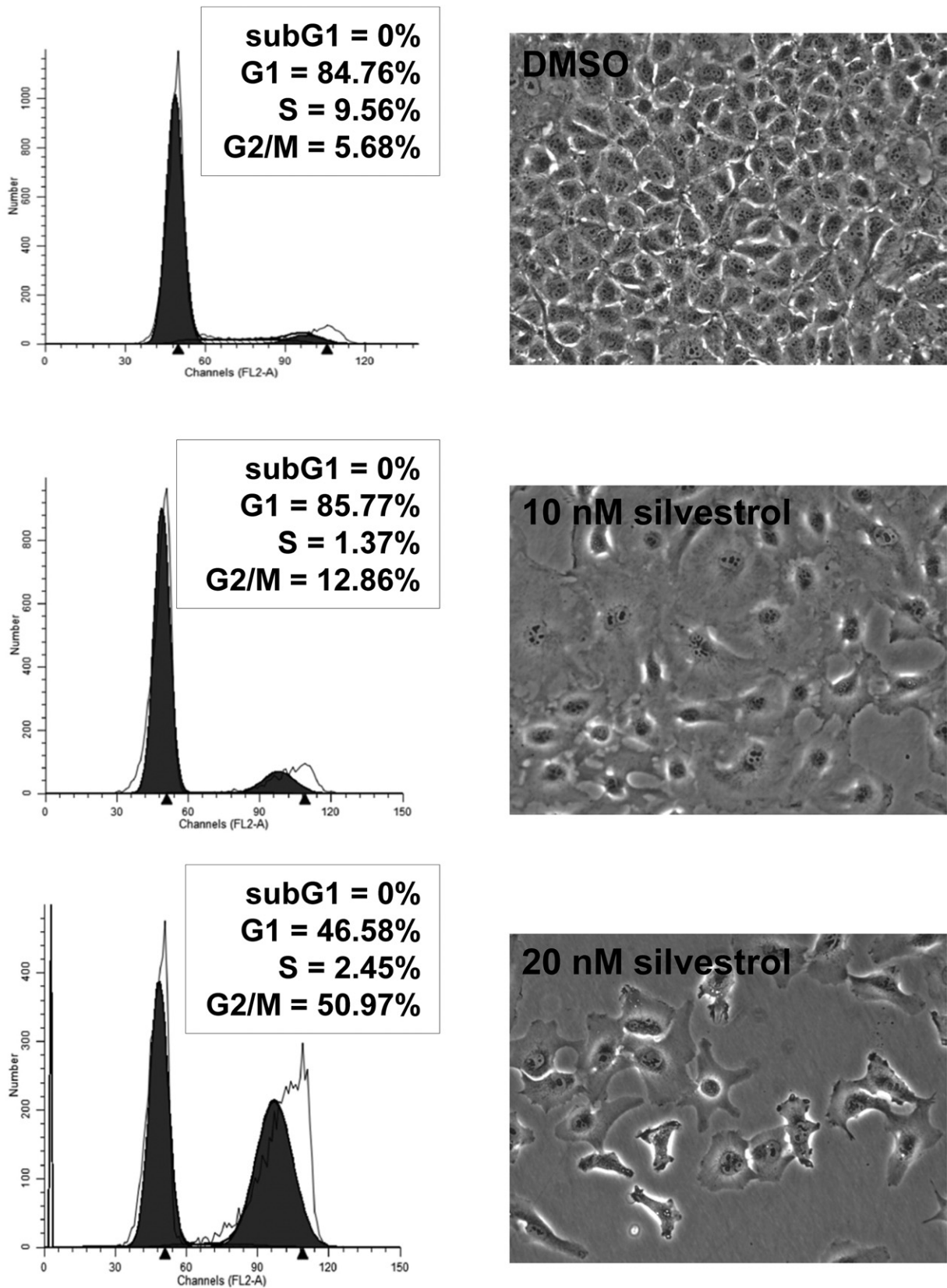


**Fig. 4.** Silvestrol induced G<sub>2</sub>/M arrest in meningioma cells. Ben-Men-1 cells were treated with the indicated concentrations of silvestrol for three days, and phase contrast images of treated cells were taken, followed by cell harvesting for flow cytometry analysis as described in the [Materials and methods](#). Cell cycle histograms of propidium iodide-labeled cells revealed a prominent increase in the G<sub>2</sub>/M peak after silvestrol treatment.

dosing schedules and toxicity in large animals. We have demonstrated that silvestrol exhibits consistent strong suppression of the growth of meningioma cells in culture (Fig. 3). Previous pharmacokinetic analysis showed that silvestrol requires intraperitoneal or intravenous delivery for maximal bioavailability (Saradhi et al., 2011). However, even with these delivery methods, the distribution to the brain is relatively low, suggesting that silvestrol may not readily cross the blood-brain barrier. Silvestrol has a bulky sugar-like dioxanyl ring, which has been shown to confer susceptibility to the multi-drug resistance protein 1 (MDR1) transporter (Gupta et al., 2011). This characteristic may limit the distribution of silvestrol to the brain. Intriguingly, rocaglaol, a silvestrol-related compound lacking this ring, possesses antitumor activity and a synthetic analog of rocaglaol displays activity in drug-resistant promyelocytic leukemia cells that overexpress MDR1 (Mi et al., 2006b; Thuaud et al., 2011; Pan et al., 2013). The finding that the growth-suppressive effects of rocaglaol are also mediated by inhibiting protein translation indicates that the dioxanyl ring of silvestrol is dispensable for eIF4A inhibition (Ohse et al., 1996). Moreover, rocaglaol analogs may exhibit cardioprotective and/or neuroprotective effects (Bernard et al., 2011; Thuaud et al., 2011). A halogenated rocaglaol derivative has been shown to be capable of crossing the blood-brain barrier (Fahrig et al., 2005; Thuaud et al., 2011). In addition, our preliminary study has identified several silvestrol-related rocaglates that lack the dioxanyl ring but exhibit potent growth-inhibitory activity in meningioma cells (data not shown). Nevertheless, it should be noted that

meningiomas may disrupt the blood-brain barrier. Experiments are in progress to evaluate the anti-tumor effects of silvestrol and a series of silvestrol-related rocaglates lacking this dioxanyl ring in an orthotopic mouse model for meningioma (Burns et al., 2013). Identification of an effective treatment for meningioma would significantly advance our efforts to improve clinical care and long-term treatment outcomes for these patients.

### Conflict of interest statement

The authors declare no conflict of interest.

### Authorship

Conception and design of the study: JLO, SSB, and LSC.

Performance of experiments: JLO, SSB, JH, LP, YR, ADK, and LSC.

Analysis and interpretation of the data: JLO, SSB, RS, DBW, and LSC.

Manuscript writing: JLO and LSC.

### Acknowledgements

We sincerely thank Drs. Aaron Moberly and Oliver Adunka for meningioma specimens and the OSU Cooperative Human Tissue Network and Tissue Archives for tissue sections. This study was supported by grants from the US Department of Defense (W81XWH-16-1-0104), Advocure NF2, the Galloway family, Meningioma Mommas, and CancerFree Kids to LSC and from the National Cancer Institute to ADK (P01 CA125066) and to the OSU Comprehensive Cancer Center (P30 CA16058).

### References

- Ammoun, S., Flaiz, C., Ristic, N., Schuldt, J., Hanemann, C.O., 2008. Dissecting and targeting the growth factor-dependent and growth factor-independent extracellular signal-regulated kinase pathway in human schwannoma. *Cancer Res.* 68, 5236–5245.
- Ammoun, S., Provenzano, L., Zhou, L., Barczyk, M., Evans, K., Hilton, D.A., Hafizi, S., Hanemann, C.O., 2014. Axl/Gas6/NF- $\kappa$ B signalling in schwannoma pathological proliferation, adhesion and survival. *Oncogene* 33, 336–346.
- Anjum, R., Blenis, J., 2008. The RSK family of kinases: emerging roles in cellular signalling. *Nat. Rev. Mol. Cell Biol.* 9, 747–758.
- Bauer, C., Diesinger, I., Brass, N., Steinhart, H., Iro, H., Meese, E.U., 2001. Translation initiation factor eIF-4G is immunogenic, overexpressed, and amplified in patients with squamous cell lung carcinoma. *Cancer* 92, 822–829.
- Berkel, H.J., Turbat-Herrera, E.A., Shi, R., de Benedetti, A., 2001. Expression of the translation initiation factor eIF4E in the polyp-cancer sequence in the colon. *Cancer Epidemiol. Biomark. Prev.* 10, 663–666.
- Bernard, Y., Ribeiro, N., Thuaud, F., Türkeri, G., Dirr, R., Boulberdaa, M., Nebigil, C.G., Désaubry, L., 2011. Flavaglines alleviate doxorubicin cardiotoxicity: implication of Hsp27. *PLoS One* 6, e25302.
- Blagden, S.P., Willis, A.E., 2011. The biological and therapeutic relevance of mRNA translation in cancer. *Nat. Rev. Clin. Oncol.* 8, 280–291.
- Brastianos, P.K., Horowitz, P.M., Santagata, S., Jones, R.T., McKenna, A., Getz, G., Ligon, K.L., Palescandolo, E., Van Hummelen, P., Ducar, M.D., Raza, A., Sunkavalli, A., Macconail, L.E., Stemmer-Rachamimov, A.O., Louis, D.N., Hahn, W.C., Dunn, I.F., Beroukhim, R., 2013. Genomic sequencing of meningiomas identifies oncogenic SMO and AKT1 mutations. *Nat. Genet.* 45, 285–289.
- Burns, S.S., Akhrametyeva, E.M., Oblinger, J.L., Bush, M.L., Huang, J., Senner, V., Chen, C.-S., Jacob, A., Welling, D.B., Chang, L.-S., 2013. Histone deacetylase inhibitor AR-42 differentially affects cell-cycle transit in meningeal and meningioma cells, potentially inhibiting NF2-deficient meningioma growth. *Cancer Res.* 73, 792–803.
- Chang, L.S., Welling, D.B., 2009. Molecular biology of vestibular schwannomas. *Methods Mol. Biol.* 493, 163–177.
- Clark, V.E., Erson-Omay, E.Z., Serin, A., Yin, J., Cotney, J., Ozduman, K., Avşar, T., Li, J., Murray, P.B., Henegariu, O., Yilmaz, S., Günel, J.M., Carrión-Grant, G., Yilmaz, B., Grady, C., Tanrikulu, B., Bakircioğlu, M., Kaymakçalan, H., Caglayan, A.O., Sencar, L., Ceyhan, E., Atik, A.F., Bayri, Y., Bai, H., Kolb, L.E., Hebert, R.M., Omay, S.B., Mishra-Gorur, K., Choi, M., Overton, J.D., Holland, E.C., Mane, S., State, M.W., Bilgüvar, K., Baehring, J.M., Gutin, P.H., Piepmeyer, J.M., Vortmeyer, A., Brennan, C.W., Pamiir, M.N., Kiliç, T., Lifton, R.P., Noonan, J.P., Yasuno, K., Günel, M., 2013. Genomic analysis of non-NF2 meningiomas reveals mutations in TRAF7, KLF4, AKT1, and SMO. *Science* 339, 1077–1080.
- Clark, V.E., Harmanci, A.S., Bai, H., Youngblood, M.W., Lee, T.I., Baranoski, J.F., Ercan-Sencicek, A.G., Abraham, B.J., Weintraub, A.S., Hniz, D., Simon, M., Kirschek, B., Erson-Omay, E.Z., Henegariu, O., Carrión-Grant, G., Mishra-Gorur, K., Durán, D., Goldmann, J.E., Schramm, J., Goldbrunner, R., Piepmeyer, J.M., Vortmeyer, A.O.,

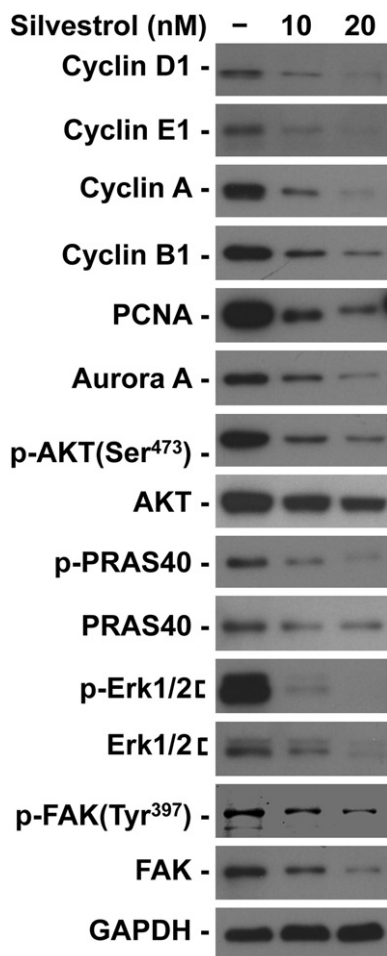


**Fig. 5.** Silvestrol suppressed the expression of multiple cell cycle proteins and mitogenic kinases. Ben-Men-1 cells were treated with 1× and 2× the IC<sub>50</sub> dose of silvestrol for 24 h followed by cell lysis and Western blotting for the indicated proteins. GAPDH served as a loading control.

- Günel, J.M., Bilgüvar, K., Yasuno, K., Young, R.A., Günel, M., 2016. Recurrent somatic mutations in *POLR2A* define a distinct subset of meningiomas. *Nat. Genet.* 48, 1253–1259.
- Comtesse, N., Keller, A., Diesinger, I., Bauer, C., Kayser, K., Huwer, H., Lenhof, H.P., Meese, E., 2007. Frequent overexpression of the genes *FXR1*, *CLAMP1* and *EIF4G* located on amplicon 3q26–27 in squamous cell carcinoma of the lung. *Int. J. Cancer* 120, 2538–2544.
- Culjkovic, B., Tan, K., Orolicki, S., Amri, A., Meloche, S., Borden, K.L., 2008. The *elf4E* RNA regulon promotes the Akt signaling pathway. *J. Cell Biol.* 181, 51–63.
- De Benedetti, A., Graff, J.R., 2004. *elf4E* expression and its role in malignancies and metastases. *Oncogene* 23, 3189–3199.
- Endo, M., Yamamoto, H., Setsu, N., Kohashi, K., Takahashi, Y., Ishii, T., Iida, K., Matsumoto, Y., Hakozi, M., Aoki, M., Iwasaki, H., Dobashi, Y., Nishiyama, K., Iwamoto, Y., Oda, Y., 2013. Prognostic significance of AKT/mTOR and MAPK pathways and antitumor effect of mTOR inhibitor in NF1-related and sporadic malignant peripheral nerve sheath tumors. *Clin. Cancer Res.* 19, 450–461.
- Fahrig, T., Gerlach, I., Horváth, E., 2005. A synthetic derivative of the natural product rosciglaol is a potent inhibitor of cytokine-mediated signaling and shows neuroprotective activity in vitro and in animal models of Parkinson's disease and traumatic brain injury. *Mol. Pharmacol.* 67, 1544–1555.
- Galicía-Vázquez, G., Cencic, R., Robert, F., Agenor, A.Q., Pelletier, J., 2012. A cellular response linking *elf4A1* activity to *elf4AII* transcription. *RNA* 18, 1373–1384.
- Gkogkas, C.G., Khoutorsky, A., Ran, I., Lampakakis, E., Nevarko, T., Weatherill, D.B., Vasuta, C., Yee, S., Truitt, M., Dallaire, P., Major, F., Lasko, P., Ruggero, D., Nader, K., Lacaille, J.C., Sonenberg, N., 2013. Autism-related deficits via dysregulated *elf4E*-dependent translational control. *Nature* 493, 371–377.
- Gkogkas, C.G., Khoutorsky, A., Cao, R., Jafarnejad, S.M., Prager-Khoutorsky, M., Giannakas, N., Kaminari, A., Fragkouli, A., Nader, K., Price, T.J., Konicek, B.W., Graff, J.R., Tzinia, A.K., Lacaille, J.C., Sonenberg, N., 2014. Pharmacogenetic inhibition of *elf4E*-dependent *Mmp9* mRNA translation reverses fragile X syndrome-like phenotypes. *Cell Rep.* 9, 1742–1755.
- Goldbrunner, R., Minniti, G., Preusser, M., Jenkinson, M.D., Sallabanda, K., Houdart, E., von Deimling, A., Stavrinou, P., Lefranc, F., Lund-Johansen, M., Moyal, E.C., Brandsma, D., Henriksson, R., Soffietti, R., Weller, M., 2016. EANO guidelines for the diagnosis and treatment of meningiomas. *Lancet Oncol.* 17, e383–e391.
- Gupta, S.V., Sass, E.J., Davis, M.E., Edwards, R.B., Lozanski, G., Heerema, N.A., Lehman, A., Zhang, X., Jarjoura, D., Byrd, J.C., Pan, L., Chan, K.K., Kinghorn, A.D., Phelps, A.K., Grever, M.R., Lucas, D.M., 2011. Resistance to the translation initiation inhibitor silvestrol is mediated by ABCB1/P-glycoprotein overexpression in acute lymphoblastic leukemia cells. *AAPS J.* 13, 357–364.
- Hilton, D.A., Ristic, N., Hanemann, C.O., 2009. Activation of ERK, AKT and JNK signalling pathways in human schwannomas in situ. *Histopathology* 55, 744–749.
- Hilton, D.A., Shivane, A., Kirk, L., Bassiri, K., Enki, D.G., Hanemann, C.O., 2016. Activation of multiple growth factor signalling pathways is frequent in meningiomas. *Neuropathology* 36, 250–261.
- Holland, E.C., Sonenberg, N., Pandolfi, P.P., Thomas, G., 2004. Signaling control of mRNA translation in cancer pathogenesis. *Oncogene* 23, 3138–3144.
- Jackson, R.J., Hellen, C.U., Pestova, T.V., 2010. The mechanism of eukaryotic translation initiation and principles of its regulation. *Nat. Rev. Mol. Cell Biol.* 11, 113–127.
- Jacob, A., Lee, T.X., Neff, B.A., Miller, S., Welling, B., Chang, L.S., 2008. Phosphatidylinositol 3-kinase/AKT pathway activation in human vestibular schwannoma. *Otol. Neurotol.* 29, 58–68.
- Kinghorn, A.D., Pan, L., Fletcher, J.N., Chai, H., 2011. The relevance of higher plants in lead compound discovery programs. *J. Nat. Prod.* 74, 1539–1555.
- Kleiner, H.E., Krishnan, P., Tubbs, J., Smith, M., Meschonat, C., Shi, R., Lowery-Nordberg, M., Adegboyega, P., Unger, M., Cardelli, J., Chu, Q., Mathis, J.M., Clifford, J., De Benedetti, A., Li, B.D., 2009. Tissue microarray analysis of *elf4E* and its downstream effector proteins in human breast cancer. *J. Exp. Clin. Cancer Res.* 28, 5.
- Lazaris-Karatzas, A., Montine, K.S., Sonenberg, N., 1990. Malignant transformation by a eukaryotic initiation factor subunit that binds to mRNA 5' cap. *Nature* 345, 544–547.
- Li, B.D., Liu, L., Dawson, M., De Benedetti, A., 1997. Overexpression of eukaryotic initiation factor 4E (*elf4E*) in breast carcinoma. *Cancer* 79, 2385–2390.
- Li, Y., Fan, S., Koo, J., Yue, P., Chen, Z.G., Owonikoko, T.K., Ramalingam, S.S., Khuri, F.R., Sun, S.Y., 2012. Elevated expression of eukaryotic translation initiation factor 4E is associated with proliferation, invasion and acquired resistance to erlotinib in lung cancer. *Cancer Biol. Ther.* 13, 272–280.
- Ma, X.M., Blenis, J., 2009. Molecular mechanisms of mTOR-mediated translational control. *Nat. Rev. Mol. Cell Biol.* 10, 307–318.
- Menon, S., Manning, B.D., 2008. Common corruption of the mTOR signaling network in human tumors. *Oncogene* 27 (Suppl. 2), S43–S51.
- Mi, Q., Kim, S., Hwang, B.Y., Su, B.N., Chai, H., Arbieve, Z.H., Kinghorn, A.D., Swanson, S.M., 2006a. Silvestrol regulates G2/M checkpoint genes independent of p53 activity. *Anticancer Res.* 26, 3349–3356.
- Mi, Q., Su, B.N., Chai, H., Cordell, G.A., Farnsworth, N.R., Kinghorn, A.D., Swanson, S.M., 2006b. Rosciglaol induces apoptosis and cell cycle arrest in LNCaP cells. *Anticancer Res.* 26, 947–952.
- Oblinger, J.L., Burns, S.S., Akhrametyeva, E.M., Huang, J., Pan, L., Ren, Y., Shen, R., Miles-Markley, B., Moberly, A.C., Kinghorn, A.D., Welling, D.B., Chang, L.S., 2016. Components of the *elf4F* complex are potential therapeutic targets for malignant peripheral nerve sheath tumors and vestibular schwannomas. *Neuro-Oncology* 18, 1265–1277.
- Ohse, T., Ohba, S., Yamamoto, T., Koyano, T., Umezawa, K., 1996. Cyclopentabenzofuran lignan protein synthesis inhibitors from *Aglaia odorata*. *J. Nat. Prod.* 59, 650–652.
- Ostrom, Q.T., Gittleman, H., Fulop, J., Liu, M., Blanda, R., Kromer, C., Wolinsky, Y., Kruchko, C., Barnholtz-Sloan, J.S., 2015. CBTRUS statistical report: primary brain and central nervous system tumors diagnosed in the United States in 2008–2012. *Neuro-Oncology* 17 (Suppl. 4), iv1–iv62.
- Pachow, D., Andrae, N., Kliese, N., Angenstein, F., Stork, O., Wilisch-Neumann, A., Kirches, E., Mawrin, C., 2013. mTORC1 inhibitors suppress meningioma growth in mouse models. *Clin. Cancer Res.* 19, 1180–1189.
- Pan, L., Acuña, U.M., Li, J., Jena, N., Ninh, T.N., Pannell, C.M., Chai, H., Fuchs, J.R., Carcache de Blanco, E.J., Soejarto, D.D., Kinghorn, A.D., 2013. Bioactive flavaglines and other constituents isolated from *Aglaia perviridis*. *J. Nat. Prod.* 76, 394–404.
- Pan, L., Woodard, J.L., Lucas, D.M., Fuchs, J.R., Kinghorn, A.D., 2014. Rocaglamide, silvestrol and structurally related bioactive compounds from *Aglaia* species. *Nat. Prod. Rep.* 31, 924–939.
- Pines, J., 1996. Cyclin from sea urchins to HeLas: making the human cell cycle. *Biochem. Soc. Trans.* 24, 15–33.
- Poulidakos, P.I., Xiao, G.H., Gallagher, R., Jablonski, S., Jhanwar, S.C., Testa, J.R., 2006. Re-expression of the tumor suppressor NF2/merlin inhibits invasiveness in mesothelioma cells and negatively regulates FAK. *Oncogene* 25, 5960–5968.
- Rogers, L., Barani, I., Chamberlain, M., Kaley, T.J., McDermott, M., Raizer, J., Schiff, D., Weber, D.C., Wen, P.Y., Vogelbaum, M.A., 2015. Meningiomas: knowledge base, treatment outcomes, and uncertainties. A RANO review. *J. Neurosurg.* 122, 4–23.
- Rosenwald, I.B., Kaspar, R., Rousseau, D., Gehrke, L., Leblouh, P., Chen, J.J., Schmidt, E.V., Sonenberg, N., London, I.M., 1995. Eukaryotic translation initiation factor 4E regulates expression of cyclin D1 at transcriptional and post-transcriptional levels. *J. Biol. Chem.* 270, 21176–21180.
- Rouleau, G.A., Merel, P., Lutchman, M., Sanson, M., Zucman, J., Marineau, C., Hoang-Xuan, K., Demczuk, S., Desmaze, C., Plougastel, B., 1993. Alteration in a new gene encoding a putative membrane-organizing protein causes neuro-fibromatosis type 2. *Nature* 363, 515–521.
- Saradhi, U.V., Gupta, S.V., Chiu, M., Wang, J., Ling, Y., Liu, Z., Newman, D.J., Covey, J.M., Kinghorn, A.D., Marcucci, G., Lucas, D.M., Grever, M.R., Phelps, M.A., Chan, K.K., 2011. Characterization of silvestrol pharmacokinetics in mice using liquid chromatography-tandem mass spectrometry. *AAPS J.* 13, 347–356.
- Scoles, D.R., Yong, W.H., Qin, Y., Wawrowsky, K., Pulst, S.M., 2006. Schwannomin inhibits tumorigenesis through direct interaction with the eukaryotic initiation factor subunit c (*elf3c*). *Hum. Mol. Genet.* 15, 1059–1070.
- Shuda, M., Kondoh, N., Tanaka, K., Ryo, A., Wakatsuki, T., Hada, A., Goseki, N., Igari, T., Hatsuse, K., Aihara, T., Horiuchi, S., Shichita, M., Yamamoto, N., Yamamoto, M., 2000. Enhanced expression of translation factor mRNAs in hepatocellular carcinoma. *Anticancer Res.* 20, 2489–2494.
- Silvera, D., Formenti, S.C., Schneider, R.J., 2010. Translational control in cancer. *Nat. Rev. Cancer* 10, 254–266.
- Sorrells, D.L., Meschonat, C., Black, D., Li, B.D., 1999. Pattern of amplification and overexpression of the eukaryotic initiation factor 4E gene in solid tumor. *J. Surg. Res.* 85, 37–42.
- Tejada, S., Lobo, M.V., García-Villanueva, M., Sacristán, S., Pérez-Morgado, M.I., Salinas, M., Martín, M.E., 2009. Eukaryotic initiation factors (*elf*) 2alpha and 4E expression, localization, and phosphorylation in brain tumors. *J. Histochem. Cytochem.* 57, 503–512.
- Thuaud, F., Ribeiro, N., Gaidon, C., Cresteil, T., Désaubry, L., 2011. Novel flavaglines displaying improved cytotoxicity. *J. Med. Chem.* 54, 411–415.
- Trofatter, J.A., MacCollin, M.M., Rutter, J.L., Murrell, J.R., Duyao, M.P., Parry, D.M., Eldridge, R., Kley, N., Menon, A.G., Pulaski, K., 1993. A novel moesin-, ezrin-, radixin-like gene is a candidate for the neurofibromatosis 2 tumor suppressor. *Cell* 72, 791–800.
- Wang, X., Gong, Y., Wang, D., Xie, Q., Zheng, M., Zhou, Y., Li, Q., Yang, Z., Tang, H., Li, Y., Hu, R., Chen, X., Mao, Y., 2012. Analysis of gene expression profiling in meningioma: deregulated signaling pathways associated with meningioma and EGFL6 overexpression in benign meningioma tissue and serum. *PLoS One* 7, e2707.
- Wolfe, A.L., Singh, K., Zhong, Y., Drewe, P., Rajasekhar, V.K., Sanghvi, V.R., Mavrikis, K.J., Jiang, M., Roderick, J.E., Van der Meulen, J., Schatz, J.H., Rodrigo, C.M., Zhao, C., Rondou, P., de Stanchina, E., Teruya-Feldstein, J., Kelliher, M.A., Speleman, F., Porco, J.A., Pelletier, J., Ratsch, G., Wendel, H.G., 2014. RNA G-quadruplexes cause *elf4A*-dependent oncogene translation in cancer. *Nature* 513, 65–70.

# Preclinical assessment of MEK1/2 inhibitors for neurofibromatosis type 2–associated schwannomas reveals differences in efficacy and drug resistance development

Marisa A. Fuse, Christine T. Dinh, Jeremie Vitte, Joanna Kirkpatrick, Thomas Mindos, Stephani Klingeman Plati, Juan I. Young, Jie Huang, Annemarie Carlstedt, Maria Clara Franco, Konstantin Brnjos, Jackson Nagamoto, Alejandra M. Petrilli, Alicja J. Copik, Julia N. Soualakova, Olena Bracho, Denise Yan, Rahul Mittal, Rulong Shen, Fred F. Telischi, Helen Morrison, Marco Giovannini, Xue-Zhong Liu, Long-Sheng Chang, and Cristina Fernandez-Valle

*Burnett School of Biomedical Sciences, College of Medicine, University of Central Florida (UCF), Orlando, Florida, USA (M.A.F., S.K.P., M.C.F., K.B., J.N., A.P., A.J.C., J.N.S., C.F.V.); Department of Otolaryngology, University of Miami Miller School of Medicine, Miami, Florida, USA (C.T.D., O.B., D.Y., R.M., F.F.T., X.Z.-L.); Department of Head and Neck Surgery, David Geffen School of Medicine at UCLA and Jonsson Comprehensive Cancer Center, University of California at Los Angeles (UCLA), Los Angeles, California, USA (J.V., M.G.); Leibniz Institute on Aging, Fritz Lipmann Institute, Jena, Germany (J.K., T.M., A.C., H.M.); Department of Human Genetics, University of Miami Miller School of Medicine, Miami, Florida, USA (J.I.Y., X.-Z.L.); Center for Childhood Cancer and Blood Diseases, Nationwide Children's Hospital (J.H., L.S.C.) and Departments of Pediatrics (J.H., L.-S.C.) and Pathology, The Ohio State University (R.S.), Columbus, Ohio, USA*

**Corresponding Author:** Cristina Fernandez-Valle, Ph.D., Burnett School of Biomedical Sciences, College of Medicine, University of Central Florida, 6900 Lake Nona Blvd, Orlando, FL 32827 ([cfv@ucf.edu](mailto:cfv@ucf.edu)).

## Abstract

**Background.** Neurofibromatosis type 2 (NF2) is a genetic tumor-predisposition disorder caused by *NF2*/merlin tumor suppressor gene inactivation. The hallmark of NF2 is formation of bilateral vestibular schwannomas (VS). Because merlin modulates activity of the Ras/Raf/mitogen-activated protein kinase kinase (MEK)/extracellular signal-regulated kinase (ERK) pathway, we investigated repurposing drugs targeting MEK1 and/or MEK2 as a treatment for NF2-associated schwannomas.

**Methods.** Mouse and human merlin-deficient Schwann cell lines (MD-MSCHSC) were screened against 6 MEK1/2 inhibitors. Efficacious drugs were tested in orthotopic allograft and *NF2* transgenic mouse models. Pathway and proteome analyses were conducted. Drug efficacy was examined in primary human VS cells with *NF2* mutations and correlated with DNA methylation patterns.

**Results.** Trametinib, PD0325901, and cobimetinib were most effective in reducing MD-MSCHSC viability. Each decreased phosphorylated pERK1/2 and cyclin D1, increased p27, and induced caspase-3 cleavage in MD-MSCHSCs. Proteomic analysis confirmed cell cycle arrest and activation of pro-apoptotic pathways in trametinib-treated MD-MSCHSCs. The 3 inhibitors slowed allograft growth; however, decreased pERK1/2, cyclin D1, and Ki-67 levels were observed only in PD0325901 and cobimetinib-treated grafts. Tumor burden and average tumor size were reduced in trametinib-treated *NF2* transgenic mice; however, tumors did not exhibit reduced pERK1/2 levels. Trametinib and PD0325901 modestly reduced viability of several primary human VS cell cultures with *NF2* mutations. DNA methylation analysis of PD0325901-resistant versus -susceptible VS identified genes that could contribute to drug resistance.

**Conclusion.** MEK inhibitors exhibited differences in antitumor efficacy resistance in schwannoma models with possible emergence of trametinib resistance. The results support further investigation of MEK inhibitors in combination with other targeted drugs for NF2 schwannomas.

### Key Points

1. Cobimetinib and trametinib reduced NF2 schwannoma model cell proliferation in vitro and in vivo.
2. Biochemical/proteome analyses reveal cell cycle arrest and apoptosis of trametinib-treated cells.
3. Human vestibular schwannoma cell viability is modestly inhibited by PD0325901 and trametinib.

### Importance of the Study

There are currently no FDA-approved drug therapies for the treatment of NF2-associated schwannomas. Clinical trials for selumetinib and cobimetinib are ongoing for assessment of efficacy for NF2-associated tumors and hearing loss; however, little preclinical data have been published. Here, we evaluated 6 MEK1/2 inhibitors for efficacy in mouse and human cell and animal models as well as

patient-derived vestibular schwannoma cells with *NF2* mutations. We observed differences in efficacy among the inhibitors as well as the possibility of drug resistance development. Our work highlights the importance of comprehensive drug screening in multiple model systems and supports further investigation of MEK inhibitors alone and in combination with other targeted therapies.

Neurofibromatosis type 2 (NF2) is caused by mutations in the *NF2* gene encoding the merlin tumor suppressor.<sup>1,2</sup> NF2 patients classically present with bilateral vestibular schwannomas (VS) involving the cochleovestibular nerves important for hearing and balance, and can develop additional peripheral schwannomas, meningiomas, and ependymomas.<sup>3</sup> Management of NF2 requires a complex, multidisciplinary approach focused on balancing tumor control and nerve function preservation to improve quality of life and maximize survival.<sup>4</sup> Whereas microsurgical resection of tumors risks permanent nerve injury, radiation therapy increases the chance of malignant transformation of benign tumors and secondary malignancies.<sup>5–10</sup> Therefore, there is an ongoing search for effective drug therapies for NF2.

Schwann cells with loss of merlin tumor suppressor function have elevated levels of Ras/Raf/mitogen-activated protein kinase (MEK)/extracellular signal-regulated kinase (ERK) signaling that promotes cell proliferation.<sup>11–13</sup> Sixteen small molecule MEK inhibitors have entered clinical trials for various cancers.<sup>14</sup> Among these MEK inhibitors, selumetinib (AZD6244) was recently granted Orphan Drug Designation by the FDA for treatment of inoperable plexiform neurofibromas in children with NF1.<sup>15</sup> Additionally, selumetinib reduced growth of an in vitro human schwannoma model.<sup>16,17</sup> This success has prompted additional trials of selumetinib for NF1 and NF2 (NCT numbers: 01089101, 01362803, 02839720, 03259633, 03095248).

Trametinib (Mekinist, GSK1120212, JTP-74057, GlaxoSmithKline) is an allosteric, second-generation, adenosine triphosphate non-competitive reversible MEK1/2 inhibitor that also blocks Raf-dependent phosphorylation

of MEK Ser218.<sup>14</sup> Trametinib promotes cell cycle arrest and caspase cleavage in cultured colorectal cells, and demonstrates more potent antitumor activity than other second-generation MEK inhibitors, PD0325901 and selumetinib. It is FDA approved for metastatic melanoma and is in phase I clinical trial for NF1-associated plexiform neurofibromas (NCT02124772).<sup>18</sup>

PD0325901 (Pfizer) is also an allosteric MEK1/2 inhibitor and is a synthetic analog of the first-generation MEK1/2 inhibitor, CI-1040.<sup>14,19</sup> In an *Nf1* genetically engineered mouse model, PD0325901 prolonged survival of mice with malignant peripheral nerve sheath tumors and decreased neurofibroma size in over 80% of mice.<sup>20</sup> Tumor regrowth was observed when treatment was suspended.<sup>21</sup> A phase II open-label study is ongoing for PD0325901 in NF1 (NCT02096471).<sup>14</sup>

Cobimetinib (XL518, GDC-0973, Cotellic, Exelixis/Genentech) is derived from methanone and was FDA approved in 2015 for use in combination with vemurafenib, a BRAF inhibitor, for advanced melanoma with *BRAF* mutations.<sup>22,23</sup> Cobimetinib inhibited growth of tumors with *BRAF* and *KRAS* mutations in xenograft models.<sup>24–26</sup> Phase I studies of cobimetinib for solid tumors reported a manageable toxicity profile with signs of efficacy in tumors with *BRAF*<sup>V600E</sup> mutations.<sup>27</sup> Cobimetinib is in clinical trial for pediatric and young adult patients with rasopathies, including NF2 (NCT02639546), treated previously for solid tumors.

Here, we used mouse and human merlin-deficient Schwann cell lines (MD-MSC/HSC) and animal models to evaluate the growth-inhibitory and antitumor activities of a panel of MEK inhibitors. Also, we assessed their efficacy in primary human VS with NF2 mutations.

## Materials and Methods

### Cell Culture

Wild-type (WT)-MSCs and MD-MSCs were generated and characterized in 2010.<sup>28</sup> MD-MSCs were transduced with lentiviral luciferase as previously reported.<sup>29</sup> MD-schwannoma (MD-SCN) cells were derived from paraspinal schwannomas of *Periostin-Cre:Nf2<sup>flox2/flox2</sup>* mice with *Nf2* inactivation (provided by Dr Wade Clapp, Indiana University). Human Schwann cells (HSCs) were purchased from ScienCell Research Laboratories (catalog #1700, lot #7228), and the generation of a merlin-deficient HSC (MD-HSC) line using lentiviral short hairpin (sh)RNA targeting *NF2* (Sigma Mission, SHCLNV-TRCN0000237845) was previously described.<sup>30</sup> Cells were tested monthly for *Mycoplasma* contamination (Lookout *Mycoplasma* PCR Detection Kit, Sigma).

### Mouse Model Systems

NSG (*NOD.Cg-Prkdcscid Il2rgtm1Wjl/SzJ*) mice were used at 6–10 weeks of age. *P0-SCH-Δ(39–121)-27* transgenic mice<sup>31</sup> in the BALB/c background were used as a genetically engineered mouse (GEM) model of NF2 schwannomas. Animal use was approved by the Institutional Animal Care and Usage Committees of UCF and UCLA, and the Animal Care and Use Review Office of the United States Army Medical Research and Materiel Command.

### Human VS Samples

Through an institutional review board (IRB) approved protocol, the University of Miami Tissue Bank Core Facility (UM-TBCF) consented patients undergoing surgery for brain tumors to harvest samples for research purposes. De-identified fresh human VS were obtained from UM-TBCF through an IRB-exempt protocol. Primary VS cells were prepared and cultured as previously reported.<sup>29,30</sup>

### Drug Formulations

MEK inhibitors were purchased from MedChemExpress. Drugs were prepared in dimethyl sulfoxide (DMSO) (stock 10 mM) and diluted to final concentrations in cell culture medium for in vitro work. For animal studies, drugs were solubilized in DMSO at 50–100 mg/mL and diluted in 0.1 M citrate buffer (pH 3) for oral dosing.

### Cell Viability Assays

Cells were seeded in 384-well CellBind plates (Corning) at 2000–2500 cells/well in phenol red-free growth medium. WT-MSCs were seeded at 15000 cells/well in 96-well plates coated with poly-L-lysine (200 µg/mL) and laminin (25 µg/mL). Attached cells were treated with drug or DMSO for 48 h (mouse) or 72 h (human); viability was measured with the CellTiter-Fluor Assay (Promega). Primary human VS

cells were seeded (passage 1 or 2) in 96-well plates at 10000 cells/well. After 24 hours, cells were treated with drug or DMSO for 72 h. Crystal violet assay was performed using a SpectraMax 190 microplate reader (Molecular Devices) to assess cell number, as previously described.<sup>29,30</sup>

### Membrane Asymmetry Assay

MD-MSCs were grown at 200000 cells/well in 12-well CellBind plates (Corning). When at ~80% confluency, cells were treated with drug for 18–24 h, then harvested with 0.05% trypsin and resuspended in Hanks Balanced Salt Solution. The Violet Ratiometric Membrane Asymmetry Assay (Invitrogen) was used to detect apoptosis per the manufacturer's instructions. Cell populations were measured by flow cytometry (Cytotflex, Beckman Coulter) and analyzed with CytExpert software (Beckman Coulter).

### Mouse Studies

For pharmacokinetic analysis, at each timepoint 3 mice received drug (1 mg/kg trametinib, 1.5 mg/kg PD0325901, or 20 mg/kg cobimetinib); one mouse received vehicle alone (0.1 M citrate, pH 3, 2% DMSO). Mice were sacrificed after 0.5–32 h; blood and sciatic nerve samples were collected and analyzed by mass spectrometry at Sanford Burnham Prebys Medical Discovery Institute (Lake Nona, Florida).

The orthotopic allograft model using luciferase-expressing MD-MSCs was generated as previously described.<sup>29</sup> Upon confirmation of successful grafting, mice were randomized into treatment groups and received drug or vehicle at the above concentrations daily by oral gavage. Mice were imaged weekly for bioluminescence using the In Vivo Imaging System (IVIS, Caliper) or Bruker MI Imaging System. After 13–14 days of treatment, mice were sacrificed; grafts and contralateral sciatic nerves were removed, weighed, and photographed. Grafts were fixed overnight in 4% paraformaldehyde and stored in 30% sucrose (0.02% azide in phosphate buffered saline) at 4°C. List of antibodies used is provided in Supplementary Methods.

Four-week-old *P0-SCH-Δ(39–121)-27* transgenic mice<sup>31</sup> were treated daily with trametinib (1 mg/kg) or vehicle (0.1 M citrate buffer pH 3, 0.2% DMSO) by oral gavage for 8 weeks. Spinal nerve roots were histopathologically scored at the endpoint as previously described.<sup>32</sup> Following a blind procedure, measurements of tumors and nerve root areas were performed using Zeiss Axiovision software on hematoxylin and eosin stained parasagittal sections of cervical, thoracic, lumbar, and sacral spinal cord segments. The total area of nerve root analyzed was comparable between the trametinib and vehicle-treated groups ( $P = 0.1541$ ).

### Western Blotting

Western blots were performed as previously described.<sup>29</sup> Protein was extracted from human VS tumors using radio-immunoprecipitation buffer with protease and phosphatase inhibitors (ThermoFisher). Human VS blots were blocked in 3% bovine serum albumin and incubated

overnight in primary antibody solution at 4°C, followed by incubation with Alexa Fluor 488 and 647 conjugated secondary antibodies (1:200; ThermoFisher) for 2 hours at room temperature and imaged using the ImageQuant LAS 4000 Imager (GE Healthcare).

### NF2 Mutation Analysis

Total DNA was extracted from fresh tumor tissues using the QIAamp DNA Mini Kit (Qiagen) and purified using the QIAquick PCR Purification Kit (Qiagen). All VS were tested for mutations within the NF2 gene with multiplex ligation-dependent probe amplification using the Salsa MLPA NF2 Kit (MRC-Holland) per the manufacturer's instructions. Copy number alterations in all 17 exons of the NF2 gene (NM\_000268.3) were analyzed with Coffalyser. Additional details are provided in the [Supplementary Methods](#).

### DNA Methylation Analysis

High-throughput DNA methylation analysis was performed for 7 human VS tumors using the Infinium MethylationEPIC Kit (Illumina) according to the manufacturer's instructions. Methylation patterns were compared between VS that had a statistically significant decrease in cell number following a 72 hour incubation with 3  $\mu$ M PD0325901 and those with no response. Additional details are provided in [Supplementary Methods](#).

### Proteome

Protein from cell pellets of MD-MSCs treated with trametinib or vehicle was extracted, denatured and prepared for liquid chromatography–tandem mass spectrometry (LC-MS/MS) as described in the [Supplementary Methods](#). MS/MS spectra were searched against the *Mus Musculus* Swiss-Prot entries of the Uniprot KB (database release 2016\_01, 16755 entries) using the Andromeda search engine.<sup>33</sup> The specific search criteria and analytics used are provided in [Supplementary Methods](#). Protein differential expression between the trametinib and vehicle control samples was evaluated using the Limma package.<sup>34</sup>

### Statistics

Using GraphPad Prism 6, ANOVA with Bonferroni posttest, or Kruskal–Wallis test with Dunn's comparison was applied to all in vitro data. For in vivo allograft studies, we used SAS version 9.4 to test the overall differences in median tumor weight and median fold change in flux after 14 days treatment among the 4 cohorts (vehicle treatment served as the control). Nonparametric ANOVA with Bonferroni adjustments were used to adjust for small group sample sizes and non-normal distributions. The ANOVA for the median tumor weight and median fold change in flux indicated the overall significance differences. We tested 1-tailed hypothesis of improvements. For the *P0-SCH-Δ(39–121)-27* NF2 mouse model, 2-tailed unpaired Student's *t*-test was used to compare tumor burden and sizes in the trametinib- and vehicle-treated groups.

## Results

We screened selumetinib, trametinib, PD0325901, MEK162, cobimetinib, and refametinib for effectiveness in reducing viability of 9 WT and MD-MSC/HSC lines after 48-hour (mouse) and 72-hour (human) treatments. Based upon 50% inhibitory concentration ( $IC_{50}$ ) values, the inhibitors were overall more effective in MSCs compared with HSCs. Maximum loss of cell viability at 10  $\mu$ M observed for all inhibitors tested was ~90–95% in MD-MSCs, compared with ~60% in MD-HSCs ([Fig. 1A–B](#)). The lowest inhibitor concentration tested produced a 20–40% reduction in MD-MSC viability. MEK inhibitors promoted a dose-dependent decrease in incorporation of 5-ethynyl-2'-deoxyuridine in both MD-MSC and MD-HSC ([Supplementary Fig. 1](#)). All 6 MEK inhibitors also exhibited less selectivity between WT- and MD-HSCs compared with MSC lines (2–5 fold compared with 6–15 fold; [Fig. 1A–B](#) and [Supplementary Fig. 2](#)).

Trametinib, PD0325901, and cobimetinib were further evaluated in vitro and in an allograft mouse model because each reduced viability of both MD-MSCs and MD-HSCs with submicromolar  $IC_{50}$  values and had some selectivity in HSCs. Each drug decreased phosphorylated pERK levels in MD-MSCs at 5 and 24 hours of treatment ([Fig. 2A–B](#), [Supplementary Fig. 3](#)). Trametinib was the most potent, as pERK was not detected in the 0.001  $\mu$ M sample. Among these 3 MEK1/2 inhibitors, cobimetinib was the least effective, based on sustained reduction of pERK levels over 24 hours. Higher cobimetinib concentrations (0.3–1  $\mu$ M) were required to achieve an equivalent pERK reduction observed with 0.001  $\mu$ M trametinib and PD0325901. As reported in other cell types, MEK inhibition is associated with a compensatory increase in pMEK levels ([Fig. 2A–B](#), [Supplementary Fig. 3](#)).<sup>35</sup> In MD-MSCs, a more robust increase in pMEK levels was observed in cells treated with cobimetinib at 5 hours and PD0325901 at 24 hours. Because trametinib uniquely blocks Raf-dependent MEK phosphorylation,<sup>14</sup> the lowest increase in pMEK was observed in trametinib-treated cells. MD-HSCs also exhibited decreased pERK and increased pMEK following MEK inhibition, but at higher drug concentrations compared with MD-MSCs ([Supplementary Fig. 4](#)).

An examination of downstream MEK/ERK effectors in MD-MSCs treated with these inhibitors revealed decreased levels of cyclin D1, and increased p27<sup>kip1</sup> and cleaved caspase 3 levels ([Fig. 2C–D](#)). Membrane asymmetry assays confirmed an increase in apoptotic cell populations from ~2% in DMSO-treated to 20% and 45% in trametinib- and cobimetinib-treated MD-MSCs, respectively ([Fig. 2E](#), [Supplementary Fig. 4](#)).

A proteomic analysis of trametinib-treated MD-MSCs was conducted to assess global changes in protein expression. The results were consistent with effective inhibition of MEK1/2 and downstream effectors and induction of apoptotic pathways. Trametinib-treated MD-MSCs had reduced expression of Ras/Raf/MEK/ERK pathway effectors including cyclin D1 and c-Myc and increased expression of pro-apoptotic proteins such as Bcl-2 interacting protein 3 like (BNIP3L) at 24 hours, compared with DMSO control ([Fig. 3A](#)). Ingenuity Pathway Analysis identified upstream regulators whose

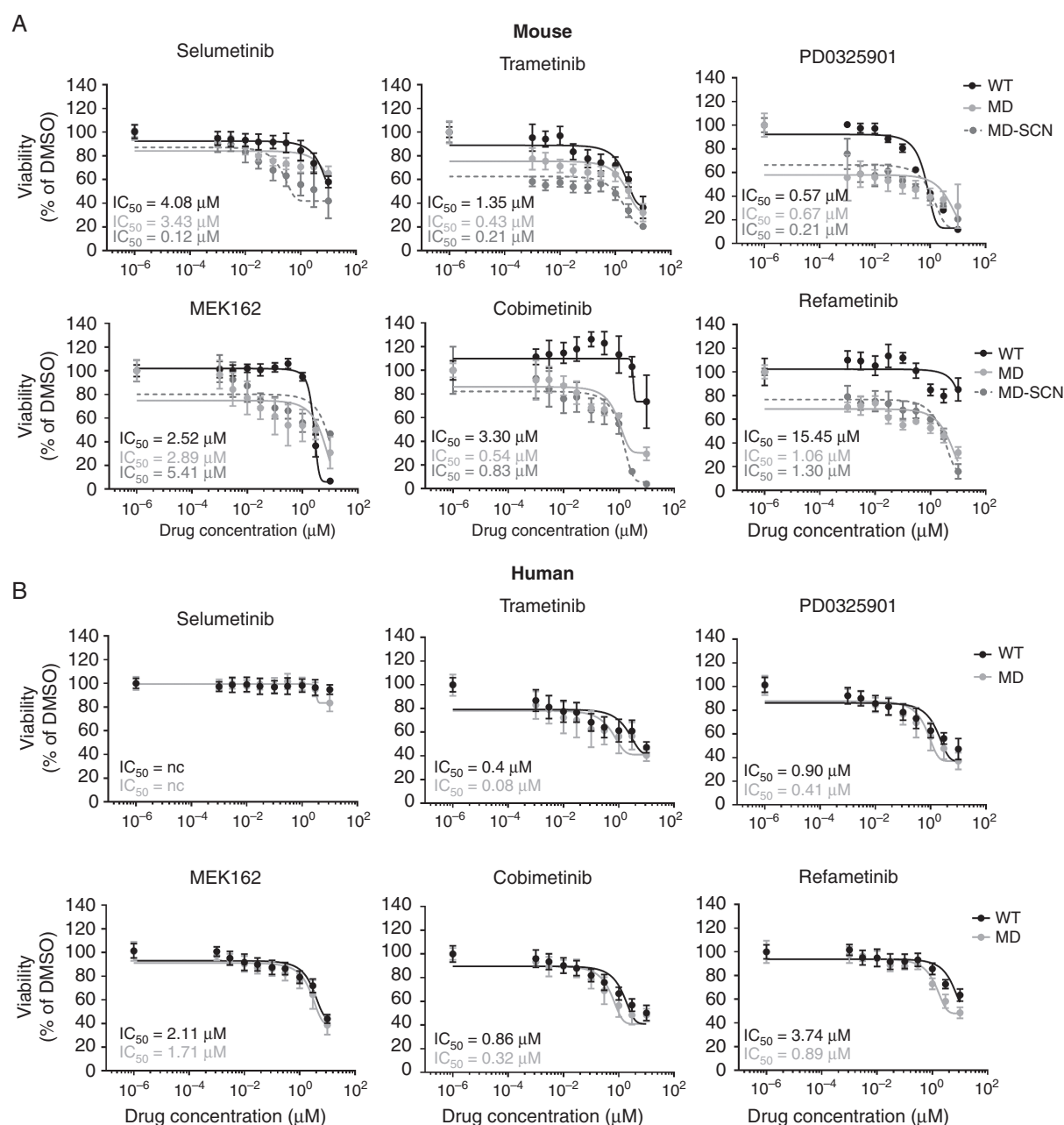


**Fig. 1** MEK inhibitors reduce MD-MSC and MD-HSC viability. Screen of 6 MEK inhibitors against (A) mouse and (B) human WT and MD-SC lines treated for 48–72 h. Mean viability is plotted with  $IC_{50}$  values ( $n = 1$ –3 independent experiments; 8 replicates each).

modulation is consistent with the observed changes in protein levels. These included transforming growth factor beta (TGF $\beta$ ), specificity protein 1, and p53 levels, whose levels were higher in trametinib-treated MD-MSCs compared with DMSO-treated controls (Fig. 3B–D).

To assess in vivo efficacy, we employed an orthotopic allograft model by grafting luciferase-expressing MD-MSCs into the sciatic nerves of NSG mice.

Pharmacokinetic studies revealed that trametinib and cobimetinib had long  $t_{1/2}$  values ( $\sim 8$  h and 4.8 h, respectively) and their nerve/plasma ratios increased with time (Fig. 4A). Upon confirmation of successful grafting (Supplementary Fig. 5), mice were gavaged daily for 14 days with trametinib (1 mg/kg), PD0325901 (1.5 mg/kg), or cobimetinib (20 mg/kg). All 3 MEK inhibitors significantly reduced the median tumor weight by 60–70% and the median fold change in flux from 0 to 14 days

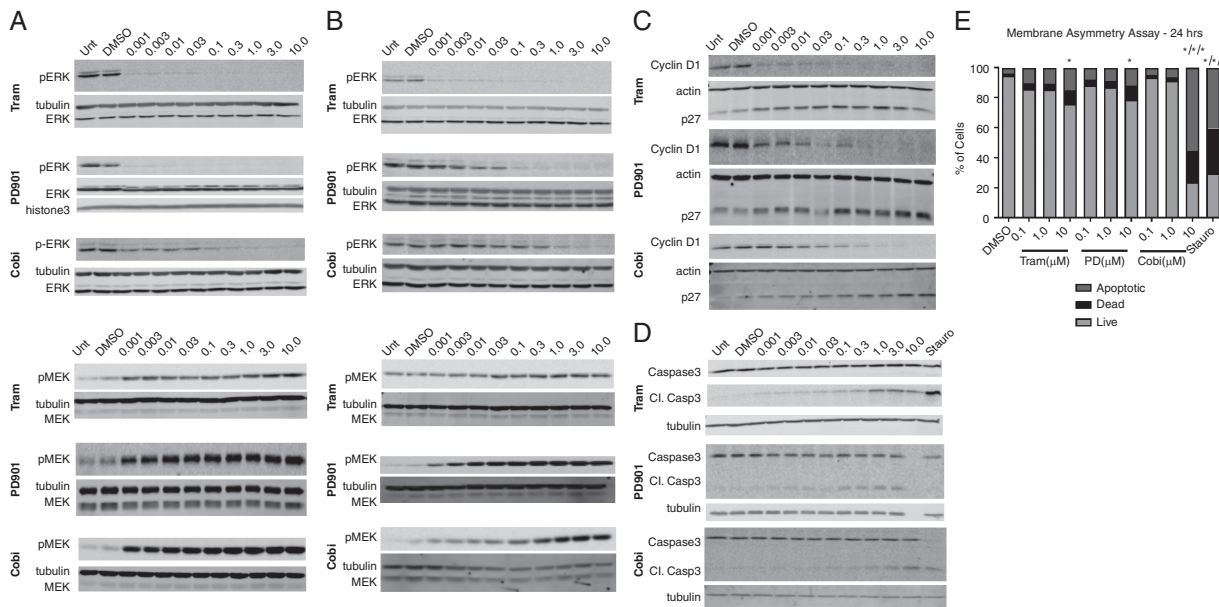


**Fig. 2** MEK inhibitors promote G1 arrest and caspase-dependent apoptosis of MD-MSC in vitro. pERK1/2, pMEK1/2, cyclin D1, p27, and caspase-3 western blots of MD-MSC treated as indicated for (A) 5 h and (B–D) 24 h. All western blots are representative of 3–5 independent experiments. (E) Quantitation of membrane asymmetry assay of MD-MSC treated for 20 h with MEK inhibitors. Staurosporine (0.1 μM) served as a positive control for apoptosis ( $n = 3$  independent experiments, 2-way ANOVA,  $*P < 0.05$ ).

by at least 80% compared with controls (Fig. 4B–D, Supplementary Fig. 6). Immunohistochemical analysis revealed that PD0325901 and cobimetinib were superior to trametinib in reducing pERK levels compared with the vehicle-treated group (Fig. 4E). Additionally, both inhibitors caused a more robust decrease in Ki-67 and cyclin D1 than trametinib, suggesting they were more potent inhibitors of graft growth in vivo. None of the inhibitors produced detectable caspase 3 cleavage nor did they affect vascularity as evidenced by CD31 staining (Fig. 4E).

Because trametinib is a well-tolerated FDA-approved drug and outperformed cobimetinib in cell assays, we assessed its efficacy in an 8-week study using the *P0-SCH-Δ(39–121)-27 NF2* schwannoma mouse model.<sup>31,32</sup> In this GEM model, trametinib efficacy was assessed by comparing the tumor burden, as defined by the percentage of tumor area versus total spinal nerve root area. Overall, trametinib promoted a 25% reduction in tumor burden ( $P < 0.0001$ ) and a 37% decrease of average tumor size ( $P = 0.0023$ ) (Fig. 5). Phosphorylated ERK immunohistochemistry of tumor samples revealed equivalent staining in trametinib- and vehicle-treated mice (data not shown), consistent with the allograft findings.

To examine the effect of MEK inhibition on human VS cells, primary cultures from 7 VS tumors were prepared and treated with PD0325901 or trametinib. All 7 VS tumors demonstrated  $\geq 1$  mutation in the *NF2* gene (Supplementary Table 1) and varying degrees of MEK1/2, pMEK, and pERK expression (Fig. 6A–B). Compared with DMSO-treated cells, trametinib (3 μM) moderately

reduced cell viability of 2 of 7 VS, whereas PD0325901 (3 μM) reduced cell viability of 5 of the 7 VS tested (Fig. 6C–D). No significant correlations between viabilities and MEK1/2 and pMEK protein expression levels were identified, suggesting that drug response was independent of MEK expression.

To assess whether aberrant DNA methylation of the genome was associated with a lack of drug response, we compared methylation profiles of 2 VS with no response to PD0325901 tumors (VS27 and VS32) to the remaining 5 PD0325901-responsive tumors. In an unbiased evaluation, we identified 17 299 single cytosine-phosphate-guanine (CpG) sites with significantly different methylation levels ( $P < 0.05$ ) between the drug responsive and nonresponsive VS. Among significant CpG sites, 4773 were hypermethylated (covering 3090 genes) and 12526 were hypomethylated (covering 8051 genes) in the PD0325901-resistant compared with drug-sensitive VS. Supplementary Table 2 displays the top 20 hypermethylated and hypomethylated genes between the 2 groups. However, when false discovery rate (FDR)  $< 0.05$  was applied, *ELMOD1* (NM\_001130037; Engulfment and cell motility domain 1) was the only gene that contained a CpG site (cg22355889) in the promoter region that was significantly hypermethylated in the PD0325901 nonresponsive VS.

Neighboring CpG sites often display closely related methylation patterns. To account for spatial correlations, we identified 34 differentially methylated regions (DMRs) with at least 5 consecutive

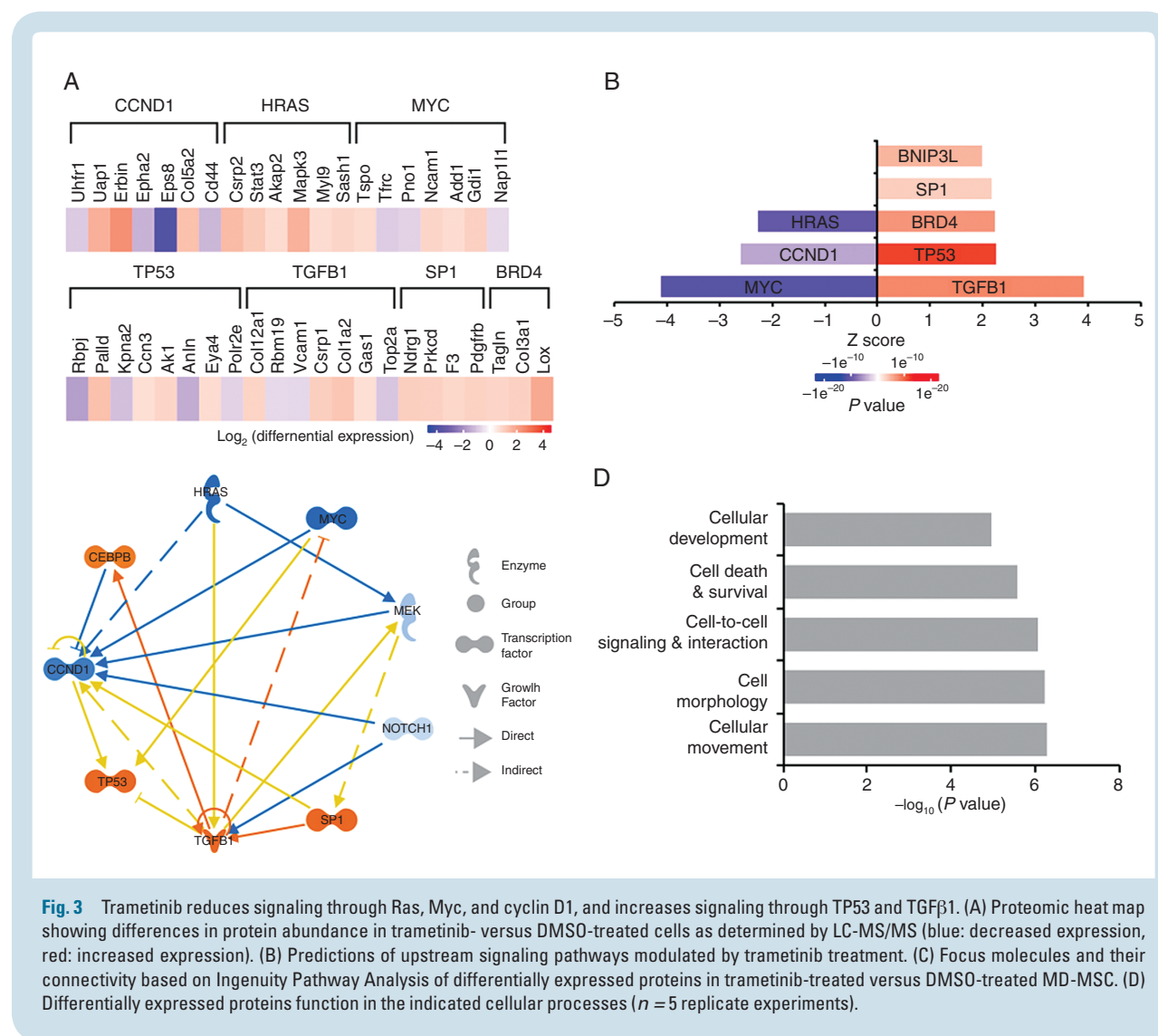


**Fig. 3** Trametinib reduces signaling through Ras, Myc, and cyclin D1, and increases signaling through TP53 and TGFβ1. (A) Proteomic heat map showing differences in protein abundance in trametinib- versus DMSO-treated cells as determined by LC-MS/MS (blue: decreased expression, red: increased expression). (B) Predictions of upstream signaling pathways modulated by trametinib treatment. (C) Focus molecules and their connectivity based on Ingenuity Pathway Analysis of differentially expressed proteins in trametinib-treated versus DMSO-treated MD-MSC. (D) Differentially expressed proteins function in the indicated cellular processes ( $n = 5$  replicate experiments).

hypermethylated or hypomethylated CpG loci in the PD0325901-nonresponsive compared with responsive VS (Supplementary Table 3). When examining individual DMRs, PD0325901 nonresponsive VS had DMRs in genes involved in non-MEK merlin signaling, including the *ATF6B* (activating transcription factor 6) and RXR (retinoid x receptor) genes associated with the phosphoinositide 3-kinase (PI3K/Akt) pathway and ATP6V1C1 (V-type proton ATPase subunit C1) of the mammalian target of rapamycin pathway. Gene ontology pathway analysis revealed no significant enrichment pathways for DMRs. However, when using a targeted approach assessing genes associated with merlin signaling, cancer, drug resistance, cell death, and survival, additional DMRs were identified. ARHRS4 pathway analysis revealed significant enrichment in epidermal growth factor receptor and tumor suppressor RPS6KA2 (ribosomal protein S6 kinase A2) human kinase pathways (<http://amp.pharm.mssm.edu/Enrichr/>. Accessed January 20, 2019).

## Discussion

NF2 is a genetic disorder involving the development of multiple nervous system tumors that each impact neurological functions. Individuals affected by NF2 develop bilateral VS that cause severe hearing loss, disabling imbalance, and even life-threatening hydrocephalus from brainstem and cerebellar compression. Observation of tumor growth rate and hearing is standard as enthusiasm for microsurgical resection in NF2 is low due to consequential and irreversible limitations on nerve function and quality of life.<sup>8</sup> In the same respect, the long-term sequelae of utilizing radiotherapy is not so uncommon to disregard the risk of developing malignant transformation of benign tumors.<sup>5-7,9,10</sup> Off-label use of select FDA-approved chemotherapeutic agents for NF2 in clinical trials show moderate tumor control at best and hearing stabilization in only some NF2 patients.<sup>36-41</sup> However, even small effects

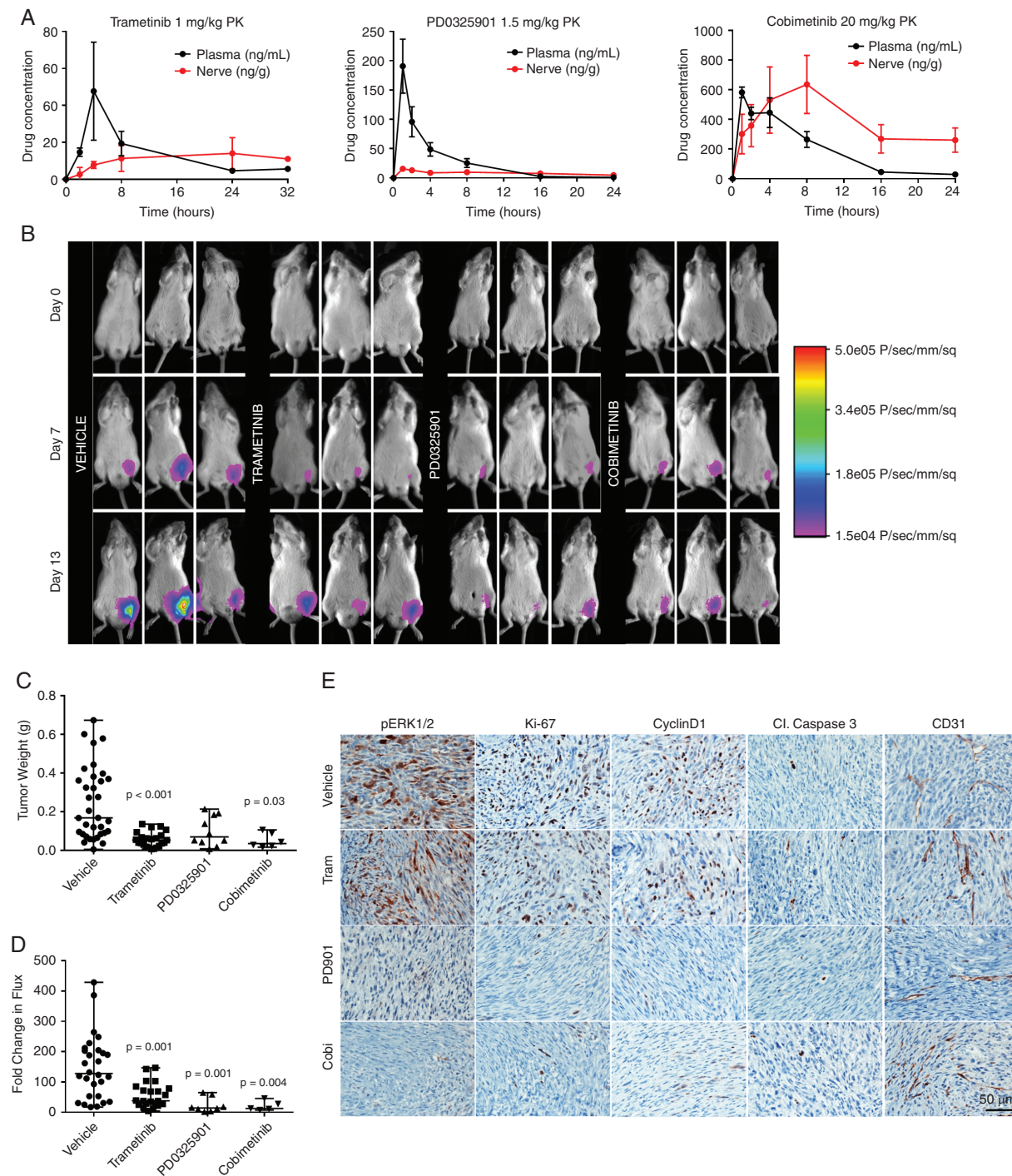


**Fig. 4** MEK inhibitors slow MD-MS growth in NSG mice. (A) Pharmacokinetic analysis for plasma and nerve following a single drug dose. (B) Representative bioluminescent (BL) images for indicated times. (C) Median tumor weights after 14 days of drug treatment compared with vehicle ( $n = 6-35$  mice, nonparametric ANOVA). (D) BL signals were normalized to day 0 for each mouse and fold change in flux (photons/sec) after 14 days of treatment is shown (nonparametric ANOVA, median values shown). (E) Representative graft immunohistochemistry images for pERK1/2, Ki-67, cyclin D1, cleaved caspase 3, and CD31.

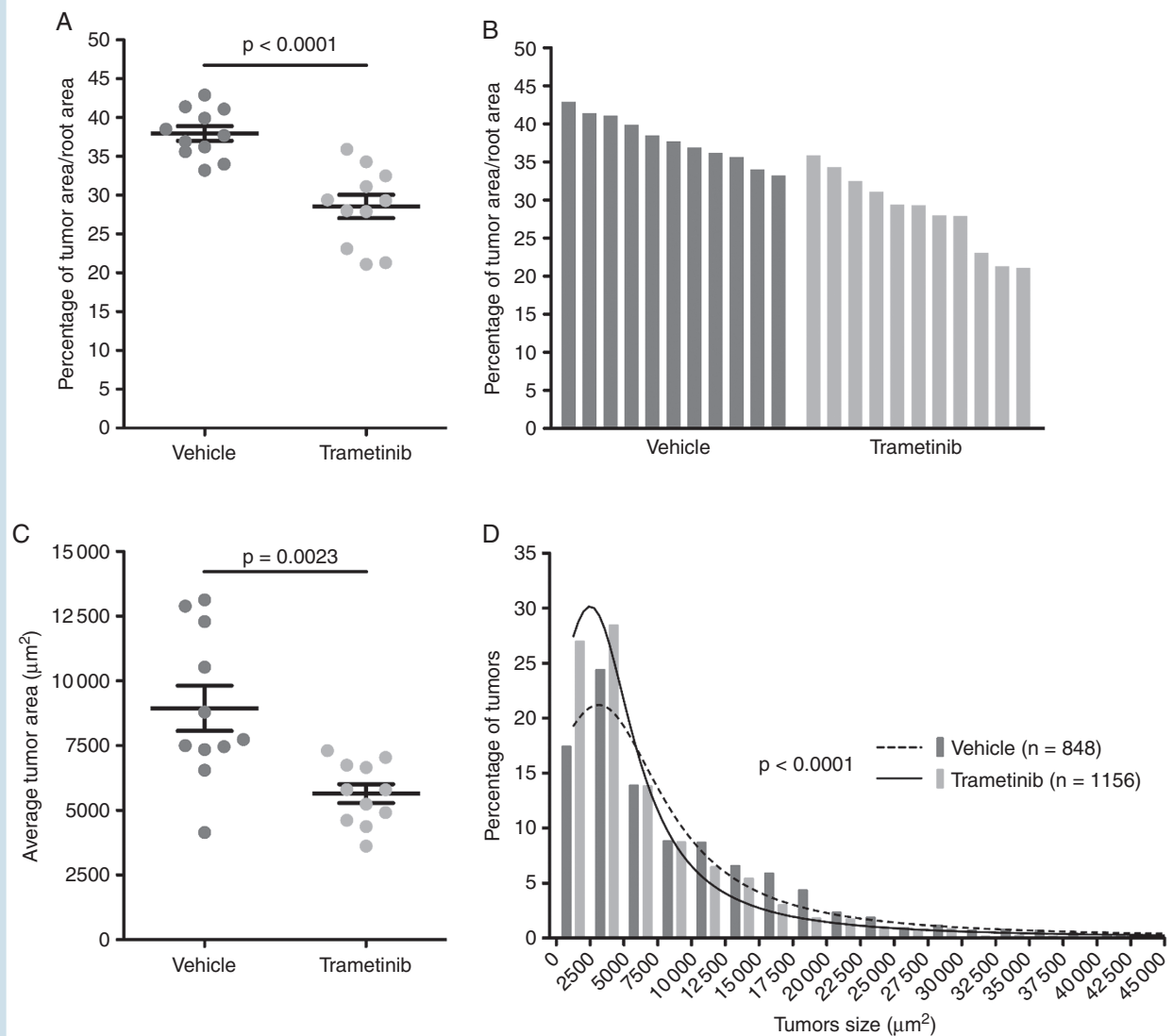


**Fig. 5** Trametinib reduces schwannoma growth in the *P0-SCH-Δ(39-121)-27NF2* mouse model. *P0-SCH-Δ(39-121)-27NF2* mice were treated daily with trametinib (1 mg/kg, p.o., 7 d/wk) for 8 weeks starting at 4 weeks of age. (A) Reduction by 25% of the average tumor burden, calculated as percentage of tumor area versus total spinal nerve root area for trametinib-treated mice ( $n = 11$ ) compared with vehicle-treated mice ( $n = 11$ ). (B) Waterfall plot showing tumor burden for each vehicle- and trametinib-treated mouse. (C) Treatment with trametinib reduced average tumor size by 37% in trametinib-treated compared with vehicle-treated mice. (D) Histogram of tumor size distribution demonstrated a significantly higher percentage of smaller tumors in trametinib-treated ( $n = 1156$  tumors) compared with vehicle-treated ( $n = 848$  tumors) mice.

can impact survival and quality of life in individual NF2 patients. Therefore, the discovery of effective NF2 drug therapies is critical.

Currently, 2 clinical trials are enrolling pediatric NF2 patients to test effectiveness of selumetinib and cobimetinib in reducing tumor volume and preserving hearing (NCT03095248 and NCT02639546). However, the preclinical efficacies for selumetinib and cobimetinib have not been established. These trials are supported by knowledge that merlin loss is associated with increased mitogen-activated protein kinase signaling, and<sup>42</sup> success of selumetinib in shrinking plexiform neurofibromas in NF1 children.<sup>15</sup> Our study is the first to evaluate

a panel of MEK inhibitors in mouse and human NF2 schwannoma models.

Of the 6 inhibitors screened against multiple mouse and human SC lines, trametinib, PD0325901, and cobimetinib reduced MD-SC viability at submicromolar  $IC_{50}$  values and were the most effective in non-immortalized human MD-SCs (Fig. 1A). Notably, selumetinib was the least effective in MD-HSCs and was not a top performer in MD-MSCs (based on maximum effect and  $IC_{50}$  values). In vitro, trametinib, PD0325901, and cobimetinib reduced pERK levels, modulated cyclin D1 and p27 levels in a manner consistent with a  $G_1/S$  cell cycle arrest, and induced caspase-dependent apoptosis in MD-MSCs. The proteomic study conducted in

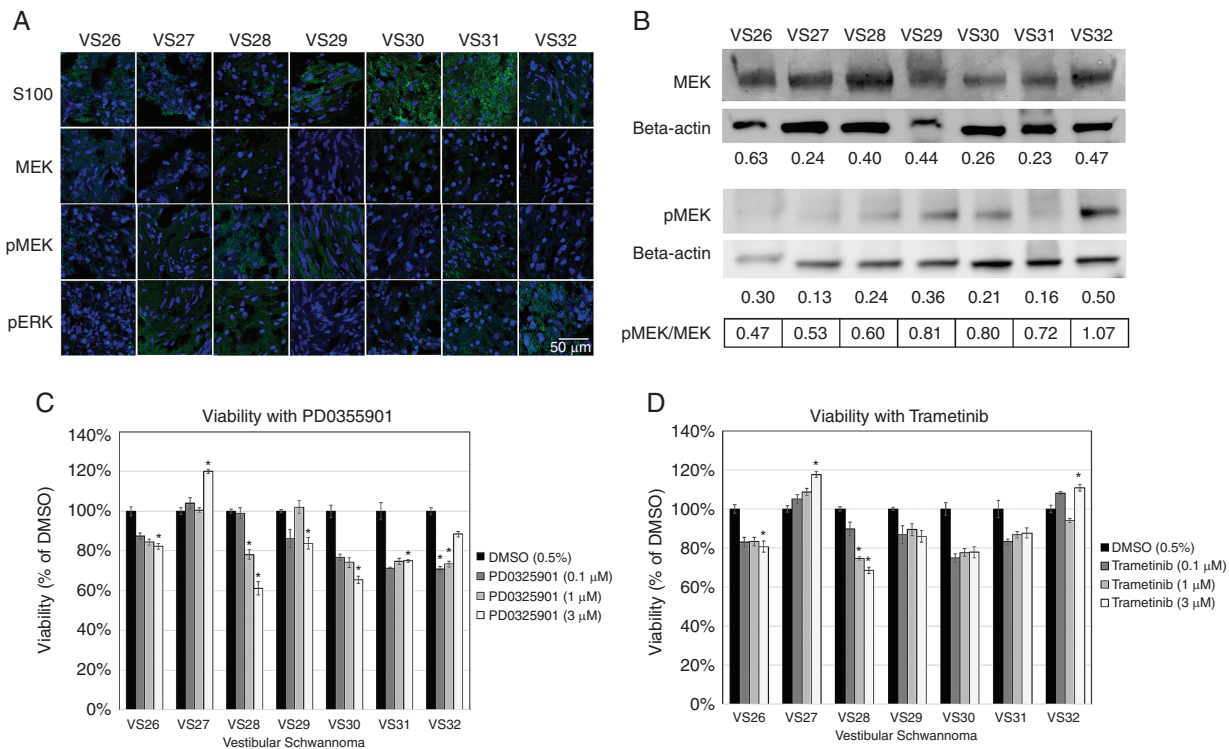


**Fig. 6** MEK inhibitors reduce viability of a subset of primary human VS cells. (A) Immunohistochemistry shows S100 positivity and variable expression levels of MEK, pMEK, and pERK (green) in VS tumors (4',6'-diamidino-2-phenylindole nuclear stain, blue). (B) Western blots demonstrate expression of MEK and pMEK for VS with beta-actin as the standard. Relative expression levels of MEK and pMEK were displayed and expressed as a ratio of pMEK/MEK. (C–D) Cell viability assays for PD0325901 and trametinib were performed and viability was normalized to 0.5% DMSO controls.

trametinib-treated MD-MSC further corroborated this conclusion by revealing decreased signaling in the Ras-ERK-cyclin D1 pathway and increased signaling from BNIP3L, a pro-apoptotic subfamily in the Bcl-2 family of proteins.

We used 2 *in vivo* models to evaluate drug efficacy: a 2-week treatment protocol aimed at slowing growth of established MD-MSCs nerve grafts in NSG mice, and an 8-week chemoprevention protocol aimed at preventing appearance of schwannomas in a GEM model. In the nerve grafts, PD0325901 and cobimetinib produced a stronger reduction in MD-MSC growth compared with trametinib, likely from persistent inhibition of pERK, cyclin D1, and Ki-67 levels. Trametinib did not significantly decrease pERK, cyclin D1 and Ki-67 levels in allografts at the study endpoint when compared with vehicle-treated controls, supporting the conclusion that cells in the allografts were developing resistance to trametinib. Similar responses to trametinib were obtained with the GEM model. Although the number and size of schwannomas were reduced in the GEM model following 8 weeks of trametinib treatment, immunohistochemically, pERK levels in trametinib-treated schwannomas were equivalent to controls. An adaptive response to trametinib has been reported in triple-negative breast cancer.<sup>43</sup> Trametinib treatment resulted in degradation of c-Myc and in assembly of bromodomain containing 4 (BRD4)-containing transcriptional enhancers on promoters

of adaptive response genes, resulting in activation of compensatory pathways associated with drug resistance.<sup>43</sup> Our proteomic analysis similarly revealed decreased c-Myc levels and increased BRD4 levels in MD-MSCs treated with trametinib (Fig. 3). BRD4 in trametinib-induced adaptive response promoter complexes can be displaced by treatment with bromodomain and extraterminal domain family (BET) bromodomain inhibitors.<sup>44</sup> A study of BET bromodomain inhibitors in ovarian cancer revealed reduced activation of ERK, Akt, and Src kinase following treatment, suggesting that these pathways may be activated by bromodomain-containing transcriptional enhancers.<sup>45</sup> Additionally, BET family bromodomains were involved in reactivation of the Src/focal adhesion kinase pathway in breast cancer cells following inhibition of ErbB2 with lapatinib.<sup>46</sup> Collectively, these studies suggest that trametinib treatment may promote assembly of BRD-containing transcriptional enhancers that can activate compensatory proliferative pathways. Future studies examining the effects of bromodomain and Src inhibitors in combination with MEK inhibitors are warranted.

Of the 7 primary human VS cultures tested, only a subset responded to either PD0325901 or trametinib by reducing cell viability by 15–40% of controls. Although the trend of response to both drugs was similar within individual VS cultures, the differing response rate to the drugs was

71% versus 29%, respectively, and did not correlate with baseline MEK or pMEK expression (Fig. 6A–D). The differing response rate can be attributed to the 10-fold higher potency of cobimetinib compared with PD0325901 (Fig. 6C–D).<sup>18,19</sup> VS cells also demonstrated a large variety of NF2 mutations, which can have differential effects on merlin-dependent cell proliferation and survival pathways. Methylome exploration identified *ELMOD1* as the single gene with a hypermethylated promoter and an FDR <0.05 in nonresponsive VS compared with responsive VS. *ELMOD1* is a GTPase activator for small GTPases in the ADP ribosylation factor (Arf) and Arf-like families (Arl2). In PD0325901 nonresponsive VS, a hypermethylated promoter in *ELMOD1* is expected to reduce *ELMOD1* expression, increase Arl2 activity, and alter normal microtubule dynamics.<sup>47</sup> This may allow VS cells to circumvent traditional mechanisms of cell cycle arrest and cell death.<sup>47</sup> Further investigation into how tumor heterogeneity in NF2 contributes to drug resistance and disease progression is imperative for identifying treatment modalities to overcome resistance to MEK inhibition.

We present a comprehensive preclinical analysis of MEK inhibitors in mouse and human NF2 schwannoma models and primary human VS. Although differences in response were observed between drugs, species, and models, our cumulative results support MEK inhibitors for the treatment of a subset of NF2 schwannomas. We demonstrate that differences in treatment response to MEK inhibitors depends on genetic and epigenetic differences between tumors that can impact downstream merlin signaling, drug resistance mechanisms, and adaptive pathways to evade cell death or arrest. By understanding the mechanisms of drug response and resistance to MEK inhibitors in individual tumors, we can identify optimal combination therapies to maximize tumor control, determine important genetic and molecular biomarkers to predict patient outcomes, and develop precision medicine algorithms for NF2 treatment.

## Supplementary Material

Supplementary data are available at *Neuro-Oncology* online.

## Keywords

merlin tumor suppressor | methylome | NF2 transgenic mice | MEK inhibitors | patient-derived vestibular schwannomas

## Funding

This work was supported by Department of Defense Congressionally Directed Medical Research Program (W81XWH-15-1-0446 to CFV and W81XWH-16-1-0104 to LSC), National Institutes of Health/National Institute on Deafness and Other Communication Disorders (R01-DC005575 and R01-DC012115 to XZL), and the Children's Tumor Foundation with contracts to CFV and MAF.

## Acknowledgments

We thank Drs Jacques Morcos and Michael Ivan for their efforts harvesting human VS tumors and patients for donated tumor samples. We acknowledge Anthony Griswold, PhD, Division Head of the Center for Genetic Epidemiology and Statistical Genetics at the University of Miami Miller School of Medicine, for bioinformatics and statistical analysis of DNA methylation experiments.

**Conflict of interest statement.** CFV is a named inventor on unrelated patents. MG and JV receive research funding from Recursion Pharmaceuticals. Other authors report that no conflicts of interest exist.

**Authorship statement.** *Designed experiments:* CFV, MCF, MAF, JV, MG, JK and CTD. *Supervised work:* CFV, CTD, MG, HM, and LSC. *Cell and allograft studies:* MAF, SKP, JN, KB, AP, MCF. *Human VS work:* CTD, OB, RM, DY, XL, FT, JIY. *GEM model:* MG, JV. *Proteome analysis:* AC, JK, TM, HM. *Histology:* LSC, RS, JH. *Flow cytometry analysis:* AJC. *Statistical analysis:* JNS. CFV, MAF and LSC wrote the initial draft and all authors edited the manuscript.

Portions of Figs. 1, 3, and 5 were presented at the annual Neurofibromatosis Conference in Washington DC in June 2017.

## References

1. Rouleau GA, Merel P, Lutchman M, et al. Alteration in a new gene encoding a putative membrane-organizing protein causes neuro-fibromatosis type 2. *Nature*. 1993;363(6429):515–521.
2. Trofatter JA, MacCollin MM, Rutter JL, et al. A novel moesin-, ezrin-, radixin-like gene is a candidate for the neurofibromatosis 2 tumor suppressor. *Cell*. 1993;72(5):791–800.
3. Evans DG. Neurofibromatosis type 2 (NF2): a clinical and molecular review. *Orphanet J Rare Dis*. 2009;4:16.
4. Blakeley JO, Evans DG, Adler J, et al. Consensus recommendations for current treatments and accelerating clinical trials for patients with neurofibromatosis type 2. *Am J Med Genet A*. 2012;158A(1):24–41.
5. Chung LK, Nguyen TP, Sheppard JP, et al. A systematic review of radio-surgery versus surgery for neurofibromatosis type 2 vestibular schwannomas. *World Neurosurg*. 2018;109:47–58.
6. Evans DG, Birch JM, Ramsden RT, Sharif S, Baser ME. Malignant transformation and new primary tumours after therapeutic radiation for benign disease: substantial risks in certain tumour prone syndromes. *J Med Genet*. 2006;43(4):289–294.
7. Kim BS, Seol HJ, Lee JI, et al. Clinical outcome of neurofibromatosis type 2-related vestibular schwannoma: treatment strategies and challenges. *Neurosurg Rev*. 2016;39(4):643–653.

8. Nowak A, Dziedzic T, Czernicki T, et al. Strategy for the surgical treatment of vestibular schwannomas in patients with neurofibromatosis type 2. *Neurol Neurochir Pol*. 2015;49(5):295–301.
9. Seferis C, Torrens M, Paraskevopoulou C, Psichidis G. Malignant transformation in vestibular schwannoma: report of a single case, literature search, and debate. *J Neurosurg*. 2014;121(Suppl):160–166.
10. Sun S, Liu A. Long-term follow-up studies of Gamma Knife surgery for patients with neurofibromatosis type 2. *J Neurosurg*. 2014;121(Suppl):143–149.
11. Hilton DA, Ristic N, Hanemann CO. Activation of ERK, AKT and JNK signalling pathways in human schwannomas in situ. *Histopathology*. 2009;55(6):744–749.
12. Morrison H, Sperka T, Manent J, Giovannini M, Ponta H, Herrlich P. Merlin/neurofibromatosis type 2 suppresses growth by inhibiting the activation of Ras and Rac. *Cancer Res*. 2007;67(2):520–527.
13. Petrilli AM, Fernández-Valle C. Role of merlin/NF2 inactivation in tumor biology. *Oncogene*. 2016;35(5):537–548.
14. McDermott L, Qin C. Allosteric MEK1/2 inhibitors for the treatment of cancer: an overview. *J Drug Res Dev*. 2015;1:1–9. doi: 10.16966/jdrd.101.
15. Dombi E, Baldwin A, Marcus LJ, et al. Activity of selumetinib in neurofibromatosis type 1–related plexiform neurofibromas. *N Engl J Med*. 2016;375(26):2550–2560.
16. Ammoun S, Schmid MC, Ristic N, et al. The role of insulin-like growth factors signaling in merlin-deficient human schwannomas. *Glia*. 2012;60(11):1721–1733.
17. Ammoun S, Schmid MC, Triner J, Manley P, Hanemann CO. Nilotinib alone or in combination with selumetinib is a drug candidate for neurofibromatosis type 2. *Neuro Oncol*. 2011;13(7):759–766.
18. Yamaguchi T, Kakefuda R, Tajima N, Sowa Y, Sakai T. Antitumor activities of JTP-74057 (GSK1120212), a novel MEK1/2 inhibitor, on colorectal cancer cell lines in vitro and in vivo. *Int J Oncol*. 2011;39(1):23–31.
19. Barrett SD, Bridges AJ, Dudley DT, et al. The discovery of the benzhydryloxamate MEK inhibitors CI-1040 and PD 0325901. *Bioorg Med Chem Lett*. 2008;18(24):6501–6504.
20. Jessen WJ, Miller SJ, Jousma E, et al. MEK inhibition exhibits efficacy in human and mouse neurofibromatosis tumors. *J Clin Invest*. 2013;123(1):340–347.
21. Jousma E, Rizvi TA, Wu J, et al. Preclinical assessments of the MEK inhibitor PD-0325901 in a mouse model of Neurofibromatosis type 1. *Pediatr Blood Cancer*. 2015;62(10):1709–1716.
22. Signorelli J, Shah Gandhi A. Cobimetinib. *Ann Pharmacother*. 2017;51(2):146–153.
23. Wong H, Vernillet L, Peterson A, et al. Bridging the gap between preclinical and clinical studies using pharmacokinetic-pharmacodynamic modeling: an analysis of GDC-0973, a MEK inhibitor. *Clin Cancer Res*. 2012;18(11):3090–3099.
24. Choo EF, Ng CM, Berry L, et al. PK-PD modeling of combination efficacy effect from administration of the MEK inhibitor GDC-0973 and PI3K inhibitor GDC-0941 in A2058 xenografts. *Cancer Chemother Pharmacol*. 2013;71(1):133–143.
25. Hoefflich KP, Merchant M, Orr C, et al. Intermittent administration of MEK inhibitor GDC-0973 plus PI3K inhibitor GDC-0941 triggers robust apoptosis and tumor growth inhibition. *Cancer Res*. 2012;72(1):210–219.
26. Rice KD, Aay N, Anand NK, et al. Novel carboxamide-based allosteric MEK inhibitors: discovery and optimization efforts toward XL518 (GDC-0973). *ACS Med Chem Lett*. 2012;3(5):416–421.
27. Rosen LS, LoRusso P, Ma WW, et al. A first-in-human phase I study to evaluate the MEK1/2 inhibitor, cobimetinib, administered daily in patients with advanced solid tumors. *Invest New Drugs*. 2016;34(5):604–613.
28. Petrilli AM, Fuse MA, Donnan MS, et al. A chemical biology approach identified PI3K as a potential therapeutic target for neurofibromatosis type 2. *Am J Transl Res*. 2014;6(5):471–493.
29. Fuse MA, Plati SK, Burns SS, et al. Combination therapy with c-Met and Src inhibitors induces caspase-dependent apoptosis of merlin-deficient schwann cells and suppresses growth of schwannoma cells. *Mol Cancer Ther*. 2017;16(11):2387–2398.
30. Petrilli AM, Garcia J, Bott M, et al. Ponatinib promotes a G1 cell-cycle arrest of merlin/NF2-deficient human schwann cells. *Oncotarget*. 2017;8(19):31666–31681.
31. Giovannini M, Robanus-Maandag E, Niwa-Kawakita M, et al. Schwann cell hyperplasia and tumors in transgenic mice expressing a naturally occurring mutant NF2 protein. *Genes Dev*. 1999;13(8):978–986.
32. Giovannini M, Bonne NX, Vitte J, et al. mTORC1 inhibition delays growth of neurofibromatosis type 2 schwannoma. *Neuro Oncol*. 2014;16(4):493–504.
33. Cox J, Neuhauser N, Michalski A, Scheltema RA, Olsen JV, Mann M. Andromeda: a peptide search engine integrated into the MaxQuant environment. *J Proteome Res*. 2011;10(4):1794–1805.
34. Smyth GK, Michaud J, Scott HS. Use of within-array replicate spots for assessing differential expression in microarray experiments. *Bioinformatics*. 2005;21(9):2067–2075.
35. Gilmartin AG, Bleam MR, Groy A, et al. GSK1120212 (JTP-74057) is an inhibitor of MEK activity and activation with favorable pharmacokinetic properties for sustained in vivo pathway inhibition. *Clin Cancer Res*. 2011;17(5):989–1000.
36. Blakeley JO, Plotkin SR. Therapeutic advances for the tumors associated with neurofibromatosis type 1, type 2, and schwannomatosis. *Neuro Oncol*. 2016;18(5):624–638.
37. Goutagny S, Raymond E, Esposito-Farese M, et al. Phase II study of mTORC1 inhibition by everolimus in neurofibromatosis type 2 patients with growing vestibular schwannomas. *J Neurooncol*. 2015;122(2):313–320.
38. Karajannis MA, Legault G, Hagiwara M, et al. Phase II trial of lapatinib in adult and pediatric patients with neurofibromatosis type 2 and progressive vestibular schwannomas. *Neuro Oncol*. 2012;14(9):1163–1170.
39. Karajannis MA, Legault G, Hagiwara M, et al. Phase II study of everolimus in children and adults with neurofibromatosis type 2 and progressive vestibular schwannomas. *Neuro Oncol*. 2014;16(2):292–297.
40. Plotkin SR, Halpin C, McKenna MJ, Loeffler JS, Batchelor TT, Barker FG 2<sup>nd</sup>. Erlotinib for progressive vestibular schwannoma in neurofibromatosis 2 patients. *Otol Neurotol*. 2010;31(7):1135–1143.
41. Plotkin SR, Merker VL, Halpin C, et al. Bevacizumab for progressive vestibular schwannoma in neurofibromatosis type 2: a retrospective review of 31 patients. *Otol Neurotol*. 2012;33(6):1046–1052.
42. Yi C, Troutman S, Fera D, et al. A tight junction-associated merlin-angiotensin complex mediates merlin's regulation of mitogenic signaling and tumor suppressive functions. *Cancer Cell*. 2011;19(4):527–540.
43. Bevil SM, Zawistowski JS, Johnson GL. Enhancer remodeling regulates epigenetic adaptation and resistance to MEK1/2 inhibition in triple-negative breast cancer. *Mol Cell Oncol*. 2017;4(6):e1300622.
44. Zawistowski JS, Bevil SM, Goulet DR, et al. Enhancer remodeling during adaptive bypass to MEK inhibition is attenuated by pharmacologic targeting of the P-TEFb complex. *Cancer Discov*. 2017;7(3):302–321.
45. Kurimchak AM, Shelton C, Duncan KE, et al. Resistance to BET bromodomain inhibitors is mediated by kinome reprogramming in ovarian cancer. *Cell Rep*. 2016;16(5):1273–1286.
46. Stuhlmiller TJ, Miller SM, Zawistowski JS, et al. Inhibition of lapatinib-induced kinome reprogramming in ERBB2-positive breast cancer by targeting BET family bromodomains. *Cell Rep*. 2015;11(3):390–404.
47. Zhou C, Cunningham L, Marcus AI, Li Y, Kahn RA. Arl2 and Arl3 regulate different microtubule-dependent processes. *Mol Biol Cell*. 2006;17(5):2476–2487.

Abstract presented at the 2016 NF Conference, Austin, TX. (Jun. 2016)

## **Similarities and Differences in Tumor Characteristics and Treatment Response in NF2-Associated Vestibular Schwannomas and Meningiomas**

**Sarah S. Burns, BA**

*Nationwide Children's Hospital and The Ohio State University*

Neurofibromatosis type 2 (NF2) is characterized by the development of multiple nervous system tumors, including vestibular schwannomas (VS) and meningiomas. These tumors cause considerable morbidities, including profound deafness, tinnitus, facial nerve paralysis, ataxia, and brainstem compression; however, an effective medical therapy is presently not available. Previously, we showed that the histone deacetylase inhibitor (HDACi) AR-42 causes tumor regression and inhibits tumor growth in animal models of *NF2*-deficient meningioma and schwannoma, respectively. Similarly, AR-42 reduced tumor size in meningiomas while slowing the growth of VS in an NF2 patient. To investigate this difference in treatment response, we screened for genetic mutations in 405 cancer-related genes in VS and meningiomas from two NF2 patients treated with AR-42. In addition to mutations in *NF2*, VS from both patients harbored mutations in *NUP98*, which is important for nuclear transport, mitotic checkpoint, and immunity. Also, we detected a duplication of exon 2-3 of the *MYC* gene in one of these patients. Analysis of blood samples from these patients and their parents confirmed that these mutations were present in the germline. Intriguingly, in a patient with multiple tumors, we observed the same genetic changes in both VS and meningiomas, implicating additional factors in treatment response. Interestingly, we detected a significant number of CD163+ macrophages in a majority of meningiomas, whereas little or no macrophages were present in the 20 VS examined. The *MYC* protein has been shown to regulate tumor microenvironment, which can be affected by HDACi's. Importantly, strong nuclear *MYC* expression was detected in the majority of VS specimens but not in meningiomas. Experiments are in progress to evaluate *MYC* inhibitors for their ability to inhibit tumor growth and to enhance sensitivity to AR-42. Our results suggest that targeting tumor microenvironment may enhance therapeutic response in NF2-associated tumors.

Full List Authors: Sarah S. Burns, BA<sup>1,2</sup>, Elena M. Akhmametyeva, MD, PhD<sup>1,2</sup>, Jaishri Blakeley, MD<sup>4</sup>, D. Bradley Welling, MD, PhD<sup>5</sup>, and Long-Sheng Chang, PhD<sup>1,2,3</sup>

<sup>1</sup>*Center for Childhood Cancer and Blood Diseases, Nationwide Children's Hospital and Departments of* <sup>2</sup>*Pediatrics and* <sup>3</sup>*Otolaryngology, The Ohio State University,* <sup>4</sup>*Departments of Neurology, Neurosurgery, and Oncology, Johns Hopkins University,* and <sup>5</sup>*Department of Otology and Laryngology, Harvard Medical School and Massachusetts General Hospital*

Funding: The Galloway Family, Advocure NF2, Meningioma Mommas, CTF, and the Department of Defense

Abstract presented at the 2016 NF Conference, Austin, TX. (Jun. 2016)

**ErbB3 and IGF-1R blockade as a potential treatment for vestibular schwannomas and meningiomas**

**Janet Oblinger, Ph.D.**

*Nationwide Children's Hospital & The Ohio State University*

Vestibular schwannomas (VS) and meningiomas are intracranial tumors that are frequently caused by inactivation of the *NF2*/merlin tumor suppressor gene. These neoplasms incur significant patient morbidities, such as deafness, vertigo, facial paralysis, hydrocephalus, cranial nerve palsy, seizures, and brainstem compression. Currently, treatments for these tumors include surgical excision or radiation; however, an FDA-approved targeted therapy is not available. One of merlin's functions is to suppress aberrant signaling from receptor tyrosine kinases (RTKs) on the cell surface. Indeed, VS and meningiomas often exhibit abnormal activation of RTKs, including members of the epidermal growth factor receptor (EGFR) family and insulin-like growth factor 1 receptor (IGF-1R). However, the EGFR inhibitors erlotinib and lapatinib exhibit only minimal efficacy in VS or meningioma patients, suggesting that additional RTKs provide survival signals for these tumors. We show that treatment of NF2 patient schwannoma and Ben-Men-1 benign meningioma cells with MM-121, an antibody that targets the EGFR member ErbB3, abrogates ligand-induced receptor activation and AKT phosphorylation. Similarly, treatment with MM-141, a bispecific antibody which blocks ErbB3 and IGF-1R signaling, also reduces activation of these receptors and downstream AKT. Importantly, prolonged treatment with MM-121 or MM-141 strongly suppresses ligand-mediated cell proliferation of NF2 schwannoma cells by 65% and 81%, respectively. We also found that Ben-Men-1 cells possess autocrine ErbB3 activation, which drives robust AKT signaling. Addition of MM-121 or MM-141 to Ben-Men-1 cells reduces ligand-induced cell growth and S-phase entry. These promising results warrant further *in vivo* evaluation of MM-121 and MM-141. Our study implicates ErbB3 and IGF-1R as important in VS and meningioma cell growth and indicates that blockade of these RTKs should be considered in the treatment of these tumors.

Full List Authors: Janet Oblinger<sup>1,2</sup>, Sarah Burns<sup>1,2</sup>, Michael Curley<sup>4</sup>, Long-Sheng Chang<sup>1,2,3</sup>

<sup>1</sup>Center for Childhood Cancer, The Research Institute at Nationwide Children's Hospital, Depts of <sup>2</sup>Pediatrics & <sup>3</sup>Otolaryngology, The Ohio State University, <sup>4</sup>Merrimack Pharmaceuticals, Inc.

Funding: Galloway Family Fund, Advocure NF2, CTF, Department of Defense

Abstract presented at the 2017 NF Conference, Washington, DC. (Jun. 2017)

**A strategy to identify an effective therapy for NF2-associated vestibular schwannomas**

**Janet Oblinger, Ph.D.**

*Nationwide Children's Hospital & The Ohio State University*

Current treatment options for neurofibromatosis type 2 (NF2)-associated vestibular schwannomas (VS) and meningiomas are limited to surgery and radiation; however, serious complications can occur with these treatments, and radiation can induce secondary malignancies. Also, incomplete tumor resection is not uncommon and is a main cause of tumor recurrence. Development of an effective medical therapy for NF2-associated tumors is urgently needed. Previously we reported that while the histone deacetylase inhibitor AR-42 caused tumor regression in *NF2*-deficient meningiomas, it merely inhibited tumor growth in schwannomas. Similar findings were observed in a clinical trial of AR-42 in NF2 patients. Meningiomas treated with AR-42 exhibited tumor regression; in contrast, AR-42 only slowed VS growth. In one patient with multiple tumors, his meningiomas remained small while the growth of his VS rebounded after cessation of AR-42 treatment. These results suggest that a more effective treatment of VS may require a drug combination. To investigate possible underlying causes for the differential response of meningiomas and VS to AR-42, we performed mutational analysis of tumors from two NF2 patients. In addition to *NF2* mutations, VS from both patients harbored mutations in the *NUP98* gene. Also, a duplication of exon 2-3 in the *MYC* gene was detected in one of the patients. Intriguingly, we detected the same genetic changes in the left and right VS and meningioma from the same patient. Immunostaining revealed strong nuclear MYC staining in 20 VS analyzed, but meningiomas showed little nuclear MYC expression. Depletion of MYC by shRNAs suppressed VS but not meningioma cell growth, suggesting that drugs targeting MYC expression may be effective in VS. Consistently, we showed that the bromodomain inhibitor JQ1, which transcriptionally downregulates MYC, inhibited VS cell proliferation. Combining JQ1 with AR-42 resulted in enhanced growth suppression. We are presently investigating additional drug combinations with the ultimate goal of identifying an effective therapy for VS. Further, we have established telomerase-immortalized cell lines from NF2 patient tumors for further investigation.

Full List Authors: Sarah Burns<sup>1,2</sup>, Janet Oblinger<sup>1,2</sup>, Elena Akhmametyeva,<sup>1,2</sup> D. Bradley Welling,<sup>3,4</sup> Long-Sheng Chang<sup>1,2,3</sup>

<sup>1</sup>*Center for Childhood Cancer and Blood Diseases, Nationwide Children's Hospital, Departments of* <sup>2</sup>*Pediatrics and* <sup>3</sup>*Otolaryngology, The Ohio State University, and* <sup>4</sup>*Department of Otolaryngology, Harvard Medical School/Massachusetts General Hospital*

Support: The Galloway Family, the Franklin/Goodkind Family, Advocure NF2, CTF, Department of Defense

Abstract presented at the 2017 NF Conference, Washington, DC. (Jun. 2017)

**Natural Silvestrol-Related Rocaglates as Potential Treatments for Vestibular Schwannomas and Meningiomas**

**Janet Oblinger, Ph.D.**

*Nationwide Children's Hospital & The Ohio State University*

Vestibular schwannomas (VS) and meningiomas are intracranial tumors that are often caused by inactivation of the *NF2*/merlin tumor suppressor gene. These tumors cause serious morbidities, including deafness, vertigo, facial paralysis, hydrocephalus, cranial nerve palsies, seizures, and brainstem compression. Currently, surgical excision and radiation are the treatment options for these tumors, since an FDA-approved targeted therapy is not yet available. We and others have previously shown that VS and meningiomas often exhibit high levels of activated AKT, which can promote protein biosynthesis. As uncontrolled growth of tumor cells often requires a high degree of protein translation, we found that both of these tumors frequently over-express eIF4A, eIF4E, and eIF4G, components of the eukaryotic initiation factor 4F (eIF4F) complex that critically regulates protein translation initiation. Intriguingly, the eIF4A inhibitor silvestrol, which is a member of the rocaglate family isolated from *Aglaia* plants in tropical rainforests, was consistently found to be a potent inhibitor of VS and meningiomas. However, due to its complex structure and large molecular weight, silvestrol has suboptimal pharmacokinetic and pharmacodynamic properties. To this end, we have investigated the growth-inhibitory activity of 10 silvestrol-related compounds isolated from *Aglaia perviridis*. These compounds have the same scaffold as silvestrol, but lack the bulky, sugar-like dioxanyl ring that is thought to hinder silvestrol's bioavailability. We found that three of these silvestrol related rocaglates, didesmethylrocaglamide, methyl 4'-demethoxy-3',4'-methylenedioxyrocaglate, and rocaglaol, strongly inhibited the growth of schwannoma and meningioma cells with IC<sub>50</sub> values similar to or better than that of silvestrol (less than 100 nM). Importantly, the IC<sub>50</sub> values for these rocaglates in normal meningeal cells were greater than 300 nM, suggesting an improved therapeutic window. Like silvestrol, didesmethylrocaglamide and rocaglaol decreased the levels of phospho-AKT, PCNA, cyclin D1, and Aurora A. Studies are in progress to verify the *in vivo* efficacy of these compounds in our tumor models.

Full List Authors: Janet Oblinger<sup>1,2</sup>, Sarah Burns<sup>1,2</sup>, A. Douglas Kinghorn<sup>4</sup>, Long-Sheng Chang<sup>1,2,3</sup>

<sup>1</sup>Center for Childhood Cancer and Blood Diseases, The Research Institute at Nationwide Children's Hospital, Departments of <sup>2</sup>Pediatrics & <sup>3</sup>Otolaryngology, The Ohio State University, <sup>4</sup>Division of Medicinal Chemistry and Pharmacognosy, College of Pharmacy

Funding: Advocure NF2, the Galloway Family, CTF, and the Department of Defense

Abstract presented at the 2017 NF Conference, Washington, DC. (Jun. 2017)

## **Merlin plays an important role in centrosome disjunction**

Long-Sheng Chang, PhD

*Nationwide Children's Hospital and The Ohio State University*

Neurofibromatosis type 2 (NF2) is a genetic disorder characterized by the development of multiple nervous system tumors, such as vestibular schwannomas. NF2 is caused by mutations in the *NF2* gene, which encodes the merlin protein that regulates multiple signaling pathways in several cellular compartments. In addition, somatic *NF2* mutations have been detected in multiple cancer types, including breast cancer. Presently, the mechanism by which *NF2* inactivation leads to tumorigenesis is not completely understood. We have shown that *NF2* is strongly expressed in the developing brain and in regions containing migrating cells, including the neural tube closure. Using *Nestin-CreER*, we demonstrated that *Nf2* inactivation during early gestation impaired neuroprogenitor cell proliferation and caused neural tube defects. In contrast, mice with *Nf2* inactivation during mid-to-late gestation developed schwannomas at a high frequency. Similarly, we showed that *Nf2* inactivation in luminal epithelial cells during mid-to-late pregnancy using *Wap1-Cre* and during early pregnancy using *Blg-Cre* markedly decreased cell proliferation, leading to impaired lobuloalveolar morphogenesis. Interestingly, 100% of these mice with *Nf2* knockout in mammary epithelial cells developed mammary tumors following multiple gestation cycles. The decreased cell proliferation during development and tumor formation at later stages due to *Nf2* loss in neural and mammary epithelial cells implies that merlin either inhibits or supports cell proliferation depending on the biological context. To further examine the role of merlin during tumorigenesis, we found that mitotic neuroprogenitor and mammary epithelial cells lacking *Nf2* displayed abnormal spindle formation and chromosome segregation due to defects in centrosome duplication and separation. We have generated merlin-deficient MCF10A mammary epithelial cells using shRNA or the CRISPR/Cas 9 technology. Both *NF2*-depleted and *NF2*-null MCF10A cells also exhibited abnormal centrosome separation, resulting in abnormal centrosome clustering or multiple centrosome formation. Double immunostaining detected merlin in the centrosomes. As  $\beta$ -catenin is a Nek2 substrate involved in centrosome separation, we found that depletion of merlin affected  $\beta$ -catenin phosphorylation at the centrosome. Together, these results suggest that merlin plays an important role during the centrosome separation process. Experiments are in progress to examine possible therapeutic implications of our findings.

Full List Authors: Long-Sheng Chang,<sup>1,2,3</sup> Jie Huang,<sup>1,2</sup> Elena Akhmametyeva,<sup>1,2</sup> Sarah Burns<sup>1,2</sup>

<sup>1</sup>*The Research Institute at Nationwide Children's Hospital and* <sup>2</sup>*Department of Pediatrics, The Ohio State University*

Funding: the Department of Defense. We sincerely thank Dr. Marco Giovannini for *Nf2*<sup>flox/flox</sup> mice.

# Abstract Submission

*Basic and translational research*

*NF2/Schwannomatosis*

NF2018/ABS-151

## **Preclinical Assessment of MEK1/2 Inhibitors for Neurofibromatosis Type 2-Associated Schwannomas Reveals Differences in Efficacy and Drug Resistance Development.**

Cristina Fernandez-Valle\*<sup>1</sup>, Marisa Fuse<sup>1</sup>, Christine Dinh<sup>2</sup>, Jeremie Vitte<sup>3</sup>, Joanna Kirkpatrick<sup>4</sup>, Thomas Mindos<sup>4</sup>, Stephani Champion<sup>5</sup>, Konstantin Brnjos<sup>1</sup>, Maria Clara Franco<sup>6</sup>, Jie Huang<sup>7</sup>, Juan Young<sup>2</sup>, Alejandra Petrilli<sup>1</sup>, Denise Yan<sup>2</sup>, Rahul Mittal<sup>2</sup>, Rulong Shen<sup>8</sup>, Fred Telischki<sup>2</sup>, Long-Sheng Chang<sup>7</sup>, Helen Morrison<sup>4</sup>, Marco Giovannini<sup>3</sup>, Xue-Zhong Liu<sup>2</sup>

<sup>1</sup>University of Central Florida, Orlando, <sup>2</sup>University of Miami Miller School of Medicine, Miami, <sup>3</sup>David Geffen School of Medicine, UCLA, Los Angeles, United States, <sup>4</sup>Leibniz Institute on Aging, Jena, Germany, <sup>5</sup>Orlando Health, Orlando, <sup>6</sup>Oregon State University, Corvallis, <sup>7</sup>Nationwide Children's Hospital, <sup>8</sup>Ohio State University, Columbus, United States

**Select your preferred type of presentation:** Platform presentation

**Background:** Neurofibromatosis type 2 (NF2) is a genetic tumor disorder caused by loss of function of the *NF2*/merlin tumor suppressor gene. A hallmark of NF2 is formation of bilateral vestibular schwannomas (VS) for which no FDA-approved drug is presently available. Because merlin modulates activity of the Ras/Raf/MEK/ERK pathway, we investigated repurposing drugs targeting MEK1/2 to treat NF2-associated schwannomas.

**Methods:** Mouse and human merlin-deficient Schwann cell (MD-MSCHSC) lines were screened against six MEK1/2 inhibitors. Efficacious drugs were tested in orthotopic allograft and *NF2* transgenic mouse models. Proteome and pathway analyses were conducted. Drug efficacy was examined in primary human VS cells with *NF2* mutations and correlated with differential DNA methylation patterns.

**Results:** Trametinib, PD0325901, and cobimetinib were the most potent in reducing MD-MSCHSC viability. Each decreased pERK1/2 and cyclin D<sub>1</sub>, increased p27, and induced caspase 3 cleavage in MD-MSCHSCs. Proteome analysis was consistent with cell cycle arrest and activation of pro-apoptotic pathways in trametinib-treated MD-MSCHSCs. The three inhibitors slowed the growth of MD-MSCHSC allografts compared to controls. However, decreased pERK1/2, cyclin D<sub>1</sub>, and Ki67 levels were observed in PD0325901 and cobimetinib, but not trametinib treated grafts. Eight weeks of trametinib treatment reduced tumor burden and average tumor size compared to controls in the *NF2* transgenic mouse model; tumors did not exhibit reduced pERK1/2 staining compared to control. Both trametinib and PD0325901 modestly reduced viability of several primary human VS cells with *NF2* mutations. DNA methylation analysis of PD0325901-resistant versus -susceptible VS identified differentially methylated regions in genes that could contribute to drug-resistance.

**Conclusions:** This comprehensive pre-clinical study demonstrates efficacy differences and possible emergence of drug resistance among MEK inhibitors in schwannoma models and supports further investigation of MEK inhibitors alone and in combination with other targeted drugs as treatments for NF2-associated schwannomas.

**Disclosure of Interest:** None Declared

**Keywords:** None

# Abstract Submission

*Basic and translational research*

*NF2/Schwannomatosis*

NF2018/ABS-184

## **Novel drug discovery for NF2-deficient meningiomas: Brigatinib causes tumor shrinkage in NF2-deficient meningiomas**

Long-Sheng Chang<sup>\*1</sup>, Sarah S Burns<sup>1</sup>, Janet L Oblinger<sup>1</sup>, Marc Ferrer<sup>2</sup>, Jie Huang<sup>1</sup>, Ming Poi<sup>3</sup>, Vijaya Ramesh<sup>4</sup>, On behalf of the Synodos for NF2 Consortium<sup>5</sup> and Full list of Investigators of the Children's Tumor Foundation (CTF)-supported Synodos for NF2 Consortium: <https://www.synapse.org/#!Synapse:syn2343195/wiki/62126>

<sup>1</sup>Center for Childhood Cancer & Blood Diseases/Department of Pediatrics, The Res Inst at Nationwide Children's Hosp/The Ohio State Univ College of Medicine, Columbus, OH, <sup>2</sup>National Center for Advancing Translational Sciences, NIH, Bethesda, MD, <sup>3</sup>Division of Pharmacy Practice & Science, The Ohio State Univ College of Pharmacy, Columbus, OH, <sup>4</sup>Center for Genomic Medicine and Department of Neurology, Massachusetts General Hospital, Boston, MA, <sup>5</sup>The CTF-supported Synodos for NF2 Consortium, NY, United States

**Select your preferred type of presentation:** Platform presentation

**Background:** Originating from meningotheelial cells of the arachnoid layer lining the brain, meningiomas cause significant morbidities by compressing adjacent brain tissues, cranial nerves, and blood vessels. Meningiomas can occur spontaneously or are frequently found in NF2 patients carrying *NF2* mutations. As an FDA-approved drug is presently not available for *NF2*-deficient meningioma, we aimed to identify novel targeted drugs that delay tumor progression or cause tumor shrinkage.

**Methods:** A panel of isogenic *NF2* and *NF2*<sup>+</sup> arachnoidal cells and *NF2* meningioma cells was used to screen ~2000 compounds of diverse mechanisms of action. The anti-tumor activity of the selected drug combination, pharmacokinetic (PK) analysis, PathScan RTK Signaling Antibody Arrays, and Western blots were performed.

**Results:** From the single agent screen, 45 potent compounds were selected for further combination screening, and 33 drug combinations, including the combination of brigatinib, an inhibitor of multi-RTKs including ALK, and MK2206, an AKT inhibitor, were identified that exhibited a greater synergistic growth inhibition in *NF2* cells versus *NF2*<sup>+</sup> cells. As a single agent, brigatinib effectively blocked tumor growth and reduced tumor size in the intracranial *NF2*-deficient Ben-Men-1-LucB meningioma model, while MK2206 only modestly suppressed tumor growth. Combined treatment with brigatinib and MK2206 further reduced tumor size. Upon cessation of treatment, the tumors treated with brigatinib or the brigatinib/MK2206 combination regrew. Importantly, these regrown tumors were responsive to these drugs when retreated again. PK analysis revealed that both brigatinib and MK2206 crossed the blood-brain barrier and accumulated in tumor-containing brain tissues. Intriguingly, Ben-Men-1 cells did not express ALK but expressed several phospho-RTKs (p-RTKs) with strong expression of p-ErbB2, ErbB3, FGFR1, TrkA, and VEGFR2. Brigatinib treatment reduced the levels of most of these p-RTKs with the most significant reduction in EGFR, ErbB2, ErbB3, VEGFR2, several Eph receptor members, as well as FAK. In addition, brigatinib treatment attenuated the downstream signals of these kinases, including p-AKT and p-ERKs.

**Conclusions:** The anti-tumor effects of brigatinib in *NF2*-deficient meningiomas are mediated through inhibition of multiple growth-promoting RTKs but not ALK. Brigatinib and its combination with an AKT inhibitor should be further evaluated in patients with *NF2*-deficient meningiomas (Support: the CTF and US Department of Defense)

**Disclosure of Interest:** None Declared

**Keywords:** None

# Abstract Submission

*Basic and translational research*

*NF1*

NF2018/ABS-185

## Identification of silvestrol-related rocaglates with better bioavailability and high potency against malignant peripheral nerve sheath tumors

Long-Sheng Chang<sup>1</sup>, Janet L Oblinger<sup>1</sup>, Sarah S Burns<sup>1</sup>, Jie Huang<sup>1</sup>, Larry Anderson<sup>2</sup>, Rulong Shen<sup>3</sup>, Li Pan<sup>4</sup>, Yulin Ren<sup>4</sup>, Barry R O'Keefe<sup>5</sup>, A Douglas Kinghorn<sup>4</sup>, Jerry M Collins<sup>2</sup>

<sup>1</sup>Center for Childhood Cancer & Blood Diseases/Department of Pediatrics, The Research Institute at Nationwide Children's Hospital/The Ohio State University College of Medicine, Columbus, OH, <sup>2</sup>Division of Cancer Treatment and Diagnosis, National Cancer Institute, NIH, Bethesda, MD, <sup>3</sup>Department of Pathology, The Ohio State University College of Medicine, <sup>4</sup>Division of Medicinal Chemistry and Pharmacognosy, The Ohio State University College of Pharmacy, Columbus, OH, <sup>5</sup>Division of Cancer Treatment and Diagnosis and Molecular Targets Program, Center for Cancer Research, National Cancer Institute, NIH, Bethesda, MD, United States

**Select your preferred type of presentation:** Platform presentation

**Background:** Malignant peripheral nerve sheath tumors (MPNSTs) frequently overexpress eIF4F components, and the eIF4A inhibitor silvestrol effectively suppresses MPNST growth. However, silvestrol has suboptimal drug-like properties, including a bulky structure and poor oral bioavailability. Our objectives are to identify potent silvestrol-related rocaglates and to determine their bioavailability, anti-tumor effects, and mechanisms of action.

**Methods:** *NF1*<sup>+/+</sup> STS26T and *NF1*<sup>-/-</sup> ST8814 MPNST and 697 and silvestrol-resistant 697-R leukemic cells were treated with various concentrations of each rocaglate. Cell proliferation assays, flow cytometry, Western blots, and pharmacokinetic (PK) analysis were performed. A quantifiable, orthotopic *NF1*-deficient MPNST mouse model and immunohistochemistry were conducted to assess antitumor effects.

**Results:** Among 10 silvestrol-related rocaglates lacking the dioxanyl ring examined, didesmethylrocaglamide (DDR) and rocaglamide (ROC) had potent growth-inhibitory activity comparable to silvestrol in MPNST cells. Structure-activity relationship analysis revealed that the dioxanyl ring in silvestrol was dispensable while the C-8b hydroxyl group was essential for cytotoxicity. DDR and ROC arrested MPNST cells at G<sub>2</sub>/M and significantly increased the sub-G<sub>1</sub> fraction. Accordingly, these rocaglamides induced cleavage of caspases 3 and 7 and poly(ADP-ribose) polymerase, while decreasing total protein levels of these apoptotic markers, consistent with translation inhibition. Additionally, DDR and ROC reduced the levels of mitogenic kinases AKT and ERK1/2. Unlike silvestrol, DDR and ROC inhibited proliferation of silvestrol-resistant 697-R leukemic cells, which over-express the MDR1 multidrug transporter, at IC<sub>50</sub> values similar to silvestrol-sensitive 697 cells, suggesting that these rocaglamides may be more bioavailable. PK analysis confirmed that ROC had 50% oral bioavailability. Importantly, ROC, when administered intraperitoneally or orally, potently suppressed the growth of luciferase-expressing *NF1*<sup>-/-</sup> ST8814-Luc MPNST xenografts with no overt toxicity. Treated tumors had abundant phospho-histone H3 labeling and more cleaved caspase 3-positive cells, consistent with G<sub>2</sub>/M arrest and indicative of increased apoptosis, respectively.

**Conclusions:** The more favorable drug-like properties and potent anti-tumor effects suggest that ROC and DDR have potential to become viable MPNST treatments. (Support: CancerFree Kids, the US Department of Defense, and National Cancer Institute, NIH)

**Disclosure of Interest:** None Declared

**Keywords:** None

# Abstract Submission

*Clinical research*

**NF2/Schwannomatosis**

NF2018/ABS-215

## **Phase 1 and Phase 0 studies of AR-42, a pan histone deacetylase inhibitor, in subjects with neurofibromatosis type 2 (NF2)-associated vestibular schwannomas and meningiomas**

D. Bradley Welling\*<sup>1</sup>, Sarah Burns<sup>2</sup>, Janet Oblinger<sup>3</sup>, Beth Miles-Markley<sup>4</sup>, Amir Mortazavi<sup>5</sup>, Amy Quinkert<sup>6</sup>, Jaishri Blakeley<sup>7</sup>, S. Alireza Monsouri<sup>8</sup>, Brian Neff<sup>9</sup>, Robert Jackler<sup>10</sup>, Long-Sheng Chang<sup>3</sup>

<sup>1</sup>Otolaryngology, Harvard Medical School, Massachusetts Eye and Ear, Massachusetts General Hospital, Boston, <sup>2</sup>Department of Pediatrics, <sup>3</sup>Center for Childhood Cancer, Nationwide Children's Hospital, <sup>4</sup>Otolaryngology Head & Neck Surgery, <sup>5</sup>Internal Medicine, The Ohio State University, Columbus, <sup>6</sup>Otolaryngology, Harvard/MEEI, Boston, <sup>7</sup>Neurology, Neurosurgery and Oncology, <sup>8</sup>Neurosurgery, Johns Hopkins University, Baltimore, <sup>9</sup>Otolaryngology, Mayo Clinic, Rochester, <sup>10</sup>Otolaryngology, Stanford, Palo Alto, United States

**Select your preferred type of presentation:** Platform presentation

**Background:** Patients with NF2 frequently develop bilateral vestibular schwannomas (VS) and multiple meningiomas. Presently, an FDA-approved medical therapy is not available. The histone deacetylase inhibitor AR-42, suppresses schwannoma growth and causes tumor shrinkage in meningiomas in preclinical models.

**Methods:** As part of a phase I trial of AR-42 in patients with advanced or recurrent solid tumors for which no standard therapy is available or patients who decline available standard treatment options, patients with NF2-associated VS and meningiomas were enrolled and received AR-42 treatment 3 times weekly for 3 weeks followed by 1-week break. Subsequently, a phase 0 exploratory evaluation of AR-42 for intratumoral pharmacodynamics and pharmacokinetics in VS and meningioma was performed.

**Results:** In the phase I trial, 5 NF2 patients were recruited. AR-42 was overall well-tolerated, and the maximum tolerated dose (MTD) was defined at 60 mg. AR-42 demonstrated anti-tumor activity mostly in the form of tumor stability. In one NF2 patient treated for 10 months, AR-42 significantly reduced tumor size in meningiomas and slowed VS growth rates. After cessation of treatment, meningiomas remained small, but VS quickly resumed growth. Tissue samples including a bilateral VS, a skull base meningioma, and an optic meningioma were collected from this patient. A VS from a second person with NF2 and these 4 tumors underwent comprehensive genomic profiling via FoundationOne. Mutations in *NF2* and *NUP98* were found. A phase 0 study with the primary objective to estimate p-AKT and p16<sup>INK4A</sup> levels after 3 weeks of oral AR-42 at 40 mg every other day, 3 times a week for 3 weeks preceding surgery, in NF2-related and sporadic VS and meningiomas, as well as control tumor samples from a tissue bank is ongoing. The secondary objectives include assessment of audiometric changes and volumetric tumor reduction and determination of plasma and intra-tumoral AR-42 concentrations. So far, 5 patients were studied. AR-42 concentrations in the plasma and VS of treated patients reached levels around the IC<sub>50</sub> value determined *in vitro* and was more preferentially concentrated in the tumors. AR-42 decreased the levels of p-AKT, pERK1/2, p-PRAS40, and p-S6 in treated VS.

**Conclusions:** AR-42 achieves therapeutic concentrations in the tumors and hits its targets. Further investigation of AR-42 as an NF2 treatment is ongoing.

(Funding: The US Department of Defense, The Galloway Family, and Advocure NF2)

**Disclosure of Interest:** None Declared

**Keywords:** None

Abstract presented at the 2019 NF Conference, San Francisco, CA. (Sept. 2019)

## **Brigatinib as a potential therapy for malignant peripheral nerve sheath tumors**

**Janet Oblinger, Ph.D.**

*Nationwide Children's Hospital & The Ohio State University*

MPNSTs are highly aggressive soft-tissue sarcomas that have a high risk of recurrence and metastasis and are refractory to current treatment. These tumors can arise spontaneously or from pre-existing plexiform neurofibromas in patients with neurofibromatosis type 1 (NF1), a tumor predisposition syndrome caused by inactivating mutations in the *NF1* tumor suppressor gene which encodes a Ras-GTPase-activating protein. Importantly, even sporadic tumors often incur mutations in the *NF1* gene or the Ras pathway. As a consequence, MPNSTs exhibit upregulation of Ras downstream kinase signaling, including the phosphatidylinositol 3-kinase (PI3K)-AKT-mammalian target of rapamycin (mTOR) and Raf-MEK-ERK mitogen-activated protein kinases. MPNSTs also harbor other genetic alterations, such as aberrant activation of epidermal growth factor receptor (EGFR) and insulin-like growth factor-1 receptor (IGF-1R), suggesting that these receptor tyrosine kinases (RTKs) may be therapeutic targets. Previously we showed that the FDA-approved ALK inhibitor brigatinib (ALUNBRIG™) suppresses multiple RTKs and non-RTKs, including focal adhesion kinase (FAK). Here we demonstrate that brigatinib exhibited growth-inhibitory activity in *NF1*-deficient ST8814 and *NF1*-expressing STS26T MPNST cells. Combination of brigatinib with the dual mTORC1/2 inhibitor INK128 (sapanisertib) yielded enhanced anti-proliferative effects. Treatment of ST8814 cells with brigatinib decreased p-EGFR and p-IGF-1R and their downstream p-AKT and p-S6. Treatment with INK128 also profoundly inhibited p-AKT and p-S6. Interestingly, combination of brigatinib and INK128 further reduced the phosphorylation of these signaling mediators and p-FAK compared to either monotherapy, suggesting cooperation in suppressing the AKT-mTOR pathway. However, we did not detect ALK expression in ST8814 and STS26T cells, indicating that brigatinib mediates growth inhibition via targeting of other tyrosine kinases. Experiments are in progress to investigate the anti-tumor activity of brigatinib in patient-derived xenograft (PDX) models for MPNST. Collectively, our data suggest that brigatinib should be further evaluated as a potential treatment for MPNST.

Full List Authors: Janet Oblinger<sup>1,2</sup> and Long-Sheng Chang<sup>1,2,3</sup>

<sup>1</sup>*Center for Childhood Cancer and Blood Diseases, Abigail Wexner Research Institute at Nationwide Children's Hospital and Depts of* <sup>2</sup>*Pediatrics &*

<sup>3</sup>*Otolaryngology-Head & Neck Surgery, The Ohio State University*

Funding: CancerFree KIDS, Department of Defense

Abstract presented at the 2019 NF Conference, San Francisco, CA. (Sept. 2019)

## **Targeting protein translation with rocaglamide and didesmethylrocaglamide to treat NF1 and NF2 tumors**

Long-Sheng Chang

*Nationwide Children's Hospital & The Ohio State University*

To sustain uncontrolled growth, cancer cells exhibit enhanced protein synthesis by upregulation of the protein translation machinery. Previously we reported that NF1-associated malignant peripheral nerve sheath tumors (MPNSTs) and NF2-related vestibular schwannomas and meningiomas exhibit elevated expression of eIF4A, eIF4E, and eIF4G, components of the eIF4F translation initiation complex, and that the eIF4A inhibitor silvestrol potently suppresses the growth of these tumor cells. Studies by others also show strong anti-tumor activity of silvestrol in several other cancer models, suggesting that it may be a potential cancer treatment. However, silvestrol has suboptimal drug-like properties, including a bulky structure, sensitivity to inhibition by the MDR1 multidrug-resistant transporter, and poor oral bioavailability. By screening 10 silvestrol-related rocaglates lacking the dioxanyl ring, we identified rocaglamide (Roc) and didesmethylrocaglamide (DDR) with potent growth-inhibitory activity comparable to silvestrol in MPNST cells. Structure-activity relationship analysis revealed that the dioxanyl ring present in silvestrol was dispensable for, but may enhance, cytotoxicity. Both Roc and DDR arrested MPNST cells at G<sub>2</sub>/M, significantly increased the sub-G<sub>1</sub> fraction, and induced cleavage of caspases 3 and 7 and poly(ADP-ribose) polymerase, while decreasing total protein levels of these apoptotic markers and mitogenic kinases AKT and ERK1/2, consistent with translation inhibition. Additionally, these rocaglamides elevated the levels of  $\gamma$ H2AX, a marker of the DNA damage response. Unlike silvestrol, Roc and DDR were not sensitive to MDR1 inhibition. Pharmacokinetic analysis confirmed that Roc had 50% oral bioavailability. Importantly, Roc, when administered intraperitoneally or orally, potently suppressed the growth of orthotopic NF1-deficient MPNST xenografts with no overt toxicity. Treated MPNSTs had abundant phospho-histone H3 labeling and more cleaved caspase 3-positive cells, consistent with G<sub>2</sub>/M arrest and indicative of increased apoptosis, respectively. In addition, Roc exhibited anti-tumor effects in patient-derived xenograft models for several types of sarcomas, including Ewing sarcoma, osteosarcoma, and rhabdomyosarcoma. Western blot analysis revealed that Roc and DDR decreased multiple oncogenic kinases, including IGF-1R, in sarcoma cells. Further, these rocaglamides potently inhibited proliferation of NF2-deficient schwannoma and meningioma cells. The more favorable drug-like properties and potent anti-tumor effects of Roc and DDR suggest that these rocaglamides have potential to become viable treatments for NF1- and NF2-associated tumors, including MPNST, as well as other sarcomas.

Full List Authors: Long-Sheng Chang<sup>1</sup>, Janet L Oblinger<sup>1</sup>, Sarah S Burns<sup>1</sup>, Jie Huang<sup>1</sup>, Larry Anderson<sup>2</sup>, Rulong Shen<sup>3</sup>, Li Pan<sup>4</sup>, Yulin Ren<sup>4</sup>, Ryan Roberts<sup>1</sup>, Barry R O'Keefe<sup>5</sup>, A Douglas Kinghorn<sup>4</sup>, Jerry M Collins<sup>2</sup>

<sup>1</sup>*Ctr for Childhood Cancer & Blood Diseases, Nationwide Children's Hospital/Dept of Pediatrics, The Ohio State Univ*, <sup>2</sup>*Div of Cancer Treatment and Diagnosis, National Cancer Institute, NIH*, <sup>3</sup>*Dept of Pathology, The Ohio State Univ*, <sup>4</sup>*Div of Medicinal Chemistry and Pharmacognosy, The Ohio State Univ Coll of Pharmacy*, <sup>5</sup>*Div of Cancer Treatment and Diagnosis and Molecular Targets Program, Ctr for Cancer Research, National Cancer Institute, NIH*

Funding: CancerFree KIDS, Sunbeam Foundation, Department of Defense